Hilde Sande

# The Cauchy problem for a model of immiscible gas flow with large data

Thesis for the degree of Philosophiae Doctor

Trondheim, Desember 2008

Norwegian University of Science and Technology
Faculty of Information Technology, Mathematics
and Electrical Engineering
Department of Mathematical Sciences

NTNU
Norwegian University of
Science and Technology

**NTNU**
Norwegian University of Science and Technology

Thesis for the degree of Philosophiae Doctor

Faculty of Information Technology, Mathematics and Electrical Engineering
Department of Mathematical Sciences



ISBN 978-82-471-1370-7 (printed ver.)
ISBN 978-82-471-1371-4 (electronic ver.)
ISSN 1503-8181

Doctoral theses at NTNU, 2009:4

Printed by NTNU-trykk

## PREFACE

This thesis is submitted for the degree philosophiae doctor (PhD) at the Norwegian University of Science and Technology (NTNU) in Trondheim, Norway. The work has been financed and carried out at the Department of Mathematical Sciences, NTNU. The thesis is based on two research papers concerning existence of a weak solution for a system of hyperbolic conservation laws with large initial data modeling one dimensional, immiscible flow of several isentropic gases. My supervisors have been Prof. Helge Holden, NTNU, and Prof. Nils Henrik Risebro, UiO.

These past years have been filled with hard work, lots of ups and downs, but most of all, many exciting challenges. I am very grateful for the opportunity to learn so much about mathematics, research and life in general. First of all, I want to thank Helge Holden for encouraging me to do a PhD. Moreover, I sincerely thank Helge the many discussions and for his continuously support and guidance throughout these years.

During the fall 2005 I spent two and an half months at Institut Mittag–Leffler, Stockholm, Sweden, as part of the project "Wave motions". The work environment provided there was excellent, I enjoyed many good discussions with other researchers and my collaboration with Nils Henrik Risebro also started there. I want to thank Nils Henrik for many enlightening discussions, for always bringing new ideas to the table and his impressive eye for details.

I am grateful for the good working environment provided by my colleagues at the department. A warm thank goes to my fellow PhD-students and the computer guys for all the social events and the many lunch breaks. In particular, I want to thank Marte G. for many good discussions and travels, and Marte H. and Vegard for sharing many conversations as well as the office with me.

I want to thank my friends for their patience and support. A special thank to Lars Erik for always being helpful and trying to answer all my questions.

Finally, I want to express my gratitude to my family for always being there for me, for their love, support and encouragement.

Hilde Sande,
Trondheim, December 2008.

## CONTENTS

# INTRODUCTION

The system of partial differential equations studied in this thesis is a $3 \times 3$ system of hyperbolic conservation laws that models the one dimensional, immiscible flow of several isentropic gases. The main topic is showing existence of a weak solution of the Cauchy problem when the initial data have large total variation.

## The model

**Some thermodynamics.** This brief introduction to thermodynamics is included to introduce the variables and motivate the equations studied in this thesis. An introduction to compressible fluids and thermodynamics from a mathematical point of view can be found in [9].

Each point in a fluid is in a definite state of thermodynamic equilibrium that is defined by the pressure $p$, the temperature $T$, the specific volume[1] $v = 1/\rho$ where $\rho$ is the density, the specific entropy $S$, and the specific internal energy $e$. For any given medium, only two of the above parameters are independent, and they can therefore be viewed as functions of two of the others. This gives rise to relations, usually called equations of state, between the parameters.

We assume that all gases are ideal gases, that is, there are no intermolecular forces and the molecules themselves have no volume. The equation of state for an ideal gas can be given as

$$pv = RT, \tag{1}$$

where the constant $R$ is the universal gas constant divided by the effective molecular weight of the particular gas.

The change in the internal energy for a medium during a change from one state to another, is due to the heat contributed and the work done. For an infinitesimal, reversible change from one state to the neighboring one in a compressible fluid, this can be written as

$$\mathrm{d}e = T\mathrm{d}S - p\mathrm{d}v, \tag{2}$$

where $T\mathrm{d}S$, for a reversible process, is the heat acquired by conduction, and $p\mathrm{d}v$ is the compressive work due to pressure forces. For an ideal gas, the internal energy is a function of the temperature alone, as shown in [9, Ch. 1*A*4].

A polytropic gas is an ideal gas where the internal energy is proportional to the temperature. Thus,

$$e = c_V T = \frac{pv}{\gamma - 1}, \tag{3}$$

where the specific heat capacity at constant volume, $c_V$, is equal to $R/(\gamma - 1)$, where $\gamma > 1$ is the adiabatic gas constant. In this case, the caloric equation of state can be written as

$$p = p(v, S) = (\gamma - 1)v^{-\gamma} \exp((\gamma - 1)(S - S_0)/R), \tag{4}$$

where $S_0$ is a constant.

[1]The specific volume is frequently denoted by $\tau$, but $v$ is chosen here since this is the notation used in the papers.

The model we discuss in this thesis concerns isentropic gases. An isentropic flow is in [9] defined as a flow in which the entropy is everywhere and always the same. The flow is reversible and adiabatic, that is, the entropy is unchanged and there is no heat transfer. The internal energy is still given by (3), thus, equation (2) reduces to

$$c_V \mathrm{d}T = -p\mathrm{d}v. \tag{5}$$

By eliminating $p$ using the equation of state (1) and solving equation (5), we find that $Tv^{\gamma-1}$ is constant, or equivalent, that $pv^\gamma$ equals a constant. From this we obtain the following caloric equation of state for the isentropic flow

$$p = p(v) = k^2 v^{-\gamma}, \tag{6}$$

where $k$ is a constant. Whenever the pressure is given by (6), we say that the pressure is given by a $\gamma$-law. Moreover, the constant $k$ will be equal to one throughout this thesis.

With this short introduction to thermodynamics, we are ready to derive the equations for our model.

**The system.** We want to describe the one dimensional, immiscible flow of several isentropic gases. We assume that all gases are ideal gases, thus, the pressure is given by the caloric equation of state (6) for each gas. The adiabatic gas constant, $\gamma$, now varies with the different gases, and therefore, the pressure is a function of $v$ and $\gamma$,

$$p = p(v, \gamma) = v^{-\gamma}, \tag{7}$$

where we, as previously stated, have set the constant $k$ in (6) equal to one.

We furthermore assume that the different gases are separated initially and that they do not mix at any later time. It is therefore natural to look for a model in Lagrangian coordinates where the reference frame follows the particles. To do this, we attach a number, $h$, to each plane section of particles normal to the $x$-axis, so that the changing position of the plane is given by the function $x(h,t)$. When this is done, the parameters such as $v$, $u$ and $p$ can be expressed as functions of our Lagrangian variables $h$ and $t$.

Thus, we first have to choose a way to identify $h$. This can be done in many different ways, and the most natural one would be to associate $h$ with the abscissa of the particle at some initial time, $t = 0$. However, in line with [9, Ch. 1*A*18], we choose to identify $h$ based on the fundamental law of mass conservation. We may think of the flow in a tube of unit cross section along the $x$-axis, and we define a reference section, moving with the medium, to be $h = 0$. Then we define $h$ for a cross section as the amount of mass between that section and the cross section $h = 0$. Thus, $h$ is negative if the cross section identified by $h$ is to the left of the reference section on the $x$-axis, and positive if it is to the right. All cross sections now have a uniquely defined $h$ and, mathematically, $h$ is given by the relation

$$h = \int_{x(0,t)}^{x(h,t)} \rho(x,t)\mathrm{d}x, \tag{8}$$

where $\rho(x,t)$ is the density associated with the motion, that is, given in the Eulerian reference frame.

We now have a reference frame given by $h$ and $t$ that follows the particles. From this way of identifying $h$, mass conservation follows naturally. First, differentiating (8) with respect to $h$ yields

$$\rho(h,t)x_h = 1, \tag{9}$$

where we use subscripts to indicate partial derivation. The quantity $\rho(h,t)x_h$ is the reference density, that is, the density associated with a particle. This quantity does not change in time, thus,

$$(\rho x_h)_t = \rho_t x_h + \rho x_{ht} = 0.$$

From equation (9) we have $x_h = 1/\rho = v$, where $v$ is the specific volume. Furthermore, $x_t$ equals the velocity $u$, and $\rho_t = -v_t/v^2$. Thus, conservation of mass is in Lagrangian coordinates given by

$$v_t - u_h = 0. \tag{10}$$

Furthermore, we neglect the external force of gravity and assume that no force other than the pressure gradient is acting on the gases. According to Newton's second law we then have

$$\rho x_{tt} = -p_x.$$

Recall that $\rho = 1/v$, $x_t = u$, and $p_x = p_h/x_h = p_h/v$, thus, after rearranging, conservation of momentum in Lagrangian coordinates reads

$$u_t + p_h = 0. \tag{11}$$

Equations (10)–(11) model the one-dimensional flow of one isentropic gas. In order to include several gases, we need one additional equation. From the assumptions that the gases are separated and not allowed to mix, the properties specific to one gas have to be conserved. Since we have given the pressure as a function of the adiabatic gas constant for each gas, it is natural to let $\gamma$ be our third variable. In the Lagrangian reference frame, $\gamma$ does not change with time, and

$$\gamma_t = 0, \tag{12}$$

serves as our last equation, representing conservation of the gas specific properties.

Letting now $x \in \mathbb{R}$ (replacing $h$ by $x$) and $t \in (0,\infty)$ denote our Lagrangian coordinates, the model of one dimensional, immiscible flow of several isentropic gases can be described by the system

$$\begin{aligned} v_t - u_x &= 0, \\ u_t + p(v,\gamma)_x &= 0, \\ \gamma_t &= 0, \end{aligned} \tag{13}$$

where $v$ is the specific volume, $u$ is the velocity, and $p$ is the pressure function given by (7). Note that if the specific volume, $v$, becomes infinite, which corresponds to zero density and zero pressure, we have *vacuum*.

We discuss the properties of this $3 \times 3$ system of hyperbolic conservation laws later. For now, we note that system (13) can be rewritten as a $2 \times 2$ system with discontinuous flux. We get

$$\begin{aligned} v_t - u_x &= 0, \\ u_t + p(v,\gamma(x))_x &= 0, \end{aligned}$$

where the adiabatic gas constants for the different gases are given by the discontinuous function $\gamma(x)$.

**From Lagrangian to Eulerian coordinates.** We have chosen to work with Lagrangian coordinates throughout this thesis mainly due to the nice form system (13) then has. In Eulerian coordinates with $x \in \mathbb{R}$ as the physical space variable and $t \in (0, \infty)$ as the time, the system reads

$$\begin{aligned} \rho_t + (\rho u)_x &= 0, \\ (\rho u)_t + (\rho u^2 + p(\rho, \gamma))_x &= 0, \\ (\rho\gamma)_t + (\rho u\gamma)_x &= 0, \end{aligned} \tag{14}$$

which can be obtained from system (13) by a transformation of reference frames. Let $(x, t)$ be the Eulerian coordinates and $(h, t)$ the Lagrangian coordinates. Let furthermore the time derivative in Lagrangian coordinates be denoted by a dot, like $\dot{f}$. The transition between the Lagrangian and the Eulerian reference frame is given by

$$\dot{x} = u(x, t), \tag{15}$$

since $x(h, t)$ is the physical changing position of the particle and $u$ is the velocity. Thus, we have

$$\dot{f} = f_t + \dot{x} f_x, \tag{16}$$

for any function $f$. Starting from mass conservation given by (10) in Lagrangian coordinates, the above relation gives us

$$0 = \dot{v} - u_h = v_t + \dot{x} v_x - x_h u_x = -\frac{\rho_t}{\rho^2} - u\frac{\rho_x}{\rho^2} - \frac{1}{\rho} u_x,$$

where we have used that $\dot{x} = u$, $x_h = v$ and $\rho = 1/v$. Multiplying the equation with $-\rho^2$ and writing $u_x\rho + u\rho_x = (\rho u)_x$, we obtain the first equation of system (14) given in Eulerian coordinates.

For the conservation of momentum given in Lagrangian coordinates by (11), we get

$$0 = \dot{u} + p_h = u_t + \dot{x} u_x + x_h p_x = u_t + u u_x + \frac{p_x}{\rho}.$$

To get this equation into the standard conservative form, we first multiply with $\rho$, and then use that $\rho_t + (\rho u)_x = 0$ by mass conservation;

$$0 = \rho u_t + \rho u u_x + p_x = \rho u_t + \rho u u_x + p_x + (\rho_t + (\rho u)_x)u = (\rho u)_t + (\rho u^2 + p)_x,$$

and we have obtained the second equation of system (14).

Finally, we transform the last equation given in Lagrangian coordinates by (12), and obtain

$$0 = \dot{\gamma} = \gamma_t + \dot{x}\gamma_x = \gamma_t + u\gamma_x.$$

Once more, we first multiply by $\rho$, then exploit the equation of mass conservation to obtain the last equation of system (14) in its conservative form;

$$0 = \rho\gamma_t + \rho u\gamma_x = \rho\gamma_t + \rho u\gamma_x + (\rho_t + (\rho u)_x)\gamma = (\rho\gamma)_t + (\rho u\gamma)_t.$$

By the results of Wagner [27], there is a one-to-one correspondence between a weak solution of a system given in Lagrangian coordinates and a weak solution of the same system given in Eulerian coordinates. Thus, proving existence results for system (13) in Lagrangian coordinates also gives existence results for system (14) in Eulerian coordinates.

**Some other models.** System (13) is an extension of the $2 \times 2$ system modeling the flow of one isentropic gas,

$$\begin{aligned} v_t - u_x &= 0, \\ u_t + p(v)_x &= 0, \end{aligned} \tag{17}$$

where $\gamma$ is constant and the pressure, $p(v) = v^{-\gamma}$, depends solely on $v$. This system is known as the $p$-system, and is a classic textbook example of systems of hyperbolic conservation laws, see, e.g., [10, 15, 24].

To the best of our knowledge, system (13) has not been discussed earlier. Several other $3 \times 3$ systems are extensions of the $p$-system (17), and we mention a few. In order to model multiphase flow, Amadori and Corli [1] extend the $p$-system with an extra equation,

$$\begin{aligned} v_t - u_x &= 0, \\ u_t + p(v, \lambda)_x &= 0, \\ \lambda_t &= 0, \end{aligned} \tag{18}$$

where $\lambda \in [0, 1]$ is the mass density fraction of vapor in the fluid. The pressure function, $p(v, \lambda) = a^2(\lambda)/v$, is a function of both $v$ and the new variable, $\lambda$, as it is for system (13), making the two systems similar. However, the adiabatic gas constant is equal to one for system (18), and therefore the properties of the two systems are quite different. For instance, vacuum can never form for the model in [1] as it can for system (13). Moreover, the wave curves of system (18) are monotone in $\lambda$, making the analysis of the interactions less complicated than for system (13), where the wave curves are not monotone in $\gamma$. The model in [1] is a simplified version of the model discussed by Fan in [13]. Similar models, but with a rather different pressure laws, are also considered in [12] and [19] applying completely different methods. A model in the context of the Navier–Stokes equation with finitely many independent pressure laws has been studied in [6].

We furthermore mention the Euler equations modeling polytropic gas flow which in Lagrangian variables reads

$$\begin{aligned} v_t - u_x &= 0, \\ u_t + p_x &= 0, \\ E_t + (pu)_x &= 0, \end{aligned} \tag{19}$$

where the last equation is conservation of energy, $E = e + \frac{1}{2}u^2$, and $e$ is the internal energy. The gas is assumed to be ideal and polytropic, thus, the pressure is given by the caloric equation of state (4), as discussed earlier. Note that there is only one gas present in this model, hence, $\gamma$ is constant. System (19) is also frequently discussed in textbooks on conservation laws, see, e.g., [24]

## Systems of hyperbolic conservation laws

The theory of hyperbolic conservation laws dates back to the mid of the 19th century and has developed in close relations with gas dynamics. The Riemann problem was, however, already formulated by Riemann in the 18th century in connection with isentropic gas dynamics. Courant and Friedrichs [9] give a survey of this field up to 1948. The mathematical formulation of the theory for systems of hyperbolic conservation laws in one space dimension we use, was established in the paper by Lax [16]. Several books give an up-to-date overview of the theory of hyperbolic conservation laws, see, e.g., [4, 10, 15, 24]. This introduction briefly gives the theory and definitions needed to discuss the results proved in this thesis.

An $n \times n$ system of hyperbolic conservation laws is $n$ nonlinear partial differential equations of the form

$$U_t + f(U)_x = 0, \tag{20}$$

where $U = U(x,t)$ and $f \in C^2$ are vectors in $\mathbb{R}^n$. We restrict our discussion to systems in one space dimension, that is, $x \in \mathbb{R}$.

The Jacobian of the flux, $\mathrm{d}f$, for system (20) has $n$ real eigenvalues, $\lambda_1, \ldots, \lambda_n$, with corresponding right eigenvectors $r_1, \ldots, r_n$. If the $n$ eigenvalues are distinct, then the system is *strictly hyperbolic*. Furthermore, if

$$\nabla \lambda_j(U) \cdot r_j(U) \neq 0,$$

we say that the $j$th family is *genuinely nonlinear*, and if

$$\nabla \lambda_j(U) \cdot r_j(U) = 0,$$

the $j$th family is *linearly degenerate*. In this thesis we are only concerned with strictly hyperbolic systems of the form (20) where each family is either genuinely nonlinear or linearly degenerate.

**The Riemann problem.** The problem solving system (20) with initial data consisting of two constant states, that is,

$$U(x,0) = \begin{cases} U_l, & \text{if } x < 0, \\ U_r, & \text{if } x > 0, \end{cases} \tag{21}$$

where $U_l, U_r \in \mathbb{R}^n$ are constants, is called the Riemann problem. Understanding this fundamental problem is essential in order to obtain results for system (20) for more general initial data.

For an $n \times n$ system of hyperbolic conservation laws where each family is either genuinely nonlinear or linearly degenerate, the two initial states of the Riemann problem are connected by up to $n$ elementary waves. There is at most one wave from each family, and the waves have increasing wave speeds.

For a genuinely nonlinear family there are two types of waves; *rarefaction waves* which are continuous waves of the form $U(x,t) = w(x/t)$ satisfying

$$\dot{w}(x/t) = r_j(w(x/t)), \qquad \lambda_j(w(x/t)) = x/t, \tag{22}$$

where $\lambda_j$ is increasing along the wave, and *shock waves* which are solutions

$$U(x,t) = \begin{cases} U_l, & \text{if } x < \sigma_j t, \\ U_r, & \text{if } x > \sigma_j t, \end{cases} \tag{23}$$

satisfying the Rankine–Hugoniot condition

$$\sigma_j(U_r - U_l) = f(U_r) - f(U_l), \tag{24}$$

for a shock velocity $\sigma_j$. To rule out the non-physical shock waves, we use an entropy condition: The admissible shock waves are those satisfying the Lax entropy conditions

$$\lambda_{j-1}(U_l) < \sigma_j < \lambda_j(U_l), \qquad \lambda_j(U_r) < \sigma_j < \lambda_{j+1}(U_r). \tag{25}$$

For a linearly degenerate family there is only one type of waves called *contact discontinuities*. These waves are solutions of the form (23) that satisfy the Rankine–Hugoniot condition (24) with $\sigma = \lambda_j$.

The *$j$-wave curve* consists of all states $U$ that can be connected to a given left state $U_l$ by a wave of family $j$, and is often denoted $W_j(U_l)$. Thus, to solve the Riemann problem

we have to find (up to) $n-1$ intermediate states $U_i$ so that $U_1 \in W_1(U_l)$, $U_i \in W_i(U_{i-1})$, and $U_r \in W_n(U_{n-1})$. By Lax's theorem [15, Thm. 5.17], we have a unique solution of the Riemann problem for system (20) in a small neighborhood of $U_l$.

**The Cauchy problem.** Solving the Cauchy problem for system (20) means solving the system with general initial data

$$U(x,0) = U_0(x). \tag{26}$$

It is well-known that systems of hyperbolic conservation laws do not in general have smooth solutions, even for smooth initial data. Thus, by a solution of the Cauchy problem for system (20) we mean a *weak solution* in the distributional sense with $U \in L^1(\mathbb{R} \times [0,\infty))$ so that

$$\iint_{\mathbb{R}\times[0,\infty)} (U\phi_t - f(U)\phi_x)\,\mathrm{d}x\mathrm{d}t + \int_{\mathbb{R}} U_0(x)\phi(x,0)\,\mathrm{d}x = 0, \tag{27}$$

for all infinitely differentiable functions $\phi(x,t)$ with compact support.

Glimm [14] proved global existence of a weak solution of the Cauchy problem with small initial data for strictly hyperbolic systems where each family is either genuinely nonlinear or linearly degenerate. This includes system (13) with sufficiently small initial data.

Proving existence of a solution for systems of hyperbolic conservation laws is typically done in a constructive manner. Through an approximate method one obtains a sequence of approximate solutions and thereafter shows that a subsequence converges to a weak solution. Two frequently used methods are the Glimm scheme [14, 24] and the front-tracking method [15, 4]. Both methods rely on solving several Riemann problems in order to obtain an approximate solution.

For $n \times n$ systems of hyperbolic conservation laws with large initial data, there is no general result similar to the theorem by Glimm [14] for small data. The topic for this thesis has therefore been to extend the result by Glimm to obtain existence of a weak solution of system (13) with large initial data.

## Some properties of the system

System (13) is a $3 \times 3$ system of hyperbolic conservation laws that is strictly hyperbolic for $p > 0$ with eigenvalues;

$$\lambda_1 = -\lambda, \qquad \lambda_2 = 0, \qquad \lambda_3 = \lambda, \tag{28}$$

where $\lambda := \sqrt{-p_v} = \sqrt{\gamma v^{-\gamma-1}}$. The corresponding eigenvectors are

$$r_1 = (1,\lambda,0), \qquad r_2 = (-p_\gamma, 0, p_v)\,, \qquad r_3 = (-1,\lambda,0). \tag{29}$$

Furthermore, the first and third wave family are genuinely nonlinear, while the second wave family is linearly degenerate.

Recall that vacuum corresponds to infinite $v$, or equivalently, $p = 0$. The properties of the system change at vacuum, and the methods used in this thesis do not apply then, see [18]. Therefore we only consider system (13) for finite $v$, that is, $p > 0$. Furthermore, we have from the thermodynamics that $\gamma > 1$.

The Riemann invariants for system (13) are given in **Appendix A** where we prove that the system does not have a coordinate system of Riemann invariants, only a 2-Riemann coordinate. **Appendix A** also includes the discussion of entropy/entropy flux pair for system (13).

**Wave curves.** For system (13) the rarefaction and shock waves of the first and third family have constant $\gamma$, thus, they are equal to the wave curves of the corresponding $p$-system (17). Along the contact discontinuities of the second family, $p$ and $u$ are constant, and only $\gamma$ changes. It is therefore easier to describe the wave curves, and other properties of the system, using $p$, $u$ and $\gamma$ as our variables. For $p > 0$, the wave curves are then given as

$$\Phi_1(p, U_l) := \begin{cases} (p, u_l - r(p, p_l, \gamma_l), \gamma_l), & p < p_l, \\ (p, u_l - s(p, p_l, \gamma_l), \gamma_l), & p > p_l, \end{cases} \tag{30}$$

$$\Phi_2(\gamma, U_l) := (p_l, u_l, \gamma), \quad \gamma > 1, \tag{31}$$

$$\Phi_3(p, U_l) := \begin{cases} (p, u_l + r(p, p_l, \gamma_l), \gamma_l), & p > p_l, \\ (p, u_l - s(p, p_l, \gamma_l), \gamma_l), & p < p_l, \end{cases} \tag{32}$$

where

$$r(p, p_l, \gamma_l) := \frac{2\sqrt{\gamma_l}}{\gamma_l - 1}\left(p^{\frac{\gamma_l - 1}{2\gamma_l}} - p_l^{\frac{\gamma_l - 1}{2\gamma_l}}\right), \tag{33}$$

$$s(p, p_l, \gamma_l) := \left(\left(p_l^{-\frac{1}{\gamma_l}} - p^{-\frac{1}{\gamma_l}}\right)(p - p_l)\right)^{1/2}, \tag{34}$$

and the shock velocities are

$$\sigma_1(U_l, U) = -\sqrt{\frac{p_l - p}{p^{-1/\gamma_l} - p_l^{-1/\gamma_l}}}, \qquad \sigma_3(U_l, U) = \sqrt{\frac{p - p_l}{p_l^{-1/\gamma_l} - p^{-1/\gamma_l}}}. \tag{35}$$

The wave curves through two different left states are depicted in Figure 1 where the notation

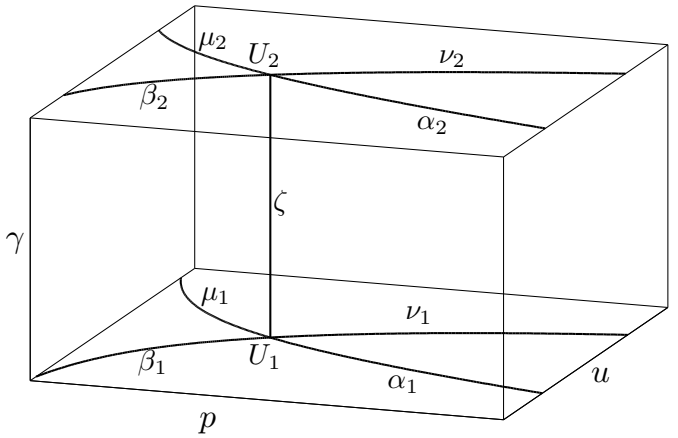


FIGURE 1. The wave curves through $U_1 = (p_l, u_l, \gamma_1)$ and $U_2 = (p_l, u_l, \gamma_2)$ where $\gamma_1 < \gamma_2$.

of the different waves is consistent with the notation used throughout this thesis. That is, we let

| | | |
|---|---|---|
| $\epsilon$ define a 1-wave, | $\alpha$ a 1-shock wave, | $\mu$ a 1-rarefaction wave, |
| $\eta$ a 3-wave, | $\beta$ a 3-shock wave, | $\nu$ a 3-rarefaction wave, |
| $\zeta$ a 2-wave. | | |

The backward 3-wave curve consists of all left states, $U$, that can be connected to a given right state $U_r$ by a 3-wave. This curve is useful when describing the Riemann problem and is given by

$$\tilde{\Phi}_3(p, U_r) := \begin{cases} (p, u_r - r(p_r, p, \gamma_r), \gamma_r), & p < p_r, \\ (p, u_r + s(p_r, p, \gamma_r), \gamma_r), & p > p_r, \end{cases} \tag{36}$$

where $r$ and $s$ are given by (33) and (34).

The 1-wave curve is strictly decreasing as a function of $p$, while the 3-wave curve and the backward 3-wave curve are strictly increasing. Several properties of the wave curves are given in the papers, but in this introduction we only include the most important one: The rarefaction and shock waves are not monotone in $\gamma$, that is, the projected wave curves onto the $(p, u)$-plane might intersect. Depending on the value of $\frac{\partial}{\partial p} r$ at the left state, the projected wave curves going either to the left or to the right will intersect, see Figure 2. This

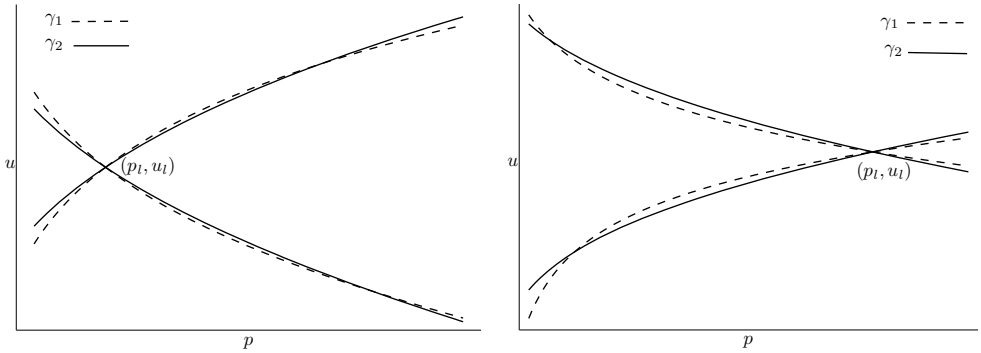


(a) When $\frac{\partial}{\partial p} r(p_l, p_l, \gamma_l) > \frac{\partial}{\partial p} r(p_l, p_l, \gamma_2)$, the projected wave curves going to the right intersect.

(b) When $\frac{\partial}{\partial p} r(p_l, p_l, \gamma_l) < \frac{\partial}{\partial p} r(p_l, p_l, \gamma_2)$, the projected wave curves going to the left intersect.

FIGURE 2. The wave curves through $U_1 = (p_l, u_l, \gamma_1)$ (dashed lines) and $U_2 = (p_l, u_l, \gamma_2)$, where $\gamma_1 < \gamma_2$, projected onto the $(p, u)$-plane.

property considerably complicates the interactions of waves with different values of $\gamma$.

**The Riemann problem.** Given the wave curves we can solve the Riemann problem for system (13) with initial data given by (21). From the general discussion of systems of hyperbolic conservation laws, it follows that the solution of the Riemann problem consists of up to three waves, one from each family. Since $p$ and $u$ are constant along the contact discontinuities, we look for the intersection between the 1-wave curve of the left state and the backward 3-wave curve of the right state projected onto the $(p, u)$-plane. Thus, the solution of the Riemann problem $(U_l, U_r)$ for system (13) is constructed as follows: Let $(\tilde{p}, \tilde{u})$ be the intersection point between the projections of $\Phi_1(p, U_l)$ and $\tilde{\Phi}_3(p, U_r)$ onto the $(p, u)$-plane. We connect $U_l = (p_l, u_l, \gamma_l)$ to $\tilde{U}_1 = (\tilde{p}, \tilde{u}, \gamma_l)$ by a 1-curve, then we go from $\tilde{U}_1$ to $\tilde{U}_2 = (\tilde{p}, \tilde{u}, \gamma_r)$ along a contact discontinuity, and finally connect $\tilde{U}_2$ to $U_r = (p_r, u_r, \gamma_r)$ by a 3-wave. The solution of a Riemann problem is shown in Figure 3.

We only consider system (13) away from vacuum, that is, for $p > 0$. Because the wave curves are monotone with respect to $p$, there is at most one intersection point between the projections of $\Phi_1(p, U_l)$ and $\tilde{\Phi}_3(p, U_r)$. The only case where the two projected curves never

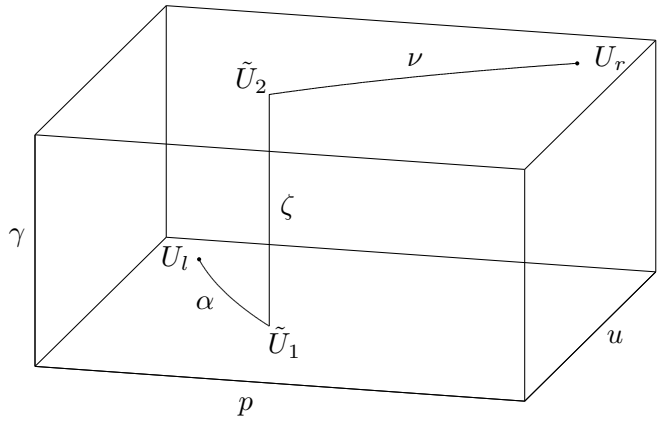


FIGURE 3. The solution of the Riemann problem $(U_l, U_r)$ consisting of a 1-shock wave $\alpha$, a contact discontinuity $\zeta$, and a 3-rarefaction wave $\nu$.

intersect, is if the projection of the backward 3-rarefaction wave from $U_r$ always lies above the projection of the 1-rarefaction wave from $U_l$. Thus, the Riemann problem for system (13) has a unique solution if

$$u_r - u_l < r(p_r, 0, \gamma_r) - r(0, p_l, \gamma_l). \tag{37}$$

It is important to note that if $\gamma_l = \gamma_r$, then the Riemann problem reduces to the Riemann problem for the $p$-system (17) with $\gamma = \gamma_l$, and the solution consists of at most two waves, a 1-wave and a 3-wave. We are therefore able to use results for the $p$-system, in particular due to Nishida and Smoller [21], for problems where $\gamma$ does not change.

Another important problem for system (13) is that its invariant region includes vacuum. A region $\Omega$ is invariant for the Riemann problem if for any Riemann problem with initial data in $\Omega$, its solution is also in $\Omega$. Since $\gamma$ never takes any other values than those of the initial data, we find the invariant region for the $p$-system for each $\gamma$ and take the union of these to get the invariant region for system (13). This invariant region gives an upper and lower bound on $u$ and an upper bound on $p$, but includes $p = 0$.

### The Cauchy problem with large initial data

As already noted, there is no general result for systems with large data, in contrast to the case of small data. Therefore, the topic for this thesis has been solving system (13) for large initial data. However, there are several results with large data for other specific systems, or systems with some given properties, and we give a short overview of some of these.

**Some existence result for systems with large data.** For $3 \times 3$ systems with a 2-Riemann coordinate, Temple and Young [26] showed existence of a solution for initial data with arbitrary large total variation, provided that the oscillations are small. This result applies to our system as well, but we want to avoid the restriction on the oscillations.

For the $p$-system (17) with $\gamma = 1$, Nishida [20] showed existence of a global solution for arbitrary, bounded initial data. This is a special case, since no vacuum can form and the wave curves are translation invariant. For $\gamma > 1$, Nishida and Smoller [21] proved existence of a solution for initial data where $(\gamma - 1)$ times the total variation of the initial data is

sufficiently small. The case with large initial data for $2 \times 2$ systems is also discussed in [5, 11].

Since system (13) does not have a coordinate system of Riemann invariants, we do not have the advantage of changing variables to Riemann invariants as for the $p$-system and other $2 \times 2$ systems. Liu [17] proved existence of a solution for the Euler equations (19) with large initial data. This system does not have a coordinate system of Riemann invariants, however, in [17] Liu changes variables inspired by the use of Riemann invariants. This clever approach does not simplify system (13) because $\gamma$ is a function of $x$.

The general results by Temple [25] includes both the results of [21] and [17]. In [25] one considers the flux function as a smooth one parameter family of functions where one has existence of a solution for arbitrary large initial data for the system with the parameter, $\epsilon$, equal to zero. Then the system with $0 \leq \epsilon \leq 1$ has a unique solution if $\epsilon$ times the total variation of the initial data is sufficiently small. Letting $\epsilon = \gamma - 1$ for the $p$-system (17) and the Euler equations (19), one obtains similar results as in [21] and [17]. However, this cannot be used for system (13) since $\gamma$ is one of the variables.

In [28] Wissman proved a large data existence theorem for the $3 \times 3$ system of relativistic Euler equations in the ultra-relativistic limit. Applying a change of coordinates, the shock waves become translation invariant and a Nishida-type of analysis is used. Peng [23, 22] also considered certain $3 \times 3$ systems (Lagrangian gas dynamics for a perfect gas and a model originating in multiphase flow modeling) with large initial data.

All these existence results are proved using the Glimm scheme. Asakura applies front tracking to show existence of a solution for the $p$-system [3] and for the Euler equations [2] with large initial data. The conditions on the initial data are the same as obtained in [21] and [17]. Amadori and Corli [1] also use front tracking to prove existence of a weak solution of (18) when the initial data have large total variation.

In [7, 8] front tracking is used to study systems of conservation laws whose flux functions depend on a parameter vector, $\mu$, similar to those in [25]. An approach for establishing $L^1$-estimate pointwise in time between entropy solutions for $\mu \neq 0$ and $\mu = 0$ is given. In particular, the $L^1$-estimate between entropy solutions in the large for the isentropic Euler equations, that is, system (17) with $\gamma > 1$, and the isothermal Euler equations, system (17) with $\gamma = 1$, is established in [7] and between entropy solutions in the large for the the Euler equations (19) and the isothermal Euler equations, system (17) with $\gamma = 1$, in [8]. For both cases $\mu = \gamma - 1$ where the adiabatic gas constant $\gamma$ tends to one.

**Existence results for system** (13) **with large initial data.** In this thesis we prove existence of a time-global, weak, entropy solution of system (13) for initial data

$$v(x,0) = v_0(x), \qquad u(x,0) = u_0(x), \qquad \gamma(x,0) = \gamma_0(x), \qquad x \in \mathbb{R}, \tag{38}$$

satisfying

$$\begin{aligned} (\sup(\gamma_0) - 1)\text{T.V.}(p_0, u_0) &\leq \min\left\{ \frac{C}{9kC_1}, C_3 \right\}, \\ \text{T.V.}(\gamma_0) &\leq \frac{C}{9C_2}, \end{aligned} \tag{39}$$

where $k$, $C$, $C_1$, $C_2$ and $C_3$ are constants that only depend on the initial data. Note that by reducing the supremum of $\gamma_0$, we can allow arbitrary large total variation in $p_0$ and $u_0$.

We prove this using the Glimm scheme in **Paper I** and using front tracking in **Paper II**. Through these numerical methods, we obtain a sequence of approximate solutions of system (13). The first step towards showing convergence to a weak solution, is for both methods

to prove that the approximate solutions have bounded total variation. To do this, we define a Glimm type functional, and show that it decreases in time. This involves identifying and estimating all possible interactions that might occur. We use the same functional in both papers, even though the definition of an interaction is different for the Glimm scheme compared to front tracking. Note, however, that the interactions between two waves or two fronts are the same for both methods. Since interactions that do not involve a contact discontinuity are equal to the interactions for the $p$-system, our choice of the Glimm type functional is inspired by the functional used in [21] by Nishida and Smoller, adding one extra term to account for the interactions with a contact discontinuity. Furthermore, the estimates we use for interactions between two waves or fronts where none of them are contact discontinuities, are obtained by transferring the estimates in [21] to our variables. Due to space limitations, this transformation is not included in the papers, and we have therefore included the detailed discussion of these estimates in **Appendix B**. The estimates for interactions between a contact discontinuity and another wave, or front, are in both papers found using an estimate proved in **Paper I** on how different two waves, or fronts, with different values of $\gamma$ are.

In **Paper I** we use the Glimm scheme for which the first step is to approximate the initial data as piecewise constants, then solve the Riemann problems at each jump. This gives us an approximate solution for small $t > 0$. Before any of the waves in the solutions of the initial Riemann problems interact, we sample the solution at some random sampling points, making it constant for each grid cell. Then the Riemann problems at the grid points are solved, and this process is continued up to any given time. The grid points, $x_i$, make up a staggered grid as shown in Figure 4. Connecting the sampling points with lines called

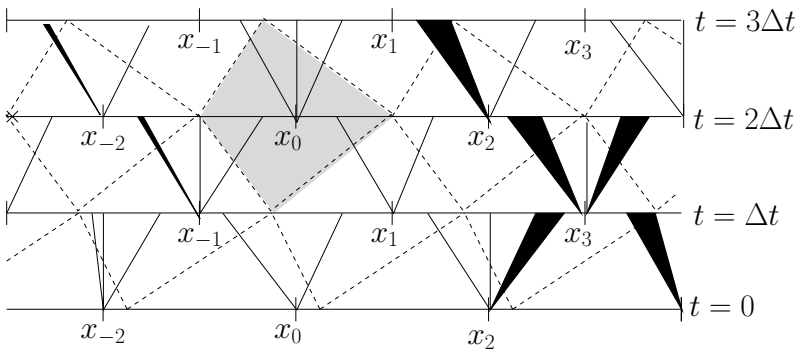


FIGURE 4. The staggered grid for the Glimm scheme with the diamond structure.

mesh curves, we get a diamond structure, also depicted in Figure 4. Since the values at the sampling points are the left and right state of the leftmost and rightmost wave entering the diamond, respectively, we say that the waves entering one diamond interact. Due to this diamond structure, and the wave speeds, at most four waves can enter one diamond. Thus, the most complicated interactions we get in the Glimm scheme are interactions between four waves.

For interactions with three or more incoming waves, we present a formal way of dividing the interaction into several steps to obtain the estimates needed to show that the Glimm functional is decreasing. The idea is to introduce intermediate mesh curves and inner diamonds so that only some of the waves enter the inner diamond and interact, while the rest is left unchanged. Typically, two waves enter an inner diamond, see Figure 5, and we already

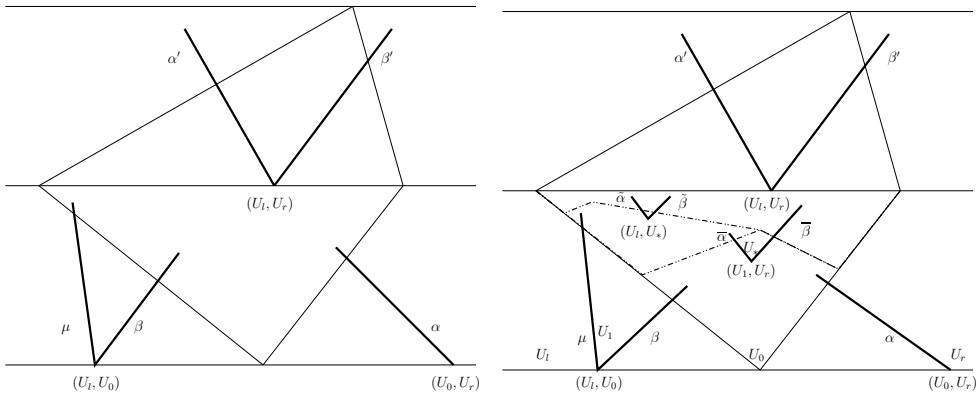


(a) The interaction before division.

(b) The interaction divided into three steps with two new mesh curves and two inner diamonds.

FIGURE 5. A typical interaction in the Glimm scheme.

have interaction estimates for these interactions. Thus, we know that the Glimm functional is decreasing for each step. The process of letting some waves interact while the rest is unchanged is continued until we have a collection of waves that we are able to compare to the outgoing waves. It is important to note that this is only a formal tool in order to prove that the Glimm functional is decreasing, and that no interactions in the Glimm scheme are altered.

In this way we prove that the Glimm functional decreases in time, from which we obtain bounded total variation of the approximate solution. Then, convergence to a weak solution follows by standard arguments.

In **Paper II** we use front tracking to show the existence result for system (13). Again we start by approximating the initial data as piecewise constants and then solve the Riemann problems at the jumps. However, all solutions to Riemann problems in front tracking must be piecewise constant, thus, we have to approximate rarefaction waves by step functions. Each discontinuity in the solution is called a front; a shock wave or a contact discontinuity is one front, while a rarefaction wave is approximated by several small fronts. We now have an approximate solution for small $t > 0$, and we track all fronts until some of them collide. Then we solve the Riemann problem with the left state of the leftmost front and the right state of the rightmost front as initial data, and we continue this process of tracking fronts and solving Riemann problems. However, to ensure that we always have a finite number of fronts, and hence, interactions, we have to introduce a simplified solver generating non-physical fronts we denoted by $\theta^{\text{NP}}$. The simplified solver is only used when fronts of the same family collide with a contact discontinuity and the sum of the strengths of the incoming fronts times the strength of the contact discontinuity is less than some given threshold parameter. Then, the solution of the Riemann problem consists of a non-physical front and two or three physical waves, depending on the number of incoming fronts, see Figure 6. Unlike the standard front-tracking algorithm with non-physical fronts, see [4], we introduce non-physical fronts traveling to the left as well as to the right, to retain the nice symmetry property of system (13). Still, all non-physical fronts have absolute speed greater than the speed of any other front.

In front tracking an interaction is an actually collision between fronts, and therefore arbitrary many fronts might interact. However, using a stepping procedure by letting two

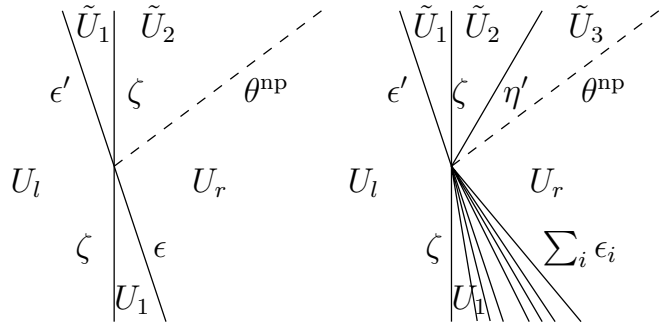


(a) A contact discontinuity interacts with one front of the first family.

(b) A contact discontinuity interacts with several fronts of the first family.

FIGURE 6. The simplified Riemann solver with non-physical fronts (dashed lines).

and two fronts interact, we obtain estimates for interaction between arbitrary many fronts of the same family. In this way we get the estimates needed for all possible interaction in front tracking, including the ones involving non-physical fronts. Figure 7 shows a typical interaction in front tracking where the interaction is divided into three steps. At the first step we use the result for interactions between fronts of the same family and at the second step we have an interaction between three fronts. Dividing the interaction into steps like this is just a formal trick to show that the Glimm type functional decreases, and no fronts or speeds are altered in the front-tracking algorithm.

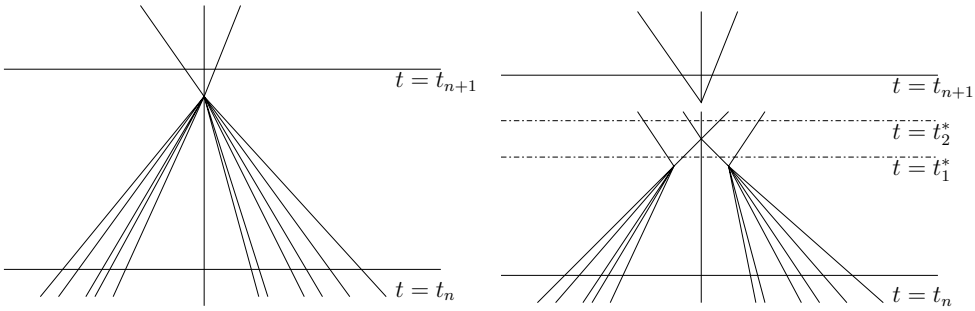


(a) The original interaction.

(b) The interaction divided into steps.

FIGURE 7. A typical interaction in front tracking.

Using the decreasing Glimm type functional we obtain bounded total variation of the approximate solution, and furthermore, prove that there is a finite number of physical and non-physical fronts. Thus, front tracking gives an approximate solution for any given time in a finite number of steps. We also bound the total amount of non-physical fronts that are generated. Finally, we show that a subsequence of the approximate solutions converges, and that the limit is a weak solution. To do this, we have to estimate the errors we do by approximating the initial data and the rarefaction waves, and by introducing non-physical fronts.

Moreover, **Paper I** and **Paper II** include numerical examples solved using the Glimm scheme and front tracking, respectively. One of these examples is common for both papers, and in **Paper II** we compare the solutions found by the two methods.

## References


[1] D. Amadori and A. Corli. On a model of multiphase flow. *SIAM J. Math. Anal*, 40(1):134–166, 2008.

[2] F. Asakura. Wave-front tracking for the equation of non-isentropic gas dynamics. *RIMS Kokyuroku*, 1495:78–91, 2006.

[3] F. Asakura. Wave-front tracking for the equation of isentropic gas dynamics. *Quart. Appl. Math.*, 63(1):20–33, 2005.

[4] A. Bressan. *Hyperbolic Systems of Conservation Laws.* Oxford University Press, 2000.

[5] A. Bressan and R. M. Colombo. Unique solutions of $2 \times 2$ conservation laws with large data. *Indiana Univ. Math. J.*, 44(3):677–725, 1993.

[6] C. Chalons and F. Coquel. Navier–Stokes equations with several independent pressure laws and explicit predictor-corrector schemes. *Numer. Math.* 101:451–478, 2005.

[7] G.-Q. Chen, C. Christoforou, and Y. Zhang. Dependence of entropy solutions in the large for the Euler equations on nonlinear flux functions. *Indiana Univ. Math. J.* 56(5):2535–2567, 2007.

[8] G.-Q. Chen, C. Christoforou, and Y. Zhang. Continuous dependence of entropy solutions to the Euler equations on the adiabatic exponent and Mach number *Arch. Ration. Mech. Anal.* 189:97–130, 2008.

[9] R. Courant and K. O. Friedrichs. *Supersonic Flow and Shock Waves.* Springer-Verlag, 1976.

[10] C. Dafermos *Hyperbolic Conservation Laws in Continuum Physics.* Springer-Verlag, 2005.

[11] R. J. DiPerna. Existence in the large for quasilinear hyperbolic conservation laws. *Arch. Rational Mech. Anal.*, 52:244–257, 1973.

[12] S. Evje and K. H. Karlsen. Global existence of weak solutions for a viscous two-phase model. *J. Differential Equations*, to appear.

[13] H. Fan. On a model of the dynamics of liquid/vapor phase transitions. *SIAM J. Appl. Math.*, 60(4):1270–1301. 2000.

[14] J. Glimm. Solution in the large for nonlinear hyperbolic systems of equations. *Comm. Pure Appl. Math.*, 18:697–715, 1965.

[15] H. Holden and N. H. Risebro. *Front Tracking for Hyperbolic Conservation Laws.* Springer-Verlag, 2002.

[16] P. D. Lax. Hyperbolic systems of conservation laws. *Comm. Pure Appl. Math.*, 10:537–566, 1957.

[17] T.-P. Liu. Solutions in the large for the equations of nonisentropic gas dynamics. *Indiana Univ. Math. J-*, 26(1):147–177, 1977.

[18] T. P. Liu and J. A. Smoller. On the vacuum state for the isentropic gas dynamics equations. *Adv. in Appl. Math.*, 1(4):345–359, 1980.

[19] Y. Lu. *Hyperbolic Conservation Laws and the Compensated Compactness Method.* Shapman&Hall/CRC, 2003.

[20] T. Nishida. Global solution for an initial boundary value problem for a quasilinear hyperbolic system. *Proc. Japan Acad.*, 44:642–646, 1968.

[21] T. Nishida and J. A. Smoller. Solution in the large for some nonlinear hyperbolic conservation laws. *Comm. Pure Appl. Math.*, 26:183–200, 1973.

[22] Y.-J. Peng. Solutions faibles globales pour l'quation d'Euler d'un fluide compressible avec de grandes donnees initales. *Comm. Partial Differential Equations*, 17(1-2):161–187, 1992.

[23] Y.-J. Peng. Solutions faibles globales pour un modèle d'écoulements diphasiques. *Ann. Scuola Norm. Sup. Pisa Cl. Sci.*, 21(4):523–540, 1994.

[24] J. Smoller. *Shock Waves and Reaction-Diffusion Equations.* Springer-Verlag, second edition, 1994.

[25] J. B. Temple. Solution in the large for the nonlinear hyperbolic concervation laws of gas dynamics. *J. Differential Equations*, 41:96–161, 1981.

[26] B. Temple and R. Young. The large time stability of sound waves. *Comm. Math. Phys.*, 179(2):417–466, 1996.

[27] D. H. Wagner. Equivalence of the Euler and Lagrangian equations of gas dynamics for weak solutions. *J. Differential Equations*, 68(1):118–136, 1987.

[28] B. D. Wissmann. Global soutions to the ultra-relativistic Euler equations. arXiv:0705.1333v1 [math.AP] 9 May 2007.

## Paper I

# The solution of the Cauchy problem with large data for a model of a mixture of gases

H. Holden, N. H. Risebro and H. Sande

Accepted for publication in *Journal of Hyperbolic Differential Equations*

# THE SOLUTION OF THE CAUCHY PROBLEM WITH LARGE DATA FOR A MODEL OF A MIXTURE OF GASES

HELGE HOLDEN, NILS HENRIK RISEBRO, AND HILDE SANDE

Abstract. In this paper we study mixture of gases, each governed by a gamma law. The system is modeled by the $p$-system with variable gamma. We use this model to study immiscible gas flow. The main result is that the Cauchy problem with large data is shown to have a solution. We use the Glimm scheme for the proof. The result is illustrated by numerical examples.

## 1. Introduction

We want to describe the one dimensional flow for several isentropic gases. The different gases are initially separated, and the pressure is for all gases given by a $\gamma$-law, that is, $p = \rho^\gamma$, where $\rho$ is the density and $\gamma$ is the adiabatic gas constant for each gas. The different gases cannot mix, therefore, in Lagrangian coordinates $\gamma$ only depends on $x$ and does not change in time. The flow of these gases is thus in Lagrangian coordinates described for $x \in \mathbb{R}$ and $t \in (0, \infty)$ by the system

$$\begin{aligned} v_t - u_x &= 0, \\ u_t + p(v,\gamma)_x &= 0, \\ \gamma_t &= 0, \end{aligned} \tag{1.1}$$

where $v = 1/\rho$ is the specific volume, $u$ is the velocity, and $p(v,\gamma) = v^{-\gamma}$ is the pressure function. We assume $\gamma(x,t) > 1$. This $3 \times 3$ system of hyperbolic conservation laws is strictly hyperbolic. The first and third family are genuinely nonlinear and the second family is linearly degenerate.

We consider the Cauchy problem for this system, that is, the system (1.1) with general initial data

$$v(x,0) = v_0(x), \qquad u(x,0) = u_0(x), \qquad \gamma(x,0) = \gamma_0(x), \qquad x \in \mathbb{R}. \tag{1.2}$$

Glimm [9] proved global existence of a weak solution of the Cauchy problem with small initial data for strictly hyperbolic systems where each family is either genuinely nonlinear or linearly degenerate, thus including the present system. This solution is found by using the Glimm scheme [9, 19, 20] or by using front tracking [11] by which one can prove stability of the Cauchy problem. Here we extend the existence result to large initial data for (1.1).

System (1.1) is an extension of the $2 \times 2$ system known as the $p$-system,

$$\begin{aligned} v_t - u_x &= 0, \\ u_t + p(v)_x &= 0, \end{aligned} \tag{1.3}$$

2000 *Mathematics Subject Classification.* Primary: 35L65, 76N15; Secondary: 35A05.

*Key words and phrases.* $p$-system, gamma law, mixture of gases.

This version contains graphics in colors and some typos are corrected.

which describes the flow of an isentropic gas, with only one gas is present here, thus $\gamma$ is constant and the pressure, still given by a $\gamma$-law, is a function of $v$ only.

For the $p$-system with $\gamma = 1$, Nishida [15] showed existence of a global solution for arbitrary bounded initial data. For $\gamma > 1$, Nishida and Smoller [16] proved existence of a solution for initial data where $(\gamma - 1)$ times the total variation of the initial data is sufficiently small. The case with large initial data for $2 \times 2$ systems is also discussed in [6, 4].

System (1.1) does not have a coordinate system of Riemann invariants, only a 2-Riemann coordinate. Therefore we do not have the advantage of changing variables to Riemann invariants as for the $p$-system and other $2 \times 2$ systems. Liu [12] proved existence of a solution for the full Euler system with large initial data, another $3 \times 3$ system without a coordinate system of Riemann invariants. Liu's change of variables is inspired by the use of Riemann invariants, but a similar approach does not simplify system (1.1), because $\gamma$ is a function of $x$. The general results by Temple [21] includes both the results of [16] and [12]. In [21] one considers the flux function as a smooth one parameter family of functions where one has existence of a solution for arbitrary large initial data for the system with the parameter, $\epsilon$, equal to zero. Then the system with $0 \leq \epsilon \leq 1$ has a unique solution if $\epsilon$ times the total variation of the initial data is sufficiently small. Letting $\epsilon = \gamma - 1$ for the $p$-system and the Euler equations, one obtains similar results as in [16] and [12]. However, this cannot be used for system (1.1) since $\gamma$ is one of the variables. Wissman proves in [25] a large data existence theorem for the $3 \times 3$ system of relativistic Euler equations in the ultra-relativistic limit. Applying a change of coordinates the shock waves become translation invariant and a Nishida-type of analysis is used.

For $3 \times 3$ systems with a 2-Riemann coordinate, Temple and Young [22] showed existence of a solution for initial data with arbitrary large total variation, provided that the oscillations are small. This result applies to our system as well, but we want to avoid this restriction on the oscillations. Peng [18, 17] also considered certain $3 \times 3$ systems (Lagrangian gas dynamics for a perfect gas and a model originating in multiphase flow modeling) with large initial data.

All these existence results are proved using the Glimm scheme. Asakura applies front tracking to show existence of a solution for the $p$-system [3] and for the Euler equations [2] with large initial data. The conditions on the initial data are the same as obtained in [16] and [12].

Amadori and Corli [1] extend the $p$-system with an extra equation, $\lambda_t = 0$, to model multiphase flow, and they use front tracking to prove existence of a weak solution. As for system (1.1), the pressure function in [1] is a function of both $v$ and the new variable, $\lambda$, making the two systems similar. However, since the adiabatic gas constant, $\gamma$, is equal to one in [1], vacuum can never occur for their system as it can for system (1.1). Furthermore, the wave curves in [1] are monotone in $\lambda$, resulting in a considerably simpler analysis of the wave interactions compared to the system considered here. The system treated in [1] is a simplified version of the model discussed by Fan in [8]. Similar models, but with a rather different pressure law, are also considered in [7] and [14] applying completely different methods. A model in the context of the Navier–Stokes equation with finitely many independent pressure laws has been studied in [5].

System (1.1) can also be rewritten as a $2 \times 2$ system with discontinuous flux. We get

$$\begin{aligned} v_t - u_x &= 0, \\ u_t + p(v, \gamma(x))_x &= 0, \end{aligned}$$

where the adiabatic gas constant of the different gases is given by the discontinuous function $\gamma(x)$.

This paper is organized as follows: In Section 2 we discuss the wave curves of the system. The variable $\gamma$ is constant along the rarefaction and shock waves of the first and third family, therefore these curves are similar to the wave curves of the $p$-system. However, these curves are not monotone in $\gamma$, which considerably complicates the interactions of waves with different values of $\gamma$. The second family is linearly degenerate and gives rise to a contact discontinuity along which $p$ and $u$ are constant. Thus, by changing variables to $p$, $u$ and $\gamma$, the Riemann problem is easy to describe. The invariant region for the Riemann problem includes vacuum. This is a problem since the interaction estimates are not valid when $p$ tends to zero, see [13].

In Section 3 we describe the Glimm scheme and discuss all possible interactions before we define the Glimm functional. In Lemma 3.3 we give the conditions needed on the initial data for the Glimm functional to be decreasing in time. The main part of this paper is the proof of Lemma 3.3, and we devote Section 4 to this. Here all possible interactions are discussed, estimates are found and we show that the Glimm functional is decreasing for each of them. The presentation aims at being self-contained.

In Section 5 we show convergence, and Lemma 5.1 states that given some conditions on the total variation of the initial data, we have stability of the total variation. This follows from the decreasing Glimm functional and is only valid when the approximate solution is bounded away from vacuum. The conditions for this is given by Lemma 5.2. The main result reads as follows:

**Theorem 5.3.** *The Cauchy problem for system* (1.1) *has a global, weak solution if* $(\sup(\gamma) - 1)\text{T.V.}(p(\,\cdot\,,0), u(\,\cdot\,,0))$ *and* $\text{T.V.}(\gamma(\,\cdot\,,0))$ *are sufficiently small.*

Observe that by reducing the total variation of $\gamma$ and reducing its supremum, one can allow for large total variation of $p$ and $u$. Due to Wagner [23], this result translates into existence for the system in Eulerian coordinates as stated in Theorem 5.4.

In the last section we study two examples numerically. In the first example we have one gas confined to an interval, surrounded by another gas. The two gases have distinct but constant gammas. The constants that limit the total variation of the initial data are computed, and the initial data are chosen so that they satisfy the conditions in the theorem. The Glimm functional is explicitly computed, and shown to decay in accordance with the theorem. In the second example we consider a case with a continuously varying gamma. Again the initial data are chosen so that they satisfy the explicitly computed constants that appear in Theorem 5.3. Finally, the decaying Glimm functional is computed and displayed for this example.

Further numerical experiments reveal that, as expected, the Glimm functional decays also in cases where the fairly stringent restrictions on the initial data are violated. A necessary condition for the Glimm scheme to work is that the Riemann problems that occur all are solvable, but no conjecture as to the maximum size of the Glimm functional can be made at this stage.

We intend to discuss the same system using the front-tracking method in a subsequent paper. The basic interactions between two waves (fronts) in front-tracking are similar to those of the Glimm scheme. Interactions between more waves (fronts) are different from the interactions discussed in Section 4, but the same methods apply. In addition, the front-tracking method requires a close control of the number of fronts at all times, possibly by removing weak fronts according to some measure. These issues are not yet fully resolved for our system, therefore we choose to use the Glimm scheme in this paper.

## 2. The System

It is well-known that systems of hyperbolic conservation laws such as (1.1) do not in general have smooth solutions, even for smooth initial data. Thus, by a solution of (1.1) with the initial data (1.2) we mean a *weak solution* in the distributional sense with $v, u, \gamma \in L^\infty(\mathbb{R} \times [0, \infty))$ so that

$$\iint_{\mathbb{R}\times[0,\infty)} (v\phi_t - u\phi_x)\,\mathrm{d}x\mathrm{d}t + \int_{\mathbb{R}} v_0(x)\phi(x,0)\,\mathrm{d}x = 0,$$
$$\iint_{\mathbb{R}\times[0,\infty)} (u\phi_t + p\phi_x)\,\mathrm{d}x\mathrm{d}t + \int_{\mathbb{R}} u_0(x)\phi(x,0)\,\mathrm{d}x = 0,$$
$$\iint_{\mathbb{R}\times[0,\infty)} \gamma\phi_t\,\mathrm{d}x\mathrm{d}t + \int_{\mathbb{R}} \gamma_0(x)\phi(x,0)\,\mathrm{d}x = 0,$$

for all infinitely differentiable functions $\phi(x,t)$ with compact support.

If the specific volume, $v$, becomes infinite, which corresponds to zero density and zero pressure, we have *vacuum*. At vacuum, the properties of the system change and the methods used here do not apply, therefore we only consider system (1.1) for $v(x,t) < \infty$. Furthermore, we assume $\gamma(x,t) > 1$.

We write $U(x,t) = (v(x,t), u(x,t), \gamma(x,t))$. Often we will work with $p$ instead of $v$, and then also write $U(x,t) = (p(x,t), u(x,t), \gamma(x,t))$.

For $v < \infty$, or equivalently, $p > 0$, the system (1.1) is strictly hyperbolic with eigenvalues

$$\lambda_1 = -\lambda, \qquad \lambda_2 = 0, \qquad \lambda_3 = \lambda, \tag{2.1}$$

where $\lambda := \sqrt{-p_v} = \sqrt{\gamma v^{-\gamma-1}}$, and corresponding eigenvectors

$$r_1 = (1, \lambda, 0), \qquad r_2 = (-p_\gamma, 0, p_v)\,, \qquad r_3 = (-1, \lambda, 0). \tag{2.2}$$

Note that the eigenvalues and eigenvectors do not depend on $u$. The first and the third family are genuinely nonlinear, while the second family is linearly degenerate. Moreover, the system does not possess a coordinate system of Riemann invariants, but $\gamma$ is a Riemann coordinate for the second family.

Before we can turn to solving system (1.1) for general initial data, we need to solve the Riemann problem for (1.1), that is, when the initial data consists of two constant states separated by a jump, cf. (2.26). The solution of the Riemann problem consists of up to three elementary *waves*, one from each family, and up to two intermediate constant states separating these waves. Thus, we start by looking at the wave curves.

### 2.1. Wave curves.

For a genuinely nonlinear family there are two types of waves; *rarefaction waves* which are continuous waves of the form $U(x,t) = w(x/t)$ satisfying

$$\dot{w}(x/t) = r_j(w(x/t)), \qquad \lambda_j(w(x/t)) = x/t, \quad j = 1, 3, \tag{2.3}$$

where $\lambda_j$ is increasing along the wave, and *shock waves* which are solutions

$$U(x,t) = \begin{cases} U_l, & \text{if } x < \sigma t, \\ U_r, & \text{if } x > \sigma t, \end{cases} \tag{2.4}$$

satisfying the Rankine–Hugoniot condition

$$\sigma(U_r - U_l) = f(U_r) - f(U_l), \tag{2.5}$$

for a shock velocity $\sigma$. The admissible shock waves are those satisfying the Lax entropy conditions

$$\lambda_{j-1}(U_l) < \sigma < \lambda_j(U_l), \qquad \lambda_j(U_r) < \sigma < \lambda_{j+1}(U_r), \quad j = 1, 3. \tag{2.6}$$

For the linearly degenerate family $j = 2$ there is only one type of waves called *contact discontinuities*. These waves are solutions of the form (2.4) that satisfy the Rankine–Hugoniot condition (2.5) with $\sigma = \lambda_2$.

We fix a left state $U_l$. For each family the *wave curve* consists of all states $U$ that can be connected to the given left state by a wave of this family. The rarefaction solution is of the form

$$U(x,t) = \begin{cases} U_l, & \text{if } x < \lambda_j(U_l)t, \\ w(x/t), & \text{if } \lambda_j(U_l)t < x < \lambda_j(U)t, \\ U, & \text{if } x > \lambda_j(U)t. \end{cases} \tag{2.7}$$

The rarefaction wave curve is the set of all right states $U$ that can be connected to the left state by a rarefaction wave. For system (1.1) these are

$$R_1(v, U_l) := \left( v, u_l - \frac{2\sqrt{\gamma_l}}{\gamma_l - 1} \left( v^{\frac{1-\gamma_l}{2}} - v_l^{\frac{1-\gamma_l}{2}} \right), \gamma_l \right), \qquad v > v_l,$$

$$R_3(v, U_l) := \left( v, u_l + \frac{2\sqrt{\gamma_l}}{\gamma_l - 1} \left( v^{\frac{1-\gamma_l}{2}} - v_l^{\frac{1-\gamma_l}{2}} \right), \gamma_l \right), \qquad v < v_l.$$

The shock curves of all states which can be connected to $U_l$ by an admissible shock wave are

$$S_1(v, U_l) : = \left( v, u_l - \left( (v_l - v)(v^{-\gamma_l} - v_l^{-\gamma_l}) \right)^{1/2}, \gamma_l \right), \qquad v < v_l,$$

$$S_3(v, U_l) : = \left( v, u_l - \left( (v_l - v)(v^{-\gamma_l} - v_l^{-\gamma_l}) \right)^{1/2}, \gamma_l, \right), \qquad v > v_l,$$

with the shock velocities

$$\sigma_1(U_l, U_r) = -\sqrt{\frac{v_l^{-\gamma_l} - v^{-\gamma_l}}{v - v_l}} = -\sqrt{\frac{p_l - p}{p^{-1/\gamma_l} - p_l^{-1/\gamma_l}}}, \tag{2.8}$$

$$\sigma_3(U_l, U_r) = \sqrt{\frac{v^{-\gamma_l} - v_l^{-\gamma_l}}{v_l - v}} = \sqrt{\frac{p - p_l}{p_l^{-1/\gamma_l} - p^{-1/\gamma_l}}}, \tag{2.9}$$

respectively. Note that the shock velocities do not depend on $u$. The curve of all right states which can be connected to $U_l$ by a contact discontinuity is

$$C_2(\gamma, U_l) : = \left( v_l^{\gamma_l/\gamma}, u_l, \gamma \right), \qquad \gamma > 1,$$

with the velocity $\sigma_2 = \lambda_2 = 0$.

Note that $\gamma$ only changes along the contact discontinuities. Furthermore, both $u$ and $p = v^{-\gamma}$ are constant along a contact discontinuity, and we therefore choose to work with $p$, $u$ and $\gamma$. A shock or a rarefaction curve through $U_l$ lies in the plane $\gamma = \gamma_l$ and is equal to the corresponding wave curve for the $p$-system (1.3) with $\gamma = \gamma_l$. We proceed by defining the wave curves using $p$, $u$, and $\gamma$;

$$\Phi_1(p, U_l) := \begin{cases} (p, u_l - r(p, p_l, \gamma_l), \gamma_l), & p < p_l, \\ (p, u_l - s(p, p_l, \gamma_l), \gamma_l), & p > p_l, \end{cases} \tag{2.10}$$

$$\Phi_2(\gamma, U_l) := (p_l, u_l, \gamma), \quad \gamma > 1, \tag{2.11}$$

$$\Phi_3(p,U_l) := \begin{cases} (p, u_l + r(p,p_l,\gamma_l),\gamma_l)\,, & p > p_l, \\ (p, u_l - s(p,p_l,\gamma_l),\gamma_l)\,, & p < p_l, \end{cases} \tag{2.12}$$

where

$$r(p,p_l,\gamma_l) := \frac{2\sqrt{\gamma_l}}{\gamma_l - 1}\left(p^{\frac{\gamma_l-1}{2\gamma_l}} - p_l^{\frac{\gamma_l-1}{2\gamma_l}}\right), \tag{2.13}$$

$$s(p,p_l,\gamma_l) := \left(\left(p_l^{-\frac{1}{\gamma_l}} - p^{-\frac{1}{\gamma_l}}\right)(p-p_l)\right)^{1/2}. \tag{2.14}$$

Recall that if $p = 0$, we have vacuum, and thus the wave curves are only well-defined for $p > 0$ and $p_l > 0$. All results are for waves contained in

$$\mathcal{D} = \{(p,u,\gamma) \mid p \in [p_{\min}, p_{\max}], |u\,| < \infty, \gamma \in (1,\overline{\gamma}]\}, \tag{2.15}$$

where $p_{\min} > 0$, $p_{\max} < \infty$ and $\overline{\gamma} \in (1,\infty)$ are constants. For initial data given by (1.2) we will later establish the upper and lower bound on $p$ and argue that

$$\overline{\gamma} := \sup_x(\gamma_0(x)), \tag{2.16}$$

for all waves.

The projection onto the $(p,u)$-plane of two wave curves with different $\gamma$'s are shown in Figure 1. Note that the projected curves intersect. Before we discuss this and other important properties of the wave curves, we mention the *backward wave curves*. These are the curves of all left states $U$ that can be connected to a given right state $U_r$ by a wave of the given family. We denote these wave curves by $\tilde{\Phi}_i$. We will use the backward 3-wave curve several times and this is given by

$$\tilde{\Phi}_3(p,U_r) := \begin{cases} (p, u_r - r(p_r,p,\gamma_r),\gamma_r)\,, & p < p_r, \\ (p, u_r + s(p_r,p,\gamma_r),\gamma_r)\,, & p > p_r, \end{cases} \tag{2.17}$$

where $r$ and $s$ are given by (2.13) and (2.14). We now turn to the properties of the wave curves.

**Lemma 2.1.** *Assume that the wave curves are contained in $\mathcal{D}$. Then they have the following properties:*

*(i) Viewed as functions of $p$, $\Phi_1$ is strictly decreasing and $\Phi_3$ is strictly increasing.*

*(ii) Given two wave curves, $\Phi_j(p,U_1)$ and $\Phi_j(p,U_2)$ where $j \in \{1,3\}$, so that $U_1$ is not on $\Phi_j(p,U_2)$ and $U_2$ is not on $\Phi_j(p,U_1)$. Then the two wave curves never intersect. Moreover, if $\gamma_1 = \gamma_2$, then also the projected wave curves onto the $(p,u)$-plane never intersect. However, if $\gamma_1 \neq \gamma_2$, then the projected wave curves can intersect.*

*(iii) Consider the projections onto the $(p,u)$-plane of the wave curves through $U_1 = (p_l,u_l,\gamma_1)$ and $U_1 = (p_l,u_l,\gamma_2)$ where $\gamma_1 \leq \gamma_2$. If*

$$\frac{\partial}{\partial p} r(p_l,p_l,\gamma_l) < \frac{\partial}{\partial p} r(p_l,p_l,\gamma_2),$$

*then the projected wave curves going to the right (with respect to p) will never intersect, while the projected wave curves going to the left will intersect as p decreases. If*

$$\frac{\partial}{\partial p} r(p_l,p_l,\gamma_l) > \frac{\partial}{\partial p} r(p_l,p_l,\gamma_2),$$

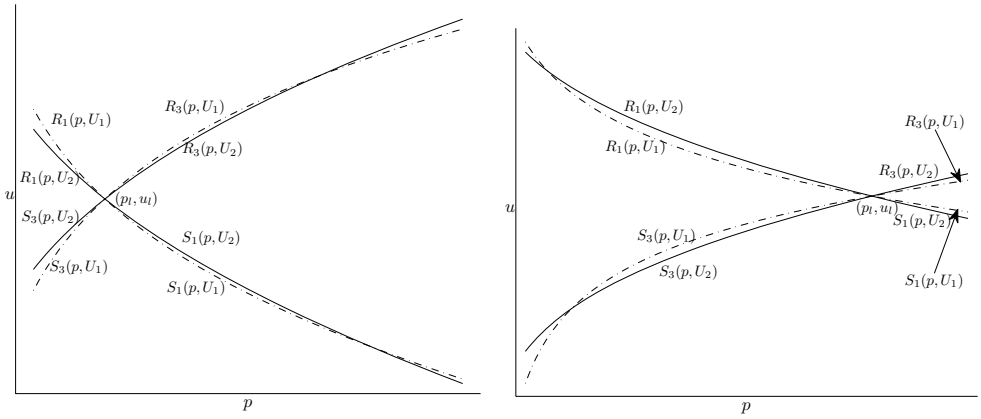


(a) The projected curves going to the left do not intersect, while the curves going to the right do.

(b) The projected curves going to the left intersect, while the curves going to the right do not.

FIGURE 1. The wave curves through $U_1 = (p_l, u_l, \gamma_1)$ (dotted line) and $U_2 = (p_l, u_l, \gamma_2)$, where $\gamma_1 < \gamma_2$, projected onto the $(p,u)$-plane are depicted for two different values of the parameters.

*then the projected wave curves going to the right will intersect, while the projected wave curves going to the left will not. If*

$$\frac{\partial}{\partial p} r(p_l, p_l, \gamma_l) = \frac{\partial}{\partial p} r(p_l, p_l, \gamma_2),$$

*then none of the projected wave curves will intersect.*

*(iv) The slope of a rarefaction wave in the plane $\gamma = \gamma_l$, $\partial r/\partial p$, only depends on $p$ and $\gamma_l$, not on $p_l$. Furthermore, there exist two constants $r'_{\min}$ and $r'_{\max}$ only depending on $p_{\min}$, $p_{\max}$ and $\overline{\gamma}$ so that*

$$r'_{\min} \leq \frac{\partial}{\partial p} r(p, p_l, \gamma_l) \leq r'_{\max}.$$

*(v) The slope of a shock wave in the plane $\gamma = \gamma_l$, $\partial s/\partial p$, depends on $p$, $\gamma_l$ and $p_l$. Furthermore, there exist two constants $s'_{\min}$ and $s'_{\max}$ only depending on $p_{\min}$, $p_{\max}$ and $\overline{\gamma}$ so that*

$$s'_{\min} \leq \frac{\partial}{\partial p} s(p, p_l, \gamma_l) \leq s'_{\max}.$$

*(vi) The wave curves have a continuous derivative at $U_l$,*

$$\lim_{p \to p_l} \frac{\partial}{\partial p} s(p, p_l, \gamma_l) = \frac{\partial}{\partial p} r(p_l, p_l, \gamma_l).$$

*Furthermore,*

$$\frac{\partial}{\partial p} s(p, p_l, \gamma_l) \geq \frac{\partial}{\partial p} r(p, p_l, \gamma_l),$$

*for all $p_l$. Hence, a shock wave is always steeper than a rarefaction wave at a given $p \neq p_l$ provided both waves lie in the plane $\gamma = \gamma_l$.*

*(vii) Rarefaction waves are additive; if a rarefaction wave connects $U_1$ to $U_2$ and another rarefaction wave of the same family connects $U_2$ to $U_3$, then the rarefaction wave connecting $U_1$ to $U_3$ equals the sum of the other two rarefaction waves.*

*(viii) Given two 1-shock waves starting at $(p_1, u, \gamma)$ and $(p_2, u, \gamma)$, respectively, and assume $p_1 < p_2$. Then the shock wave starting at $p_1$ is steeper than the shock wave starting at $p_2$ at any given point $p$, that is,*

$$\frac{\partial}{\partial p} s(p, p_2, \gamma) < \frac{\partial}{\partial p} s(p, p_1, \gamma),$$

*for all $p \geq p_2 > p_1$.*

*(ix) Given two 3-shock waves starting at $(p_1, u, \gamma)$ and $(p_2, u, \gamma)$, respectively, and assume $p_1 < p_2$. Then the shock wave starting at $p_2$ is steeper than the shock wave starting at $p_1$ at any given point $p$, that is,*

$$\frac{\partial}{\partial p} s(p, p_1, \gamma) < \frac{\partial}{\partial p} s(p, p_2, \gamma),$$

*for all $p \leq p_1 < p_2$.*

*Proof.* All the properties follows from differentiating the wave curves. □

According to the above lemma, the slopes of the projected wave curves onto the $(p, u)$-plane depend on $\gamma$. The next lemma gives an estimate on how different two waves with different $\gamma$'s are.

**Lemma 2.2.** *Let $\epsilon_1$ and $\epsilon_2$ be 1-waves of the same type such that $\epsilon_1$ connects $(p_0, u_0, \gamma_1)$ to $(p, u_1, \gamma_1)$ and $\epsilon_2$ connects $(p_0, u_0, \gamma_2)$ to $(p, u_2, \gamma_2)$, or let $\eta_1$ and $\eta_2$ be 3-waves of the same type such that $\eta_1$ connects $(p, u_1, \gamma_1)$ to $(p_0, u_0, \gamma_1)$ and $\eta_2$ connects $(p, u_2, \gamma_2)$ to $(p_0, u_0, \gamma_2)$. Assume that all waves are contained in $\mathcal{D}$ and furthermore that $u_1 < u_2$. Then*

$$u_2 - u_1 \leq c_2 \left| p - p_0 \right| \left| \gamma_2 - \gamma_1 \right|, \tag{2.18}$$

*where $c_2$ only depends on $p_{\min}$, $p_{\max}$ and $\overline{\gamma}$.*

Note that for 1-waves we compare two waves where the projected waves start at the same point in the $(p, u)$-plane, while we for 3-waves compare two waves where the projected waves end at the same point. The proof is based on the same techniques as used in [24].

*Proof.* Since the projection of the 3-waves end at the same point, we make use of the 3-backward wave curves. The projected (backward) wave curves can be described by a function of two variables,

$$u(p, \gamma) = \begin{cases} u_0 - s(p, p_0, \gamma), & p > p_0, \quad \text{for 1-shock waves,} \\ u_0 - r(p, p_0, \gamma), & p < p_0, \quad \text{for 1-rarefaction waves,} \\ u_0 + s(p_0, p, \gamma), & p > p_0, \quad \text{for 3-shock waves,} \\ u_0 - r(p_0, p, \gamma), & p < p_0, \quad \text{for 3-rarefaction waves,} \end{cases} \tag{2.19}$$

where $u(p_0, \gamma_1) = u(p_0, \gamma_2) = u_0$, $u(p, \gamma_1) = u_1$ and $u(p, \gamma_2) = u_2$ for all cases. Figure 2 illustrates this when the waves are 1-shocks. If the two wave curves do not intersect between $p_0$ and $p$, then

$$\int_{\gamma_1}^{\gamma_2} \int_{p_0}^{p} u_{p\gamma}(s, t) \, \mathrm{d}s \, \mathrm{d}t = u(p, \gamma_2) - u(p, \gamma_1) - u(p_0, \gamma_2) + u(p_0, \gamma_1), \tag{2.20}$$

where $u_{p\gamma}$ denotes the second order partial derivative with respect to $p$ and $\gamma$. If the two wave curves intersect at $p = p_m$, then we integrate from $p_m$ to $p$ and replace $p_0$ by $p_m$ at

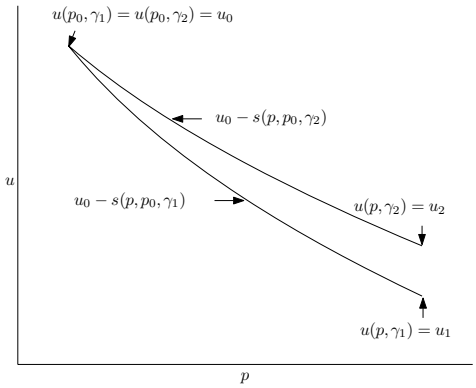


FIGURE 2. When $\epsilon_1$ and $\epsilon_2$ of Lemma 2.2 are 1-shocks.

the right-hand side. This will give us an even stronger estimate than (2.18), and therefore we can assume for the rest of the proof that the wave curves do not intersect.

If we can show that $|u_{p\gamma}| \leq c_2$, where $c_2$ is a constant only depending on $p_{\min}$, $p_{\max}$ and $\overline{\gamma}$, then

$$\begin{aligned} u_2 - u_1 &= u(p,\gamma_2) - u(p,\gamma_1) - u(p_0,\gamma_2) + u(p_0,\gamma_1) \\ &= \int_{\gamma_1}^{\gamma_2} \int_{p_0}^{p} u_{p\gamma}(s,t)\,\mathrm{d}s\,\mathrm{d}t \leq c_2\,|\gamma_2 - \gamma_1|\,|p - p_0|\,, \end{aligned}$$

and we have proved (2.18).

Let us first consider when the waves are either 1- or 3-rarefaction waves. Then we find that

$$\frac{\partial^2 r}{\partial p \partial \gamma}(p,p_0,\gamma) = -\frac{\partial^2 r}{\partial p \partial \gamma}(p_0,p,\gamma) = \frac{1}{2}\gamma^{-5/3} p^{-(1+\gamma)/2\gamma}(\ln p - \gamma). \tag{2.21}$$

For a fixed $\gamma$, we see that (2.21) is negative for $\ln p < \gamma$. By differentiating (2.21) with respect to $p$, we find that it is increasing in $p$ until it reaches its maximum value,

$$0 < \gamma^{-\frac{2}{3}} \exp\left(-\frac{3+\gamma}{2}\right) \leq 1,$$

at $\ln p = \gamma(3+\gamma)/(1+\gamma)$. After this point, (2.21) is strictly decreaseing towards zero as $p$ grows large. Thus, if $\ln p_{\min} \leq \gamma$, then the minimum value of (2.21) is obtained at $p = p_{\min}$, otherwise (2.21) is positive for all $p_{\min} \leq p \leq p_{\max}$. Define

$$c := \max_{\gamma \in (1,\overline{\gamma}]} \frac{1}{2}\gamma^{-5/3} p_{\min}^{-(1+\gamma)/2\gamma}\,|\ln p_{\min} - \gamma|\,, \tag{2.22}$$

which is a constant depending only on $p_{\min}$ and $\overline{\gamma}$. We conclude that when the waves are either 1- or 3-rarefaction waves, then

$$|u_{p\gamma}| \leq \max\{c, 1\}.$$

For shock waves we have

$$\frac{\partial^2 s}{\partial p \partial \gamma}(p, p_0, \gamma) = -\frac{\partial^2 s}{\partial p \partial \gamma}(p_0, p, \gamma) = f, \tag{2.23}$$

where

$$f := \frac{-sp^{-\frac{\gamma+1}{\gamma}}(p-p_0) + \gamma(p_0^{-\frac{1}{\gamma}} \ln p_0 - p^{-\frac{1}{\gamma}} \ln p)((p-p_0)\frac{\partial s}{\partial p} + s)}{2\gamma^3 s^2}, \tag{2.24}$$

and $s = s(p, p_0, \gamma)$. By differentiating with respect to $p$, we find that (2.24) does in general behave similar to (2.21); its minimum value is obtained at the limit when $p$ tends to $p_0$, and this limit equals the value of (2.21) at $p = p_0$. Furthermore, also (2.24) increases until it reaches its maximum value, which is positive and less than one, before it decreases towards zero as $p$ grows large. However, (2.24) does depend on $p_0$ while (2.21) does not, therefore the two expressions behave different for small $p_0$. Then (2.24) is negative and increasing for all $p$, but still its minimum value is obtained at the limit when $p$ goes to $p_0$. Therefore,

$$|u_{p\gamma}| \leq \max\{c, 1\},$$

also when the waves are shock waves where $c$ is given by (2.22). We define

$$c_2 := \max\{c, 1\}, \tag{2.25}$$

and conclude that $|u_{p\gamma}| \leq c_2$ for $u$ given by any of the cases in (2.19), and for all $p \in [p_{\min}, p_{\max}]$ and $\gamma \in (1, \overline{\gamma}]$. This ends the proof of the lemma. □

2.2. **The Riemann Problem.** We have the following fundamental definition.

**Definition 2.3.** The Riemann problem for (1.1) is the Cauchy problem with initial data

$$U(x, 0) = \begin{cases} U_l, & \text{if } x < 0, \\ U_r, & \text{if } x > 0, \end{cases} \tag{2.26}$$

where $U = (v, u, \gamma)$ and $U_l, U_r \in \mathbb{R}^3$ are constants.

**Lemma 2.4.** *The Riemann problem for* (1.1) *where $U_l$ and $U_r$ are contained in $\mathcal{D}$, cf.* (2.15)*, has a unique solution with no vacuum if*

$$u_r - u_l < r(p_r, 0, \gamma_r) - r(0, p_l, \gamma_l). \tag{2.27}$$

*Proof.* Note that if $\gamma_l = \gamma_r$, then the Riemann problem for (1.1) reduces to the Riemann problem for the $p$-system (1.3). The solution of this problem is described in detail in [20, Ch. 17, §A], and it is unique if (2.27) is satisfied with $\gamma_l = \gamma_r$.

A 2-wave takes us from one plane, $\gamma = \gamma_1$, to another plane, $\gamma = \gamma_2$, while $p$ and $u$ remain constant. Therefore, the Riemann problem has a unique solution if the projections onto the $(p, u)$-plane of the 1-wave curve, $\Phi_1(p, U_l)$, and the backward 3-wave curve, $\tilde{\Phi}_3(p, U_r)$, have a unique intersection point. From property (i) we have that the projection of $\Phi_1$ is strictly decreasing in $p$ and it follows that the projection of $\tilde{\Phi}_3$ is strictly increasing in $p$. Hence, the projected curves intersect at most once. The only case where the two curves do not intersect is if the projection of the backward 3-rarefaction wave from $U_r$ always lies above the projection of the 1-rarefaction wave from $U_l$. Thus, if

$$u_r - r(p_r, 0, \gamma_r) < u_l - r(0, p_l, \gamma_l),$$

then the projections of $\tilde{\Phi}_3(p, U_r)$ and $\Phi_1(p, U_l)$ onto the $(p, u)$-plane have a unique intersection point, and the Riemann problem has a unique solution. □

The solution of the Riemann problem $(U_l, U_r)$ is constructed as follows: Let $(\tilde{p}, \tilde{u})$ be the unique intersection between the projections of $\Phi_1(p, U_l)$ and $\tilde{\Phi}_3(p, U_r)$ onto the $(p, u)$-plane. We connect $U_l = (p_l, u_l, \gamma_l)$ to $\tilde{U}_1 = (\tilde{p}, \tilde{u}, \gamma_l)$ by a 1-curve, then we go from $\tilde{U}_1$ to $\tilde{U}_2 = (\tilde{p}, \tilde{u}, \gamma_r)$ along a contact discontinuity, and finally connect $\tilde{U}_2$ to $U_r = (p_r, u_r, \gamma_r)$ by a 3-wave.

2.3. **Invariant region and vacuum.** A region $\Omega$ is invariant for the Riemann problem if for any Riemann problem with initial data in $\Omega$, its solution is also in $\Omega$. For the $p$-system we know from [10, Ex. 3.5] that the convex region in the $(v, u)$-plane between the integral curves of the eigenvectors is invariant. This region bounds $v$ from below, but not from above, thus vacuum is included in the invariant region. In the $(p, u)$-plane this corresponds to the region bounded by $p = 0$ and the two integral curves. Since $\gamma$ cannot take any other values than those of the initial data, we find the invariant region for the $p$-system for each $\gamma$ and take the union of these. This gives us an invariant region for (1.1). Moreover, this gives us the upper bound on $p$, $p_{\max}$, which we need, but $p$ is still not bounded away from vacuum.

## 3. Decreasing Glimm Functional

In order to prove existence of a unique weak solution of (1.1) with the initial data (1.2), we first find a sequence of approximate solutions of (1.1), and then show that this converges to a weak solution. We use the Glimm scheme to obtain the approximate solutions, for details on the Glimm scheme see, e.g., [20, Ch. 19]. If we can show that the total variation of the approximate solution is bounded, convergence to a weak solution of (1.1) follows. To do this we use a Glimm functional and therefore need interaction estimates which are quadratic in the incoming waves for all possible interactions. As discussed for the $p$-system by Liu and Smoller [13], it is not possible to find such estimates if the approximate solution is not bounded away from vacuum. Fortunately, using the Glimm scheme we have a region $\mathcal{U}$ which contains the approximate solution and this region is bounded by the total variation of the initial data. Therefore, given some assumptions on the initial data, we can show that this region does not contain vacuum.

3.1. **The Glimm Scheme.** Before we define the Glimm functional and prove it is decreasing, we need to introduce the Glimm scheme and some more notation.

Choose the spatial mesh size $\Delta x = h$ and the temporal mesh size $\Delta t$ so that

$$\frac{h}{\Delta t} > \max_{U \in \mathcal{U}} |\lambda_j(U)|, \quad j = 1, 2, 3, \tag{3.1}$$

and define $x_i := ih$ for $i = 0, \pm 1, \pm 2, \dots$, and $t_n := n\Delta t$ for $n = 0, 1, 2, \dots$. The *mesh points* $(x_i, t_n)$ with $i + n$ even, $n = 0, 1, 2, \dots$, make up a staggered grid, see Figure 3. Let furthermore $a = \{a_0, a_1, \dots\}$ be a random sequence, equidistributed in the interval $[-1, 1]$, and let

$$y_i^n := x_i + a_n h, \quad i + n \text{ odd}, \tag{3.2}$$

be the *sampling points*. Figure 3 shows the characteristic diamonds we get by drawing the lines between the sampling points, each diamond containing exactly one mesh point. A curve going from the left to the right along the edges of the diamonds, connecting $y_i^n$ to either $y_{i+1}^{n-1}$ or $y_{i+1}^{n+1}$, is called a *mesh curve*. Two mesh curves, $J_{j-1}$ and $J_j$, are indicated by dotted lines in Figure 3. These curves are called *successive mesh curves* since they only differ at one point.

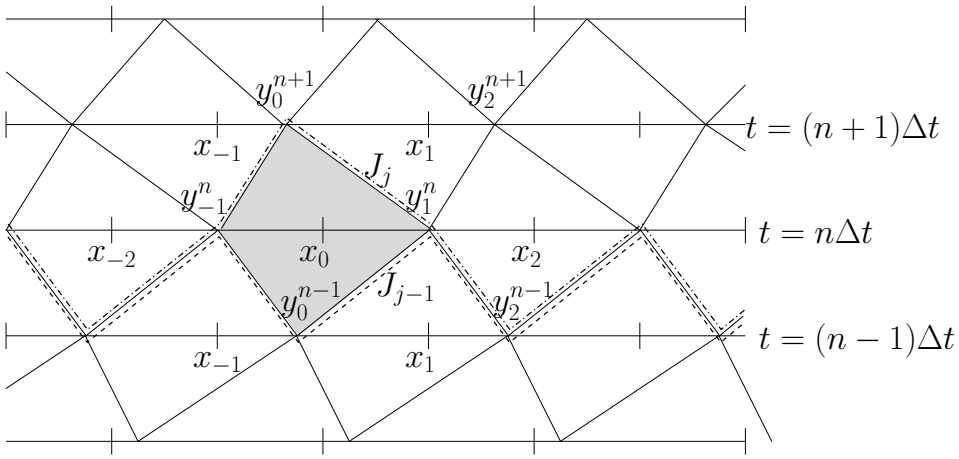


FIGURE 3. The staggered grid with the diamonds and two successive mesh curves indicated by dotted lines. Here $n$ is even.

We approximate the initial data by piecewise constants,

$$U_h(x,0) = U_0(y_i^0-), \qquad (i-1)h \le x \le (i+1)h, \quad i \text{ odd}, \tag{3.3}$$

and at each time step we use the solution already found for $0 \le t < t_n$ to define $U_h(x,t_n)$ as a piecewise constant function by

$$U_h(x,t_n) = U_h(y_i^n-,t_n-), \qquad (i-1)h \le x \le (i+1)h, \quad i+n \text{ odd}, \tag{3.4}$$

i.e., by using the values of the solution at the sampling points. We solve all Riemann problems at $t = t_n$ and together these waves give the approximate solution for $t_n \le t < t_{n+1}$. None of the waves will interact before the next time step because the ratio between the spatial mesh and the temporal mesh is larger than the speed of any of the waves, cf. (3.1).

We now turn to what happens inside one diamond. Waves may enter a diamond through its lower left or lower right edge. A shock wave or a contact discontinuity either enters the diamond or not. For a rarefaction wave one part of the wave can enter one diamond, while the rest of the rarefaction wave enters the nearby diamond. As stated in property (vii), rarefaction waves are additive and therefore this corresponds to one rarefaction wave entering each diamond. We call waves that are entering a diamond *incoming waves*.

At the grid point inside the diamond we solve the Riemann problem $(U_l, U_r)$ where $U_l$ and $U_r$ are the values at the sampling points. Since the sampling points are the corners of the diamond, $U_l$ is the leftmost state (with respect to $x$) among the incoming waves and $U_r$ is the rightmost state. The solution of the Riemann problem $(U_l, U_r)$ consists of up to three waves. These waves are called *outgoing waves* and are the only waves leaving the diamond. Let $U_i$, $i = 1, \dots, 3$, be the intermediate states among the incoming waves and $\tilde{U}_j$, $j = 1, 2$, the intermediate states among the outgoing waves. Note that $\tilde{p}_1 = \tilde{p}_2$ and $\tilde{u}_1 = \tilde{u}_2$, and we refer to them by $\tilde{p}$ and $\tilde{u}$.

We define an *interaction* between incoming waves as solving the Riemann problem with the leftmost state among the incoming waves as the left state and the rightmost state among the incoming waves as the right state. We also say that two or more *waves interact* meaning the interaction between these waves. In other words, the waves entering one diamond interacts and the result of this interaction is the outgoing waves. Note that there is no actual

interaction in the Glimm scheme because the grid is constructed so that no waves can collide at any time.

The goal is to estimate the *total strength* of the outgoing waves, that is, the sum of the strengths of the outgoing waves, in terms of the strengths of the incoming waves. First we define *the strength of a* 1*-wave or a* 3*-wave* as the jump in $p$ across the wave, and *the strength of a* 2*-wave* as the jump in $\gamma$ across the wave. Furthermore, we let

| | | |
|---|---|---|
| $\epsilon$ define a 1-wave, | $\alpha$ a 1-shock wave, | $\mu$ a 1-rarefaction wave, |
| $\eta$ a 3-wave, | $\beta$ a 3-shock wave, | $\nu$ a 3-rarefaction wave, |
| $\zeta$ a 2-wave, | $\delta$ a 1- or 3-wave. | |

The strength of a wave is written $|\delta|$. We use a prime, like $\delta'$, to indicate an outgoing wave and write an interaction as $\delta_1 + \delta_2 \to \delta_1' + \delta_2'$ where $\delta_1$ enters the diamond through its left edge and $\delta_2$ through its right edge. If more than two waves interact, we use parentheses to indicate which waves enter the diamond through the left and the right edge.

Since $\gamma$ only changes along $\zeta$-waves, the incoming and outgoing $\zeta$-waves will always be equal and we write them all as $\zeta$. Moreover, the incoming and outgoing $\zeta$-waves have the same strength and we therefore omit them from the interaction estimates.

3.2. **Possible interactions in a diamond.** Due to the staggered grid used in the Glimm scheme, the number of possible interactions in one diamond is limited. All contact discontinuities have zero speed, therefore at most one contact discontinuity can enter one diamond. Moreover, it follows from the wave speeds that two rarefaction waves of the same family can only enter the same diamond if there is another wave between them. Furthermore, it is not possible to have both a 1-wave and a 3-wave entering through both the left and the right edge. Therefore we do not get interactions between more than four waves.

We divide all possible interactions into four main types:

(A) Waves entering through only one edge, see Figure 4: $(\epsilon + \zeta + \eta)$ where one or two of the waves can be absent.
(B) Two waves entering the diamond through different edges, see Figure 5:
  (a) Both waves are of the same family: $\epsilon_1 + \epsilon_2$ or $\eta_1 + \eta_2$ where at least one wave is a shock wave.
  (b) Different families, but no contact discontinuity: $\eta + \epsilon$.
  (c) With a contact discontinuity: $\zeta + \epsilon$ or $\eta + \zeta$.
(C) Three waves entering the diamond, see Figure 6:
  (a) No contact discontinuity: $(\epsilon + \eta) + \epsilon$ or $\eta + (\epsilon + \eta)$.
  (b) A contact discontinuity as the leftmost or rightmost wave: $(\zeta + \eta) + \epsilon$ or $\eta + (\epsilon + \zeta)$.
  (c) A contact discontinuity as the middle wave: $(\epsilon_1 + \zeta) + \epsilon_2$ or $\eta_1 + (\zeta + \eta_2)$.
(D) Four waves entering the diamond, see Figure 7: $(\epsilon_1 + \zeta + \eta) + \epsilon_2$ or $\eta_1 + (\epsilon + \zeta + \eta_2)$.
  (a) Waves of the same family are also of the same type.
  (b) Waves of the same family are not of the same type.

Even though we have at most four interacting waves, we get a notable number of interactions. However, symmetries of the system considerably reduce the number of cases that need to be discussed. The symmetries are summarized in the following lemma.

**Lemma 3.1** (Symmetry property)**.** *By letting $x$ go to $-x$, a* 1*-wave connecting $U_l$ to $U_r$ becomes a* 3*-wave connecting $U_r$ to $U_l$, and vice versa. A* 2*-wave is unchanged under this transformation. Furthermore, the leftmost wave with respect to $x$ will be the rightmost wave with respect to $-x$.*

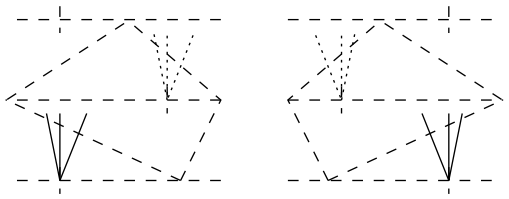

FIGURE 4. Interactions of type A.

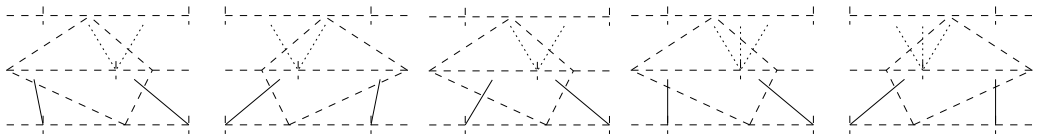

(a) Type Ba (b) Type Bb (c) Type Bc

FIGURE 5. Interactions of type B.

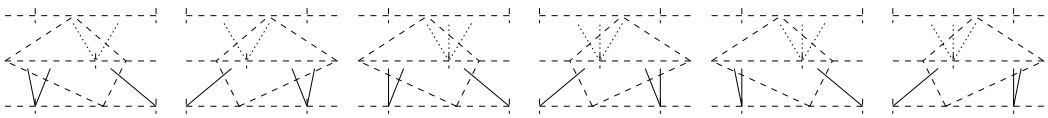

(a) Type Ca (b) Type Cb (c) Type Cc

FIGURE 6. Interactions of type C.

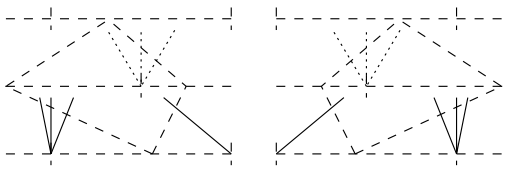

FIGURE 7. Interactions of type D.

*Proof.* Consider first a 1-rarefaction wave connecting $U_l$ to $U_r$. In the $(x,t)$-plane this wave is the fan between the lines $x = \lambda_1(U_l)\,t$ and $x = \lambda_1(U_r)\,t$ where $\lambda_1(U_l) \le \lambda_1(U_r)$. Recall that $\lambda_1 = -\lambda_3$. Changing variables from $x$ to $y = -x$, we get

$$\frac{\mathrm{d}y}{\mathrm{d}t} = \frac{\mathrm{d}y}{\mathrm{d}x}\frac{\mathrm{d}x}{\mathrm{d}t} = -\frac{\mathrm{d}x}{\mathrm{d}t},$$

thus, in the new variables, we have the fan between $y = -\lambda_1(U_r)\,t = \lambda_3(U_r)\,t$ and $y = -\lambda_1(U_l)\,t = \lambda_3(U_l)\,t$, or in other words, we have obtained the 3-rarefaction wave connecting $U_r$ to $U_l$.

In the $(x,t)$-plane, a 1-shock wave connecting $U_l$ to $U_r$ is given by the line $x = \sigma_1(U_l,U_r)\,t$. Note that $p_l < p_r$ according to (2.10) and that the shock velocity $\sigma_1(U_l,U_r)$ satisfies the

Rankine–Hugoniot condition (2.5). Changing variables from $x$ to $y = -x$, we get

$$\sigma = \frac{\mathrm{d}y}{\mathrm{d}t} = \frac{\mathrm{d}y}{\mathrm{d}x}\frac{\mathrm{d}x}{\mathrm{d}t} = -\frac{\mathrm{d}x}{\mathrm{d}t} = -\sigma_1(U_l, U_r) = \sigma_3(U_r, U_l),$$

where the last equality follows from (2.8) and (2.9). Thus, the 1-shock wave changes into the line $x = \sigma\, t = \sigma_3(U_r, U_l)\, t$. The Rankine–Hugoniot condition must still be satisfied after the change of variables, thus

$$\begin{aligned} \sigma(U_r - U_l) &= f(U_r) - f(U_l), \\ \Leftrightarrow -\sigma_1(U_l, U_r)(U_r - U_l) &= f(U_r) - f(U_l), \\ \Leftrightarrow \sigma_3(U_r, U_l)(U_l - U_r) &= f(U_l) - f(U_r). \end{aligned}$$

Hence, we have a wave connecting $U_r$ to $U_l$ with the shock velocity $\sigma_3(U_r, U_l)$ satisfying the Rankine–Hugoniot condition. Furthermore, $p_r > p_l$, therefore it is an admissible 3-shock wave connecting $U_r$ to $U_l$.

The fact that a 3-wave becomes a 1-wave under this transformation follows by the same arguments.

For a 2-wave we have $\sigma = \lambda = 0$, therefore a 2-wave is unchanged when sending $x$ to $-x$. □

For instance, it follows from Lemma 3.1 that $\zeta + \nu + \alpha$ becomes $\beta + \mu + \zeta$ under the transformation from $x$ to $-x$ and therefore the two interactions are symmetric. This means that all estimates found for $\zeta + \nu + \alpha$ will apply to $\beta + \mu + \zeta$ as well, and we only need to consider one of them.

3.3. **The Glimm functional.** Our Glimm functional is defined on a mesh curve $J$ by

$$G(J) := F(J) + 3C_1(\overline{\gamma} - 1)Q_1(J) + 3C_2Q_2(J), \tag{3.5}$$

where $C_1$ is the constant appearing in the estimates given by (4.3) for the interaction between two shock waves, cf. the case Bb-ii (see Subsection 4.2.2), and

$$C_2 := \frac{c_2}{\min\{r'_{\min}, s'_{\min}\}} = kc_2, \tag{3.6}$$

where $c_2$ is the constant from Lemma 2.2 defined by (2.25) and

$$k := \frac{1}{\min\{r'_{\min}, s'_{\min}\}}. \tag{3.7}$$

Note that both $C_1$ and $C_2$ are constants only depending on $p_{\min}$, $p_{\max}$ and $\overline{\gamma}$. The linear functional $F$ and the two quadratic functionals $Q_1$ and $Q_2$ are defined by

$$F(J) := \sum\{|\delta\,| \mid \text{all shock waves } \delta \text{ crossing } J\}, \tag{3.8}$$

$$Q_1(J) := \sum\{|\alpha\,||\beta\,| \mid \text{all approaching 1- and 3-shock waves crossing } J\}, \tag{3.9}$$

$$Q_2(J) := \sum\{|\zeta\,||\delta\,| \mid \text{all approaching pairs of } \zeta \text{ and } \delta \text{ crossing } J\}, \tag{3.10}$$

where two waves of different families are *approaching* if the wave of the lowest family is the rightmost wave with respect to $x$. Note that $F$ and $Q_1$ only sum over shock waves.

**Remark 3.2.** The Glimm functional used in [16] is similar to the two first terms of our Glimm functional (3.5), only the constants differ slightly.

We need two more functionals, one summing over all shock and rarefaction waves crossing a mesh curve $J$ and one summing over the contact discontinuities crossing $J$. We define

$$L(J) := \sum \{|\delta| \mid \text{all } \delta \text{ crossing } J\}, \tag{3.11}$$

and

$$F_\gamma(J) = F_\gamma := \sum \{|\zeta| \mid \text{all } \zeta \text{ crossing } J\}. \tag{3.12}$$

Note that the sum of all contact discontinuities, $F_\gamma$, is constant for all mesh curves.

The key point in order to show convergence, is to prove that this Glimm functional is a decreasing functional in time. Define the constant

$$C = \min\{\tilde{C}, 1\}, \tag{3.13}$$

where the minimum is taken over all the constants $\tilde{C}$ appearing in the estimates for interactions of type Ba considered in Subsection 4.2.1. Note that $0 < C \leq 1$ depends only on $p_{\min}$, $p_{\max}$ and $\overline{\gamma}$. We can now state the following lemma.

**Lemma 3.3.** *Assume that all waves are contained in $\mathcal{D}$ and let $G(J)$ be the Glimm functional defined by* (3.5)*. If*

$$(\overline{\gamma} - 1)L(J_0) \leq \frac{C}{9C_1}, \tag{3.14}$$

$$F_\gamma \leq \frac{C}{9C_2}, \tag{3.15}$$

*then $G(J)$ is a decreasing functional, that is, $G(J_N) \leq G(J_{N-1}) \leq \cdots \leq G(J_0)$. Furthermore, $F(J_N) \leq \frac{5}{3}L(J_0)$.*

We prove this lemma by going through every possible interaction we can get in the Glimm scheme, and we devote the next section to this.

## 4. Proof of Lemma 3.3

We prove that the Glimm functional (3.5) is decreasing by induction on successive mesh curves. Since two successive mesh curves only differ at the edges of one diamond, we have to consider all possible interactions that can take place in one diamond and show that $G$ is decreasing across these.

Before we start on the induction, we prove the last part of Lemma 3.3. Assume that $G$ is decreasing for successive mesh curves up to $J_n$ and assume furthermore that $L_0 = L(J_0)$ and $F_\gamma$ satisfy (3.14) and (3.15), respectively. To simplify the notation we write $G_j = G(J_j)$, $F_j = F(J_j)$, and $Q_{k,j} = Q_k(J_j)$. We get

$$\begin{aligned} F_n \leq G_n \leq G_{n-1} \leq \cdots \leq G_0 &= F_0 + 3C_1(\overline{\gamma} - 1)Q_{1,0} + 3C_2Q_{2,0} \\ &\leq F_0 + 3C_1(\overline{\gamma} - 1)(F_0)^2 + 3C_2L_0F_\gamma \\ &\leq (1 + 3C_1(\overline{\gamma} - 1)F_0 + 3C_2F_\gamma)L_0 \\ &\leq (1 + 3C_1(\overline{\gamma} - 1)L_0 + 3C_2F_\gamma)L_0 \\ &\leq \left(1 + \frac{C}{3} + \frac{C}{3}\right)L_0 \leq \frac{5}{3}L_0, \end{aligned} \tag{4.1}$$

where we have used that $C \leq 1$. This proves that if $G$ is decreasing, then $F(J_N) \leq \frac{5}{3}L(J_0)$.

We now turn to the induction argument. The first step is to show that $G_1 - G_0 \leq 0$ where $J_0$ is the unique mesh curve connecting the sampling points at $t = 0$ to the sampling points

at $t = \Delta t$. Then we assume that $G$ is decreasing for successive mesh curves up to $J_n$, that is, $G_n \leq G_{n-1} \leq \cdots \leq G_0$. The induction step is to show that $\Delta G := G_{n+1} - G_n \leq 0$. For a given interaction, the calculations needed to estimate $G_1 - G_0$ and $\Delta G$ are the same. The sum over all shock waves or all contact discontinuities crossing the first of the two successive mesh curves most often show up in the estimates, and we use conditions (3.14) and (3.15) in addition to (4.1) to show that the estimates are nonpositive. Thus, the only difference in the estimates for $G_1 - G_0$ and $\Delta G$ is that for the first one we might get terms with $F_0 \leq L_0$, while for the second one these terms involve $F_n \leq \frac{5}{3} L_0$. We only include the calculations for $\Delta G$.

In Section 3.2 we discussed all the possible interactions and divided them into four main types. Recall that the projection of 1- or 3-wave curves onto the $(p, u)$-plane can intersect if they have different $\gamma$'s, cf. property (ii) in Lemma 2.1, therefore each interaction has up to four possible outcomes and they all have to be considered. Fortunately, the symmetry properties of system (1.1) stated in Lemma 3.1 nearly halve the number of interactions we have to consider.

Before we start considering each interaction, we describe our general approach. We start by proving that the Glimm functional is decreasing for all interactions of type B, that is, interactions between two waves. This is either done by using estimates and properties of the wave curves given in [16] and translating these into estimates using $p$ and $u$ as the variables, or by applying Lemma 2.2.

To show that $\Delta G \leq 0$ for interactions between more than two waves, we use a strategy of dividing the interaction into several steps. As long as we can show that $G$ is decreasing across each step, it follows that $G$ is decreasing going from the first to the last step and that $\Delta G \leq 0$ across the interaction. Based on this, we divide the interaction into steps for which we already know that $G$ is decreasing. Thus, at each step we let two (or sometimes three) waves interact. As long as this is an interaction already analyzed, we know that $G$ decreases across this step. We continue this until we at some point easily can show that $G$ is decreasing across the last step, that is, we are able to find sufficiently strong estimates of the outgoing waves in terms of the collection of waves obtained through the previous steps.

Formally, we can describe the division of the interaction into $k$ steps using inner diamonds and intermediate mesh curves. Start by identifying two (or three) nearby waves among the incoming waves for which we already have established that the Glimm functional is decreasing across the interaction. Introduce an *intermediate mesh curve*, $J_1^*$, which coincides with $J_n$ everywhere except near the lower corner of the original diamond. Near the lower corner $J_1^*$ lies above $J_n$ so that $J_1^*$ and $J_n$ enclose a small *inner diamond* inside the original diamond. This is done so that the waves interacting at the first step enter the inner diamond, while the waves left unchanged at this step cross $J_n$ and $J_1^*$ outside the inner diamond. Observe that $J_n$ and $J_1^*$ act as successive mesh curves. Since the waves entering this inner diamond correspond to an interaction already analyzed, we have $\Delta G_1 := G(J_1^*) - G(J_n) \leq 0$. Note that $J_1^*$ is not a real mesh curve by the definition given above, since it inside the original diamond does not consist of lines connecting sampling points. However, the outcome of the interaction inside an inner diamond is found by solving the Riemann problem where the left and right states are the values at the corners of the inner diamond, so the corners act as sampling points. Let the fan of the outgoing waves be situated somewhere on the line between the left and the right corner of the inner diamond in such a way that the waves interacting at the next step enter the next inner diamond while the rest of the waves do not. Thus, both the intermediate mesh curves and the inner diamonds resemble the real mesh

curves and diamonds. One example of an interaction divided into steps and the introduced intermediate mesh curves and inner diamonds is shown in Figure 8.

For each step $i = 2, \dots, k-1$ we introduce a new mesh curve $J_i^*$ which acts as a successive mesh curve to $J_{i-1}^*$, that is, the two intermediate mesh curves enclose an inner diamond which the interacting waves enter. Since the waves entering an inner diamond correspond to an interaction already analyzed, we have that $\Delta G_i := G(J_i^*) - G(J_{i-1}^*) \le 0$ for $i = 2 \dots k-1$. We stop this process when we after step $k-1$ are able to show that $\Delta G_k := G(J_{n+1}) - G(J_{k-1}^*) \le 0$. In other words, we divide the interaction into steps until we after step $k-1$ have a collection of waves which are easy to compare (possibly using Lemma 2.2) with the outgoing waves so that we are able show that $\Delta G_k \le 0$. Then we have $G(J_{n+1}) \le G(J_{k-1}^*) \le \cdots \le G(J_i^*) \le \cdots \le G(J_1^*) \le G(J_n)$, thus, $\Delta G = G(J_{n+1}) - G(J_n) \le 0$.

In most cases only a few extra steps are needed in order to show $\Delta G \le 0$. However, for the cases where many steps are required, we change our strategy slightly. At the first step[1] we replace the incoming waves with a new set of waves connecting $U_l$ to $U_r$. We introduce inner diamonds and intermediate mesh curves as before, thus, all the incoming waves enter the first inner diamond and the introduced waves leave this diamond. The only difference from before is that these outgoing waves of the first diamond is not a result of some known interaction. Therefore, we have to obtain estimates on these introduced waves in terms of the original incoming waves, so that we can show $\Delta G_1 \le 0$. After this step of replacing one interaction with a new one, we carry on as before. We identify nearby waves among the introduced waves for which we already have analyzed the corresponding interaction, and then carry on as above. The advantage of this method is that it requires only a few extra steps for an interaction where we otherwise would need many steps.

We use the notation $\xrightarrow{\Delta G_i}$ to indicate the different steps of an interaction and square brackets to group the waves that interact at each step. Recall that we use ordinary parentheses to indicate which waves enter through the same edge. In the figures displaying the interactions we see the projection of the interaction onto the $(p, u)$-plane. The left and right states are drawn as circles, the incoming waves are drawn by dashed lines and the outgoing waves with dash-dotted lines. The contact discontinuities, $\zeta$, are indicated by asterisks. For most of the interactions that are divided into steps, we have included the intermediate waves drawn by dotted lines. Furthermore, any wave drawn by a solid line is a introduced wave which is not a result of an interaction.

We are now ready to prove that $\Delta G \le 0$ across all possible interactions.

4.1. **Type A: Waves entering through only one edge.** These interactions are trivial: If one, two or three waves all enter one diamond through the same edge, then they are by definition the solution of a Riemann problem $(U_l, U_r)$. If no more waves enter the diamond, then the Riemann problem to be solved inside the diamond is also $(U_l, U_r)$. Thus we have

$$(\epsilon + \zeta + \eta) \to \epsilon' + \zeta + \eta', \qquad \text{where} \qquad \epsilon = \epsilon', \qquad \eta = \eta',$$

and since the incoming and outgoing waves are equal, so are their strengths and $\Delta G = 0$ for all interactions of type A.

4.2. **Type B: Two waves entering the diamond.** The interactions between two waves that do not include a contact discontinuity, are the same interactions as for the $p$-system and are discussed in [16] where the waves are measured by the jumps in the Riemann invariants for the $p$-system, $r$ and $s$, defined by [16, Eq. (5)]. We use the estimates given in [16] and transform these into estimates using the jump in $p$ to measure the strength of the waves. The

[1]For the last case of interaction Db-iv we actually do this replacement at the second step.

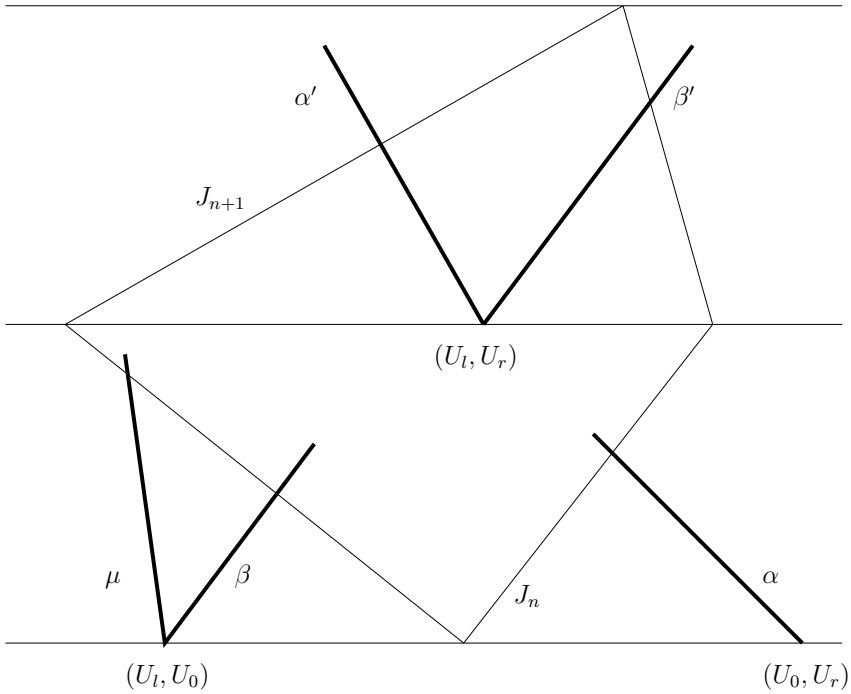


(a) The interaction before division.

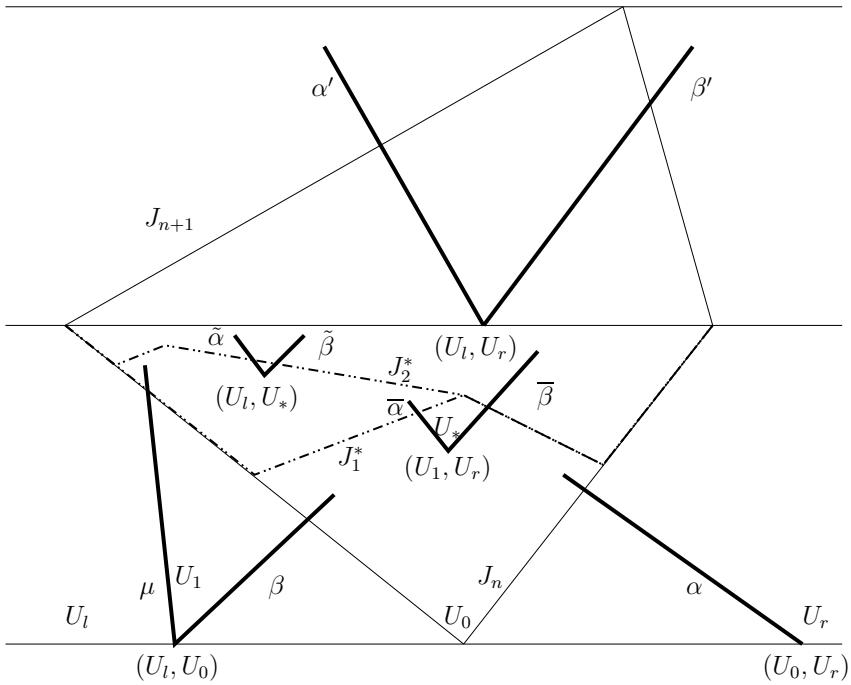


(b) The interaction divided into three steps with two new mesh curves, $J_1^*$ and $J_2^*$, and two inner diamonds.

FIGURE 8. An interaction divided into three steps: $\mu + \beta + \alpha \to \alpha' + \beta'$ which is the second case of Ca-v. The projection onto the $(p, u)$-plane is shown in Figure 16(b).

map from $(p,u)$ to $(r,s)$ is one-to-one and onto for all $p>0$. We state the estimates and skip the detailed transformations going from the estimates and properties in $(r,s)$-coordinates to estimates in $(p,u)$-coordinates. Note that the constants appearing in [16] depend on $p_{\min}$, $p_{\max}$ and $\gamma$. However, for a given $p_{\min}$ and $p_{\max}$ we take the maximum or minimum over all $\gamma$ and find an upper bound of these constants that only depend on $p_{\min}$, $p_{\max}$ and $\overline{\gamma}$. For the interactions involving a contact discontinuity, we obtain the needed estimates using Lemma 2.2.

Recall that for all interactions of type B we have one wave entering through each edge, otherwise the interaction is a trivial interaction of type A.

4.2.1. *Type* Ba*: Two waves of the same family.*

(i) $\alpha_1+\alpha_2\to\alpha'+\nu'$ (and $\beta_1+\beta_2\to\mu'+\beta'$): Property (viii) implies that $\alpha_2$ lies above $\alpha'$

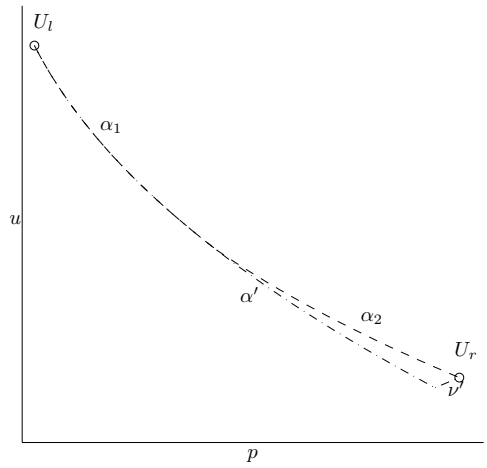


FIGURE 9. The interaction $\alpha_1+\alpha_2\to\alpha'+\nu'$.

and there is only one possible outcome of this interaction, see Figure 9. We have that

$$|\alpha'\,|-|\alpha_1\,|-|\alpha_2\,|=-|\nu'\,|\,,$$

from which we get

$$\Delta F=-|\nu'\,|\,,\qquad\qquad \Delta Q_1\le 0,\qquad\qquad \Delta Q_2\le|\nu'\,|\,F_\gamma,$$

where $\Delta F:=F_{n+1}-F_n$ and $\Delta Q_i:=Q_{i,n+1}-Q_{i,n}$. Thus,

$$\Delta G\le|\nu'\,|\,(-1+3C_2F_\gamma)\le|\nu'\,|\left(-1+\frac{C}{3}\right)\le|\nu'\,|\left(-1+\frac{1}{3}\right)\le 0.$$

By the symmetry property $\Delta G\le 0$ also across the interaction $\beta_1+\beta_2$.

(ii) $\alpha+\mu$ (and $\nu+\beta$): There are two possible outcomes of this interaction.

- $\alpha+\mu\to\mu'+\beta'$: In this case $U_r$ is to the left of the 3-shock curve starting at $U_l$, see Figure 10(a). From [16] we find that there exists a $\tilde{C}$ depending only on $p_{\min}$, $p_{\max}$ and $\overline{\gamma}$ such that

$$|\mu'\,|\le|\mu\,|\,,\qquad\qquad |\beta'\,|-|\alpha\,|\le-\tilde{C}\,|\beta'\,|\le-C\,|\beta'\,|\,.$$

Recall that $C$ is defined as minimum over all $\tilde{C}$. This gives us

$$\Delta F=-C\,|\beta'\,|\,,$$

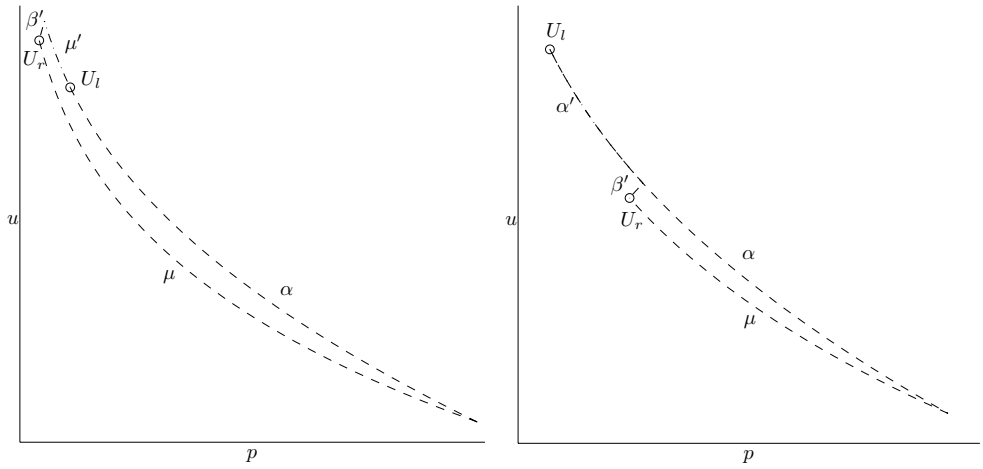


(a) $\alpha + \mu \to \mu' + \beta'$. (b) $\alpha + \mu \to \alpha' + \beta'$.

FIGURE 10. The interaction $\alpha + \mu$.

$$\Delta Q_1 \le |\beta'|\, F_n \le \frac{5}{3}\,|\beta'|\, L_0,$$
$$\Delta Q_2 \le |\beta'|\, F_\gamma,$$

and we find

$$\Delta G \le |\beta'| \left(-C + 3C_1(\overline{\gamma} - 1)\frac{5}{3}L_0 + 3C_2F_\gamma\right)$$
$$\le |\beta'| \left(-C + \frac{5}{3}\frac{C}{3} + \frac{C}{3}\right) \le 0.$$

- $\alpha + \mu \to \alpha' + \beta'$: In this case $U_r$ is to the right of the 3-shock curve starting at $U_l$, see Figure 10(b). Then there exists a constant $\tilde{C} \ge C$ so that

$$|\alpha'| + |\beta'| - |\alpha| \le -\tilde{C}\,|\beta'| \le -C\,|\beta'|\,.$$

As above we find

$$\Delta F = -C\,|\beta'|\,,$$
$$\Delta Q_1 \le |\beta'|\, F_n \le \frac{5}{3}\,|\beta'|\, L_0,$$
$$\Delta Q_2 \le |\beta'|\, F_\gamma,$$

thus, $G \le 0$.

Due to symmetry, $\Delta G \le 0$ across the interaction $\nu + \beta$.

(iii) $\mu + \alpha$ (and $\beta + \nu$): There are two possible outcomes of this interaction.

- $\mu + \alpha \to \mu' + \beta'$: In this case $U_r$ is to the left of the 3-shock curve starting at $U_l$, see Figure 11(a). There exists a $\tilde{C} \ge C$ so that

$$|\mu'| \le |\mu|\,, \qquad |\beta'| - |\alpha| \le -\tilde{C}\,|\beta'| \le -C\,|\beta'|\,. \tag{4.2}$$

Thus, $\Delta G \le 0$ by the same calculation as we just did for $\alpha + \mu$.

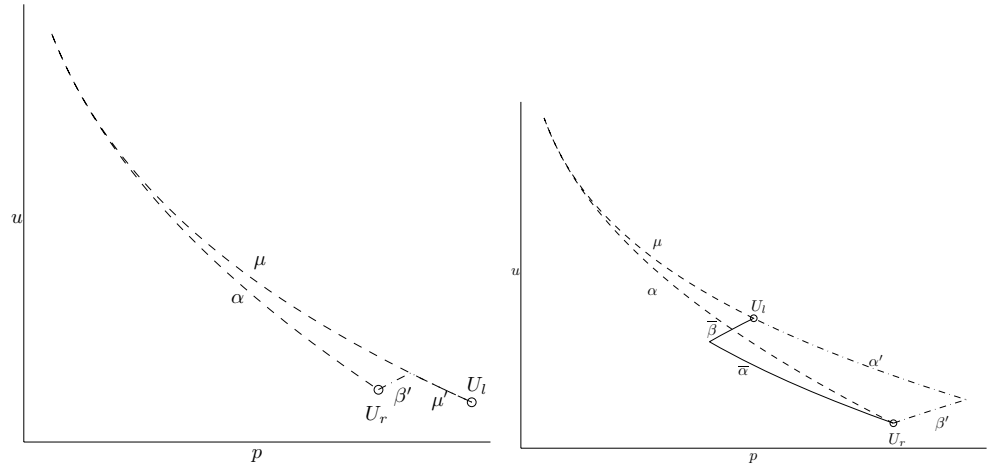


(a) $\mu + \alpha \to \mu' + \beta'$. (b) $\mu + \alpha \to \alpha' + \beta'$.

FIGURE 11. The interaction $\mu + \alpha$.

- $\mu + \alpha \to \alpha' + \beta'$: In this case $U_r$ is to the right of the 3-shock curve starting at $U_l$, see Figure 11(b). For this interaction we use the same approach as in [16] and replace the interaction by a new one. There exists two waves, $\overline{\beta}$ and $\overline{\alpha}$, so that

$$|\overline{\alpha}\,| + \left|\overline{\beta}\,\right| - |\alpha\,| \le -\tilde{C}\left|\overline{\beta}\,\right| \le -C\left|\overline{\beta}\,\right|,$$

and

$$\overline{\beta} + \overline{\alpha} \to \alpha' + \beta'.$$

We write the interaction as

$$\mu + \alpha \xrightarrow{\Delta G_1} [\overline{\beta} + \overline{\alpha}] \xrightarrow{\Delta G_2} \alpha' + \beta',$$

where the square brackets indicate that the two waves interact at the second step, unlike the first step where we just replace the waves.

For the first step we find using the above estimate that

$$\begin{aligned}
\Delta F &= -C\left|\overline{\beta}\,\right|, \\
\Delta Q_1 &\le |\overline{\alpha}\,|\left|\overline{\beta}\,\right| + \left|\overline{\beta}\,\right| \sum_i |\alpha_i\,| \le \left|\overline{\beta}\,\right| F_n \le \frac{5}{3}\left|\overline{\beta}\,\right| L_0, \\
\Delta Q_2 &\le \left|\overline{\beta}\,\right| F_\gamma,
\end{aligned}$$

where $\alpha_i$ are all 1-shock waves that are approaching $\overline{\beta}$, that is, all 1-shock waves to the right of the diamond. From this we find that $\Delta G_1 \le 0$ at the first step when passing from $\mu + \alpha$ to $\overline{\beta} + \overline{\alpha}$, regardless of the introduced approaching waves. The interaction at the second step is of type Bb-ii and by the estiamate (4.3) below we have $\Delta G_2 \le 0$.

We have now proved that the Glimm functional is decreasing for both steps, thus, $\Delta G \le 0$.

Due to symmetry, $\Delta G \le 0$ across the interaction $\beta + \nu$.

All the constants $\tilde{C}$ in the above estimates consist of one constant from the estimates in [16], let us call this $C_0$, and one constant due to the transformation into estimates

using $p$ to measure the wave strengths. From [16] we have $C_0 > 0$, thus, $\tilde{C} > 0$ for all the above estimates and $0 < C \leq 1$ since $C$ is the minimum of all $\tilde{C}$ and 1.

4.2.2. *Type* Bb*: Different families, no contact discontinuity.*

(i) $\nu + \mu \to \mu' + \nu'$: This interaction has only one outcome, see Figure 12(a), and we obtain

$$|\mu'\,| \leq |\mu\,|\,, \qquad\qquad |\nu'\,| \leq |\nu\,|\,,$$

thus $\Delta G \leq 0$.

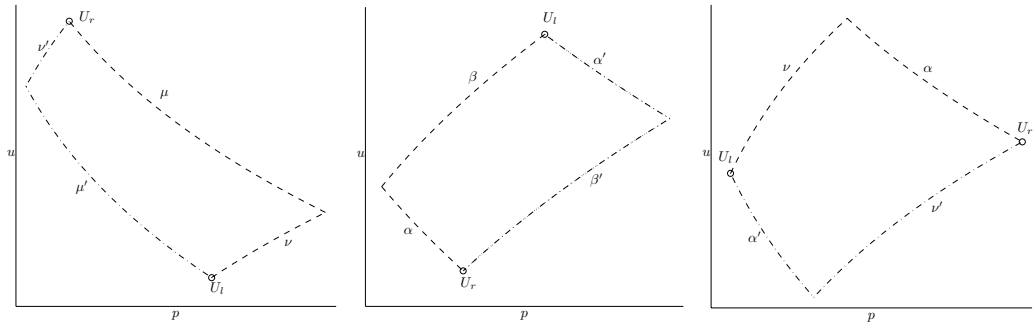


(a) $\nu + \mu \to \mu' + \nu'$. (b) $\beta + \alpha \to \alpha' + \beta'$. (c) $\nu + \alpha \to \alpha' + \nu'$.

FIGURE 12. The interactions of type Bb

(ii) $\beta + \alpha \to \alpha' + \beta'$: This interaction has only one outcome, see Figure 12(b), and we obtain

$$|\alpha'\,| - |\alpha\,| \leq C_1(\overline{\gamma} - 1)\,|\alpha\,|\,|\beta\,|\,, \qquad\qquad |\beta'\,| - |\beta\,| \leq C_1(\overline{\gamma} - 1)\,|\alpha\,|\,|\beta\,|\,, \tag{4.3}$$

where $C_1$ is a constant depending only on $p_{\min}$, $p_{\max}$ and $\overline{\gamma}$, see Remark 4.1. From these estimates we find

$$\begin{aligned}
\Delta F &\leq 2C_1(\overline{\gamma} - 1)\,|\alpha\,|\,|\beta\,|\,,\\
\Delta Q_1 &\leq C_1(\overline{\gamma} - 1)\,|\alpha\,|\,|\beta\,|\,F_n - |\alpha\,|\,|\beta\,| \leq \frac{5}{3}C_1(\overline{\gamma} - 1)\,|\alpha\,|\,|\beta\,|\,L_0 - |\alpha\,|\,|\beta\,|\,,\\
\Delta Q_2 &\leq C_1(\overline{\gamma} - 1)\,|\alpha\,|\,|\beta\,|\,F_\gamma.
\end{aligned}$$

Thus,

$$\begin{aligned}
\Delta G &\leq C_1(\overline{\gamma} - 1)\,|\alpha\,|\,|\beta\,|\left(2 + \frac{5}{3}3C_1(\overline{\gamma} - 1)L_0 - 3 + 3C_2F_\gamma\right)\\
&\leq C_1(\overline{\gamma} - 1)\,|\alpha\,|\,|\beta\,|\left(\frac{5}{3}\frac{C}{3} + \frac{C}{3} - 1\right) \leq 0.
\end{aligned}$$

**Remark 4.1.** In Nishida–Smoller [16], where the strength of the waves are measured using the Riemann invariants $r$ and $s$, interaction Bb-ii is divided into three different cases with different estimates. However, when transforming these estimates into estimates using $p$ to measure the strength of the waves, we get the same estimate for all the three cases. Similar to $C$, the constant $C_1$ is computed from the estimate in [16] and the transformation back from Riemann invariants, and it does only depend on $p_{\min}$, $p_{\max}$ and $\overline{\gamma}$.

(iii) $\nu + \alpha \to \alpha' + \nu'$ (and $\beta + \mu \to \mu' + \beta'$): There is only one outcome for this interaction, see Figure 12(c), and we find that

$$|\alpha'| - |\alpha| = -q, \qquad |\nu'| - |\nu| = q,$$

where $q$ is a positive constant. We get that

$$\Delta F = -q, \qquad \Delta Q_1 \le 0, \qquad \Delta Q_2 \le q F_\gamma,$$

and furthermore,

$$\Delta G \le q\left(-1 + 3C_2 F_\gamma\right) \le q\left(-1 + \frac{C}{3}\right) \le 0.$$

Due to symmetry, $\Delta G \le 0$ across the interaction $\beta + \mu$.

4.2.3. *Type* Bc*: With a contact discontinuity.* Interactions of this type do not occur in [16] and we prove all estimates.

(i) $\zeta + \mu$ (and $\nu + \zeta$): In general we do not know which of the curves $\mu$ with $\gamma_r$ or $\mu'$ with $\gamma_l$ lies above the other, or whether they cross, and therefore there are two possible outcomes of this interaction, see Figure 13. Recall that contact discontinuities are denoted by asteriks in the figures.

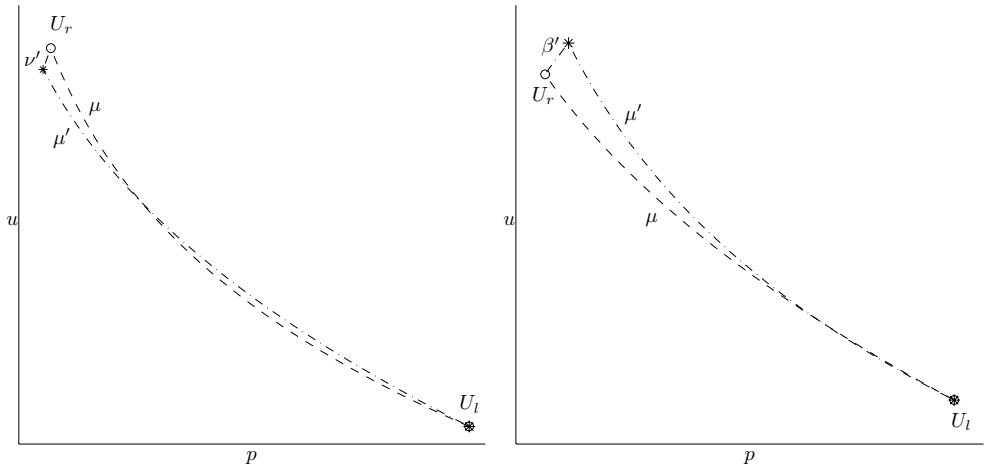


(a) $\zeta + \mu \to \mu' + \zeta + \nu'$. (b) $\zeta + \mu \to \mu' + \zeta + \beta'$.

FIGURE 13. The interaction $\zeta + \mu$.

- $\zeta + \mu \to \mu' + \zeta + \nu'$: In this case $U_r$ lies above $\mu'$, see Figure 13(a). We have that $|\mu'| - |\mu| = |\nu'|$, and want an estimate on $|\nu'|$. Let $\overline{u}$ denote the point on $\mu'$ where $p = p_r$ and apply Lemma 2.2 on the two rarefaction waves $\mu$ and $\mu'$ on the interval from $p_l = p_1$ to $p_r$, then

$$u_r - \overline{u} \le c_2 |\mu| |\zeta|.$$

From the mean value theorem we have $|u_r - \tilde{u}| = |r'(p_*, p_l, \gamma)| |p_r - \tilde{p}|$ for some $p_* \in (\tilde{p}, p_r)$ where the derivative is with respect to the first variable. Recall from

property (iv) that $|r'(p_*, p_l, \gamma)| \geq r'_{\min}$ where $r'_{\min}$ is a constant only depending on $p_{\min}$, $p_{\max}$ and $\overline{\gamma}$. We get

$$|\nu'| = |p_r - \tilde{p}| \leq \frac{1}{r'_{\min}} |u_r - \overline{u}| \leq \frac{c_2}{r'_{\min}} |\mu| |\zeta|.$$

This proves the estimate

$$|\mu'| - |\mu| = |\nu'| \leq C_2 |\mu| |\zeta|, \tag{4.4}$$

where $C_2$ is defined by (3.6). Using this estimate we find

$$\begin{aligned} \Delta F &= 0, \\ \Delta Q_1 &= 0, \\ \Delta Q_2 &\leq C_2 |\mu| |\zeta| F_\gamma - |\mu| |\zeta|, \end{aligned}$$

which gives

$$\Delta G \leq C_2 |\mu| |\zeta| (3C_2 F_\gamma - 3) \leq C_2 |\mu| |\zeta| \left(\frac{C}{3} - 3\right) \leq 0.$$

- $\zeta + \mu \to \mu' + \zeta + \beta'$: In this case $U_r$ lies below $\mu'$, see Figure 13(b). We have $|\mu'| - |\mu| \leq 0$. Let $\overline{u}$ be the point on $\mu$ with $p = \tilde{p}$ and apply Lemma 2.2 to $\mu$ and $\mu'$ on the interval from $p_l = p_1$ to $\tilde{p}$, then

$$\tilde{u} - \overline{u} \leq c_2 |\zeta| |\mu'| \leq c_2 |\zeta| |\mu|.$$

From the mean value theorem, for a $p_* \in (p_r, \tilde{p})$, and property (v), we get

$$\begin{aligned} |\beta'| = |p_r - \tilde{p}| &= \frac{1}{|s'(\tilde{p}, p_*, \gamma_r)|} |\tilde{u} - u_r| \\ &\leq \frac{1}{s'_{\min}} |\tilde{u} - \overline{u}| \leq \frac{c_2}{s'_{\min}} |\mu| |\zeta|, \end{aligned}$$

where the derivative is with respect to the first variable. This proves the estimates

$$|\mu'| - |\mu| \leq 0, \qquad |\beta'| \leq C_2 |\mu| |\zeta|, \tag{4.5}$$

where $C_2$ is defined by (3.6). We get

$$\begin{aligned} \Delta F &\leq C_2 |\mu| |\zeta|, \\ \Delta Q_1 &\leq C_2 |\mu| |\zeta| F_n \leq \frac{5}{3} C_2 |\mu| |\zeta| L_0, \\ \Delta Q_2 &\leq C_2 |\mu| |\zeta| F_\gamma - |\mu| |\zeta|, \end{aligned}$$

which gives

$$\begin{aligned} \Delta G &\leq C_2 |\mu| |\zeta| \left(1 + \frac{5}{3} 3C_1(\overline{\gamma} - 1) L_0 + 3C_2 F_\gamma - 3\right) \\ &\leq C_2 |\mu| |\zeta| \left(\frac{5}{3}\frac{C}{3} + \frac{C}{3} - 2\right) \leq 0. \end{aligned}$$

By symmetry it follows that $\Delta G \leq 0$ across the interaction $\nu + \zeta$.

(ii) $\zeta + \alpha$ (and $\beta + \zeta$): We do not know in general which of the curves $\alpha$ with $\gamma_r$ or $\alpha'$ with $\gamma_l$ lies above the other, therefore this interaction has two possible outcomes. Since this interaction is very similar to the interaction between a contact discontinuity and a rarefaction wave discussed above, we do not include all details.

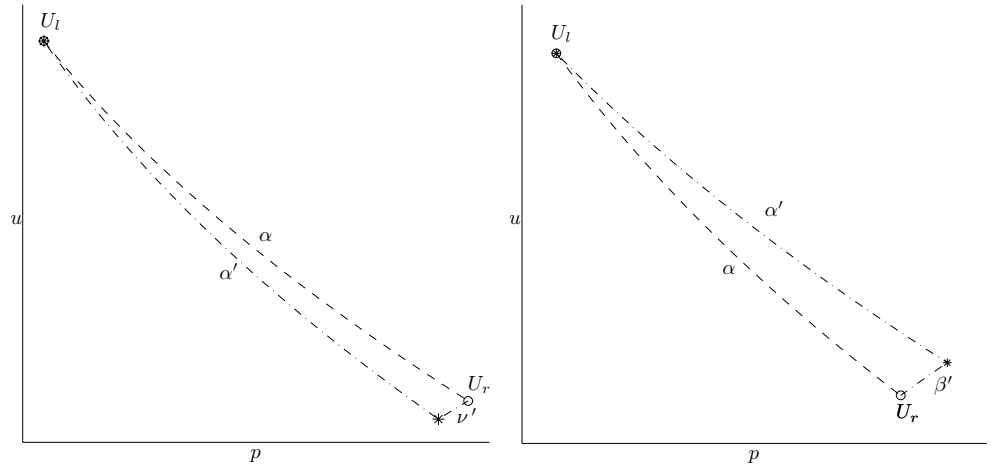


(a) $\zeta + \alpha \to \alpha' + \zeta + \nu'$. (b) $\zeta + \alpha \to \alpha' + \zeta + \beta'$.

FIGURE 14. The interaction $\zeta + \alpha$.

- $\zeta + \alpha \to \alpha' + \zeta + \nu'$: In this case $U_r$ is above $\alpha'$, see Figure 14(a). We have that

$$|\alpha'| - |\alpha| \le 0, \qquad |\nu'| \le C_2 |\alpha| |\zeta|,$$

where $C_2$ is defined by (3.6). This follows by applying Lemma 2.2 to $\alpha$ and $\alpha'$ similar to what we did for the interaction $\zeta + \mu \to \mu' + \zeta + \beta'$. We get

$$\begin{aligned} \Delta F &\le 0, \\ \Delta Q_1 &\le 0, \\ \Delta Q_2 &\le C_2 |\alpha| |\zeta| F_\gamma - |\alpha| |\zeta|, \end{aligned}$$

which gives

$$\Delta G \le C_2 |\alpha| |\zeta| (3C_2 F_\gamma - 3) \le C_2 |\alpha| |\zeta| \left( \frac{C}{3} - 3 \right) \le 0.$$

- $\zeta + \alpha \to \alpha' + \zeta + \beta'$: In this case $U_r$ is below $\alpha'$, see Figure 14(b). We have that

$$|\alpha'| - |\alpha| = |\beta'| \le C_2 |\alpha| |\zeta|,$$

where $C_2$ is defined by (3.6). This estimate is obtained using Lemma 2.2 on $\alpha$ and $\alpha'$, similar to what we did for the interaction $\zeta + \mu \to \mu' + \zeta + \nu'$. From this estimate we find

$$\begin{aligned} \Delta F &\le 2C_2 |\alpha| |\zeta|, \\ \Delta Q_1 &\le C_2 |\alpha| |\zeta| F_n \le \frac{5}{3} C_2 |\alpha| |\zeta| L_0, \\ \Delta Q_2 &\le C_2 |\alpha| |\zeta| F_\gamma - |\alpha| |\zeta|, \end{aligned}$$

which gives

$$\Delta G \le C_2 |\alpha| |\zeta| \left( 2 + \frac{5}{3} 3C_1(\overline{\gamma} - 1) L_0 + 3C_2 F_\gamma - 3 \right)$$

$$\leq C_2\,|\alpha\,|\,|\zeta\,|\left(\frac{5}{3}\frac{C}{3}+\frac{C}{3}-1\right)\leq 0.$$

Due to symmetry, $\Delta G\leq 0$ across the interaction $\beta+\zeta$.

### 4.3. **Type C: Three waves entering the diamond.**

4.3.1. *Type* Ca*: No contact discontinuities.* The interactions of this type are also present for the $p$-system and are covered by [16], although the detailed estimates are not given there. We choose to include the discussion of this type of interactions in detail since we measure the waves in $p$ and since the methods are useful for later interactions. Note the increase of complexity one gets for the later interactions involving a contact discontinuity. Recall that regular parentheses are used to indicate which edge the waves enter through, while square brackets are used to indicate which waves interact at each step.

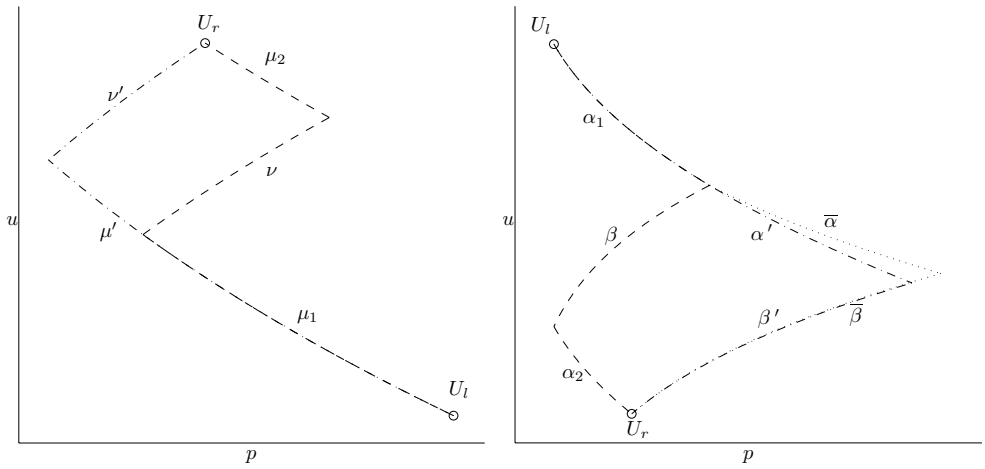


(a) $(\mu_1+\nu)+\mu_2\to\mu'+\nu'$.

(b) $(\alpha_1+\beta)+\alpha_2\to\alpha'+\beta'$.

(c) $(\mu_1+\beta)+\mu_2\to\mu'+\beta'$.

(d) $(\alpha_1+\nu)+\alpha_2\to\alpha'+\nu'$.

FIGURE 15. Some interactions of type Ca.

(i) $(\mu_1+\nu)+\mu_2 \to \mu'+\nu'$ (and $\nu_1+(\mu+\nu_2)\to\mu'+\nu'$): This interaction has only one outcome, see Figure 15(a), and we divide it into two steps,

$$\mu_1+[\nu+\mu_2] \xrightarrow{\Delta G_1} \mu_1+\overline{\mu}+\overline{\nu} \xrightarrow{\Delta G_2} \mu'+\nu'.$$

We have $\Delta G_1 \le 0$ because the interaction at the first step is of type Bb-i. From property (iv) and property (vii) it follows that $\mu_1+\overline{\mu}=\mu'$ and $\overline{\nu}=\nu'$, therefore $\Delta G_2 = 0$.

By symmetry it follows that $\Delta G \le 0$ across $\nu_1+(\mu+\nu_2)$.

(ii) $(\alpha_1+\beta)+\alpha_2 \to \alpha'+\beta'$ (and $\beta_1+(\alpha+\beta_2)\to\alpha'+\beta'$): There is only one outcome of this interaction, see Figure 15(b), and we divide it into two steps,

$$\alpha_1+[\beta+\alpha_2] \xrightarrow{\Delta G_1} \alpha_1+\overline{\alpha}+\overline{\beta} \xrightarrow{\Delta G_2} \alpha'+\beta'.$$

We have $\Delta G_1 \le 0$ because the interaction at the first step is of type Bb-ii. Due to properties (viii) and (ix) we have

$$|\alpha'|-|\alpha_1|-|\overline{\alpha}|\le 0, \qquad |\beta'|-\left|\overline{\beta}\right|\le 0,$$

and it follows that $\Delta G_2 \le 0$.

By symmetry we have $\Delta G \le 0$ across $\beta_1+(\alpha+\beta_2)$.

(iii) $(\mu_1+\beta)+\mu_2 \to \mu'+\beta'$ (and $\nu_1+(\alpha+\nu_2)\to\alpha'+\nu'$): There is only one possible outcome of this interaction, see Figure 15(c), and we divide it into two steps,

$$\mu_1+[\beta+\mu_2] \xrightarrow{\Delta G_1} \mu_1+\overline{\mu}+\overline{\beta} \xrightarrow{\Delta G_2} \mu'+\beta'.$$

The first interaction is of type Bb-iii, thus $\Delta G_1 \le 0$. From property (iv) and property (vii) it follows that $\mu_1+\overline{\mu}=\mu'$, therefore we must also have $\overline{\beta}=\beta'$, and then $\Delta G_2 = 0$.

It follows from symmetry that $\Delta G \le 0$ across $\nu_1+(\alpha+\nu_2)$.

(iv) $(\alpha_1+\nu)+\alpha_2 \to \alpha'+\nu'$ (and $\beta_1+(\mu+\beta_2)\to\mu'+\beta'$): This interaction has only one possible outcome, see Figure 15(d), and we divide it into two steps,

$$\alpha_1+[\nu+\alpha_2] \xrightarrow{\Delta G_1} \alpha_1+\overline{\alpha}+\overline{\nu} \xrightarrow{\Delta G_2} \alpha'+\nu'.$$

Since the first interaction is of type Bb-iii, we have $\Delta G_1 \le 0$. Property (iv) and property (viii) imply that

$$|\alpha'|-|\alpha_1|-|\overline{\alpha}|=-q, \qquad |\nu'|-|\overline{\nu}|=q,$$

for a $q>0$, and it follows that $\Delta G_2 \le 0$.

From symmetry we have that $\Delta G \le 0$ across $\beta_1+(\mu+\beta_2)$.

(v) $(\mu+\beta)+\alpha$ (and $\beta+(\alpha+\nu)$): This interaction has two possible outcomes.

- $(\mu+\beta)+\alpha \to \mu'+\beta'$: In this case $U_r$ is to the left of the 3-shock curve starting at $U_l$, see Figure 16(a). We divide the interaction into three steps,

$$\mu+[\beta+\alpha] \xrightarrow{\Delta G_1} [\mu+\overline{\alpha}]+\overline{\beta} \xrightarrow{\Delta G_2} \tilde{\mu}+\tilde{\beta}+\overline{\beta} \xrightarrow{\Delta G_3} \mu'+\beta',$$

where we have $\Delta G_1 \le 0$ because the interaction at the first step is of type Bb-ii, and $\Delta G_2 \le 0$ because the second interaction is of type Ba-iii. From property (vi) and property (ix) we know that the intersection between $\overline{\alpha}$ and $\overline{\beta}$ is to the right of $\beta'$, but still $\left|\overline{\beta}\right| \le |\beta'|$. However, from property (iv) and property (ix) it follows that $\tilde{\beta}$ starts to the left of $\beta'$ and we have

$$|\mu'|-|\tilde{\mu}|=q, \qquad |\beta'|-\left|\overline{\beta}\right|-\left|\tilde{\beta}\right|=-q,$$

from which we obtain $\Delta G_3 \le 0$.

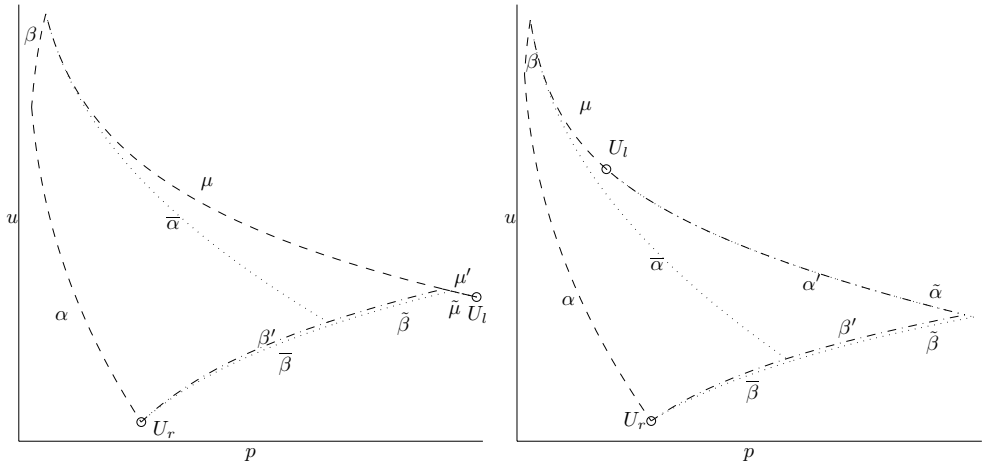


(a) $(\mu+\beta)+\alpha \to \mu'+\beta'$. (b) $(\mu+\beta)+\alpha \to \alpha'+\beta'$.

FIGURE 16. The interaction $(\mu+\beta)+\alpha$.

- $(\mu+\beta)+\alpha \to \alpha'+\beta'$: In this case $U_r$ is to the right of the 3-shock curve starting at $U_l$, see Figure 16(b). We divide the interaction into three steps,

$$\mu+[\beta+\alpha] \xrightarrow{\Delta G_1} [\mu+\overline{\alpha}]+\overline{\beta} \xrightarrow{\Delta G_2} \tilde{\alpha}+\tilde{\beta}+\overline{\beta} \xrightarrow{\Delta G_3} \alpha'+\beta'.$$

  Again we have $\Delta G_1 \le 0$ and $\Delta G_2 \le 0$ because the interactions at the first and second step are of type Bb-ii and Ba-iii, respectively. Due to property (vi) and property (ix), the intersection between $\overline{\alpha}$ and $\overline{\beta}$ is to the right of $\beta'$. Therefore, we have from property (ix) that the intersection between $\tilde{\alpha}$ and $\tilde{\beta}$ is to the right of the intersection between $\alpha'$ and $\beta'$, and

$$|\alpha'|-|\tilde{\alpha}| \le 0, \qquad |\beta'|-|\overline{\beta}|-\left|\tilde{\beta}\right| \le 0,$$

  hence $\Delta G_3 \le 0$.

By symmetry we have $\Delta G \le 0$ across $\beta+(\alpha+\nu)$.

(vi) $(\alpha+\beta)+\mu$ (and $\nu+(\alpha+\beta)$): This interaction has two outcomes.

- $(\alpha+\beta)+\mu \to \mu'+\beta'$: In this case $U_r$ is to the left of the 3-shock wave starting at $U_l$, see Figure 17(a). We divide this interaction into three steps,

$$\alpha+[\beta+\mu] \xrightarrow{\Delta G_1} [\alpha+\overline{\mu}]+\overline{\beta} \xrightarrow{\Delta G_2} \tilde{\mu}+\tilde{\beta}+\overline{\beta} \xrightarrow{\Delta G_3} \mu'+\beta',$$

  where $\Delta G_1 \le 0$ and $\Delta G_2 \le 0$ since the interactions at the first and second step are of type Bb-iii and Ba-ii, respectively. By property (vi) we know that $\overline{\mu}$ is lying below $\alpha$, and together with property (ix), this implies that the intersection between $\overline{\mu}$ and $\overline{\beta}$ is to the right of $\beta'$. From property (iv) and property (ix) we then get

$$|\mu'|-|\tilde{\mu}| = q, \qquad |\beta'|-\left|\tilde{\beta}\right|-|\overline{\beta}| = -q,$$

  and it follows that $\Delta G_3 \le 0$.

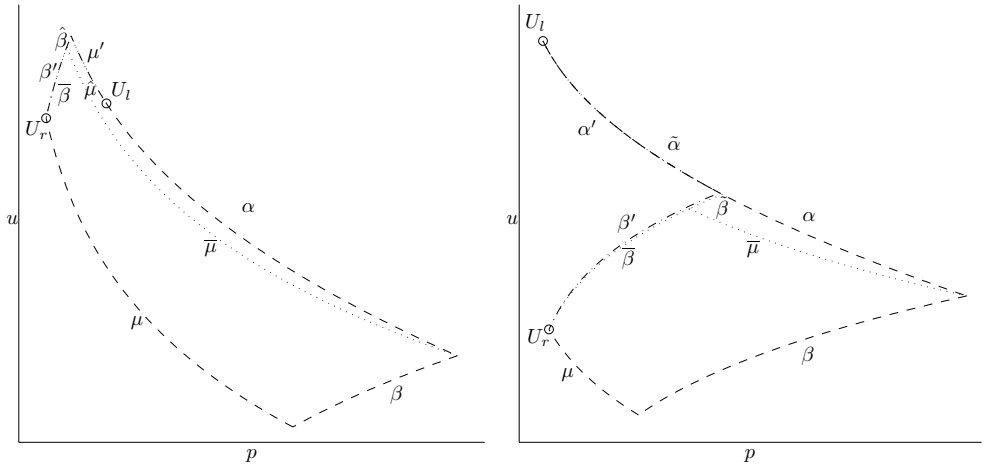


(a) $(\alpha+\beta)+\mu \to \mu'+\beta'$. (b) $(\alpha+\beta)+\mu \to \alpha'+\beta'$.

FIGURE 17. The interaction $(\alpha+\beta)+\mu$.

- $(\alpha+\beta)+\mu \to \alpha'+\beta'$: In this case $U_r$ is to the right of the 3-shock wave starting at $U_l$, see Figure 17(b). We divide this interaction into three steps,

$$\alpha+[\beta+\mu] \xrightarrow{\Delta G_1} [\alpha+\overline{\mu}]+\overline{\beta} \xrightarrow{\Delta G_2} \tilde{\alpha}+\tilde{\beta}+\overline{\beta} \xrightarrow{\Delta G_3} \alpha'+\beta,$$

  where $\Delta G_1 \le 0$ and $\Delta G_2 \le 0$ because the interactions at the first and second step are of type Bb-iii and Ba-ii, respectively. By properties (vi) and (ix) we have that the intersection between $\overline{\mu}$ and $\overline{\beta}$ is to the right of $\beta'$. Furthermore, the intersection between $\hat{\alpha}$ and $\hat{\beta}$ is then by property (viii) and property (ix) to the right of the intersection between $\alpha'$ and $\beta'$, thus

$$|\alpha'\,|-|\tilde{\alpha}\,|\le 0, \qquad\qquad |\beta'\,|-\left|\tilde{\beta}\,\right|-\left|\overline{\beta}\,\right|\le 0,$$

  and it follows that $\Delta G_3 \le 0$.

Due to symmetry, $\Delta G \le 0$ across $\nu+(\alpha+\beta)$.

Before we carry on with the last two interactions of this type, we prove the following proposition.

**Proposition 4.2.** *If $U_r$ is below the outgoing* 1*-wave for the interaction*

$$\mu+\nu+\alpha, \qquad\qquad \textit{or} \qquad\qquad \alpha+\nu+\mu,$$

*then the interaction can be replaced by*

$$\hat{\mu}+\hat{\alpha}, \qquad\qquad \textit{or} \qquad\qquad \hat{\alpha}+\hat{\mu}, \tag{4.6}$$

*respectively, where*

$$|\hat{\mu}\,|\le|\mu\,|, \qquad\qquad |\hat{\alpha}\,|\le|\alpha\,|, \tag{4.7}$$

*and $\Delta G \le 0$ for the replacement.*

*Proof.* Let us start with the second interaction. For $U_r$ to be below the outgoing 1-wave, $\mu$ has to cross $\alpha$. From property (iv) it then follows that $U_l$ can be connected to $U_r$ by following the wave $\alpha$ until the intersection point and then following $\mu$ from the

intersection point to $U_r$. Obviously, the estimates in (4.7) are then satisfied and from these it follows that $\Delta G \leq 0$.

Also for the first interaction $\alpha$ and $\mu$ have to intersect if $U_r$ is below the outgoing 1-wave. We are looking for a 1-shock wave, $\hat{\alpha}$, which ends at $U_r$ and starts somewhere on $\mu$. By property (viii) it follows that $\hat{\alpha}$ has to start to the left of the intersection point between $\mu$ and $\alpha$, but to the right of the starting point of $\alpha$. Thus, there exist a $\hat{\mu}$ and an $\hat{\alpha}$ so that (4.7) is satisfied and the interaction can be replaced by $\hat{\mu} + \hat{\alpha}$. From (4.7) we obtain $\Delta G \leq 0$. □

(vii) $(\mu + \nu) + \alpha$ (and $\beta + (\mu + \nu)$): This interaction has four possible outcomes.

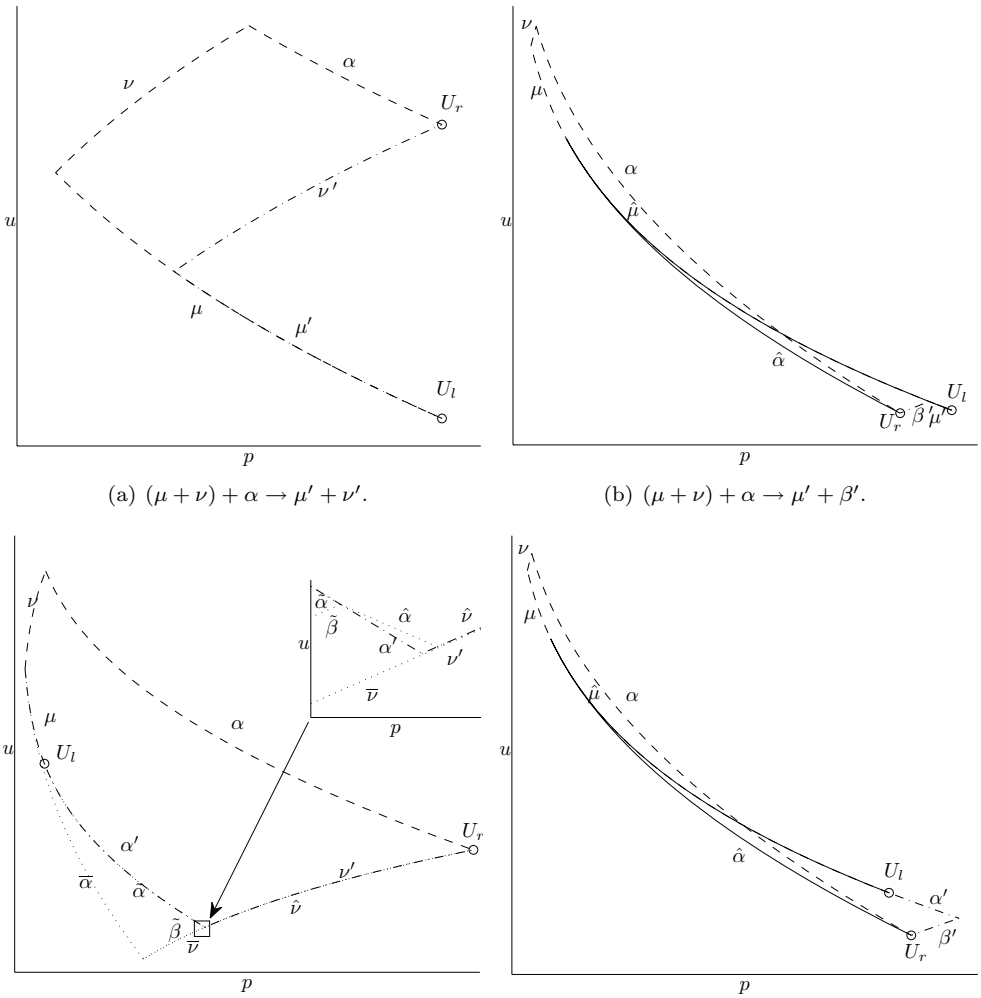


(a) $(\mu + \nu) + \alpha \to \mu' + \nu'$.

(b) $(\mu + \nu) + \alpha \to \mu' + \beta'$.

(c) $(\mu + \nu) + \alpha \to \alpha' + \nu'$.

(d) $(\mu + \nu) + \alpha \to \alpha' + \beta'$.

FIGURE 18. The interaction $(\mu + \nu) + \alpha$.

- $(\mu+\nu)+\alpha \to \mu'+\nu'$: In this case $U_r$ is above $\mu'$ and to the left of the 3-rarefaction curve starting at $U_l$, see Figure 18(a). Observe that $|\mu'| \leq |\mu|$ and $|\nu'| \leq |\alpha|$. It

then follows that

$$\begin{aligned}\Delta F &= -\,|\alpha\,|\,,\\ \Delta Q_1 &\le 0,\\ \Delta Q_2 &\le |\nu'\,|\,F_\gamma \le |\alpha\,|\,F_\gamma,\end{aligned}$$

and we obtain $\Delta G \le 0$.

- $(\mu+\nu)+\alpha \to \mu'+\beta'$: In this case $U_r$ is below $\mu'$ and to the left of the 3-shock curve starting at $U_l$, see Figure 18(b). By Proposition 4.2 we can replace this interaction by a new one,

$$\mu+\nu+\alpha \xrightarrow{\Delta G_1} [\hat\mu+\hat\alpha] \xrightarrow{\Delta G_2} \mu'+\beta',$$

where $\Delta G_1 \le 0$. Moreover, the interaction at the second step is of type Ba-iii, thus $\Delta G_2 \le 0$.

- $(\mu+\nu)+\alpha \to \alpha'+\nu'$: In this case $U_r$ is above $\alpha'$ and to the right of the 3-rarefaction wave starting at $U_l$, see Figure 18(c). We divide this interaction into four steps,

$$\begin{aligned}\mu+[\nu+\alpha] &\xrightarrow{\Delta G_1} [\mu+\overline\alpha]+\overline\nu\\ &\xrightarrow{\Delta G_2} \tilde\alpha+[\tilde\beta+\overline\nu]\\ &\xrightarrow{\Delta G_3} \tilde\alpha+\hat\alpha+\hat\nu\\ &\xrightarrow{\Delta G_4} \alpha'+\nu',\end{aligned}$$

where the interaction at the first step is of type Bb-iii, thus $\Delta G_1 \le 0$. Furthermore, $\Delta G_2 \le 0$ and $\Delta G_3 \le 0$ because the interactions at the second and third step are both of type Ba-iii. From properties (iv) and (viii) we obtain

$$|\alpha'\,| - |\tilde\alpha\,| - |\hat\alpha\,| = -q, \qquad\qquad |\nu'\,| - |\hat\nu\,| = q,$$

thus $\Delta G_4 \le 0$.

- $(\mu+\nu)+\alpha \to \alpha'+\beta'$: In this case $U_r$ is below $\alpha'$ and to the right of the 3-shock wave starting at $U_l$, see Figure 18(d). From Proposition 4.2 we know that the interaction can be replaced by $\hat\mu+\hat\alpha$,

$$\mu+\nu+\alpha \xrightarrow{\Delta G_1} [\hat\mu+\hat\alpha] \xrightarrow{\Delta G_2} \alpha'+\beta',$$

where $\Delta G_1 \le 0$. The interaction at the second step is of type Ba-iii and therefore $\Delta G_2 \le 0$.

By symmetry we have $\Delta G \le 0$ across $\beta+(\mu+\nu)$.

(viii) $(\alpha+\nu)+\mu$ (and $\nu+(\mu+\beta)$): This interaction has four possible outcomes.

- $(\alpha+\nu)+\mu \to \mu'+\nu'$: In this case $U_r$ is above $\mu'$ and to the left of the 3-rarefaction wave starting at $U_l$, see Figure 19(a). We divide this interaction into two steps,

$$\alpha+[\nu+\mu] \xrightarrow{\Delta G_1} \alpha+\overline\mu+\overline\nu \xrightarrow{\Delta G_2} \mu'+\nu',$$

where the interaction at the first step is of type Bb-i, thus $\Delta G_1 \le 0$. By property (vi) we have that $\overline\mu$ lies below $\alpha$, and therefore $|\nu'\,| \le |\overline\nu\,|$. Since also $|\mu'\,| \le |\overline\mu\,|$, we get $\Delta G_2 \le 0$.

- $(\alpha+\nu)+\mu \to \mu'+\beta'$: In this case $U_r$ is below $\mu'$ and to the left of the 3-shock wave starting at $U_l$, see Figure 19(b). According to Proposition 4.2 the interaction can be replaced by a new one,

$$\alpha+\nu+\mu \xrightarrow{\Delta G_1} [\hat\alpha+\hat\mu] \xrightarrow{\Delta G_2} \mu'+\beta',$$

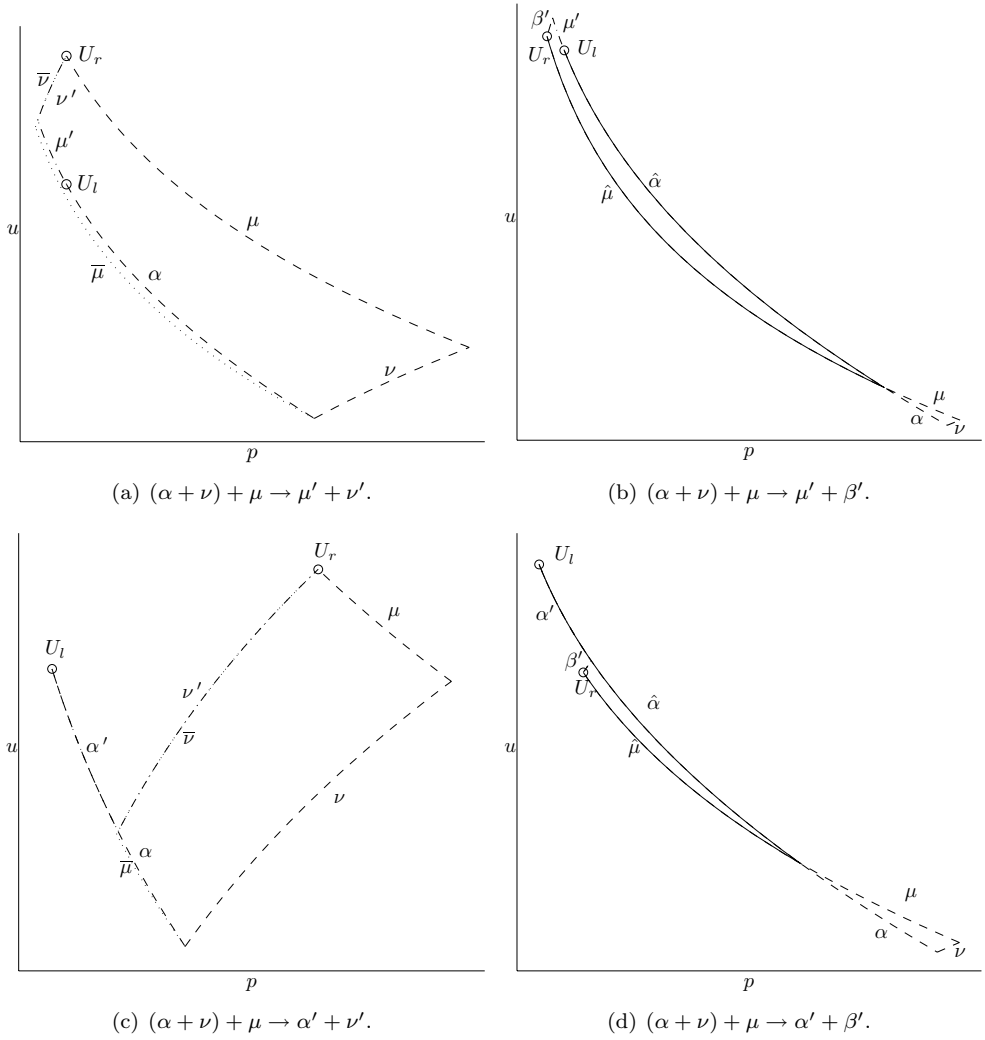


(a) $(\alpha+\nu)+\mu \to \mu'+\nu'$.

(b) $(\alpha+\nu)+\mu \to \mu'+\beta'$.

(c) $(\alpha+\nu)+\mu \to \alpha'+\nu'$.

(d) $(\alpha+\nu)+\mu \to \alpha'+\beta'$.

FIGURE 19. The interaction $(\alpha+\nu)+\mu$.

where $\Delta G_1 \le 0$. Furthermore, $\Delta G_2 \le 0$ because the interaction at the second step is of type Ba-ii.

- $(\alpha+\nu)+\mu \to \alpha'+\nu'$: In this case $U_r$ is above $\alpha'$ and to the right of the 3-rarefaction wave starting at $U_l$, see Figure 19(c). This interaction is divided into two steps,

$$\alpha + [\nu+\mu] \xrightarrow{\Delta G_1} \alpha + \overline{\mu} + \overline{\nu} \xrightarrow{\Delta G_2} \alpha' + \nu',$$

where the first interaction is of type Bb-i, thus $\Delta G_1 \le 0$. We have $|\alpha'| \le |\alpha|$. Since $\overline{\mu}$ lies below $\alpha$ by property (vi), we furthermore have $|\nu'| \le |\overline{\nu}|$, and thus, $\Delta G_2 \le 0$.

- $(\alpha+\nu)+\mu \to \alpha'+\beta'$: In this case $U_r$ is below $\alpha'$ and to the right of the 3-shock wave starting at $U_l$, see Figure 19(d). Again we can replace the interaction by a

new one,

$$\alpha+\nu+\mu \xrightarrow{\Delta G_1} [\hat{\alpha}+\hat{\mu}] \xrightarrow{\Delta G_2} \alpha'+\beta',$$

where $\Delta G_1 \le 0$ by Proposition 4.2. At the second step we have an interaction of type Ba-ii, thus $\Delta G_2 \le 0$.

It follows from symmetry that $\Delta G \le 0$ across $\nu+(\mu+\beta)$.

4.3.2. *Type* Cb*: A contact discontinuity as the leftmost or rightmost wave.* All these interactions have two possible outcomes.

(i) $(\zeta+\nu)+\mu$ (and $\nu+(\mu+\zeta)$):

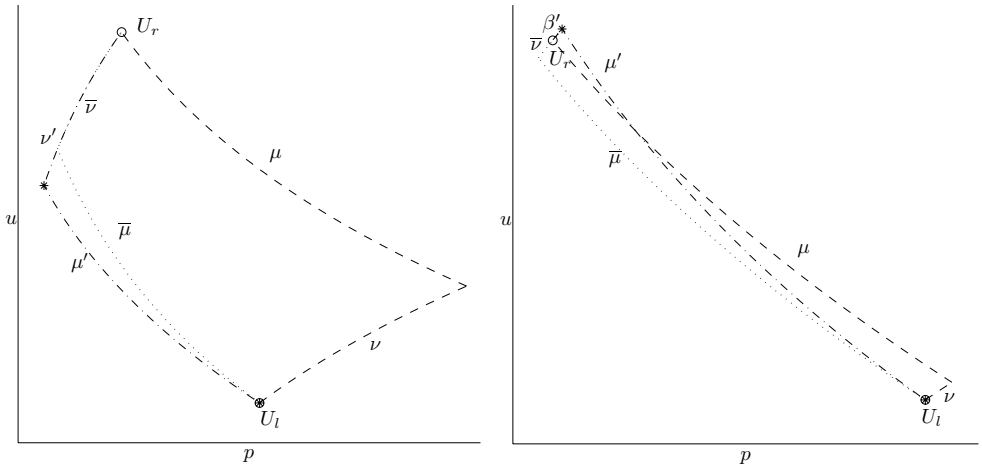


(a) $(\zeta+\nu)+\mu \to \mu'+\zeta+\nu'$. (b) $(\zeta+\nu)+\mu \to \mu'+\zeta+\beta'$.

FIGURE 20. The interaction $(\zeta+\nu)+\mu$.

- $(\zeta+\nu)+\mu \to \mu'+\zeta+\nu'$: In this case $U_r$ lies above $\mu'$, see Figure 20(a). We divide the interaction into two steps

$$\zeta+[\nu+\mu] \xrightarrow{\Delta G_1} \zeta+\overline{\mu}+\overline{\nu} \xrightarrow{\Delta G_2} \mu'+\zeta+\nu'.$$

The interaction at the first step is of type Bb-i and thus $\Delta G_1 \le 0$. If the intersection between $\overline{\mu}$ and $\overline{\nu}$ is below $\mu'$, then $|\mu'| \le |\overline{\mu}|$ and $|\nu'| \le |\overline{\nu}|$ and $\Delta G_2 \le 0$. If the intersection is above $\mu'$, then $|\mu'|-|\overline{\mu}| = |\nu'|-|\overline{\nu}|$ and by using Lemma 2.2 on $\overline{\mu}$ and $\mu'$ we get

$$|\mu'|-|\overline{\mu}| \le C_2\,|\overline{\mu}|\,|\zeta|, \qquad |\nu'|-|\overline{\nu}| \le C_2\,|\overline{\mu}|\,|\zeta|,$$

and hence, $\Delta G_2 \le 0$.

- $(\zeta+\nu)+\mu \to \mu'+\zeta+\beta'$: In this case $U_r$ lies below $\mu'$, see Figure 20(b). We divide the interaction into two steps,

$$\zeta+[\nu+\mu] \xrightarrow{\Delta G_1} \zeta+\overline{\mu}+\overline{\nu} \xrightarrow{\Delta G_2} \mu'+\zeta+\beta'.$$

The interaction at the first step is of type Bb-i and we have $\Delta G_1 \le 0$. Furthermore, we have $|\beta'| \le |\overline{\mu}|-|\mu'|$ and applying Lemma 2.2 on $\overline{\mu}$ and $\mu'$ we obtain

$$|\mu'|-|\overline{\mu}| \le 0, \qquad |\beta'| \le C_2\,|\mu'|\,|\zeta| \le C_2\,|\overline{\mu}|\,|\zeta|,$$

from which we get $\Delta G_2 \leq 0$.

Due to symmetry, $\Delta G \leq 0$ across $\nu + (\mu + \zeta)$.

(ii) $(\zeta + \nu) + \alpha$ (and $\beta + (\mu + \zeta)$):

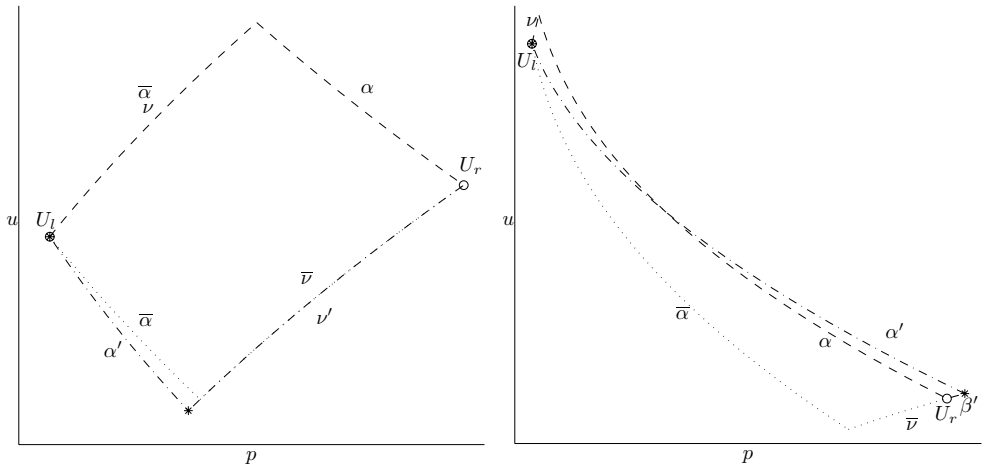


(a) $(\zeta + \nu) + \alpha \to \alpha' + \zeta + \nu'$.

(b) $(\zeta + \nu) + \alpha \to \alpha' + \zeta + \beta'$.

FIGURE 21. The interaction $(\zeta + \nu) + \alpha$.

- $(\zeta + \nu) + \alpha \to \alpha' + \zeta + \nu'$: In this case $U_r$ is above $\alpha'$, see Figure 21(a). We divide the interaction into two steps,

$$\zeta + [\nu + \alpha] \xrightarrow{\Delta G_1} \zeta + \overline{\alpha} + \overline{\nu} \xrightarrow{\Delta G_2} \alpha' + \zeta + \nu'.$$

  At the first step we have an interaction of type Bb-iii, thus $\Delta G_1 \leq 0$. If the intersection between $\overline{\alpha}$ and $\overline{\nu}$ is above $\alpha'$ as in Figure 21(a), then we have

$$|\alpha'| - |\overline{\alpha}| = -q, \qquad |\nu'| - |\overline{\nu}| = q,$$

  which results in $\Delta G_2 \leq 0$. If the intersection is below, we use Lemma 2.2 on $\overline{\alpha}$ and $\alpha'$, and get

$$|\alpha'| - |\overline{\alpha}| \leq C_2 |\zeta| |\overline{\alpha}|, \qquad |\nu'| - |\overline{\nu}| \leq 0,$$

  therefore, $\Delta G_2 \leq 0$.
- $(\zeta + \nu) + \alpha \to \alpha' + \zeta + \beta'$: In this case $U_r$ is below $\alpha'$, see Figure 21(b). We divide the interaction into two steps,

$$\zeta + [\nu + \alpha] \xrightarrow{\Delta G_1} \zeta + \overline{\alpha} + \overline{\nu} \xrightarrow{\Delta G_2} \alpha' + \zeta + \beta'.$$

  Since the interaction at the first step is of type Bb-iii we have $\Delta G_1 \leq 0$, and by construction $|\beta'| \leq |\alpha'| - |\overline{\alpha}|$. We apply Lemma 2.2 on $\overline{\alpha}$ and $\alpha'$ and find

$$|\alpha'| - |\overline{\alpha}| \leq C_2 |\zeta| |\overline{\alpha}|, \qquad |\beta'| \leq C_2 |\zeta| |\overline{\alpha}|,$$

  thus $\Delta G_2 \leq 0$.

By symmetry we have $\Delta G \leq 0$ across $\beta + (\mu + \zeta)$.

(iii) $(\zeta + \beta) + \mu$ (and $\nu + (\alpha + \zeta)$):

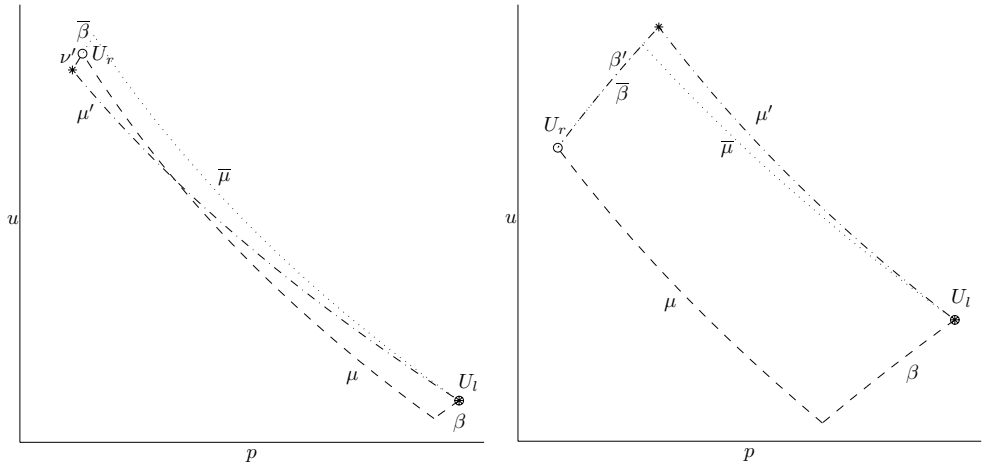


(a) $(\zeta+\beta)+\mu \to \mu'+\zeta+\nu'$. (b) $(\zeta+\beta)+\mu \to \mu'+\zeta+\beta'$.

FIGURE 22. The interaction $(\zeta+\beta)+\mu$.

- $(\zeta+\beta)+\mu \to \mu'+\zeta+\nu'$: In this case $U_r$ is above $\mu'$, see Figure 22(a). Two steps are enough,

$$\zeta+[\beta+\mu] \xrightarrow{\Delta G_1} \zeta+\overline{\mu}+\overline{\beta} \xrightarrow{\Delta G_2} \mu'+\zeta+\nu',$$

where the interaction at the first step is of type Bb-iii, thus $\Delta G_1 \le 0$. We have $|\nu'| \le |\mu'| - |\overline{\mu}|$ and apply Lemma 2.2 on $\overline{\mu}$ and $\mu'$. We get

$$|\mu'| - |\overline{\mu}| \le C_2 |\overline{\mu}|\,|\zeta|, \qquad |\nu'| \le C_2 |\overline{\mu}|\,|\zeta|,$$

and it follows that $\Delta G_2 \le 0$.

- $(\zeta+\beta)+\mu \to \mu'+\zeta+\beta'$: In this case $U_r$ is below $\mu'$, see Figure 22(b). This interaction is divided into two steps,

$$\zeta+[\beta+\mu] \xrightarrow{\Delta G_1} \zeta+\overline{\mu}+\overline{\beta} \xrightarrow{\Delta G_2} \mu'+\zeta+\nu,$$

where $\Delta G_1 \le 0$ because the interaction at the first step is of type Bb-iii. If the intersection between $\overline{\mu}$ and $\overline{\beta}$ is above $\mu'$, it follows from property (ix) that

$$|\mu'| - |\overline{\mu}| = q, \qquad |\beta'| - \left|\overline{\beta}\right| = -q,$$

thus, $\Delta G_2 \le 0$. If the intersection is below, as in Figure 22(b), it follows from property (ix) that $|\mu'| \le |\overline{\mu}|$. We then use Lemma 2.2 on $\overline{\beta}$ and $\beta'$ and obtain

$$|\mu'| - |\overline{\mu}| \le 0, \qquad |\beta'| - \left|\overline{\beta}\right| \le C_2 |\zeta|\,\left|\overline{\beta}\right|,$$

thus, $\Delta G_2 \le 0$.

Due to symmetry, $\Delta G \le 0$ across $\nu+(\alpha+\zeta)$.

(iv) $(\zeta+\beta)+\alpha$ (and $\beta+(\alpha+\zeta)$):

- $(\zeta+\beta)+\alpha \to \alpha'+\zeta+\nu'$: In this case $U_r$ is above $\alpha'$, see Figure 23(a). We can divide the interaction into steps by the same approach as above, but this is not necessary for this interaction. We have $|\alpha'| - |\alpha| \le -|\nu'|$, thus

$$\Delta F = |\alpha'| - |\alpha| - |\beta| \le -|\nu'|,$$
$$\Delta Q_1 \le 0,$$

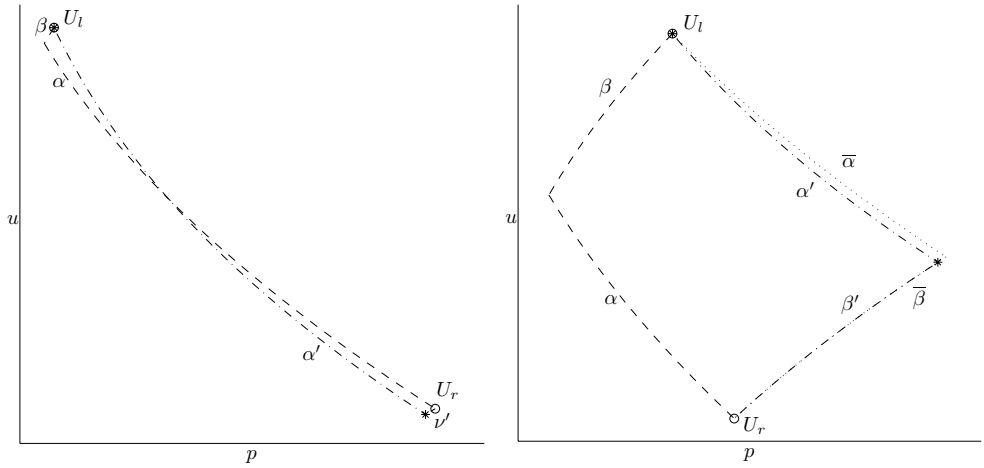


(a) $(\zeta+\beta)+\alpha \to \alpha'+\zeta+\nu'$. (b) $(\zeta+\beta)+\alpha \to \alpha'+\zeta+\beta'$.

FIGURE 23. The interaction $(\zeta+\beta)+\alpha$.

$$\Delta Q_2 \le |\nu'|\, F_\gamma,$$

which yields $\Delta G \le 0$.

- $(\zeta+\beta)+\alpha \to \alpha'+\zeta+\beta'$: In this case $U_r$ is below $\alpha'$, see Figure 23(b). Again we divide into two steps

$$\zeta+[\beta+\alpha] \xrightarrow{\Delta G_1} \zeta+\overline{\alpha}+\overline{\beta} \xrightarrow{\Delta G_2} \alpha'+\zeta+\beta',$$

where the interaction at the first step is of type Bb-iii with $\Delta G_1 \le 0$. If the intersection between $\overline{\alpha}$ and $\overline{\beta}$ is above $\alpha'$, as in Figure 23(b), it follows from property (viii) and property (ix) that

$$|\alpha'| - |\overline{\alpha}| \le 0, \qquad |\beta'| - \left|\overline{\beta}\right| \le 0,$$

hence, $\Delta G_2 \le 0$. If the intersection is below, we have $|\alpha'| - |\overline{\alpha}| = |\beta'| - \left|\overline{\beta}\right|$ and by applying Lemma 2.2 to the 1-shock curves we obtain

$$|\alpha'| - |\overline{\alpha}| \le C_2\,|\overline{\alpha}|\,|\zeta|, \qquad |\beta'| - \left|\overline{\beta}\right| \le C_2\,|\overline{\alpha}|\,|\zeta|.$$

From these estimates we obtain $\Delta G_2 \le 0$.

By symmetry we have $\Delta G \le 0$ across the interaction $\beta+(\alpha+\zeta)$.

4.3.3. *Type* Cc*: A contact discontinuities as the middle wave.*

(i) $(\mu_1+\zeta)+\mu_2$ (and $\nu_1+(\zeta+\nu_2)$): This interaction has two possible outcomes.

- $(\mu_1+\zeta)+\mu_2 \to \mu'+\zeta+\nu'$: In this case $U_r$ is above $\mu'$, see Figure 24(a). We divide the interaction into two steps,

$$\mu_1+[\zeta+\mu_2] \xrightarrow{\Delta G_1} \mu_1+\overline{\mu}+\zeta+\overline{\nu} \xrightarrow{\Delta G_2} \mu'+\zeta+\nu'.$$

The interaction at the first step is of type Bc-i, thus $\Delta G_1 \le 0$. Note that $\mu_1$, $\overline{\mu}$ and $\mu'$ all have $\gamma=\gamma_l$, and $\overline{\nu}$ and $\nu'$ have $\gamma=\gamma_r$. By property (iv) and property (vii) we therefore have $\mu_1+\overline{\mu}=\mu'$ and $\overline{\nu}=\nu$, thus $\Delta G_2 = 0$.

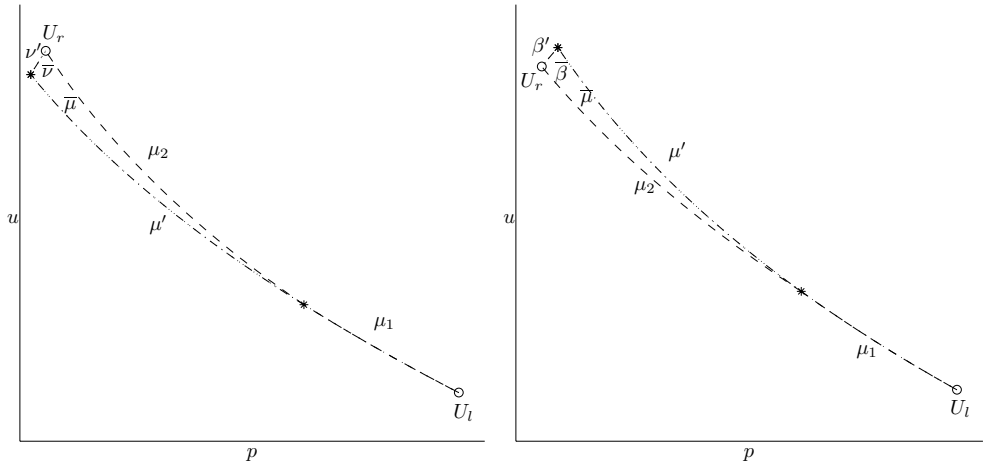


(a) $(\mu_1+\zeta)+\mu_2 \to \mu'+\zeta+\nu'$ (b) $(\mu_1+\zeta)+\mu_2 \to \mu'+\zeta+\beta'$

FIGURE 24. The interaction $(\mu_1+\zeta)+\mu_2$.

- $(\mu_1+\zeta)+\mu_2 \to \mu'+\zeta+\beta'$: In this case $U_r$ lies below $\mu'$, see Figure 24(b). This interaction is divided into two steps,

$$\mu_1+[\zeta+\mu_2] \xrightarrow{\Delta G_1} \mu_1+\overline{\mu}+\zeta+\overline{\beta} \xrightarrow{\Delta G_2} \mu'+\zeta+\beta'.$$

The interaction at the first step is of type Bc-i with $\Delta G_1 \le 0$. Furthermore, $\mu_1$, $\overline{\mu}$ and $\mu'$ all have the same $\gamma$, and so do $\overline{\beta}$ and $\beta'$. Property (iv) and property (vii) then imply that $\mu_1+\overline{\mu}=\mu'$, therefore we also have that $\overline{\beta}=\beta'$, and it follows that $\Delta G_2 = 0$.

Due to symmetry, $\Delta G \le 0$ across the interaction $\nu_1+(\zeta+\nu_2)$ as well.

(ii) $(\alpha_1+\zeta)+\alpha_2$ (and $\beta_1+(\zeta+\beta_2)$): This interaction has two possible outcomes.

- $(\alpha_1+\zeta)+\alpha_2 \to \alpha'+\zeta+\nu'$: In this case $U_r$ is above $\alpha'$, see Figure 25(a). No extra steps are needed because we have

$$|\alpha'|-|\alpha_1|-|\alpha_2|=-|\nu'|,$$

which gives us

$$\begin{aligned}\Delta F &= -|\nu|,\\ \Delta Q_1 &\le 0,\\ \Delta Q_2 &\le |\nu'|F_\gamma - |\zeta||\alpha_2| \le |\nu'|F_\gamma,\end{aligned}$$

and

$$\Delta G \le |\nu'|(-1+3C_2F_\gamma) \le |\nu'|\left(-1+\frac{C}{3}\right) \le 0.$$

- $(\alpha_1+\zeta)+\alpha_2 \to \alpha'+\zeta+\beta'$. In this case $U_r$ is below $\alpha'$, see Figure 25(b). In this case we need two steps,

$$\alpha_1+[\zeta+\alpha_2] \xrightarrow{\Delta G_1} \alpha_1+\overline{\alpha}+\zeta+\overline{\beta} \xrightarrow{\Delta G_2} \alpha'+\zeta+\beta'.$$

The interaction at the first step is of type Bc-ii, thus $\Delta G_1 \le 0$. Note that $\overline{\alpha}$ and $\alpha'$ have the same $\gamma$, and so do $\overline{\beta}$ and $\beta'$. It therefore follows from property (viii)

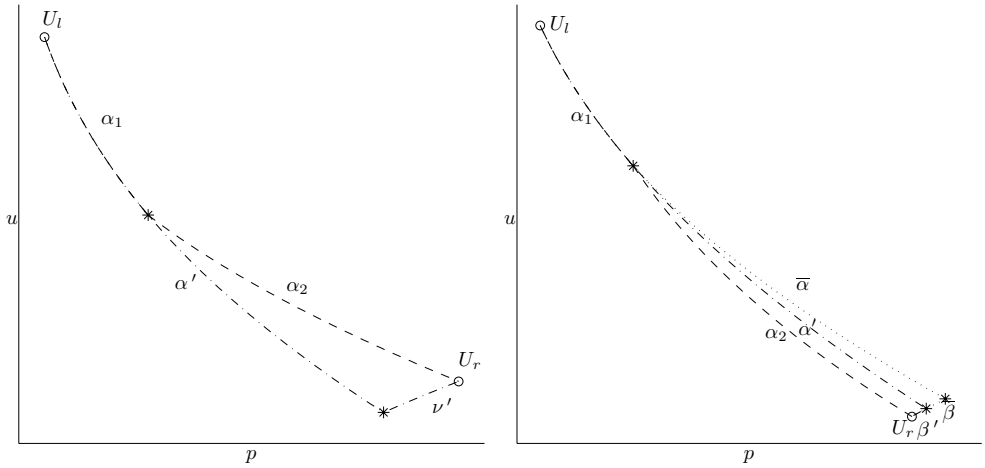


(a) $(\alpha_1 + \zeta) + \alpha_2 \to \alpha' + \zeta + \nu'$ (b) $(\alpha_1 + \zeta) + \alpha_2 \to \alpha' + \zeta + \beta'$

FIGURE 25. The interaction $(\alpha_1 + \zeta) + \alpha_2$.

and property (ix) that the intersection point between $\overline{\alpha}$ and $\overline{\beta}$ is to the right of the intersection point between $\alpha'$ and $\beta'$. This yields

$$|\alpha'| - |\alpha_1| - |\overline{\alpha}| \le 0, \qquad |\beta'| - |\overline{\beta}| \le 0,$$

and we obtain $\Delta G_2 \le 0$.

By symmetry it follows that $\Delta G \le 0$ across the interaction $\beta_1 + (\zeta + \beta_2)$.

Before discussing the last interactions of this type, we prove a useful proposition.

**Proposition 4.3.** *If $U_r$ is below the outgoing* 1*-wave for the interactions*

$$\mu + \zeta + \alpha, \qquad \text{or} \qquad \alpha + \zeta + \mu,$$

*and if*

$$\zeta + \alpha \to \overline{\alpha} + \zeta + \overline{\nu}, \qquad \text{or} \qquad \zeta + \mu \to \overline{\mu} + \zeta + \overline{\nu},$$

*respectively, then $U_l$ can be connected to $U_r$ by*

$$\hat{\mu} + \hat{\alpha} + \zeta, \qquad \text{or} \qquad \hat{\alpha} + \hat{\mu} + \zeta, \tag{4.8}$$

*respectively, where*

$$|\hat{\mu}| \le |\mu|, \qquad \text{and} \qquad |\hat{\alpha}| \le |\alpha|, \tag{4.9}$$

*and $\Delta G \le 0$ for the replacement.*

*Proof.* For the first interaction we are looking for a 1-shock wave, $\hat{\alpha}$, with $\gamma = \gamma_l$ that is starting somewhere at $\mu$ and ending at $\hat{U} = (p_r, u_r, \gamma_l)$. From property (viii) it follows that $\hat{\alpha}$ cannot reach $\hat{U}$ if it starts to the left of $\overline{\alpha}$. Moreover, since $U_r$ lies below any 1-wave starting at $U_l$, so does $\hat{U}$, and therefore $\hat{\alpha}$ has to start to the right of $U_l$. This proves that there exists a $\hat{\mu}$ and an $\hat{\alpha}$ so that $U_l$ is connected to $U_r$ by the first interaction of (4.8) and so that (4.9) is satisfied. From (4.9) it follows that $\Delta G \le 0$ for the replacement.

For the second interaction consider the backward 1-rarefaction curve from $\hat{U}$. By property (iv) this wave will stay above $\overline{\mu}$ and, since $\hat{U}$ lies below any 1-wave starting

at $U_l$, the backward rarefaction curve must intersect $\alpha$. Thus, there exists a $\hat{\mu}$ and an $\hat{\alpha}$ so that $U_l$ is connected to $U_r$ by the second interaction of (4.8) and so that (4.9) is satisfied. Furthermore, it follows from (4.9) that $\Delta G \leq 0$ for the replacement. □

(iii) $(\mu + \zeta) + \alpha$ (and $\beta + (\zeta + \nu)$): This interaction has four different outcomes.

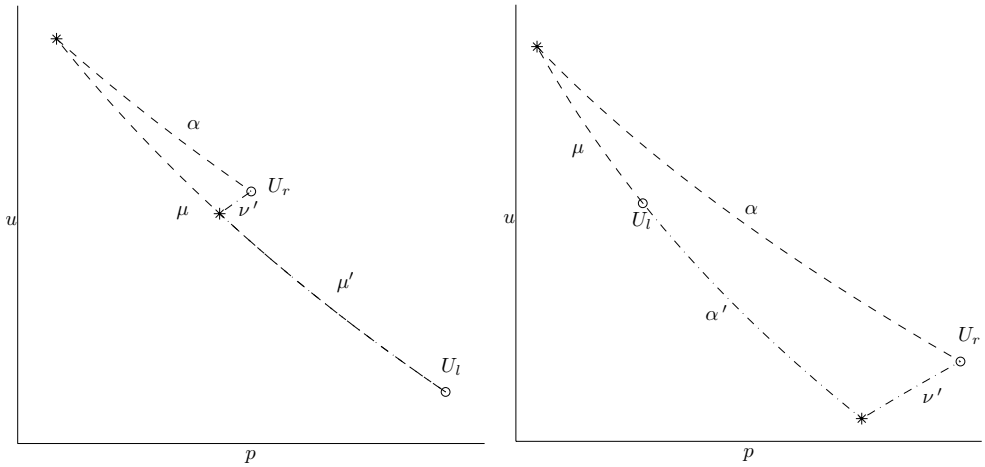


(a) $(\mu + \zeta) + \alpha \to \mu' + \zeta + \nu'$. (b) $(\mu + \zeta) + \alpha \to \alpha' + \zeta + \nu'$.

FIGURE 26. Two outcomes of the interaction $(\mu + \zeta) + \alpha$.

- $(\mu+\zeta)+\alpha \to \mu'+\zeta+\nu'$: In this case $U_r$ is above $\mu$ and to the left of the 3-rarefaction curve starting at $U_l$, see Figure 26(a). We have $|\mu'| \leq |\mu|$ and $|\nu'| \leq |\alpha|$, thus

$$\begin{aligned} \Delta F &= -|\alpha|, \\ \Delta Q_1 &\leq 0, \\ \Delta Q_2 &\leq |\nu'| F_\gamma \leq |\alpha| F_\gamma, \end{aligned}$$

  which gives

$$\Delta G \leq |\alpha| (-1 + 3C_2 F_\gamma) \leq |\alpha| \left(-1 + \frac{C}{3}\right) \leq 0.$$

- $(\mu + \zeta) + \alpha \to \mu' + \zeta + \beta'$: In this case $U_r$ is below $\mu'$ and to the left of the 3-shock curve starting at $U_l$, see Figure 27. This interaction needs several steps, and it is natural to let $\zeta$ and $\alpha$ interact first. We do not know what type of outgoing 3-wave this interaction gives, and we will have to look at each case separately. Assume first that $\zeta + \alpha \to \overline{\alpha} + \zeta + \overline{\beta}$, as in Figure 27(a), then we have

$$\begin{aligned} \mu + [\zeta + \alpha] &\xrightarrow{\Delta G_1} [\mu + \overline{\alpha}] + \zeta + \overline{\beta} \\ &\xrightarrow{\Delta G_2} \tilde{\mu} + \tilde{\beta} + \zeta + \overline{\beta} \\ &\xrightarrow{\Delta G_3} \mu' + \zeta + \beta'. \end{aligned}$$

  The interaction at step one is of type Bc-ii, therefore $\Delta G_1 \leq 0$. At the second step the interaction is of type Ba-iii, thus $\Delta G_2 \leq 0$. We do not know whether $\tilde{\beta}$

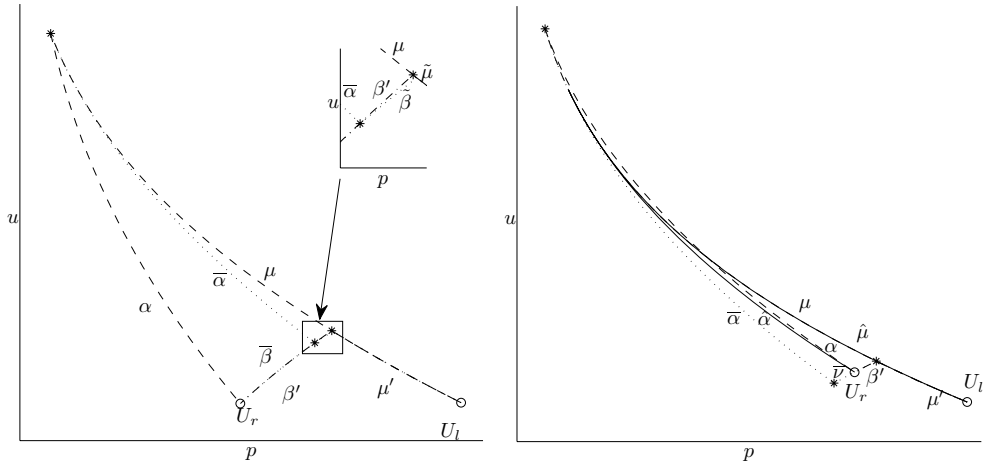


(a) When $\zeta + \alpha \to \overline{\alpha} + \zeta + \overline{\beta}$.

(b) When $\zeta + \alpha \to \overline{\alpha} + \zeta + \overline{\nu}$.

FIGURE 27. The interaction $(\mu + \zeta) + \alpha \to \mu' + \zeta + \beta'$.

starts to the left or the right of $\beta'$ because the two waves have different $\gamma$'s. If $\tilde{\beta}$ starts to the right, as in Figure 27(a), we have for a $q > 0$ that

$$|\mu'| - |\tilde{\mu}| \le q, \qquad |\beta'| - \left|\tilde{\beta}\right| - \left|\overline{\beta}\right| = -q,$$

which gives

$$\Delta F = -q, \qquad \Delta Q_1 \le 0, \qquad \Delta Q_2 \le q F_\gamma,$$

and it follows that $\Delta G_3 \le 0$. If $\tilde{\beta}$ starts to the left of $\beta'$, we claim that

$$|\mu'| - |\tilde{\mu}| \le 0, \qquad |\beta'| - \left|\overline{\beta}\right| - \left|\tilde{\beta}\right| \le C_2 \left|\tilde{\beta}\right| |\zeta|, \tag{4.10}$$

which gives us

$$\begin{aligned} \Delta F &\le C_2 \left|\tilde{\beta}\right| |\zeta|, \\ \Delta Q_1 &\le C_2 \left|\tilde{\beta}\right| |\zeta| F_n, \\ \Delta Q_2 &\le C_2 \left|\tilde{\beta}\right| |\zeta| F_\gamma - \left|\tilde{\beta}\right| |\zeta|, \end{aligned}$$

and furthermore that

$$\Delta G_3 \le C_2 \left|\tilde{\beta}\right| |\zeta| (1 + 3C_1(\overline{\gamma} - 1) F_n + 3C_2 F_\gamma - 3) \le 0.$$

Thus, we just have to prove (4.10). We introduce a 3-shock curve with $\gamma = \gamma_r$, $\beta^*$, that starts somewhere on $\mu$ and ends at the same point as $\tilde{\beta}$ ends. Since $\beta^*$ has the same $\gamma$ as $\beta'$, it follows from property (ix) that $\beta^*$ starts to the right of $\beta'$, thus $|\beta'| - \left|\tilde{\beta}\right| - \left|\overline{\beta}\right| \le |\beta^*| - \left|\tilde{\beta}\right|$. Moreover, $\beta^*$ and $\tilde{\beta}$ have different $\gamma$'s and ends at the same point, therefore we can apply Lemma 2.2 on the two shock waves and obtain $|\beta^*| - \left|\tilde{\beta}\right| \le C_2 \left|\tilde{\beta}\right| |\zeta|$. Since the estimate on the rarefaction waves follows directly from the construction, we have proved (4.10).

Assume now that $\zeta + \alpha \to \overline{\alpha} + \zeta + \overline{\nu}$, this is illustrated in Figure 27(b). By Proposition 4.3 we can replace the interaction by a new one,

$$\begin{aligned} \mu + \zeta + \alpha &\xrightarrow{\Delta G_1} [\hat{\mu} + \hat{\alpha}] + \zeta \\ &\xrightarrow{\Delta G_2} \tilde{\mu} + \tilde{\beta} + \zeta \\ &\xrightarrow{\Delta G_3} \mu' + \zeta + \beta', \end{aligned}$$

where $\Delta G_1 \leq 0$. The interaction at the second step is of type Ba-iii, thus $\Delta G_2 \leq 0$. If $\tilde{\beta}$ starts to the right of $\beta'$, we have for a $q > 0$ that

$$|\mu'| - |\tilde{\mu}| = q, \qquad |\beta'| - \left|\tilde{\beta}\right| = -q,$$

which gives $\Delta G_3 \leq 0$. If $\tilde{\beta}$ starts to the right of $\beta'$, we have $|\mu'| - |\tilde{\mu}| \leq 0$. Furthermore, since $\tilde{\beta}$ and $\beta'$ ends at the same point, but have different $\gamma$'s, it follows by applying Lemma 2.2 that

$$|\beta'| - \left|\tilde{\beta}\right| \leq C_2 \left|\tilde{\beta}\right| |\zeta|,$$

and we get $\Delta G_3 \leq 0$. Figure 27(b) do not show $\tilde{\beta}$ since it lies very close to $\beta'$.

- $(\mu + \zeta) + \alpha \to \alpha' + \zeta + \nu'$: In this case $U_r$ is above $\alpha'$ and to the right of the 3-rarefaction curve starting at $U_l$, see Figure 26(b). Since

$$|\alpha'| + |\nu'| \leq |\alpha|, \qquad \text{or} \qquad |\alpha'| - |\alpha| \leq -|\nu'|,$$

we have

$$\Delta F = -|\nu'|, \qquad \Delta Q_1 \leq 0, \qquad \Delta Q_2 \leq |\nu'| F_\gamma,$$

which gives

$$\Delta G \leq |\nu'| (-1 + 3C_2 F_\gamma) \leq |\nu'| \left(-1 + \frac{C}{3}\right) \leq 0.$$

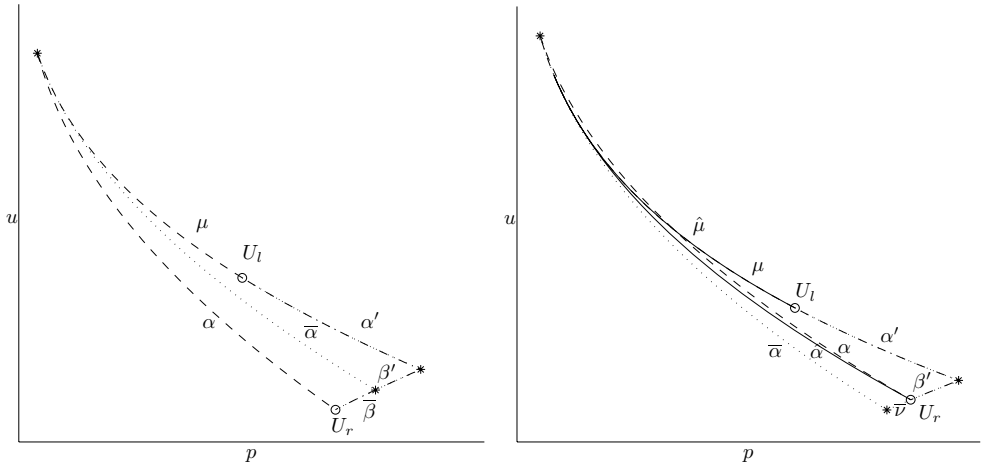


(a) When $\zeta + \alpha \to \overline{\alpha} + \zeta + \overline{\beta}$.

(b) When $\zeta + \alpha \to \overline{\alpha} + \zeta + \overline{\nu}$.

FIGURE 28. The interaction $(\mu + \zeta) + \alpha \to \alpha' + \zeta + \beta'$.

- $(\mu+\zeta)+\alpha \to \alpha'+\zeta+\beta'$: In this case $U_r$ is below $\alpha'$ and to the right of the 3-shock curve starting at $U_l$, see Figure 28. Again we do not know what type of outgoing 3-wave we get if $\zeta$ and $\alpha$ interact, and we need to consider each case separately. Assume first that $\zeta+\alpha \to \overline{\alpha}+\zeta+\overline{\beta}$, as illustrated in Figure 28(a), then we need four steps,

$$\begin{aligned}\mu+[\zeta+\alpha] &\xrightarrow{\Delta G_1} [\mu+\overline{\alpha}]+\zeta+\overline{\beta}\\ &\xrightarrow{\Delta G_2} \tilde{\alpha}+[\tilde{\beta}+\zeta+\overline{\beta}]\\ &\xrightarrow{\Delta G_3} \tilde{\alpha}+\hat{\alpha}+\zeta+\hat{\beta}\\ &\xrightarrow{\Delta G_4} \alpha'+\zeta+\beta'.\end{aligned}$$

  The interaction at the first step is of type Bc-ii, thus $\Delta G_1 \le 0$. At the second step the interaction is of type Ba-iii and $\Delta G_2 \le 0$. If $\tilde{\beta}$ starts to the right of $\beta'$, the remainding steps can be skipped because then

$$|\alpha'|-|\tilde{\alpha}| \le 0, \qquad |\beta'|-\left|\tilde{\beta}\right|-|\overline{\beta}| \le 0,$$

  and going straight to the last step we get $\Delta G_* \le 0$. If $\tilde{\beta}$ starts to the left of $\beta'$, we need one more step[2] and the interaction at the third step is of type Cc-ii, thus $\Delta G_3 \le 0$. The waves $\tilde{\alpha}$, $\hat{\alpha}$ and $\alpha'$ all have $\gamma=\gamma_l$ and $\hat{\beta}$ and $\beta'$ have $\gamma=\gamma_r$. Combining properties (viii) and (ix) it follows that

$$|\alpha'|-|\tilde{\alpha}|-|\hat{\alpha}| \le 0, \qquad |\beta'|-\left|\hat{\beta}\right| \le 0,$$

  and we have $\Delta G_4 \le 0$. The waves $\tilde{\alpha}$ and $\tilde{\beta}$ are not denoted in Figure 28(a) because they lie very close to $\alpha'$ and $\beta'$.
  Assume now that $\zeta+\alpha \to \overline{\alpha}+\zeta+\overline{\nu}$, see Figure 28(b). According to Proposition 4.3, we can replace the interaction with a new one,

$$\begin{aligned}\mu+\zeta+\alpha &\xrightarrow{\Delta G_1} [\hat{\mu}+\hat{\alpha}]+\zeta\\ &\xrightarrow{\Delta G_2} \tilde{\alpha}+\tilde{\beta}+\zeta\\ &\xrightarrow{\Delta G_3} \alpha'+\zeta+\beta',\end{aligned}$$

  where $\Delta G_1 \le 0$. At the second step we have an interaction of type Ba-iii with $\Delta G_2 \le 0$. If $\tilde{\beta}$ starts to the right of $\beta'$, we have

$$|\alpha'|-|\tilde{\alpha}| \le 0, \qquad |\beta'|-\left|\tilde{\beta}\right| \le 0,$$

  hence $\Delta G_3 \le 0$. If $\tilde{\beta}$ starts to the left of $\beta'$, we have $|\alpha'|-|\tilde{\alpha}| = |\beta'|-\left|\tilde{\beta}\right|$. Furthermore, since $\tilde{\beta}$ and $\beta'$ ends at the same point, but have different $\gamma$'s, it follows by applying Lemma 2.2 that

$$|\beta'|-\left|\tilde{\beta}\right| \le C_2\left|\tilde{\beta}\right||\zeta|,$$

  and therefore $\Delta G_3 \le 0$.

By symmetry it follows that $\Delta G \le 0$ across the interaction $\beta+(\zeta+\nu)$.

(iv) $(\alpha+\zeta)+\mu$ (and $\nu+(\zeta+\beta)$): This interaction has four different outcomes.

[2]Here we could compare $\tilde{\beta}$ to an auxiliary curve $\beta^*$ with $\gamma=\gamma_r$, similar to what we did before, but since only one more step is needed, we chose this approach.

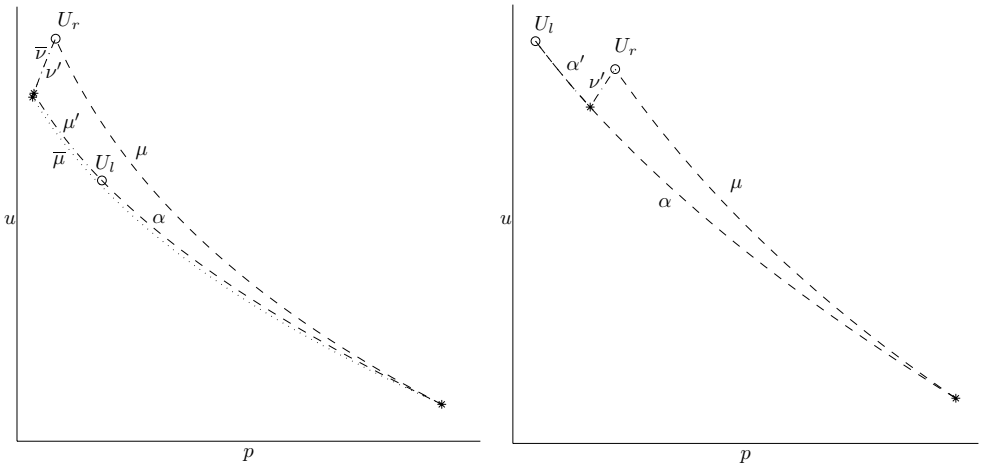


(a) $(\alpha+\zeta)+\mu \to \mu'+\zeta+\nu'$. (b) $(\alpha+\zeta)+\mu \to \alpha'+\zeta+\nu'$.

FIGURE 29. Two outcomes of the interaction $(\alpha+\zeta)+\mu$.

- $(\alpha+\zeta)+\mu \to \mu'+\zeta+\nu'$: In this case $U_r$ is above $\mu'$ and to the left of the 3-rarefaction wave starting at $U_l$, see Figure 29(a). We divide the interaction into two steps,

$$\alpha+[\zeta+\mu] \xrightarrow{\Delta G_1} \alpha+\overline{\mu}+\zeta+\overline{\nu} \xrightarrow{\Delta G_2} \mu'+\zeta+\nu',$$

where the interaction at the first step is of type Bc-i, thus $\Delta G_1 \le 0$. Since $\overline{\mu}$ has to lie below $\alpha$ by property (vi), the outgoing 3-wave of the first step is a rarefaction wave. From this it follows that

$$|\mu'|-|\overline{\mu}| \le 0, \qquad |\nu'|-|\overline{\nu}'| \le 0,$$

and therefore $\Delta G_2 \le 0$.

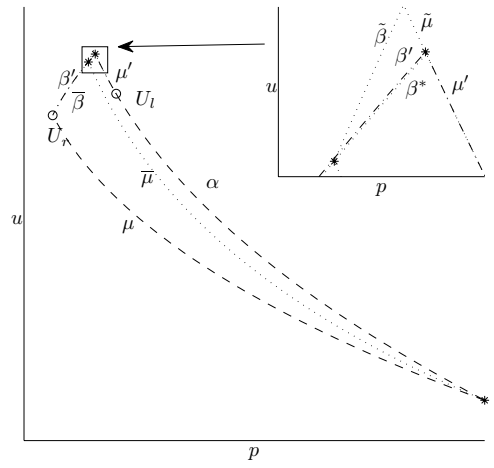


FIGURE 30. $(\alpha+\zeta)+\mu \to \mu'+\zeta+\beta'$.

- $(\alpha+\zeta)+\mu \to \mu'+\zeta+\beta'$: In this case $U_r$ is below $\mu'$ and to the left of the 3-rarefaction wave starting at $U_l$, see Figure 30. If $\zeta$ and $\mu$ interact we again do not know the type of the outgoing 3-wave we get, and we choose to look at the two cases separately. Assume first that the outgoing 3-wave is a shock wave as illustrated in Figure 30. Then we need three steps,

$$\begin{aligned}\alpha+[\zeta+\mu] &\xrightarrow{\Delta G_1} [\alpha+\overline{\mu}]+\zeta+\overline{\beta}\\ &\xrightarrow{\Delta G_2} \tilde{\mu}+\tilde{\beta}+\zeta+\overline{\beta}\\ &\xrightarrow{\Delta G_3} \mu'+\zeta+\beta'.\end{aligned}$$

  The interaction at the first step is of type Bc-i with $\Delta G_1 \le 0$. At the second step we have an interaction of type Ba-ii, thus $\Delta G_2 \le 0$. If $\tilde{\beta}$ starts to the right of $\beta'$, then

$$|\mu'|-|\tilde{\mu}| = q, \qquad |\beta'|-\left|\tilde{\beta}\right| = -q,$$

  and it follows that $\Delta G_3 \le 0$. If $\tilde{\beta}$ starts to the left of $\beta'$, as is the case in Figure 30, we once again introduce an auxiliary curve $\beta^*$, and this curve is indicated in the figure. This curve has $\gamma=\gamma_r$, starts somewhere along $\mu'$, and ends at the same point as $\tilde{\beta}$. By property (ix) the starting point of $\beta^*$ has to be to the right of $\beta'$, thus $|\beta'|-\left|\tilde{\beta}\right|-\left|\overline{\beta}\right| \le |\beta^*|-\left|\tilde{\beta}\right|$. Moreover, we apply Lemma 2.2 on $\tilde{\beta}$ and $\beta^*$, and get $|\beta^*|-\left|\tilde{\beta}\right| \le C_2\left|\tilde{\beta}\right||\zeta|$. Thus,

$$|\mu'|-|\tilde{\mu}| \le 0, \qquad |\beta'|-\left|\overline{\beta}\right|-\left|\tilde{\beta}\right| \le C_2\left|\tilde{\beta}\right||\zeta|,$$

  and $\Delta G_3 \le 0$.
  Assume now that the outgoing 3-wave of the interaction between $\zeta$ and $\mu$ is a rarefaction wave. According to Proposition 4.3 we can replace the interaction by a new one,

$$\begin{aligned}\alpha+\zeta+\mu &\xrightarrow{\Delta G_1} [\hat{\alpha}+\hat{\mu}]+\zeta\\ &\xrightarrow{\Delta G_2} \tilde{\mu}+\tilde{\beta}+\zeta\\ &\xrightarrow{\Delta G_3} \mu'+\zeta+\beta',\end{aligned}$$

  where $\Delta G_1 \le 0$. The interaction at the second step is of type Ba-ii, thus $\Delta G_2 \le 0$. If $\tilde{\beta}$ starts to the right of $\beta'$, we have

$$|\mu'|-|\tilde{\mu}| = q, \qquad |\beta'|-\left|\tilde{\beta}\right| = -q,$$

  which gives $\Delta G_3 \le 0$. If $\tilde{\beta}$ starts to the right of $\beta'$, we have $|\mu'|-|\tilde{\mu}| \le 0$. Furthermore, since $\tilde{\beta}$ and $\beta'$ end at the same point and have different $\gamma$'s, it follows by applying Lemma 2.2 that

$$|\beta'|-\left|\tilde{\beta}\right| \le C_2\left|\tilde{\beta}\right||\zeta|,$$

  and we get $\Delta G_3 \le 0$.
- $(\alpha+\zeta)+\mu \to \alpha'+\zeta+\nu'$: In this case $U_r$ is above $\alpha'$ and to the right of the 3-rarefaction wave starting at $U_l$, see Figure 29(b). We have

$$|\alpha'|+|\nu'| \le |\alpha|, \qquad \text{or} \qquad |\alpha'|-|\alpha| \le -|\nu'|,$$

which gives

$$\begin{aligned}\Delta F &= |\alpha'| - |\alpha| \le -|\nu'|,\\ \Delta Q_1 &\le 0,\\ \Delta Q_1 &\le |\nu'| F_\gamma - |\mu|\,|\zeta| \le |\nu'| F_\gamma,\end{aligned}$$

and

$$\Delta G \le |\nu'|(-1 + 3C_2F_\gamma) \le 0.$$

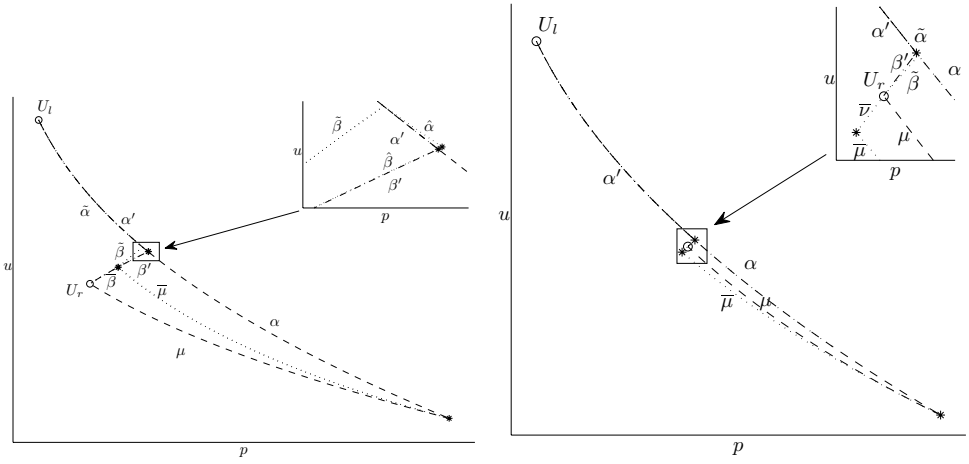


(a) When $\zeta + \mu \to \overline{\mu} + \zeta + \overline{\beta}$.

(b) When $\zeta + \mu \to \overline{\mu} + \zeta + \overline{\nu}$.

FIGURE 31. The interaction $(\alpha + \zeta) + \mu \to \alpha' + \zeta + \beta'$.

- $(\alpha + \zeta) + \mu \to \alpha' + \zeta + \beta'$: In this case $U_r$ is below $\alpha'$ and to the right of the 3-shock wave starting at $U_l$, see Figure 31. We divide the interaction into steps,

$$\begin{aligned}\alpha + [\zeta + \mu] &\xrightarrow{\Delta G_1} [\alpha + \overline{\mu}] + \zeta + \overline{\eta}\\ &\xrightarrow{\Delta G_2} \tilde\alpha + [\tilde\beta + \zeta + \overline{\eta}]\\ &\xrightarrow{\Delta G_3} \tilde\alpha + \hat\alpha + \zeta + \hat\beta\\ &\xrightarrow{\Delta G_4} \alpha' + \zeta + \beta'.\end{aligned}$$

The interaction at the first step is of type Bc-i and $\Delta G_1 \le 0$. We do not know whether the outgoing 3-wave is a shock wave or a rarefaction wave, but in this case we are able effectively to treat both case at the same time.[3] At the second step we have an interaction of type Ba-ii, thus $\Delta G_2 \le 0$. If $\tilde\beta$ starts to the right of $\beta'$, as is the case in Figure 31(b), then

$$|\alpha'| - |\tilde\alpha| \le 0, \qquad \begin{cases} |\beta'| - \left|\tilde\beta\right| \le 0, & \text{if } \overline{\eta} = \overline{\nu},\\ |\beta'| - \left|\tilde\beta\right| - \left|\overline{\beta}\right| \le 0, & \text{if } \overline{\eta} = \overline{\beta},\end{cases}$$

[3]This is the shortest way to do it, although we could for $\eta = \beta$ use Lemma 2.2 and be able to stop after step two (similar to the case $\to \mu' + \zeta + \beta'$). Moreover, for $\eta = \nu$ we could replace the interaction according to Proposition 4.3.

and going straight to the last step we get $\Delta G_* \leq 0$. However, if $\tilde{\beta}$ starts to the left of $\beta'$ as in Figure 31(a), we need more steps. We then let three waves interact at the third step. This is an interaction of type Cc-ii if $\overline{\eta} = \overline{\beta}$ and of type Cc-iv if $\overline{\eta} = \overline{\nu}$, in either case we have $\Delta G_3 \leq 0$ and the outgoing 1- and 3-waves are shock waves. By property (viii) and property (ix) we obtain

$$|\alpha'| - |\tilde{\alpha}| - |\hat{\alpha}| \leq 0, \qquad |\beta'| - \left|\hat{\beta}\right| \leq 0,$$

thus, $\Delta G_4 \leq 0$.

By symmetry we have $\Delta G \leq 0$ across $\nu + (\zeta + \beta)$.

This ends the discussion of interactions of type Cc, but before we carry on to interactions between four waves, we collect some results that will be useful when discussing the interactions of type Db. During the discussion of Cc-iii and Cc-iv we have shown the following:

**Proposition 4.4.** *For the interactions*

$$\mu + \alpha + \zeta + \beta \to \epsilon' + \zeta + \beta', \quad \textit{and} \tag{4.11}$$

$$\alpha + \mu + \zeta + \beta \to \epsilon' + \zeta + \beta', \tag{4.12}$$

*where $\epsilon'$ is either $\alpha'$ or $\mu'$, the Glimm functional is decreasing, that is, $\Delta G \leq 0$.*

Furthermore, we have also proved the following result:

**Proposition 4.5.** *For the interactions*

$$\mu + \alpha + \zeta \to \epsilon' + \zeta + \beta', \quad \textit{and} \tag{4.13}$$

$$\alpha + \mu + \zeta \to \epsilon' + \zeta + \beta', \tag{4.14}$$

*where $\epsilon'$ is either $\alpha'$ or $\mu'$, the Glimm functional is decreasing, that is, $\Delta G \leq 0$.*

## 4.4. **Type D: Four waves entering the diamond.**

4.4.1. *Type* Da*: Waves of the same family are also of the same type.* The interactions of this type all have two possible outcomes to be considered.

(i) $(\mu_1 + \zeta + \nu) + \mu_2$ (and $\nu_1 + (\mu + \zeta + \nu_2)$):

- $(\mu_1 + \zeta + \nu) + \mu_2 \to \mu' + \zeta + \nu'$: In this case $U_r$ lies above $\mu'$, see Figure 32(a). This interaction is divided into two steps,

$$\mu_1 + [\zeta + \nu + \mu_2] \xrightarrow{\Delta G_1} \mu_1 + \overline{\mu} + \zeta + \overline{\nu} \xrightarrow{\Delta G_2} \mu' + \zeta + \nu'.$$

The interaction at the first step is of type Cb-i, therefore $\Delta G_1 \leq 0$. By property (iv) and property (vii) we have $\mu_1 + \overline{\mu} = \mu'$ and $\overline{\nu} = \nu'$, thus $\Delta G_2 = 0$.

- $(\mu_1 + \zeta + \nu) + \mu_2 \to \mu' + \zeta + \beta'$: In this case $U_r$ lies below $\mu'$, see Figure 32(b). Again we need two steps,

$$\mu_1 + [\zeta + \nu + \mu_2] \xrightarrow{\Delta G_1} \mu_1 + \overline{\mu} + \zeta + \overline{\beta} \xrightarrow{\Delta G_2} \mu' + \zeta + \beta'.$$

The first interaction is of type Cb-i, thus $\Delta G_1 \leq 0$. From property (iv) and property (vii) we have $\mu_1 + \overline{\mu} = \mu'$. It then follows that $\overline{\beta} = \beta'$, and therefore $\Delta G_2 = 0$.

Due to symmetry, $\Delta G \leq 0$ across $\nu_1 + (\mu + \zeta + \nu_2)$.

(ii) $(\mu_1 + \zeta + \beta) + \mu_2$ (and $\nu_1 + (\alpha + \zeta + \nu_2)$):

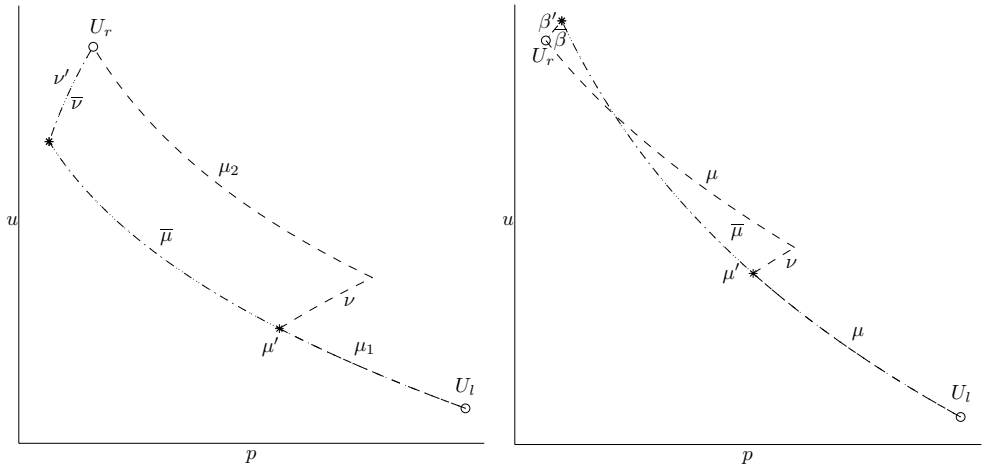


(a) $(\mu_1 + \zeta + \nu) + \mu_2 \to \mu' + \zeta + \nu'$. (b) $(\mu_1 + \zeta + \nu) + \mu_2 \to \mu' + \zeta + \beta'$.

FIGURE 32. The interaction $(\mu_1 + \zeta + \nu) + \mu_2$.

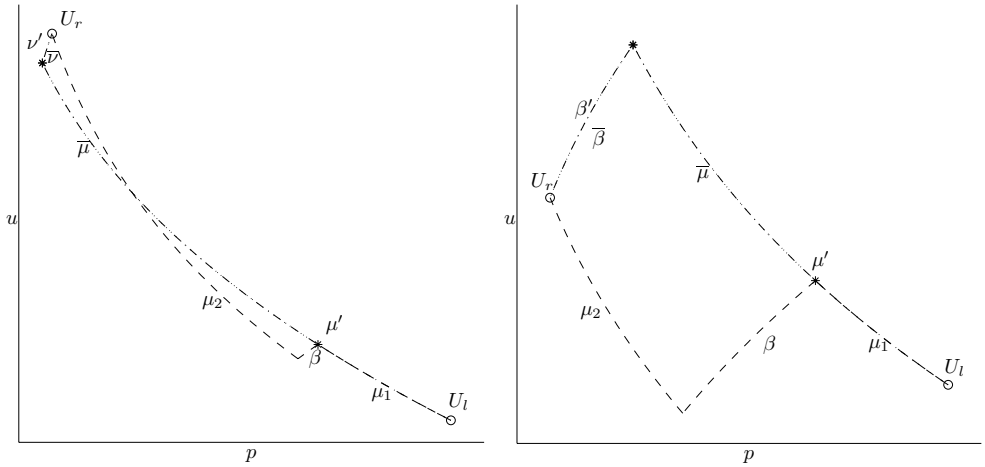


(a) $(\mu_1 + \zeta + \beta) + \mu_2 \to \mu' + \zeta + \nu'$. (b) $(\mu_1 + \zeta + \beta) + \mu_2 \to \mu' + \zeta + \beta'$.

FIGURE 33. The interaction $(\mu_1 + \zeta + \beta) + \mu_2$.

- $(\mu_1 + \zeta + \beta) + \mu_2 \to \mu' + \zeta + \nu'$: In this case $U_r$ is above $\mu'$, see Figure 33(a). Observe that $\mu_2$ crosses $\mu'$, which is possible since the two waves have different $\gamma$'s. We divide the interaction into two steps,

$$\mu_1 + [\zeta + \beta + \mu_2] \xrightarrow{\Delta G_1} \mu_1 + \overline{\mu} + \zeta + \overline{\nu} \xrightarrow{\Delta G_2} \mu' + \zeta + \nu',$$

where the interaction at the first step is of type Cb-iii, thus $\Delta G_1 \leq 0$. Due to property (iv) and property (vii) we have that $\mu_1 + \overline{\mu} = \mu'$ and $\overline{\nu} = \nu'$, and it follows that $\Delta G_2 = 0$.

- $(\mu_1+\zeta+\beta)+\mu_2 \to \mu'+\zeta+\beta'$: In this case $U_r$ is below $\mu'$, see Figure 33(b). The interaction is divided into two steps,

$$\mu_1+[\zeta+\beta+\mu_2] \xrightarrow{\Delta G_1} \mu_1+\overline{\mu}+\zeta+\overline{\beta} \xrightarrow{\Delta G_2} \mu'+\zeta+\beta',$$

  where the interaction at the first step is of type Cb-iii, thus $\Delta G_1 \le 0$. Due to property (iv) and property (vii) we have $\mu_1+\overline{\mu}=\mu'$ and therefore also $\overline{\beta}=\beta'$, thus $\Delta G_2 = 0$.

By symmetry we have $\Delta G \le 0$ across $\nu_1+(\alpha+\zeta+\nu_2)$.

(iii) $(\alpha_1+\zeta+\nu)+\alpha_2$ (and $\beta_1+(\mu+\zeta+\beta_2)$):

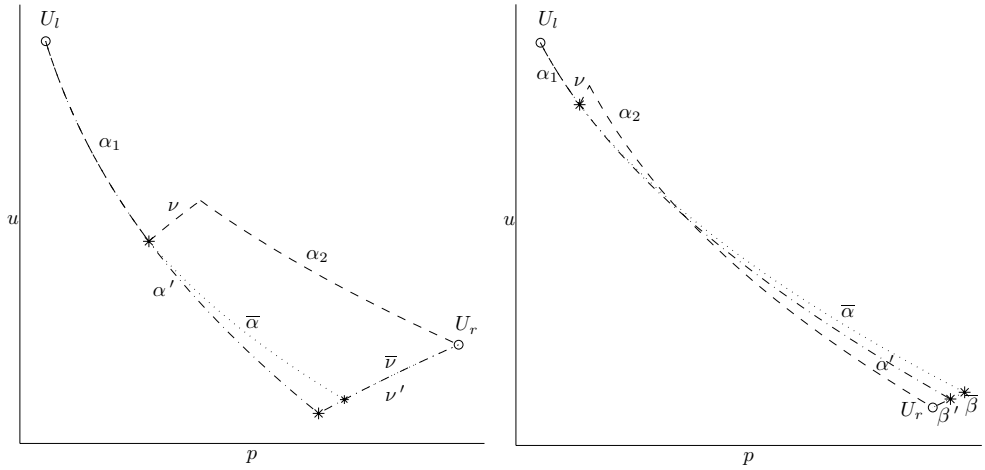


(a) $(\alpha_1+\zeta+\nu)+\alpha_2 \to \alpha'+\zeta+\nu'$ (b) $(\alpha_1+\zeta+\nu)+\alpha_2 \to \alpha'+\zeta+\beta'$

FIGURE 34. The interaction $(\alpha_1+\zeta+\nu)+\alpha_2$.

- $(\alpha_1+\zeta+\nu)+\alpha_2 \to \alpha'+\zeta+\nu'$: In this case $U_r$ is above $\alpha'$, see Figure 34(a). Two steps are needed,

$$\alpha_1+[\zeta+\nu+\alpha_2] \xrightarrow{\Delta G_1} \alpha_1+\overline{\alpha}+\zeta+\overline{\nu} \xrightarrow{\Delta G_2} \alpha'+\zeta+\nu'.$$

  The first interaction is of type Cb-ii, therefore $\Delta G_1 \le 0$. It follows from property (iv) and property (viii) that

$$|\alpha'|-|\alpha_1|-|\overline{\alpha}|=-q, \qquad |\nu'|-|\overline{\nu}|=q,$$

  for a $q>0$, and this gives $\Delta G_2 \le 0$.
- $(\alpha_1+\zeta+\nu)+\alpha_2 \to \alpha'+\zeta+\beta'$: In this case $U_r$ is below $\alpha'$, see Figure 34(b). We divide the interaction into two steps,

$$\alpha_1+[\zeta+\nu+\alpha_2] \xrightarrow{\Delta G_1} \alpha_1+\overline{\alpha}+\zeta+\overline{\beta} \xrightarrow{\Delta G_2} \alpha'+\zeta+\beta'.$$

  The first interaction is of type Cb-ii, therefore $\Delta G_1 \le 0$. The 1-shock waves $\alpha'$ and $\overline{\alpha}$ have $\gamma=\gamma_l$ and $\beta'$ and $\overline{\beta}$ have $\gamma=\gamma_r$, therefore it follows from property (viii) and property (ix) that

$$|\alpha'|-|\alpha_1|-|\overline{\alpha}|\le 0, \qquad |\beta'|-\left|\overline{\beta}\right|\le 0,$$

  resulting in $\Delta G_2 \le 0$.

It follows from symmetry that $\Delta G \le 0$ across $\beta_1 + (\mu + \zeta + \beta_2)$.

(iv) $(\alpha_1 + \zeta + \beta) + \alpha_2$ (and $\beta_1 + (\alpha + \zeta + \beta_2)$):

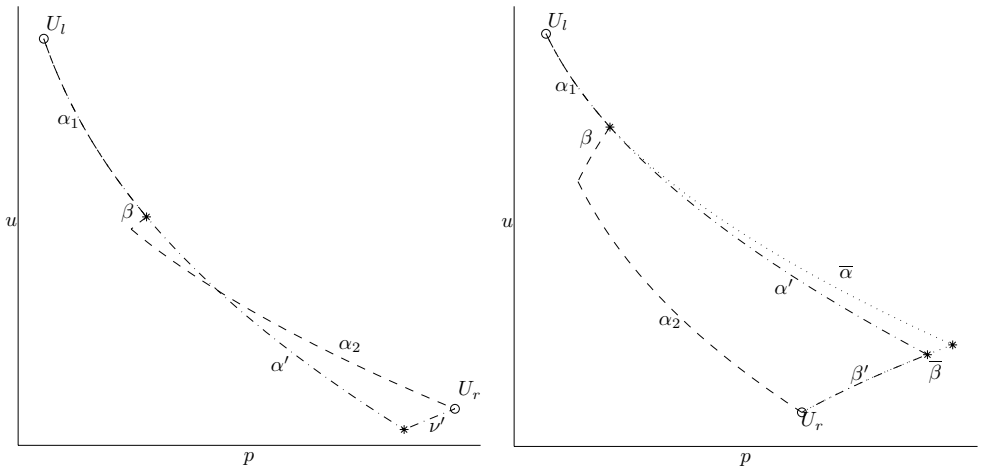


(a) $(\alpha_1 + \zeta + \beta) + \alpha_2 \to \alpha' + \zeta + \nu'$.

(b) $(\alpha_1 + \zeta + \beta) + \alpha_2 \to \alpha' + \zeta + \beta'$.

FIGURE 35. The interaction $(\alpha_1 + \zeta + \beta) + \alpha_2$.

- $(\alpha_1 + \zeta + \beta) + \alpha_2 \to \alpha' + \zeta + \nu'$: In this case $U_r$ lies above $\alpha'$, see Figure 35(a). Here $\alpha_2$ crosses $\alpha'$, which is possible since they have different $\gamma$'s. We do not need to divide this interaction because we have

$$|\alpha'| \le |\alpha_1| + |\alpha_2|,$$
$$|\alpha'| + |\nu'| \le |\alpha_1| + |\alpha_2| + |\beta|,$$

and from this we find

$$\Delta F = |\alpha'| - |\alpha_1| - |\alpha_2| - |\beta| \le -|\nu'|,$$
$$\Delta Q_1 \le 0,$$
$$\Delta Q_2 \le |\nu'| F_\gamma,$$

which gives us $\Delta G \le 0$.

- $(\alpha_1 + \zeta + \beta) + \alpha_2 \to \alpha' + \zeta + \beta'$: In this case $U_r$ lies below $\alpha'$, see Figure 35(b). We divide this interaction into two steps,

$$\alpha_1 + [\zeta + \beta + \alpha_2] \xrightarrow{\Delta G_1} \alpha_1 + \overline{\alpha} + \zeta + \overline{\beta} \xrightarrow{\Delta G_2} \alpha' + \zeta + \beta',$$

where the interaction at the first step is of type Cb-iv, thus $\Delta G_1 \le 0$. Due to property (viii) and property (ix) the intersection between $\overline{\alpha}$ and $\overline{\beta}$ is to the right of the intersection between $\alpha'$ and $\beta'$, thus

$$|\alpha'| - |\alpha_1| - |\overline{\alpha}| \le 0, \qquad |\beta| - |\overline{\beta}| \le 0,$$

and we get $\Delta G_2 \le 0$.

By symmetry we have $\Delta G \le 0$ across $\beta_1 + (\alpha + \zeta + \beta_2)$.

4.4.2. *Type* Db*: Waves of the same family are not of the same type.* Before we discuss each interaction of this type, we state some useful observations in the following propositions.

**Proposition 4.6.** *If $\mu$ and $\alpha$ cross in the interaction*

$$\mu + \zeta + \nu + \alpha, \qquad \text{or} \qquad \alpha + \zeta + \nu + \mu,$$

*then the interaction can be replaced by*

$$\hat{\mu} + \zeta + \hat{\alpha}, \qquad \text{or} \qquad \hat{\alpha} + \zeta + \hat{\mu}, \tag{4.15}$$

*respectively, where*

$$|\hat{\mu}\,| \le |\mu\,|, \qquad \text{and} \qquad |\hat{\alpha}\,| \le |\alpha\,|, \tag{4.16}$$

*and $\Delta G \le 0$ for this replacement.*

*Proof.* For the first interaction we have to prove that the backward 1-shock curve at $U_r$ crosses $\mu$, and in order to show (4.16), that this intersection is to the right of the starting point of $\alpha$. By property (viii) a 1-shock with $\gamma = \gamma_r$ that starts to the right of the intersection point between $\mu$ and $\alpha$ can never reach $U_r$. Furthermore, if $\hat{\alpha}$ starts to the left of $\alpha$, it will always be steeper than $\alpha$ and hence never reach $U_r$. Thus, there is a $\hat{\alpha}$ starting at $\mu$ so that (4.15) connects $U_l$ to $U_r$ and so that (4.16) is satisfied.

Since the slope of a rarefaction wave is independent of the starting point, the proof for the second interaction is easier. Then $\hat{\alpha}$ is the part of $\alpha$ from $U_l$ to the intersection point between $\alpha$ and $\mu$, while $\hat{\mu}$ is the part of $\mu$ from the intersection point to $U_r$. Thus, (4.16) is satisfied, and the interaction can be replaced by (4.15).

For both cases it follows from (4.16) that $\Delta G \le 0$ for this replacement. □

**Proposition 4.7.** *If $U_r$ is to the right of $U_l$ and $\mu$ and $\alpha$ do not intersect for the interaction*

$$\mu + \zeta + \nu + \alpha,$$

*then the interaction can be replaced by*

$$\zeta + \hat{\nu} + \hat{\alpha}, \tag{4.17}$$

*where, for a positive constant $q$,*

$$|\hat{\alpha}\,| - |\alpha\,| = -q, \qquad \text{and} \qquad |\hat{\nu}\,| - |\nu\,| \le q, \tag{4.18}$$

*and $\Delta G \le 0$ for this replacement.*

*Proof.* We have from property (viii) and property (iv) that the backward 1-shock curve from $U_r$ has a unique intersection point with the 3-rarefaction curve starting at $(p_l, u_l, \gamma_r)$, and that this point is to the right of the starting point of $\alpha$. Thus, $|\hat{\alpha}\,| - |\alpha\,| = -q$ for a positive constant $q$. Furthermore we find that

$$|\mu\,| + |\hat{\nu}\,| + |\hat{\alpha}\,| = |\nu\,| + |\alpha\,|,$$

hence

$$|\hat{\nu}\,| - |\nu\,| = -(|\hat{\alpha}\,| - |\alpha\,|) - |\mu\,| = q - |\mu\,| \le q,$$

which proves (4.18). Moreover, $\Delta G \le 0$ follows directly from this estimate. □

**Proposition 4.8.** *If $U_r$ is to the left of $U_l$ and $\mu$ and $\alpha$ do not intersect for the interaction*

$$\alpha + \zeta + \nu + \mu,$$

*then the interaction can be replaced by*

$$\zeta + \hat{\nu} + \hat{\mu}, \tag{4.19}$$

*where*

$$|\hat{\mu}\,| - |\mu\,| \le 0, \qquad \textit{and} \qquad |\hat{\nu}\,| - |\nu\,| \le |\alpha\,|, \tag{4.20}$$

*and* $\Delta G \le 0$ *for this replacement.*

*Proof.* It follows from property (iv) that $\hat{\mu}$ starts at the point where the 3-rarefaction curve from $(p_l, u_l, \gamma_r)$ intersects $\mu$. Thus, $|\hat{\mu}\,| - |\mu\,| \le 0$ and furthermore,

$$|\mu\,| - |\hat{\mu}\,| + |\hat{\nu}\,| = |\alpha\,| + |\nu\,|,$$

hence, $|\hat{\nu}\,| - |\nu\,| = |\alpha\,| - (|\mu\,| - |\hat{\mu}\,|) \le |\alpha\,|$. This proves (4.20) from which it follows that $\Delta G \le 0$ for the replacement. □

(i) $(\mu + \zeta + \nu) + \alpha$ (and $\beta + (\mu + \zeta + \nu)$). This interaction has four different outcomes as shown in Figure 36.

- $(\mu + \zeta + \nu) + \alpha \to \mu' + \zeta + \nu'$: In this case $U_r$ is above $\mu'$ and to the left of the 3-rarefaction wave starting at $U_l$, see Figure 36(a). We have $|\mu'\,| \le |\mu\,|$ and $|\nu'\,| - |\nu\,| \le |\alpha\,|$, thus

$$\begin{aligned} \Delta F &= -\,|\alpha\,|, \\ \Delta Q_1 &\le 0, \\ \Delta Q_2 &\le (|\nu'\,| - |\nu\,|) \sum_i |\zeta_i\,| \le |\alpha\,|\, F_\gamma, \end{aligned}$$

  where $\zeta_i$ are all contact discontinuities to the right of the diamond. From this we obtain $\Delta G \le 0$.
- $(\mu + \zeta + \nu) + \alpha \to \mu' + \zeta + \beta'$: In this case $U_r$ is below $\mu'$ and to the left of the 3-shock wave starting at $U_l$, thus $\alpha$ has to cross $\mu$, see Figure 36(b). Then it follows from Proposition 4.6 that the interaction can be replaced by a new one,

$$\mu + \zeta + \nu + \alpha \xrightarrow{\Delta G_1} [\hat{\mu} + \zeta + \hat{\alpha}] \xrightarrow{\Delta G_2} \mu' + \zeta + \beta',$$

  where $\Delta G_1 \le 0$. Since the interaction at the second step is of type Cc-iii, we also have $\Delta G_2 \le 0$.
- $(\mu + \zeta + \nu) + \alpha \to \alpha' + \zeta + \nu'$: In this case $U_r$ is above $\alpha'$ and to the right of the 3-rarefaction wave starting at $U_l$, see Figure 36(c). Since $\alpha$ and $\mu$ cannot intersect, it follows from Proposition 4.7 that the interaction can be replaced by a new one,

$$\mu + \zeta + \nu + \alpha \xrightarrow{\Delta G_1} [\zeta + \hat{\nu} + \hat{\alpha}] \xrightarrow{\Delta G_2} \alpha' + \zeta + \nu',$$

  where $\Delta G_1 \le 0$. At the second step we have an interaction of type Cb-ii, thus $\Delta G_2 \le 0$.
- $(\mu + \zeta + \nu) + \alpha \to \alpha' + \zeta + \beta'$: In this case $U_r$ is below $\alpha'$ and to the right of the 3-shock wave starting at $U_l$, see Figure 36(d). If $\alpha$ crosses $\mu$, we replace the interaction according to Proposition 4.6,

$$\mu + \zeta + \nu + \alpha \xrightarrow{\Delta G_1} [\hat{\mu} + \zeta + \hat{\alpha}] \xrightarrow{\Delta G_2} \alpha' + \zeta + \beta',$$

  where $\Delta G_1 \le 0$. The interaction at the second step is of type Cc-iii, thus $\Delta G_2 \le 0$. If, however, $\alpha$ does not cross $\mu$, we use on Proposition 4.7 and replace the interaction by a new one,

$$\mu + \zeta + \nu + \alpha \xrightarrow{\Delta G_1} \zeta + \hat{\nu} + \hat{\alpha} \xrightarrow{\Delta G_2} \alpha' + \zeta + \beta',$$

  where $\Delta G_1 \le 0$. Furthermore, $\Delta G_2 \le 0$ because the interaction at the second step is of type Cb -ii.

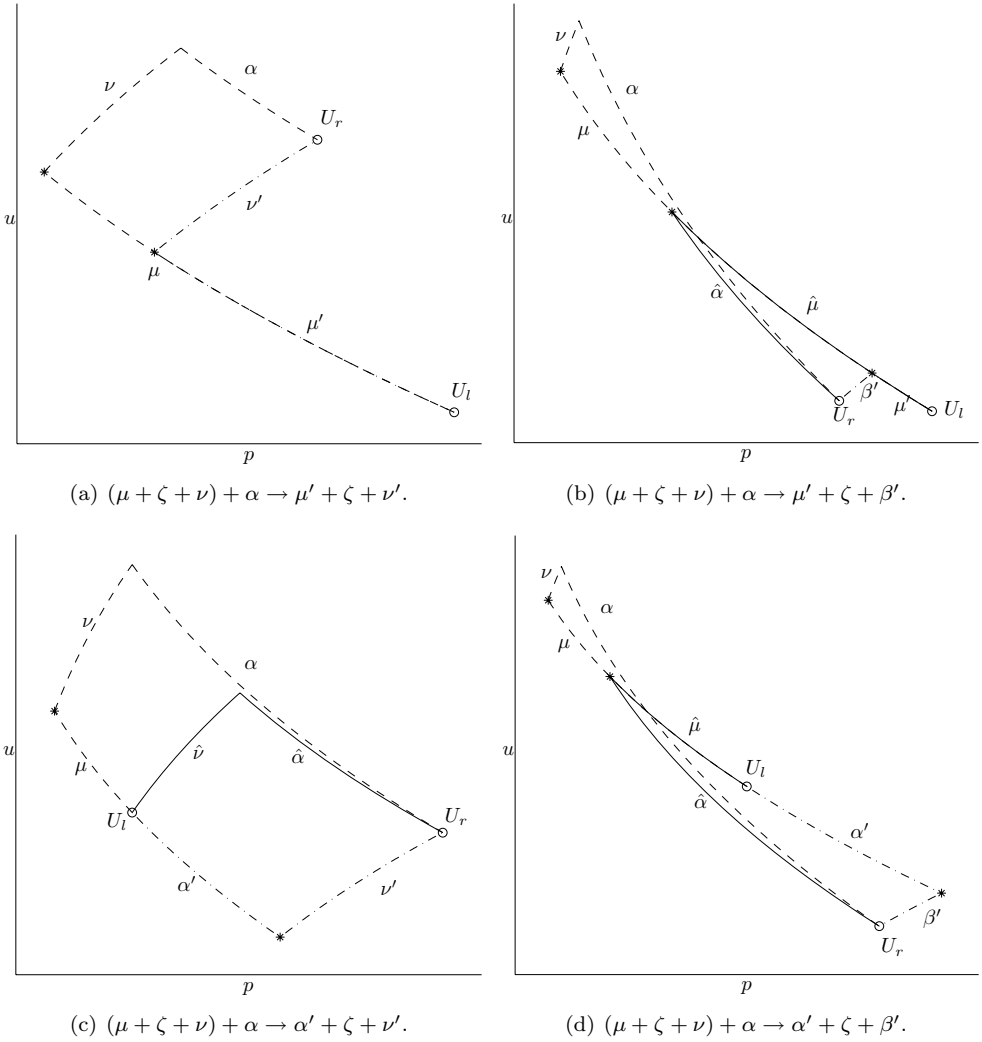


(a) $(\mu+\zeta+\nu)+\alpha \to \mu'+\zeta+\nu'$.

(b) $(\mu+\zeta+\nu)+\alpha \to \mu'+\zeta+\beta'$.

(c) $(\mu+\zeta+\nu)+\alpha \to \alpha'+\zeta+\nu'$.

(d) $(\mu+\zeta+\nu)+\alpha \to \alpha'+\zeta+\beta'$.

FIGURE 36. The interaction $(\mu+\zeta+\nu)+\alpha$.

By symmetry we have $\Delta G \leq 0$ across $\beta+(\mu+\zeta+\nu)$.

(ii) $(\alpha+\zeta+\nu)+\mu$ (and $\nu+(\mu+\zeta+\beta)$): This interaction has four possible outcomes as shown in Figure 37.

- $(\alpha+\zeta+\nu)+\mu \to \mu'+\zeta+\nu'$: In this case $U_r$ is above $\mu'$ and to the left of the 3-rarefaction curve starting at $U_l$, see Figure 37(a). Since $\alpha$ and $\mu$ do not cross, we can by Proposition 4.8 replace the interaction by a new one,

$$\alpha+\zeta+\nu+\mu \xrightarrow{\Delta G_1} [\zeta+\hat{\nu}+\hat{\mu}] \xrightarrow{\Delta G_2} \mu'+\zeta+\nu',$$

where $\Delta G_1 \leq 0$. The second interaction is of type Cb-i, thus $\Delta G_2 \leq 0$.[4]

[4]This interaction can also be divided into two steps by letting $\zeta+\nu+\mu$ interact at the first step.

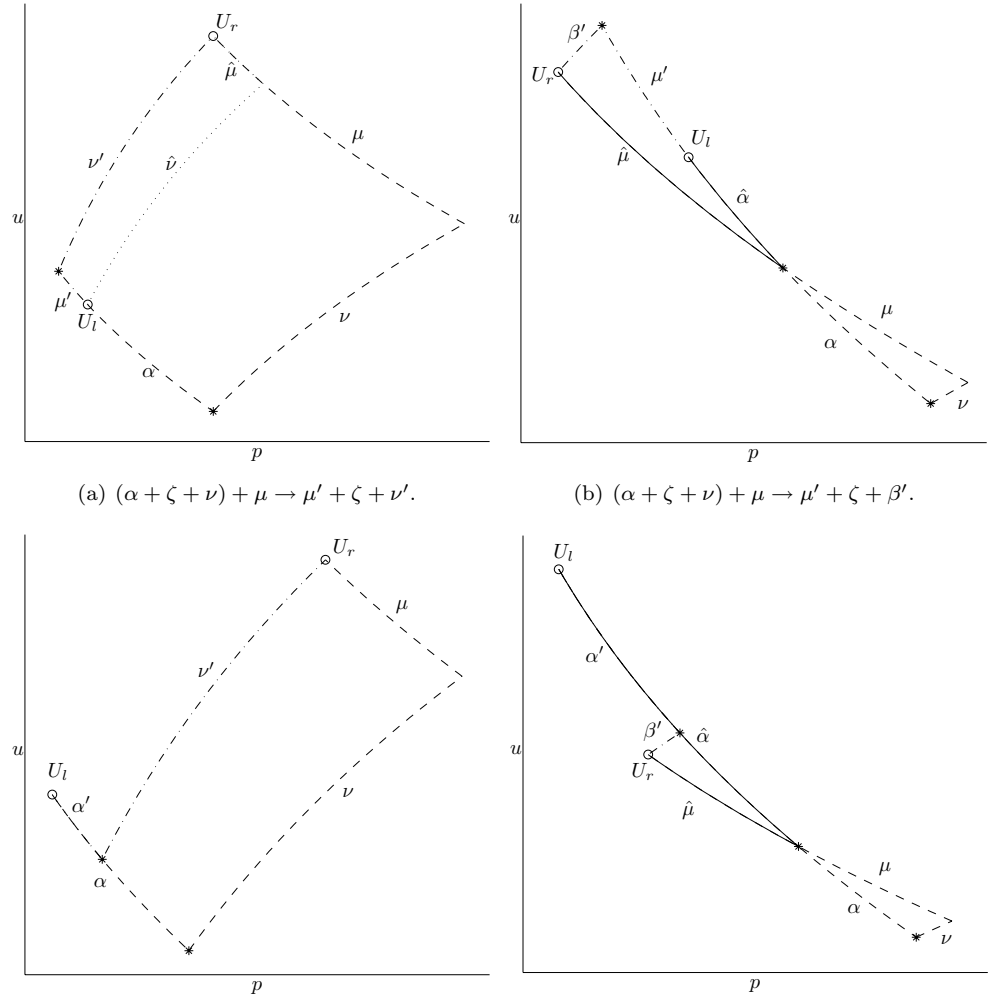


(a) $(\alpha+\zeta+\nu)+\mu \to \mu'+\zeta+\nu'$.

(b) $(\alpha+\zeta+\nu)+\mu \to \mu'+\zeta+\beta'$.

(c) $(\alpha+\zeta+\nu)+\mu \to \alpha'+\zeta+\nu'$.

(d) $(\alpha+\zeta+\nu)+\mu \to \alpha'+\zeta+\beta'$.

FIGURE 37. The interaction $(\alpha+\zeta+\nu)+\mu$.

- $(\alpha+\zeta+\nu)+\mu \to \mu'+\zeta+\beta'$: In this case $U_r$ is below $\mu'$ and to the left of the 3-shock curve starting at $U_l$, see Figure 37(b). If $\alpha$ and $\mu$ do not intersect, we use Proposition 4.8 as above and replace the interaction,

$$\alpha+\zeta+\nu+\mu \xrightarrow{\Delta G_1} [\zeta+\hat{\nu}+\hat{\mu}] \xrightarrow{\Delta G_2} \mu'+\zeta+\beta',$$

where $\Delta G_1 \le 0$.Because the interaction at the second step is of type Cb-i, we have $\Delta G_2 \le 0$. If, however, $\alpha$ and $\mu$ do intersect as in Figure 37(b), we replace the interaction according to Proposition 4.6,

$$\alpha+\zeta+\nu+\mu \xrightarrow{\Delta G_1} \hat{[}\alpha+\zeta+\hat{\mu}] \xrightarrow{\Delta G_2} \mu'+\zeta+\beta',$$

with $\Delta G_1 \le 0$. Since the interaction at the second step is of type Cc-iv, also $\Delta G_2 \le 0$.

- $(\alpha+\zeta+\nu)+\mu \to \alpha'+\zeta+\nu'$: In this case $U_r$ is above $\alpha'$ and to the right of the 3-rarefaction curve starting at $U_l$, see Figure 37(c). We have
$$|\alpha'|+|\nu'|+|\mu| = |\alpha|+|\nu|, \qquad |\alpha'|-|\alpha| = -q,$$
where $q>0$, hence,
$$|\nu'|-|\nu| = q-|\mu| \le q,$$
and
$$\begin{aligned} \Delta F &= |\alpha'|-|\alpha| = -q,\\ \Delta Q_1 &\le 0,\\ \Delta Q_1 &\le qF_\gamma, \end{aligned}$$
from which we obtain $\Delta G \le 0$.
- $(\alpha+\zeta+\nu)+\mu \to \alpha'+\zeta+\beta'$: In this case $U_r$ is below $\alpha'$ and to the right of the 3-shock curve starting at $U_l$, see Figure 37(d). Hence, $\alpha$ and $\mu$ have to intersect and by Proposition 4.6 we can replace the interaction
$$\alpha+\zeta+\nu+\mu \xrightarrow{\Delta G_1} [\hat\alpha+\zeta+\hat\mu] \xrightarrow{\Delta G_2} \mu'+\zeta+\beta',$$
where $\Delta G_1 \le 0$. The interaction at the second step is of type Cc-iv, thus $\Delta G_2 \le 0$. By symmetry we have $\Delta G \le 0$ across $\nu+(\mu+\zeta+\beta)$.

Yet another proposition is useful before discussing the last two interactions.

**Proposition 4.9.** *If $U_r$ is below the outgoing 1-wave for the interaction*
$$\mu+\zeta+\beta+\alpha, \qquad \text{or} \qquad \alpha+\zeta+\beta+\mu,$$
*and if*
$$\zeta+\beta+\alpha \to \overline\alpha+\zeta+\overline\nu, \qquad \text{or} \qquad \zeta+\beta+\mu \to \overline\mu+\zeta+\overline\nu,$$
*respectively, then $U_l$ can be connected to $U_r$ by*
$$\hat\mu+\hat\alpha+\zeta, \qquad \text{or} \qquad \hat\alpha+\hat\mu+\zeta, \tag{4.21}$$
*respectively, where*
$$|\hat\mu| \le |\mu|, \qquad \text{and} \qquad |\hat\alpha| \le |\alpha|, \tag{4.22}$$
*for the first interaction and*
$$|\hat\mu| \le |\overline\mu|, \qquad \text{and} \qquad |\hat\alpha| \le |\alpha|, \tag{4.23}$$
*for the second.*

*Proof.* The proof for the first interaction is exactly the same as for the first interaction of Proposition 4.3. Also for the second interaction the arguments are the same as for the second interaction of Proposition 4.3, but due to the extra wave, $\beta$, we here only know that the strength of $\hat\mu$ is less than the strength of $\overline\mu$. □

(iii) $(\mu+\zeta+\beta)+\alpha$ (and $\beta+(\alpha+\zeta+\nu)$): This interaction has four possible outcomes.
- $(\mu+\zeta+\beta)+\alpha \to \mu'+\zeta+\nu'$: In this case $U_r$ is above $\mu'$ and to the left of the 3-rarefaction wave starting at $U_l$, see Figure 38(a). We have $|\mu'| \le |\mu|$ and moreover, $|\nu'| \le |\alpha|$, therefore
$$\begin{aligned} \Delta F &= -|\alpha|-|\beta| \le -|\alpha|,\\ \Delta Q_1 &\le 0,\\ \Delta Q_2 &\le |\nu'|\,F_\gamma \le |\alpha|\,F_\gamma, \end{aligned}$$

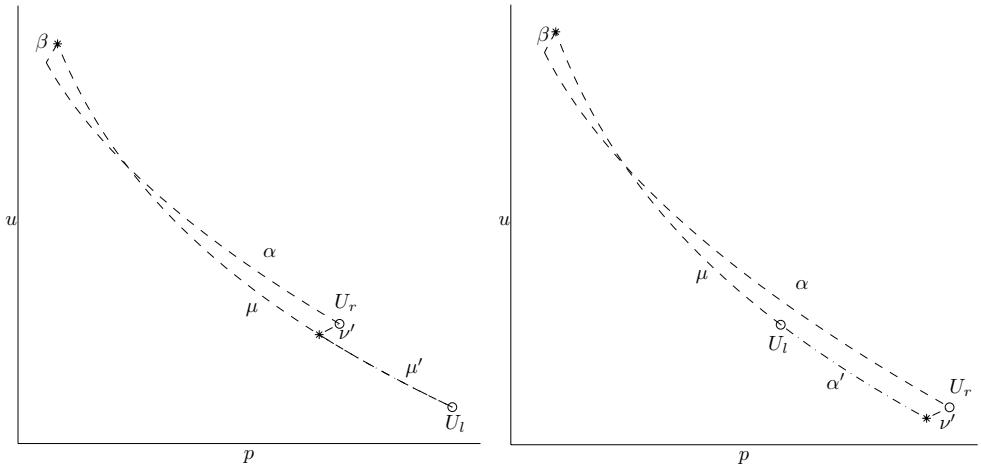


(a) $(\mu+\zeta+\beta)+\alpha \to \mu'+\zeta+\nu'$. (b) $(\mu+\zeta+\beta)+\alpha \to \alpha'+\zeta+\nu'$.

FIGURE 38. Two outcomes of the interaction $(\mu+\zeta+\beta)+\alpha$.

which gives $\Delta G \le 0$.

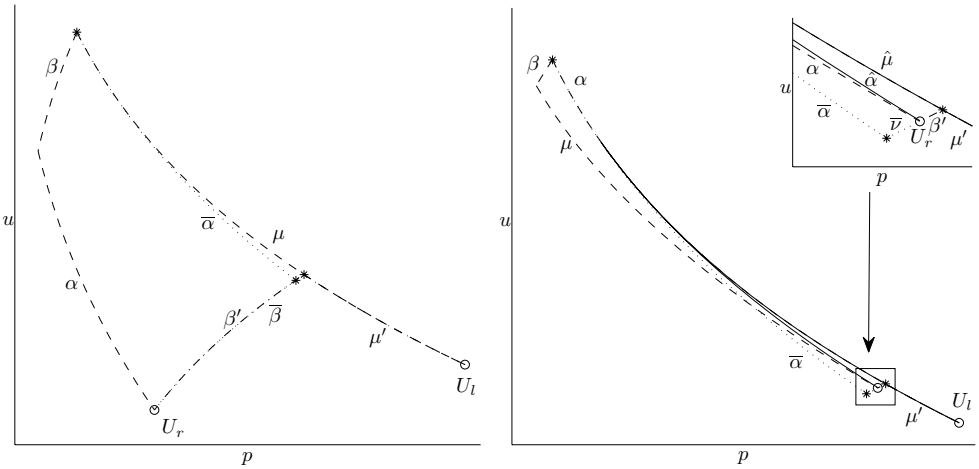


(a) When $\zeta+\beta+\alpha \to \overline{\alpha}+\zeta+\overline{\beta}$. (b) When $\zeta+\beta+\alpha \to \overline{\alpha}+\zeta+\overline{\nu}$.

FIGURE 39. $(\mu+\zeta+\beta)+\alpha \to \mu'+\zeta+\beta'$.

- $(\mu+\zeta+\beta)+\alpha \to \mu'+\zeta+\beta'$: In this case $U_r$ is below $\mu'$ and to the left of the 3-shock wave starting at $U_l$, see Figure 39. If $\zeta+\beta+\alpha \to \overline{\alpha}+\zeta+\overline{\beta}$ as in Figure 39(a), then we divide the interaction into two steps,

$$\mu+[\zeta+\beta+\alpha] \xrightarrow{\Delta G_1} \mu+\overline{\alpha}+\zeta+\overline{\beta} \xrightarrow{\Delta G_2} \mu'+\zeta+\beta',$$

where $\Delta G_1 \le 0$ because the interaction at the first step is of type Cb-iv and $\Delta G_2 \le 0$ follows from Proposition 4.4.

If, however, $\zeta+\beta+\alpha\to\overline{\alpha}+\zeta+\overline{\nu}$ as in Figure 39(b), we replace the interaction by $\hat{\mu}+\hat{\alpha}+\zeta$ according to Proposition 4.9,

$$\mu+\zeta+\beta+\alpha\xrightarrow{\Delta G_1}\hat{\mu}+\hat{\alpha}+\zeta\xrightarrow{\Delta G_2}\mu'+\zeta+\beta'.$$

It follows from (4.22) that $\Delta G_1\le 0$ and from Proposition 4.5 we have $\Delta G_2\le 0$.

- $(\mu+\zeta+\beta)+\alpha\to\alpha'+\zeta+\nu'$: In this case $U_r$ is above $\alpha'$ and to the right of the 3-rarefaction wave starting at $U_l$, see Figure 38(b). We have $|\alpha'|-|\alpha|\le-|\nu'|$, therefore

$$\begin{aligned}\Delta F&=|\alpha'|-|\alpha|-|\beta|\le-|\nu'|,\\ \Delta Q_1&\le 0,\\ \Delta Q_2&\le|\nu'|\,F_\gamma,\end{aligned}$$

and we obtain $\Delta G\le 0$.

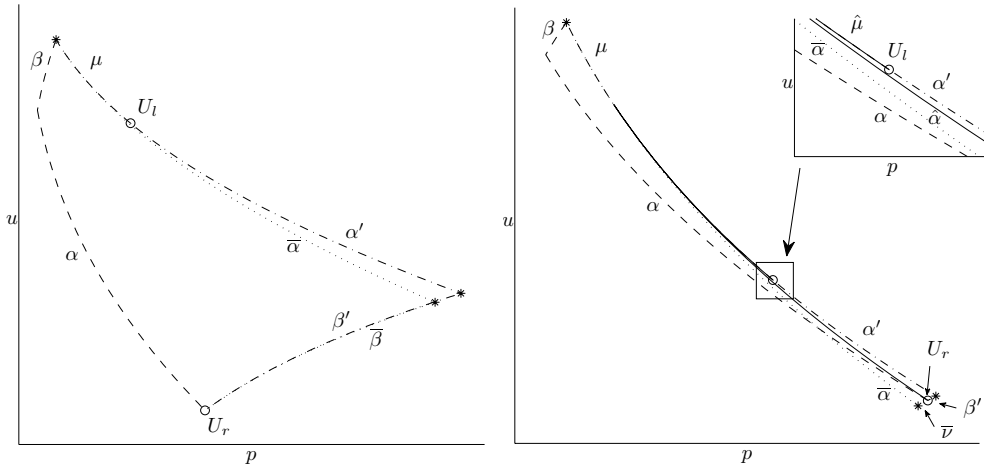


(a) When $\zeta+\beta+\alpha\to\overline{\alpha}+\zeta+\overline{\beta}$.

(b) When $\zeta+\beta+\alpha\to\overline{\alpha}+\zeta+\overline{\nu}$.

FIGURE 40. $(\mu+\zeta+\beta)+\alpha\to\alpha'+\zeta+\beta'$.

- $(\mu+\zeta+\beta)+\alpha\to\alpha'+\zeta+\beta'$: In this case $U_r$ is below $\alpha'$ and to the right of the 3-shock wave starting at $U_l$, see Figure 40. If $\zeta+\beta+\alpha\to\overline{\alpha}+\zeta+\overline{\beta}$ as in Figure 40(a), then we divide the interaction into two steps,

$$\mu+[\zeta+\beta+\alpha]\xrightarrow{\Delta G_1}\mu+\overline{\alpha}+\zeta+\overline{\beta}\xrightarrow{\Delta G_2}\alpha'+\zeta+\beta',$$

where the interaction at the first step is of type Cb-iv, thus $\Delta G_1\le 0$. Furthermore, $\Delta G_2\le 0$ follows from Proposition 4.4.
If $\zeta+\beta+\alpha\to\overline{\alpha}+\zeta+\overline{\nu}$ as in Figure 40(b), we again replace the interaction according to Proposition 4.9,

$$\mu+\zeta+\beta+\alpha\xrightarrow{\Delta G_1}\hat{\mu}+\hat{\alpha}+\zeta\xrightarrow{\Delta G_2}\alpha'+\zeta+\beta',$$

and get $\Delta G_1\le 0$ from (4.22) and $\Delta G_2\le 0$ from Proposition 4.5.

Due to symmetry, $\Delta G\le 0$ across $\beta+(\alpha+\zeta+\nu)$.

(iv) $(\alpha+\zeta+\beta)+\mu$ (and $\nu+(\alpha+\zeta+\beta)$): This interaction has four different outcomes.

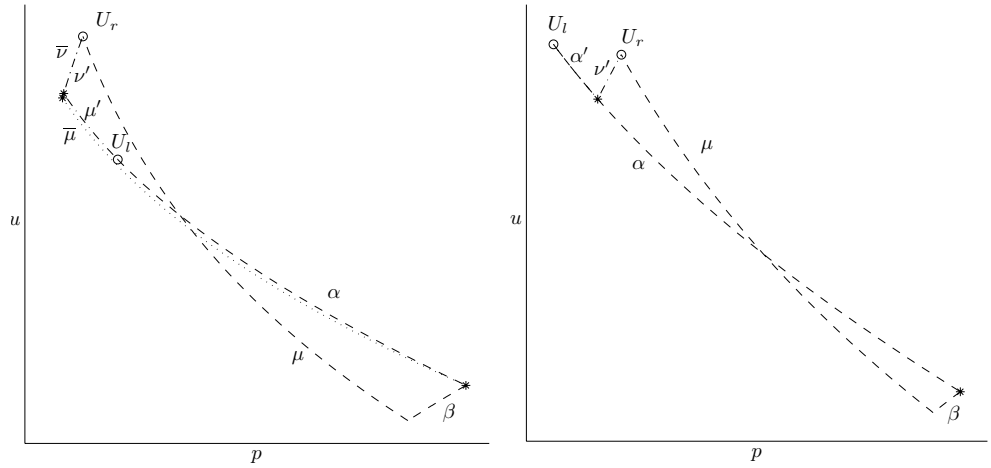


(a) $(\alpha+\zeta+\beta)+\mu \to \mu'+\zeta+\nu'$. (b) $(\alpha+\zeta+\beta)+\mu \to \alpha'+\zeta+\nu'$.

FIGURE 41. Two outcomes of the interaction $(\alpha+\zeta+\beta)+\mu$.

- $(\alpha+\zeta+\beta)+\mu \to \mu'+\zeta+\nu'$: In this case $U_r$ is above $\mu'$ and to the left of the 3-rarefaction curve starting at $U_l$, see Figure 41(a). We divide the interaction into two steps,

$$\alpha+[\zeta+\beta+\mu] \xrightarrow{\Delta G_1} \alpha+\overline{\mu}+\zeta+\overline{\nu} \xrightarrow{\Delta G_2} \mu'+\zeta+\nu',$$

where $\Delta G_1 \le 0$ since the first interaction is of type Cb-iii. From property (vi) we know that $\overline{\mu}$ lies below $\alpha$, therefore

$$|\mu'\,|-|\overline{\mu}\,| \le 0, \qquad |\nu'\,|-|\overline{\nu}\,| \le 0,$$

and we obtain $\Delta G_2 \le 0$.

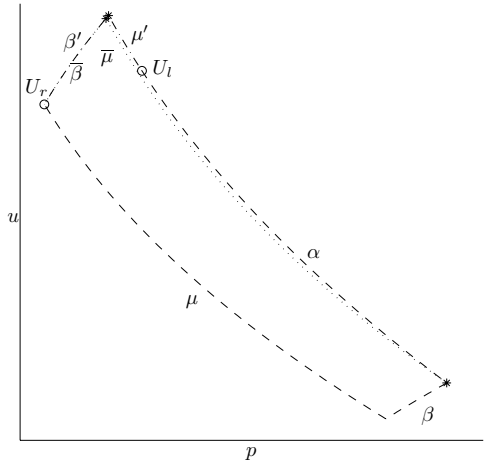


FIGURE 42. $(\alpha+\zeta+\beta)+\mu \to \mu'+\zeta+\beta'$.

- $(\alpha+\zeta+\beta)+\mu \to \mu'+\zeta+\beta'$: In this case $U_r$ is below $\mu'$ and to the left of the 3-shock curve starting at $U_l$. We first assume that $\zeta+\beta+\mu \to \overline{\mu}+\zeta+\overline{\beta}$ as in Figure 42. Then we divide the interaction into two steps

$$\alpha+[\zeta+\beta+\mu] \xrightarrow{\Delta G_1} \alpha+\overline{\mu}+\zeta+\overline{\beta} \xrightarrow{\Delta G_2} \mu'+\zeta+\beta',$$

where $\Delta G_1 \le 0$ since the first interaction is of type Cb-iii. Furthermore, it follows from Proposition 4.4 that $\Delta G_2 \le 0$.
When $\zeta+\beta+\mu \to \overline{\mu}+\zeta+\overline{\nu}$, we replace the interaction at the second step with a new one according to Proposition 4.9,

$$\begin{aligned}\alpha+[\zeta+\beta+\mu] &\xrightarrow{\Delta G_1} \alpha+\overline{\mu}+\zeta+\overline{\nu}\\ &\xrightarrow{\Delta G_2} \hat{\alpha}+\hat{\mu}+\zeta\\ &\xrightarrow{\Delta G_3} \mu'+\zeta+\beta'.\end{aligned}$$

The first interaction is of type Cb-iii, thus $\Delta G_1 \le 0$. This step is included because we are only able to relate $\hat{\mu}$ to $\overline{\mu}$, not to $\mu$. From (4.23) we obtain $\Delta G_2 \le 0$, and $\Delta G_3 \le 0$ follows from Proposition 4.5.
- $(\alpha+\zeta+\beta)+\mu \to \alpha'+\zeta+\nu'$: In this case $U_r$ is above $\alpha'$ and to the right of the 3-rarefaction curve starting at $U_l$, see Figure 41(b). We observe that $|\alpha'|-|\alpha|\le -|\nu'|$, thus

$$\begin{aligned}\Delta F &= |\alpha'|-|\alpha|-|\beta| \le -|\nu'|,\\ \Delta Q_1 &\le 0,\\ \Delta Q_2 &\le |\nu'|\,F_\gamma,\end{aligned}$$

and we have $\Delta G \le 0$.

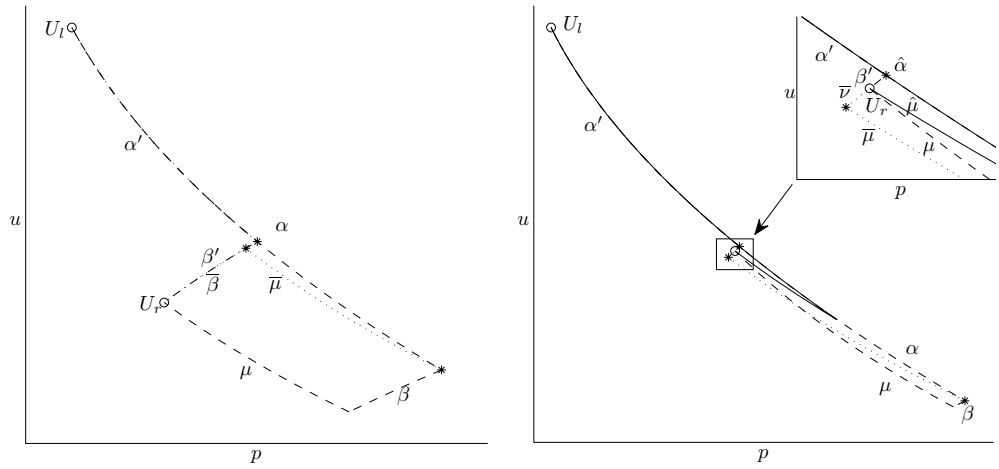


(a) When $\zeta+\beta+\mu \to \overline{\mu}+\zeta+\overline{\beta}$.

(b) When $\zeta+\beta+\mu \to \overline{\mu}+\zeta+\overline{\nu}$.

FIGURE 43. $(\alpha+\zeta+\beta)+\mu \to \alpha'+\zeta+\beta'$.

- $(\alpha+\zeta+\beta)+\mu \to \alpha'+\zeta+\beta'$: In this case $U_r$ is below $\alpha'$ and to the right of the 3-shock curve starting at $U_l$. Again we have to look at two cases. Assume first

that $\zeta+\beta+\mu \to \overline{\mu}+\zeta+\overline{\beta}$ as in Figure 43(a), then we divide the interaction into two,

$$\alpha+[\zeta+\beta+\mu] \xrightarrow{\Delta G_1} \alpha+\overline{\mu}+\zeta+\overline{\beta} \xrightarrow{\Delta G_2} \alpha'+\zeta+\beta',$$

where the interaction at step one is of type Cb-iii, thus $\Delta G_1 \le 0$. Furthermore, it follows from Proposition 4.4 that $\Delta G_2 \le 0$.
Assume now that $\zeta+\beta+\mu \to \overline{\mu}+\zeta+\overline{\nu}$ as in Figure 43(b). Then we at the second step replace the interaction with a new one according to Proposition 4.9,

$$\begin{aligned}\alpha+[\zeta+\beta+\mu] &\xrightarrow{\Delta G_1} \alpha+\overline{\mu}+\zeta+\overline{\nu}\\ &\xrightarrow{\Delta G_2} \hat{\alpha}+\hat{\mu}+\zeta\\ &\xrightarrow{\Delta G_3} \alpha'+\zeta+\beta'.\end{aligned}$$

Since the interaction at the first step is of type Cb-iii, we have $\Delta G_1 \le 0$. Moreover, $\Delta G_2 \le 0$ follows from (4.23) and $\Delta G_3 \le 0$ follows from Proposition 4.5.
By symmetry it follows that $\Delta G \le 0$ across $\nu+(\alpha+\zeta+\beta)$.

## 5. Convergence

We have to show that the approximate solution, $U_h(x,t)$ given by (3.4), converges and that the limit is a weak solution of (1.1). From [20, Ch. 19 §C] we know that an approximate solution converges to a weak solution if the approximation is uniformly bounded, has bounded total variation and is locally $L^1$ Lipschitz continuous in time. Note that the analysis in [20, Ch. 19 §C] to obtain convergence and to show that the limit is a weak solution, only relies on the above conditions and does not require a sufficiently small total variation of the initial data. Furthermore, if we have that the total variation of the approximate solution is bounded, then we can show that it is $L^1$ Lipschitz continuous in time. Thus, the requirement in the general theory that the total variation of the initial data should be sufficiently small is only needed in order to prove that the total variation of the approximate solution is bounded. Therefore, convergence to a weak solution of (1.1) follows if we can show that the total variations of $U_h(\,\cdot\,,t)$ is bounded, and we show this using the decreasing Glimm functional. Then we find the domain $\mathcal{U}$ that contains the approximate solution. As long as $\mathcal{U}$ does not include vacuum, we have that $U_h(x,t)$ is bounded.

Recall from Section 3.3 that the constant $C_1$ is the constant appearing in estimate (4.3), $C_2$ is given by (3.6), $k$ by (3.7) and $C$ is the minimum of the constants $\tilde{C}$ appearing in the estimates for interactions of type Ba, cf. Section 4.2.1. Define the constant

$$\kappa := \frac{10}{3} s'_{\max} k + 1. \tag{5.1}$$

Note that all these constants only depend on $p_{\min}$, $p_{\max}$ and $\overline{\gamma}$. We are now ready to prove that the total variation is bounded.

**Lemma 5.1.** *If the initial data satisfy*

$$(\overline{\gamma}-1)\text{T.V.}(p_0,u_0) \le \frac{C}{9kC_1}, \tag{5.2}$$

$$\text{T.V.}(\gamma_0) \le \frac{C}{9C_2}, \tag{5.3}$$

*and the approximate solution* $U_h(x,t) = (p_h(x,t), u_h(x,t), \gamma_h(x,t))$ *obtained by the Glimm scheme is bounded away from vacuum, then*

$$\text{T.V.}(p_h(\,\cdot\,,t), u_h(\,\cdot\,,t)) \le 2\kappa k \text{T.V.}(p_0,u_0), \tag{5.4}$$

$$\text{T.V.}(\gamma_h(\,\cdot\,,t)) \le \text{T.V.}(\gamma_0). \tag{5.5}$$

*Moreover, the solution is always contained in the domain*

$$\mathcal{U} = \Big\{(p,u,\gamma)\,|\max\{|p-p_-\,|\,,|p-p_+\,|\} \le 2\kappa k \text{T.V.}(p_0,u_0), \\ \max\{|u-u_-\,|\,,|u-u_+\,|\} \le 2\kappa \text{T.V.}(p_0,u_0), \gamma \in (1,\overline{\gamma}]\Big\}, \tag{5.6}$$

*where* $p_\pm = p_0(\pm\infty)$ *and* $u_\pm = u_0(\pm\infty)$.

*Proof.* Let $J_n$ be the mesh curve connecting sampling points at the times $(n+1)\Delta t$ and $n\Delta t$, and let $n\Delta t \le t < (n+1)\Delta t$. First of all, (5.5) is obvious since $\gamma$ only changes along contact discontinuities, thus

$$\text{T.V.}(\gamma_h(\,\cdot\,,t)) = F_\gamma = \text{T.V.}(\gamma_h(\cdot,0)) \le \text{T.V.}(\gamma_0). \tag{5.7}$$

We furthermore have that

$$L(J_0) \le \text{T.V.}(p_h(\,\cdot\,,0)) + k\text{T.V.}(u_h(\,\cdot\,,0)) \le k\text{T.V.}(p_h(\,\cdot\,,0), u_h(\,\cdot\,,0)), \tag{5.8}$$

where $J_0$ is the mesh curve connecting sampling points at $t=0$ and $t=\Delta t$. When (5.2) and (5.3) are satisfied, we therefore have

$$L(J_0) \le k\text{T.V.}(p_h(\,\cdot\,,0), u_h(\,\cdot\,,0)) \le k\text{T.V.}(p_0,u_0) \le \frac{C}{9C_1(\overline{\gamma}-1)}, \tag{5.9}$$

$$F_\gamma = \text{T.V.}(\gamma_h(\,\cdot\,,0)) \le \text{T.V.}(\gamma_0) \le \frac{C}{9C_2}, \tag{5.10}$$

hence, the Glimm functional is decreasing and $F(J_n) \le \frac{5}{3}L(J_0)$ by Lemma 3.3. We use this first to find a bound on $\text{T.V.}(u_h(\,\cdot\,,t))$. Since $u$ is increasing along all rarefaction waves and decreasing along all shock waves, we have

$$\sum_{\text{rf}} [\![u]\!] = \sum_{\text{shock}} [\![u]\!] + u(\infty,\,\cdot\,) - u(-\infty,\,\cdot\,), \tag{5.11}$$

where $[\![u]\!] := |u_r - u_l\,|$ for a wave connecting $U_l$ to $U_r$, and rf is short for rarefaction wave. Let $c := |u(\infty,\,\cdot\,) - u(-\infty,\,\cdot\,)\,| = |u_+ - u_-\,|$, then

$$\sum_{\text{rf}} [\![u]\!] \le \sum_{\text{shock}} [\![u]\!] + c, \tag{5.12}$$

and we have

$$\begin{aligned}
\text{T.V.}(u_h(\,\cdot\,,t)) = \text{T.V.}(u_h|_{J_n}) &= \sum_{\text{rf}} [\![u]\!] + \sum_{\text{shock}} [\![u]\!] \le 2\sum_{\text{shock}} [\![u]\!] + c \\
&\le 2\sum_{\text{shock}} |s'(\tilde{p},p_l,\gamma_l)\,|\,[\![p]\!] + c \le 2s'_{\max}\sum_{\text{shock}} [\![p]\!] + c \\
&= 2s'_{\max}F_n + c \le 2s'_{\max}\frac{5}{3}L_0 + c \\
&= \frac{10}{3}s'_{\max}k\text{T.V.}(p_0,u_0) + c \le \kappa\text{T.V.}(p_0,u_0),
\end{aligned}$$

where we have used that $c \le \text{T.V.}(u_0)$. For $\text{T.V.}(p_h(\,\cdot\,,t))$ we find

$$\begin{aligned}\text{T.V.}(p_h(\,\cdot\,,t)) &= \text{T.V.}(p_h|_{J_n}) = \sum_{\text{rf}} [\![p]\!] + \sum_{\text{shock}} [\![p]\!] \le k\left(\sum_{\text{rf}} [\![u]\!] + \sum_{\text{shock}} [\![u]\!]\right)\\ &= k\text{T.V.}(u_h) \le \kappa k \text{T.V.}(p_0,u_0),\end{aligned}$$

and moreover,

$$\begin{aligned}\text{T.V.}(p_h(\,\cdot\,,t),u_h(\,\cdot\,,t)) &= \text{T.V.}(p_h(\,\cdot\,,t)) + \text{T.V.}(u_h(\,\cdot\,,t))\\ &\le 2\kappa k \text{T.V.}(p_0,u_0).\end{aligned} \tag{5.13}$$

To show the last part of the lemma we use that

$$\sup(y) \le |y(\infty)\,| + |y(-\infty)\,| + \text{T.V.}(y),$$

and since $p_h(\pm\infty,\,\cdot\,) = p_0(\pm\infty)$, we find

$$\begin{aligned}\sup(p_h - p_0(\infty)) &\le |p_h(\infty,\,\cdot\,) - p_0(\infty)\,| + |p_h(-\infty,\,\cdot\,) - p_0(\infty)\,| + \text{T.V.}(p_h)\\ &= |p_0(\infty) - p_0(-\infty)\,| + \text{T.V.}(p_h)\\ &\le 2\text{T.V.}(p_h) \le 2\kappa k \text{T.V.}(p_0,u_0).\end{aligned}$$

Furthermore,

$$\begin{aligned}\sup(p_h - p_0(-\infty)) &\le 2\kappa k \text{T.V.}(p_0,u_0),\\ \sup(u_h - u_0(\infty)) &\le 2\kappa \text{T.V.}(p_0,u_0),\\ \sup(u_h - u_0(-\infty)) &\le 2\kappa \text{T.V.}(p_0,u_0).\end{aligned}$$

We can do the same for $\gamma$, but since $\gamma_h(\,\cdot\,,t)$ only takes the same values as $\gamma_h(\,\cdot\,,0)$, we know that $\gamma$ always lies between 1 and $\overline{\gamma}$. In other words, $U_h(\,\cdot\,,t)$ is always contained in $\mathcal{U}$ given by (5.6). □

Let us now prove that $U_h(x,t)$ is bounded, and in particular, bounded away from vacuum. First of all, the Riemann problems we solve at the first step in the Glimm scheme must have a solutions without vacuum, that is, all jumps in $U_h(x,0)$ must satisfy (2.27), cf. Lemma 2.4. If the initial data, for any $a_0 \in [-1,1]$, satisfy

$$\begin{aligned}&u_0(y^0_{r-1}-) - u_0(y^0_{r+1}-)\\ &\qquad < r(p_0(y^0_{r-1}-),0,\gamma_0(y^0_{r-1}-)) - r(0,p_0(y^0_{r+1}-),\gamma_0(y^0_{r+1}-)), \quad r \text{ even},\end{aligned} \tag{5.14}$$

where $y^0_r = x_r + a_0 h$, then no vacuum forms at the first step. The approximate solution is contained in $\mathcal{U}$ which is bounded by the total variation of the initial data, thus, by imposing an extra condition on the initial data, we ensure that all $U \in \mathcal{U}$ have $p \ge p_{\min} > 0$.

**Lemma 5.2.** *If for a $p_{min} > 0$ the initial data satisfy*

$$(\overline{\gamma} - 1)\text{T.V.}(p_0,u_0) \le C_3, \tag{5.15}$$

*where $\tilde{p} = \max\{p_0(\infty), p_0(-\infty)\}$ and*

$$C_3 := \frac{\overline{\gamma}^{1/2}}{\kappa k r'_{\max}}\left(\tilde{p}^{\frac{\overline{\gamma}-1}{2\overline{\gamma}}} - p_{\min}^{\frac{\overline{\gamma}-1}{2\overline{\gamma}}}\right). \tag{5.16}$$

*Then $p \ge p_{\min}$ for all $U \in \mathcal{U}$. Moreover, the solution obtained using the Glimm scheme is bounded and, in particular, satisfies $0 < p_{min} \le p_h(x,t) \le p_{max}$.*

*Proof.* For a $p < \min(p_0)$ we have

$$\max\{|p - p(\infty)|, |p - p(-\infty)|\} = \max\{p(\infty), p(-\infty)\} - p = \tilde{p} - p,$$

hence, $p$ is in $\mathcal{U}$ if $\tilde{p} - p \le 2\kappa k \text{T.V.}(p_0, u_0)$. Thus, if

$$2\kappa k \text{T.V.}(p_0, u_0) \le \tilde{p} - p_{\min}, \tag{5.17}$$

for a given $p_{\min}$ so that $0 < p_{\min} \le \min(p_0)$, then $p \ge p_{\min}$ for all $U \in \mathcal{U}$.

Since condition (5.2) gives restriction on $(\overline{\gamma} - 1)\text{T.V.}(p_0, u_0)$, we reformulate condition (5.17) to do the same. For a $p_0 \ge \tilde{p} \ge p_{\min}$ there is a $u_0$ so that we can write

$$u(p) = u_0 - r(p, p_0, \overline{\gamma}).$$

From the mean value theorem we get that

$$|\tilde{p} - p_{\min}| = \frac{1}{|u'(\hat{p})|} |u(\tilde{p}) - u(p_{\min})| \ge \frac{1}{r'_{\max}} (u(p_{\min}) - u(\tilde{p})),$$

for $p_{\min} \le \hat{p} \le \tilde{p}$. Furthermore,

$$\begin{aligned} u(p_{\min}) - u(\tilde{p}) &= u_0 - \frac{2\overline{\gamma}^{\frac{1}{2}}}{\overline{\gamma} - 1} \left( p_{\min}^{\frac{\overline{\gamma}-1}{2\overline{\gamma}}} - p_0^{\frac{\overline{\gamma}-1}{2\overline{\gamma}}} \right) - u_0 + \frac{2\overline{\gamma}^{\frac{1}{2}}}{\overline{\gamma} - 1} \left( \tilde{p}^{\frac{\overline{\gamma}-1}{2\overline{\gamma}}} - p_0^{\frac{\overline{\gamma}-1}{2\overline{\gamma}}} \right) \\ &= \frac{2\overline{\gamma}^{\frac{1}{2}}}{\overline{\gamma} - 1} \left( \tilde{p}^{\frac{\overline{\gamma}-1}{2\overline{\gamma}}} - p_{\min}^{\frac{\overline{\gamma}-1}{2\overline{\gamma}}} \right), \end{aligned}$$

so that

$$\tilde{p} - p_{\min} \ge \frac{2\overline{\gamma}^{1/2}}{(\overline{\gamma} - 1) r'_{\max}} \left( \tilde{p}^{\frac{\overline{\gamma}-1}{2\overline{\gamma}}} - p_{\min}^{\frac{\overline{\gamma}-1}{2\overline{\gamma}}} \right).$$

Therefore, we have that $p \ge p_{\min} > 0$ for all $p \in \mathcal{U}$ if

$$2\kappa k \text{T.V.}(p_0, u_0) \le \frac{2\overline{\gamma}^{1/2}}{(\overline{\gamma} - 1) r'_{\max}} \left( \tilde{p}^{\frac{\overline{\gamma}-1}{2\overline{\gamma}}} - p_{\min}^{\frac{\overline{\gamma}-1}{2\overline{\gamma}}} \right), \tag{5.18}$$

which proves the lemma. □

We have proved that $U_h(x,t)$ given by (3.4) is bounded and have bounded total variation. Similar to Corollary 19.8 in [20], it can then be proved that $U_h(x,t)$ is locally $L^1$ Lipschitz continuous in time. As already noted, these are the three conditions needed to ensure that $U_h(x,t)$ converges to a weak solution of (1.1). Hence, we have the following theorem:

**Theorem 5.3.** *Consider the Cauchy problem for system* (1.1) *with bounded initial data* (1.2) *where* $\inf(p_0(x)) > 0$ *and* $1 < \gamma_0(x) < \overline{\gamma}$. *Assume that the initial data satisfies* (5.14) *so that no vacuum occurs initially. If*

$$(\overline{\gamma} - 1)\text{T.V.}(p_0, u_0) \le \min\left\{ \frac{C}{9kC_1}, C_3 \right\}, \tag{5.19}$$

$$\text{T.V.}(\gamma_0(x)) \le \frac{C}{9C_2}, \tag{5.20}$$

*then there exists a time global weak entropy solution with bounded total variation of system* (1.1).

By the results of Wagner [23], there is a one-to-one correspondence between a weak solution of (1.1) and a weak solution of the system given in Eulerian coordinates,

$$\begin{aligned} \rho_t + (\rho u)_x &= 0, \\ (\rho u)_t + (\rho u^2 + p(\rho, \gamma))_x &= 0, \end{aligned} \tag{5.21}$$

$$(\rho\gamma)_t + (\rho u\gamma)_x = 0,$$

where $x \in \mathbb{R}$ is the physical space variable and $t \in (0,\infty)$ denotes time.

**Theorem 5.4.** *If there exists a global weak solution to system* (1.1) *with initial data* (1.2)*, then there exists a global weak solution of system* (5.21) *where* $0 < \rho_{\min} \le \rho(x,t) \le \rho_{\max} < \infty$.

## 6. Numerical Results

We have implemented the Glimm scheme as described in Subsection 3.1 using MATLAB. The random sequence $a(s)$ is generated using the function `rand` and `imagesc` is used to visualize the solution.

We find $p_{\max}$ as described in Subsection 2.3. Instead of using (5.15) to find $p_{\min}$, we choose a suitable candidate for $p_{\min}$ and then check that this candidate indeed satisfy $p_{\min} \le p_h(x,t)$ for all $x$ and $t$. We have chosen

$$p_{\min} = \min(p_0(x)) - (p_{\max} - \max(p_0(x))), \tag{6.1}$$

as our candidate, and for both examples this is a good lower bound on $p(x,t)$. In both examples the initial data satisfy (5.2) and (5.3). Since we also have an upper and a lower bound on $p_h(x,t)$, these initial data satisfy the conditions of Theorem 5.3.

**Example 1: Piecewise constant initial data.** The initial data in this example are piecewise constant and symmetric. We have one gas with $p = 1.26$, $u = 3.00$ and $\gamma = 1.051$ which is initially trapped between a second gas with $p = 1.30$, $u = 2.99$ and $\gamma = 1.010$. The

Table 1. The constants for Example 1.

| $p_{\max}$ | $p_{\min}$ | $\overline{\gamma}$ | $C_1$ | $C_2$ | $C$ | $k$ |
|---|---|---|---|---|---|---|
| 1.3067 | 1.2534 | 1.051 | 15.9703 | 1.3309 | 1 | 1.3309 |

constants calculated for this example are listed in Table 1, and (5.2) and (5.3) are satisfied since

$$\text{T.V.}(p_0,u_0) = 0.1 \le 0.1025 = C/(9kC_1(\overline{\gamma}-1)), \tag{6.2}$$

$$\text{T.V.}(\gamma_0) = 0.082 \le 0.0835 = C/(9C_2). \tag{6.3}$$

The solution is computed up to the time $T = 4.5$ using $\Delta x = 0.005$ and $\Delta x/\Delta t = 1.3805 = \max|\lambda(U)|$ so that condition (3.1) is satisfied. This corresponds to $1500 \times 1242$ mesh points. Figure 44 shows the solution for different times. The solution of the Riemann problem initially situated at $x = -1.0$ consists of a 1-rarefaction wave, a contact discontinuity and a 3-shock wave, while the solution of the Riemann problem at $x = 1.0$ consists of a 1-shock wave, a contact discontinuity and a 3-rarefaction wave. In Figure 45 one can see how the waves from these two initially Riemann problems evolve in time and space, and how they interact. Moreover, Figure 46 shows the decreasing Glimm functional for this example.

**Example 2: Continuous initial data.** In this example the initial data are constant for $x < -1$ and $x > 1$. For $-1 < x < 1$ we have a smooth function connecting the constant states. For $p$ and $\gamma$ this function is an increasing function based on $\sin x$, while for $u$ the two constant states are equal and connected by a function based on $\cos x$.

The constants for this example are listed in Table 2, and (5.2) and (5.3) are satisfied since

$$\text{T.V.}(p_0,u_0) = 0.0533 \le 0.0536 = C/(9kC_1(\overline{\gamma}-1)), \tag{6.4}$$

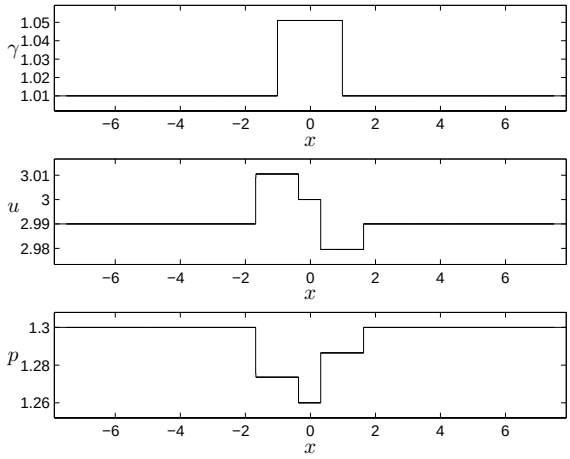


(a) $t = 0.507$.

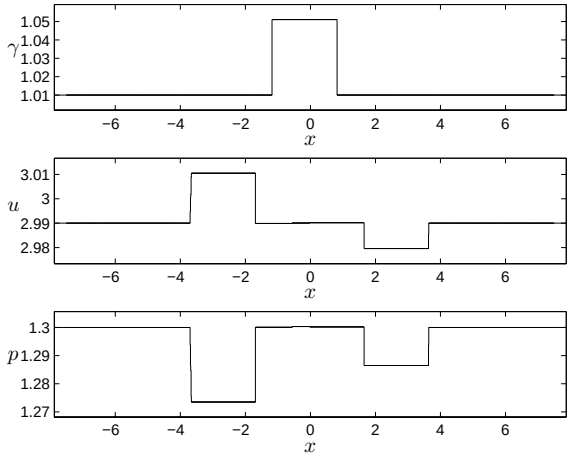


(b) $t = 2.039$.

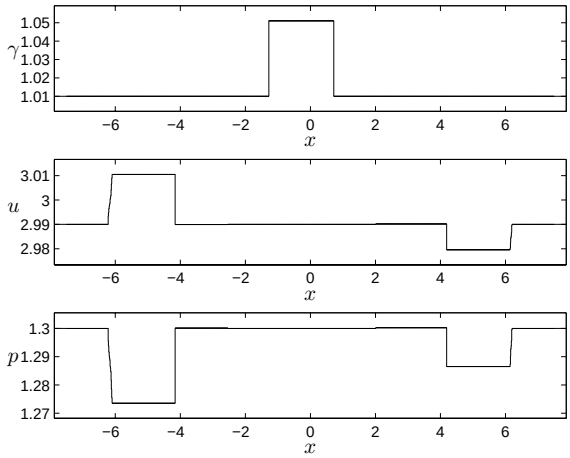


(c) $t = 4.002$.

FIGURE 44. $U_h(x, t)$ at different times.

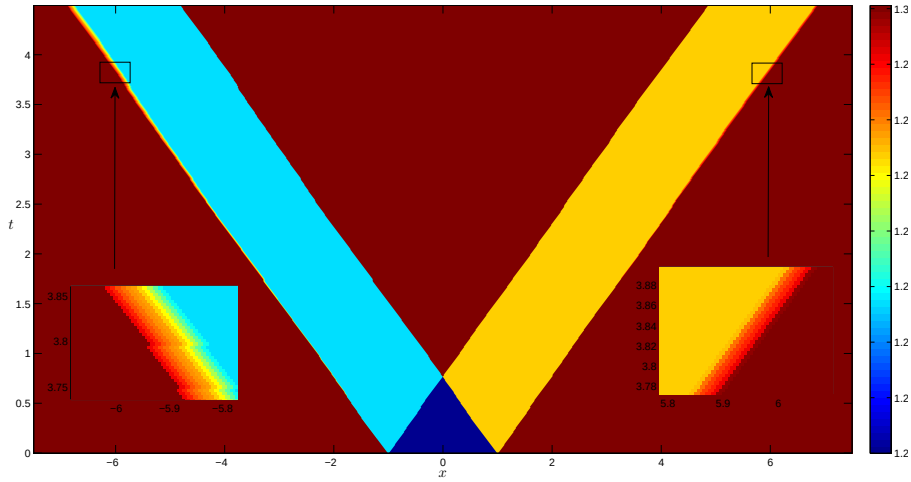


(a) $p_h(x,t)$.

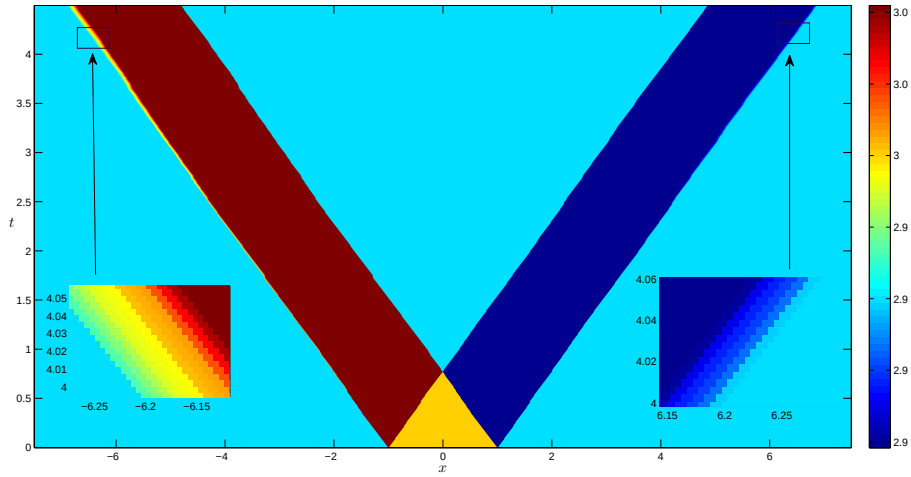


(b) $u_h(x,t)$.

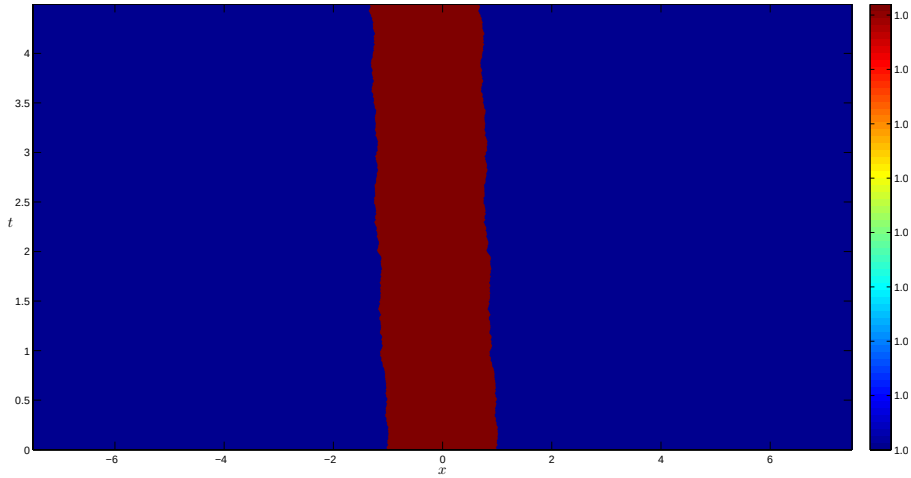


(c) $\gamma_h(x,t)$.

FIGURE 45. The solution $U_h(x,t)$ in the $(x,t)$-plane.

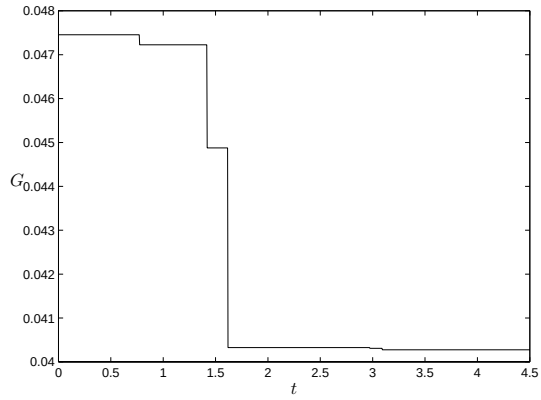


FIGURE 46. The Glimm functional for Example 1.

TABLE 2. The constants for Example 2.

| $p_{\max}$ | $p_{\min}$ | $\overline{\gamma}$ | $C_1$ | $C_2$ | $C$ | $k$ |
|---|---|---|---|---|---|---|
| 1.323 | 1.277 | 1.098 | 15.4427 | 1.3691 | 1 | 1.3691 |

$$\text{T.V.}(\gamma_0) = 0.0799 \leq 0.0812 = C/(9C_2). \tag{6.5}$$

The solution is computed up to the time $T = 1.4$ using $\Delta x = 0.002$ and $\Delta x/\Delta t = 1.4185 = \max|\lambda(U)|$ so that condition (3.1) is satisfied. This corresponds to $1600 \times 992$ mesh points. Figure 47 shows the solution at different times, and Figure 48 shows how the waves from all the initial Riemann problems interact and evolve. Finally, Figure 49 shows the decreasing Glimm functional for this example.

## ACKNOWLEDGMENTS

This research was supported in part by the Research Council of Norway.

## REFERENCES

[1] D. Amadori and A. Corli. On a model of multiphase flow. arXiv:math.AP/0605057 v2 7 July 2007.
[2] F. Asakura. Wave-front tracking for the equation of non-isentropic gas dynamics. *RIMS Kokyuroku*, 1495:78–91, 2006.
[3] F. Asakura. Wave-front tracking for the equation of isentropic gas dynamics. *Quart. Appl. Math.*, 63(1):20–33, 2005.
[4] A. Bressan and R. M. Colombo. Unique solutions of $2 \times 2$ conservation laws with large data. *Indiana Univ. Math. J.*, 44(3):677–725, 1993.
[5] C. Chalons and F. Coquel. Navier–Stokes equations with several independent pressure laws and explicit predictor-corrector schemes. *Numer. Math.* 101:451–478, 2005.
[6] R. J. DiPerna. Existence in the large for quasilinear hyperbolic conservation laws. *Arch. Rational Mech. Anal.*, 52:244–257, 1973.
[7] S. Evje and K. H. Karlsen. Global existence of weak solutions for a viscous two-phase model. *J. Differential Equations*, to appear.
[8] H. Fan. On a model of the dynamics of liquid/vapor phase transitions. *SIAM J. Appl. Math.*, 60(4):1270–1301, 2000.
[9] J. Glimm. Solution in the large for nonlinear hyperbolic systems of equations. *Comm. Pure Appl. Math.*, 18:697–715, 1965.

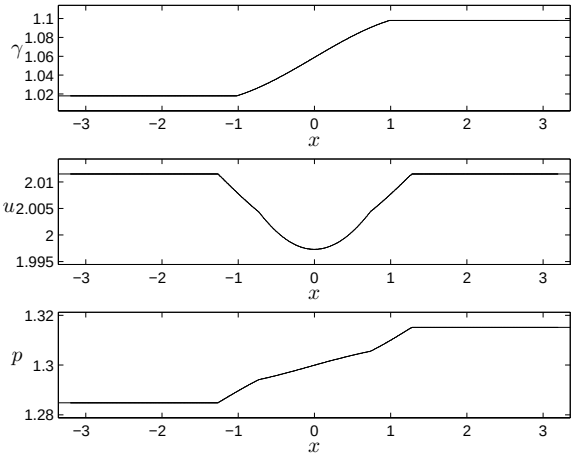


(a) $t = 0.203$.

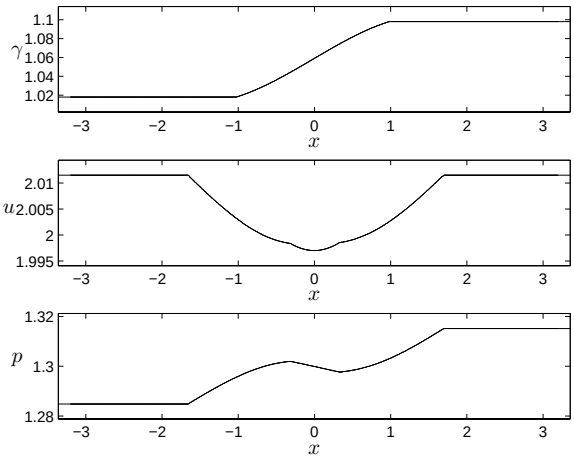


(b) $t = 0.509$.

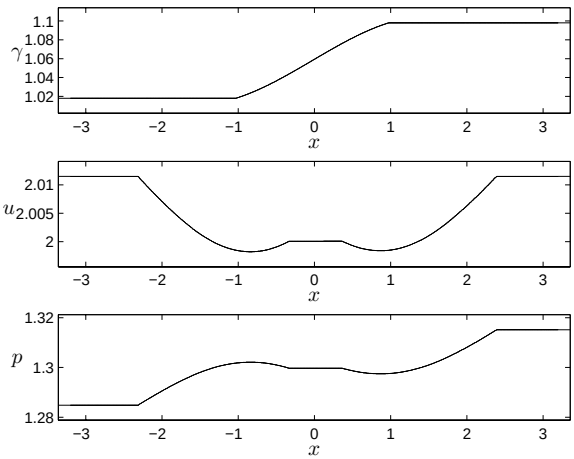


(c) $t = 1.018$.

FIGURE 47. $U_h(x,t)$ at different times.

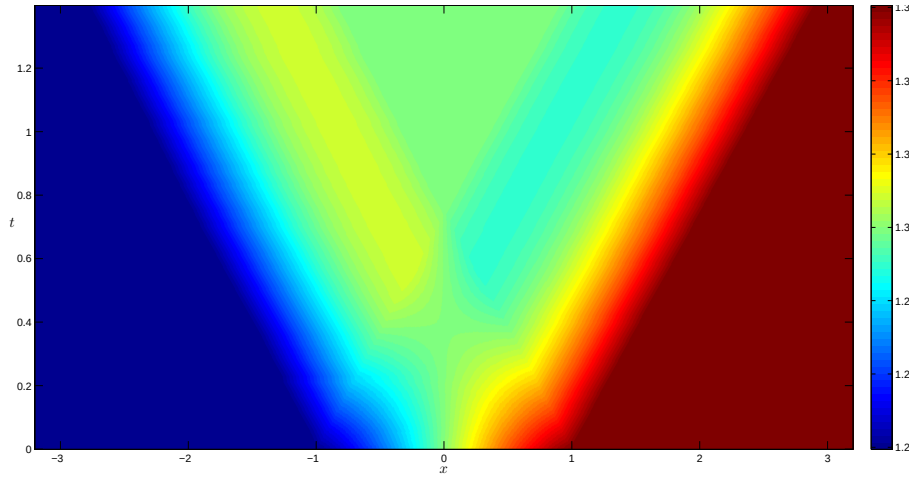


(a) $p_h(x,t)$.

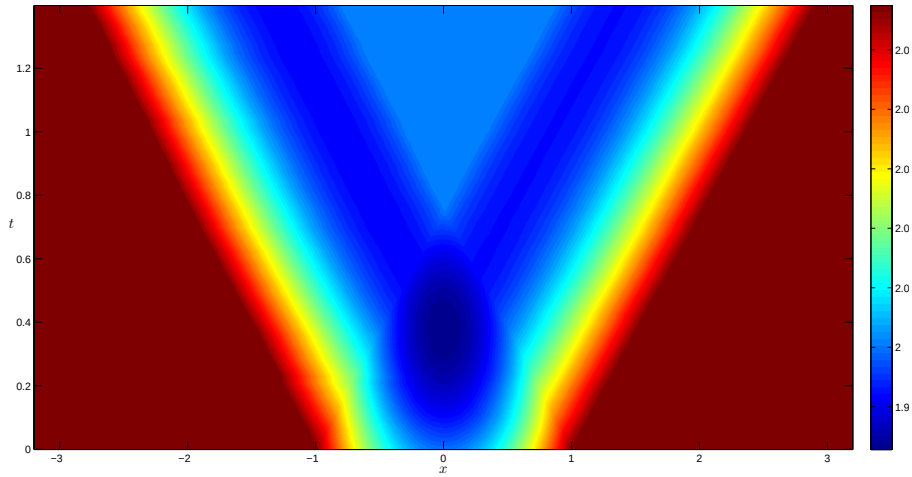


(b) $u_h(x,t)$.

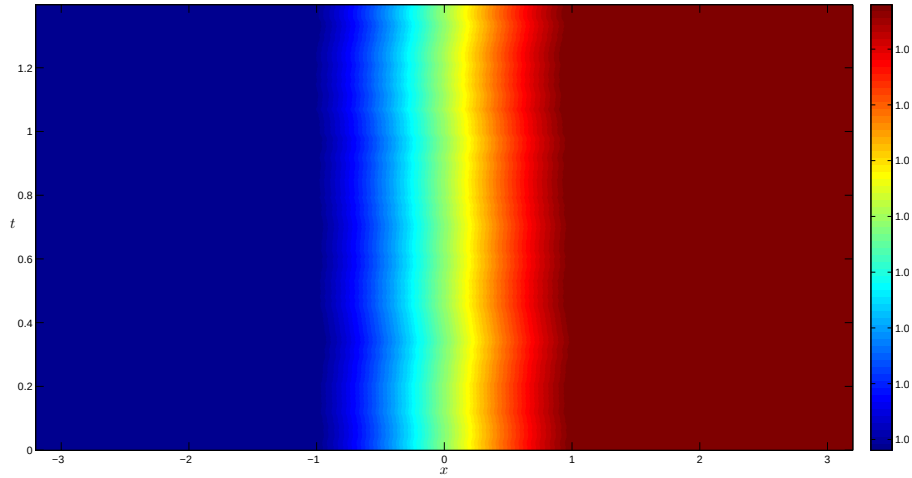


(c) $\gamma_h(x,t)$.

FIGURE 48. The solution $U_h(x,t)$ in the $(x,t)$-plane.

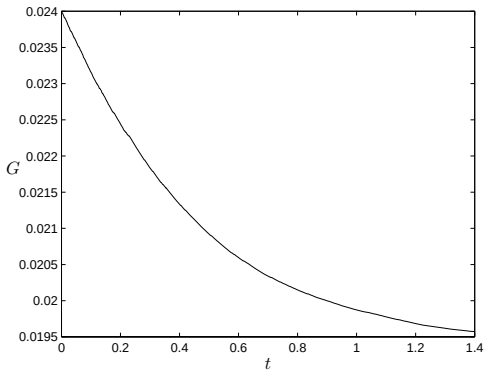


FIGURE 49. The Glimm functional for Example 2.

[10] D. Hoff. Invariant regions for systems of conservations laws. *Trans. Amer. Math. Soc.*, 289(2):591–610, 1985.
[11] H. Holden and N. H. Risebro. *Front Tracking for Hyperbolic Conservation Laws*. Springer-Verlag, 2002.
[12] T.-P. Liu. Solutions in the large for the equations of nonisentropic gas dynamics. *Indiana Univ. Math. J.*, 26(1):147–177, 1977.
[13] T. P. Liu and J. A. Smoller. On the vacuum state for the isentropic gas dynamics equations. *Adv. in Appl. Math.*, 1(4):345–359, 1980.
[14] Y. Lu. *Hyperbolic Conservation Laws and the Compensated Compactness Method*. Chapman&Hall/CRC, Boca Raton, 2003.
[15] T. Nishida. Global solution for an initial boundary value problem for a quasilinear hyperbolic system. *Proc. Japan Acad.*, 44:642–646, 1968.
[16] T. Nishida and J. A. Smoller. Solution in the large for some nonlinear hyperbolic conservation laws. *Comm. Pure Appl. Math.*, 26:183–200, 1973.
[17] Y.-J. Peng. Solutions faibles globales pour l'équation d'Euler d'un fluide compressible avec de grandes données initiales. *Comm. Partial Differential Equations*, 17(1-2):161–187, 1992.
[18] Y.-J. Peng. Solutions faibles globales pour un modèle d'écoulements diphasiques. *Ann. Scuola Norm. Sup. Pisa Cl. Sci. (4)*, 21(4):523–540, 1994.
[19] D. Serre. *System of Conservation Laws 1: Hyperbolicity, Entropies, Shock Waves*. Cambridge University Press, Cambridge, 1999.
[20] J. Smoller. *Shock Waves and Reaction-Diffusion Equations*. Springer-Verlag, second edition, 1994.
[21] J. B. Temple. Solution in the large for the nonlinear hyperbolic concervation laws of gas dynamics. *J. Differential Equations*, 41:96–161, 1981.
[22] B. Temple and R. Young. The large time stability of sound waves. *Comm. Math. Phys.*, 179(2):417–466, 1996.
[23] D. H. Wagner. Equivalence of the Euler and Lagrangian equations of gas dynamics for weak solutions. *J. Differential Equations*, 68(1):118–136, 1987.
[24] W.-A. Yong. A simple approach to Glimm's interaction estimates. *Appl. Math. Lett.*, 12(2):29–34, 1999.
[25] B. D. Wissmann. Global solutions to the ultra-relativistic Euler equations. arXiv:0705.1333v1 [math.AP] 9 May 2007.

(Holden)
Department of Mathematical Sciences, Norwegian University of Science and Technology, NO–7491 Trondheim, Norway, and
Centre of Mathematics for Applications, University of Oslo, P.O. Box 1053, Blindern, NO–0316 Oslo, Norway
*E-mail address*: holden@math.ntnu.no
*URL*: www.math.ntnu.no/~holden/

(Risebro)
Centre of Mathematics for Applications, University of Oslo, P.O. Box 1053, Blindern, NO–0316 Oslo, Norway
*E-mail address*: nilshr@math.uio.no
*URL*: www.math.uio.no/~nilshr/

(Sande)
Department of Mathematical Sciences, Norwegian University of Science and Technology, NO–7491 Trondheim, Norway
*E-mail address*: hildes@math.ntnu.no
*URL*: www.math.ntnu.no/~hildes/

## Paper II

---

**Front tracking for a model of immiscible gas flow with large data**

H. Holden, N. H. Risebro and H. Sande

Preprint

---

# FRONT TRACKING FOR A MODEL OF IMMISCIBLE GAS FLOW WITH LARGE DATA

HELGE HOLDEN, NILS HENRIK RISEBRO, AND HILDE SANDE

Abstract. In this paper we study front tracking for a model of one dimensional, immiscible flow of several isentropic gases, each governed by a gamma-law. The model consists of the $p$-system with variable gamma representing the different gases. The main result is the convergence of a front tracking algorithm to a weak solution, thereby giving existence as well. This convergence holds for general initial data with a total variation satisfying a specific bound. The result is illustrated by numerical examples.

## 1. Introduction

We want to describe the one dimensional, immiscible flow of several isentropic gases. The different gases are initially separated, and the pressure is for all gases given by a $\gamma$-law, that is, $p = \rho^\gamma$, where $\rho$ is the density and $\gamma$ is the adiabatic gas constant for each gas. We assume $\gamma(x,t) > 1$. In Lagrangian coordinates $\gamma$ only depends on $x$ because the different gases cannot mix. Thus, the flow of these gases is described for $x \in \mathbb{R}$ and $t \in (0,\infty)$ by the system

$$\begin{aligned} v_t - u_x &= 0, \\ u_t + p(v,\gamma)_x &= 0, \\ \gamma_t &= 0, \end{aligned} \tag{1.1}$$

where $v = 1/\rho$ is the specific volume, $u$ is the velocity, and $p(v,\gamma) = v^{-\gamma}$ is the pressure function. This $3 \times 3$ system of hyperbolic conservation laws is strictly hyperbolic for $v < \infty$.

We consider the Cauchy problem for this system, that is, system (1.1) with general initial data

$$v(x,0) = v_0(x),\ u(x,0) = u_0(x),\ \gamma(x,0) = \gamma_0(x), \quad x \in \mathbb{R}. \tag{1.2}$$

Glimm [13] proved global existence of a weak solution of the Cauchy problem with initial data of small total variation for strictly hyperbolic systems where each family is either genuinely nonlinear or linearly degenerate, thus including the present system. This solution is found as a limit of the Glimm scheme [13] or of the front tracking method [15, 4]. In [16] we extended the existence result to large initial data for (1.1) by using the Glimm scheme. In this paper we prove that a front tracking algorithm converges to a weak solution, thereby giving an alternative existence argument.

System (1.1) is an extension of the $2 \times 2$ system

$$\begin{aligned} v_t - u_x &= 0, \\ u_t + p(v)_x &= 0, \end{aligned} \tag{1.3}$$

2000 *Mathematics Subject Classification.* Primary: 35L65, 76N15; Secondary: 35A05.
*Key words and phrases.* $p$-system, gamma law, mixture of gases.

which describes the flow of one isentropic gas. The parameter $\gamma$ is constant, and the pressure, still given by a $\gamma$-law, is a function of $v$ only. For the $p$-system with $\gamma = 1$, Nishida [20] showed existence of a global weak solution for arbitrary bounded initial data. For $\gamma > 1$, Nishida and Smoller [21] proved existence of a weak solution for initial data where $(\gamma - 1)$ times the total variation of the initial data is sufficiently small. The case with large initial data for $2 \times 2$ systems is also discussed in [5, 9].

The system (1.1) does not have a coordinate system of Riemann invariants, only a 2-Riemann coordinate. Therefore we do not have the advantage of changing variables to Riemann invariants as for the $p$-system and other $2 \times 2$ systems. Liu [17] proved existence of a solution for the full Euler system with large initial data, another $3 \times 3$ system without a coordinate system of Riemann invariants. Liu's change of variables is inspired by the use of Riemann invariants, but a similar approach does not simplify system (1.1) because $\gamma$ is a function of $x$. The general results by Temple [25] include both the results of [21] and [17]. In [25] one considers the flux function as a smooth one-parameter family of functions where one has existence of a solution for initial data in $B.V.$ when $\epsilon = 0$. Then the system with $0 \leq \epsilon \leq 1$ has a unique solution if $\epsilon$ times the total variation of the initial data is sufficiently small. Letting $\epsilon = \gamma - 1$ for the $p$-system and the Euler equations, one obtains similar results as in [21] and [17]. However, this approach cannot be used for system (1.1) since $\gamma$ is one of the variables. Wissman proved in [29] a large data existence theorem for the $3 \times 3$ system of relativistic Euler equations in the ultra-relativistic limit. Applying a change of coordinates the shock waves become translation invariant and a Nishida-type of analysis is used.

For $3 \times 3$ systems with a 2-Riemann coordinate, Temple and Young [26] showed existence of a solution for initial data with arbitrary large total variation, provided that the oscillations are small. This result applies to (1.1) as well, but we want to avoid this restriction on the oscillations. Peng [23, 22] also considered certain $3 \times 3$ systems (Lagrangian gas dynamics for a perfect gas and a model originating in multiphase flow modeling) with large initial data.

All these existence results are proved using the Glimm scheme. Asakura shows the convergence of front tracking for the $p$-system [3] and for the Euler equations [2] with large initial data. The conditions on the initial data are the same as obtained in [21] and [17]. In [7, 8] front tracking is used to study systems of conservation laws whose flux functions depend on a parameter vector, $\mu$, similar to those in [25]. An approach for establishing $L^1$-estimate pointwise in time between entropy solutions for $\mu \neq 0$ and $\mu = 0$ is given. In particular, letting $\mu = \gamma - 1$, the $L^1$-estimate between entropy solutions in the large for the isentropic Euler equations and the isothermal Euler equations is established in [7] and between entropy solutions in the large for the the Euler equations and the isothermal Euler equations in [8].

Amadori and Corli [1] extend the $p$-system with an extra equation, $\lambda_t = 0$, to model multiphase flow, and use front tracking to prove existence of a weak solution for large data. As for system (1.1), the pressure function in [1] is a function of both $v$ and the new variable, $\lambda$, making the two systems similar. However, since the adiabatic gas constant, $\gamma$, is equal to one in [1], vacuum can never occur for their system as it can for system (1.1). Furthermore, the wave curves in [1] are monotone in $\lambda$, resulting in a considerably simpler analysis of the wave interactions compared with the analysis necessary for the model considered here. The system treated in [1] is a simplified version of the model discussed by Fan in [12]. Similar models, but with a rather different pressure law, are also considered in [11] and [19] applying completely different methods. A model in the context of the Navier–Stokes equation with finitely many independent pressure laws has been studied in [6].

System (1.1) can also be rewritten as a $2 \times 2$ system with discontinuous flux. We get

$$\begin{aligned} v_t - u_x &= 0, \\ u_t + p(v, \gamma(x))_x &= 0, \end{aligned}$$

where the adiabatic gas constant of the different gases is given by the discontinuous function $\gamma(x)$.

This rest of this paper is organized as follows: In Section 2 we discuss the wave curves of the system. The variable $\gamma$ is constant along the rarefaction and shock waves of the first and third family, therefore these curves are similar to the wave curves of the $p$-system. However, these curves are not monotone in $\gamma$, which considerably complicates the interactions of waves with different values of $\gamma$. The second family is linearly degenerate and gives rise to a contact discontinuity along which $p$ and $u$ are constant. Thus, by changing variables to $p$, $u$ and $\gamma$, the Riemann problem is easy to describe. The invariant region for the Riemann problem includes vacuum. This is a problem since the interaction estimates are not valid when $p$ tends to zero, see [18].

Section 3 is the main part of this paper where we first present the front-tracking algorithm. The solution of any Riemann problem is made piecewise constant by approximating rarefaction waves as step functions. In addition, a simplified Riemann solver generating non-physical fronts is introduced in order to ensure that the number of fronts remains finite. The simplified solver is only used for interactions where one or more fronts of the same family collide with a contact discontinuity and the sum of the strengths of the incoming fronts times the strength of the contact discontinuity is less than some threshold parameter. This solver generates non-physical fronts, traveling either to the left or the right, with absolute speed larger than any other front. Moreover, when these non-physical fronts collide with other fronts, they just pass through without changing strength. In Section 3.2 we define a Glimm functional and by considering all possible interactions we prove that it is decreasing under the conditions given in Proposition 3.7. We use this to show that there is a finite number of interactions up to any given time, hence, and thus the front-tracking algorithm is well-defined. Furthermore, we introduce a generation concept in order to bound the total amount of non-physical fronts present at any time. The approximate solution found using front tracking has bounded total variation and is bounded away from vacuum whenever the conditions on the initial data given in Lemma 3.18 and Lemma 3.19 are satisfied. We end Section 3 by proving that the sequence of approximate solutions converges to a weak solution of the system. This proves the main theorem:

**Theorem 3.20.** *Assume that* $(\sup(\gamma(\,\cdot\,,0)) - 1)\mathrm{T.V.}(p(\,\cdot\,,0), u(\,\cdot\,,0))$ *and* $\mathrm{T.V.}(\gamma(\,\cdot\,,0))$ *are sufficiently small. The the front tracking algorithm is well-defined and gives a sequence which converges to a weak solution of* (1.1).

Observe that by reducing the total variation of $\gamma$ and reducing its supremum, one can allow for arbitrary large total variation of $p$ and $u$. Due to Wagner [27], this result translates into existence for the system (3.58) in Eulerian coordinates.

In the last section we study some examples numerically. In the first example we have one gas confined to an interval, surrounded by another gas. The two gases have distinct but constant gammas. The constants that limit the total variation of the initial data are computed, and the initial data are chosen so that they satisfy the conditions in the theorem. The Glimm functional is explicitly computed, and we observe decay in accordance with the theorem. In the second example the initial data are piecewise constant, while $\gamma$ is continuously varying in the third example. For these two examples, the total variation of the

chosen initial data do not satisfy the theorem, nevertheless we still observe that the Glimm functional is decaying.

## 2. The system

It is well-known that systems of hyperbolic conservation laws such as (1.1) do not in general have smooth solutions, even for smooth initial data. Thus, by a solution of (1.1) with the initial data (1.2) we mean a *weak solution* in the distributional sense with $(v,u,\gamma)\in L^1_{\mathrm{loc}}(\mathbb{R}\times[0,\infty))$ so that

$$\begin{aligned}\iint_{\mathbb{R}\times[0,\infty)}(v\phi_t-u\phi_x)\,\mathrm{d}x\mathrm{d}t+\int_{\mathbb{R}}v_0(x)\phi(x,0)\,\mathrm{d}x=0,\\ \iint_{\mathbb{R}\times[0,\infty)}(u\phi_t+p\phi_x)\,\mathrm{d}x\mathrm{d}t+\int_{\mathbb{R}}u_0(x)\phi(x,0)\,\mathrm{d}x=0,\\ \iint_{\mathbb{R}\times[0,\infty)}\gamma\phi_t\,\mathrm{d}x\mathrm{d}t+\int_{\mathbb{R}}\gamma_0(x)\phi(x,0)\,\mathrm{d}x=0,\end{aligned}\tag{2.1}$$

for all test function $\phi\in C_0^\infty(\mathbb{R}\times[0,\infty))$.

If the specific volume, $v$, becomes infinite, which corresponds to zero density and zero pressure, we have *vacuum*. At vacuum, the properties of the system change and the methods used here do not apply, therefore we only consider system (1.1) for $v(x,t)<\infty$. Furthermore, we assume $\gamma(x,t)>1$.

We write $U(x,t)=(v(x,t),u(x,t),\gamma(x,t))$. Often we will work with $p$ instead of $v$, and then also write $U(x,t)=(p(x,t),u(x,t),\gamma(x,t))$.

For $v<\infty$, or equivalently, $p>0$, system (1.1) is strictly hyperbolic with eigenvalues

$$\lambda_1=-\lambda,\qquad\qquad \lambda_2=0,\qquad\qquad \lambda_3=\lambda,\tag{2.2}$$

where $\lambda:=\sqrt{-p_v}=\sqrt{\gamma v^{-\gamma-1}}$, and corresponding eigenvectors

$$r_1=(1,\lambda,0),\qquad\qquad r_2=(-p_\gamma,0,p_v)\,,\qquad\qquad r_3=(-1,\lambda,0).\tag{2.3}$$

Note that the eigenvalues and eigenvectors do not depend on $u$. The first and the third family are genuinely nonlinear, while the second family is linearly degenerate. Moreover, the system does not possess a coordinate system of Riemann invariants, but $\gamma$ is a Riemann coordinate for the second family.

Before we turn to solving system (1.1) with general initial data, we need to solve the Riemann problem for (1.1), that is, when the initial data consists of two constant states separated by a jump, cf. (2.21). The solution of the Riemann problem consists of up to three elementary *waves*, one from each family, and up to two intermediate constant states separating these waves. Thus, we start by looking at the wave curves.

### 2.1. Wave curves.

For the genuinely nonlinear families there are two types of waves; *rarefaction waves* which are continuous waves of the form $U(x,t)=w(x/t)$ satisfying

$$\dot w(x/t)=r_j(w(x/t)),\quad \lambda_j(w(x/t))=x/t,\quad j=1,3,\tag{2.4}$$

where $\lambda_j$ is increasing along the wave, and *shock waves* which are solutions

$$U(x,t)=\begin{cases}U_l, & \text{if } x<\sigma_j t,\\ U_r, & \text{if } x>\sigma_j t,\end{cases}\tag{2.5}$$

satisfying the Rankine–Hugoniot condition

$$\sigma_j(U_r-U_l)=f(U_r)-f(U_l),\quad j=1,3,\tag{2.6}$$

for a shock velocity $\sigma_j$. The admissible shock waves are those satisfying the Lax entropy conditions

$$\lambda_{j-1}(U_l) < \sigma < \lambda_j(U_l), \quad \lambda_j(U_r) < \sigma < \lambda_{j+1}(U_r), \quad j = 1, 3. \tag{2.7}$$

For the linearly degenerate family $j = 2$ there is only one type of waves called *contact discontinuities*. These waves are solutions of the form (2.5) which satisfy the Rankine–Hugoniot condition (2.6) with $\sigma = \lambda_2$.

Fix a left state $U_l$. For each family the *wave curve* consists of all states $U$ that can be connected to the given left state by a wave of this family. The rarefaction solution is of the form

$$U(x,t) = \begin{cases} U_l, & \text{if } x < \lambda_j(U_l)t, \\ w(x/t), & \text{if } \lambda_j(U_l)t < x < \lambda_j(U)t, \\ U, & \text{if } x > \lambda_j(U)t. \end{cases} \tag{2.8}$$

The rarefaction wave curve is the set of all right states $U$ that can be connected to the left state by a rarefaction wave. For system (1.1) these are

$$R_1(v, U_l) := \left( v, u_l - \frac{2\sqrt{\gamma_l}}{\gamma_l - 1} \left( v^{\frac{1-\gamma_l}{2}} - v_l^{\frac{1-\gamma_l}{2}} \right), \gamma_l \right), \qquad v > v_l,$$

$$R_3(v, U_l) := \left( v, u_l + \frac{2\sqrt{\gamma_l}}{\gamma_l - 1} \left( v^{\frac{1-\gamma_l}{2}} - v_l^{\frac{1-\gamma_l}{2}} \right), \gamma_l \right), \qquad v < v_l.$$

The shock curves of all right states which can be connected to $U_l$ by an admissible shock wave are

$$S_1(v, U_l) : = \left( v, u_l - \left( (v_l - v)(v^{-\gamma_l} - v_l^{-\gamma_l}) \right)^{1/2}, \gamma_l \right), \qquad v < v_l,$$

$$S_3(v, U_l) : = \left( v, u_l - \left( (v_l - v)(v^{-\gamma_l} - v_l^{-\gamma_l}) \right)^{1/2}, \gamma_l, \right), \qquad v > v_l,$$

with the shock velocities

$$\sigma_1(U_l, U) = -\sqrt{\frac{v_l^{-\gamma_l} - v^{-\gamma_l}}{v - v_l}} = -\sqrt{\frac{p_l - p}{p^{-1/\gamma_l} - p_l^{-1/\gamma_l}}}, \tag{2.9}$$

$$\sigma_3(U_l, U) = \sqrt{\frac{v^{-\gamma_l} - v_l^{-\gamma_l}}{v_l - v}} = \sqrt{\frac{p - p_l}{p_l^{-1/\gamma_l} - p^{-1/\gamma_l}}}, \tag{2.10}$$

respectively. Note that the shock velocities do not depend on $u$. The curve of all right states that can be connected to $U_l$ by a contact discontinuity is

$$C_2(\gamma, U_l) : = \left( v_l^{\gamma_l/\gamma}, u_l, \gamma \right), \qquad \gamma > 1,$$

with the velocity $\sigma_2 = \lambda_2 = 0$.

Note that $\gamma$ only changes along the contact discontinuities. Furthermore, both $u$ and $p = v^{-\gamma}$ are constant along a contact discontinuity, and we therefore choose to work with $p$, $u$ and $\gamma$. A shock or a rarefaction curve through $U_l$ lies in the plane $\gamma = \gamma_l$ and is equal to the corresponding wave curve for the $p$-system (1.3) with $\gamma = \gamma_l$. We proceed by defining the wave curves using $p$, $u$, and $\gamma$, as depicted in Figure 1,

$$\Phi_1(p, U_l) := \begin{cases} (p, u_l - r(p, p_l, \gamma_l), \gamma_l), & p < p_l, \\ (p, u_l - s(p, p_l, \gamma_l), \gamma_l), & p > p_l, \end{cases} \tag{2.11}$$

$$\Phi_2(\gamma, U_l) := (p_l, u_l, \gamma), \quad \gamma > 1, \tag{2.12}$$

$$\Phi_3(p, U_l) := \begin{cases} (p, u_l + r(p, p_l, \gamma_l), \gamma_l), & p > p_l, \\ (p, u_l - s(p, p_l, \gamma_l), \gamma_l), & p < p_l, \end{cases} \tag{2.13}$$

where

$$r(p, p_l, \gamma_l) := \frac{2\sqrt{\gamma_l}}{\gamma_l - 1}\left(p^{\frac{\gamma_l - 1}{2\gamma_l}} - p_l^{\frac{\gamma_l - 1}{2\gamma_l}}\right), \tag{2.14}$$

$$s(p, p_l, \gamma_l) := \left(\left(p_l^{-\frac{1}{\gamma_l}} - p^{-\frac{1}{\gamma_l}}\right)(p - p_l)\right)^{1/2}. \tag{2.15}$$

Recall that if $p = 0$, we have vacuum, therefore, the wave curves are only well-defined for

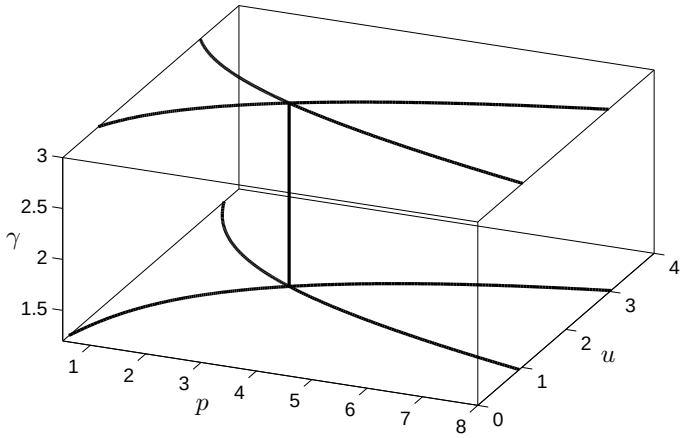


FIGURE 1. The wave curves through two left states with different $\gamma$.

$p > 0$ and $p_l > 0$. All results are for waves contained in

$$\mathcal{D} = \{(p, u, \gamma) \mid p \in [p_{\min}, p_{\max}], |u| < \infty, \gamma \in (1, \overline{\gamma}]\}, \tag{2.16}$$

where $p_{\min} > 0$, $p_{\max} < \infty$ and $\overline{\gamma} \in (1, \infty)$ are constants. For initial data given by (1.2) we will later establish the upper and lower bound on $p$ and show that

$$\overline{\gamma} := \sup_x(\gamma_0(x)), \tag{2.17}$$

for all waves. We moreover have an upper bound on the wave speed for all waves (or fronts) contained in $\mathcal{D}$, and we define

$$\lambda_{\max} = \max_{U \in \mathcal{D}}\{\lambda_i, \sigma_i\} = \max_{U \in \mathcal{D}}\{\lambda_i\}, \tag{2.18}$$

where the last equality is due to the Lax entropy condition (2.7).

Before we discuss some important properties of the wave curves, we mention the *backward wave curves*. These are the curves of all left states $U$ that can be connected to a given right state $U_r$ by a wave of the given family. We denote these wave curves by $\tilde{\Phi}_i$. The backward 3-wave curve will be used several times and this is given by

$$\tilde{\Phi}_3(p, U_r) := \begin{cases} (p, u_r - r(p_r, p, \gamma_r), \gamma_r), & p < p_r, \\ (p, u_r + s(p_r, p, \gamma_r), \gamma_r), & p > p_r, \end{cases} \tag{2.19}$$

where $r$ and $s$ are given by (2.14) and (2.15). We now turn to the properties of the wave curves.

**Lemma 2.1.** *The wave curves in $\mathcal{D}$ have the following properties:*

*(i) The function $\Phi_1$ is strictly decreasing and the function $\Phi_3$ is strictly increasing when considered as functions of $p$.*

*(ii) Given two wave curves, $\Phi_j(p, U_1)$ and $\Phi_j(p, U_2)$ where $j \in \{1, 3\}$, so that $U_1$ is not on $\Phi_j(p, U_2)$ and $U_2$ is not on $\Phi_j(p, U_1)$. Then the two wave curves never intersect.*

*(iii) Consider the projections onto the $(p, u)$-plane of the wave curves through $U_1 = (p_l, u_l, \gamma_1)$ and $U_1 = (p_l, u_l, \gamma_2)$ where $\gamma_1 \leq \gamma_2$. If*

$$\frac{\partial}{\partial p} r(p_l, p_l, \gamma_1) < \frac{\partial}{\partial p} r(p_l, p_l, \gamma_2),$$

*then the projected wave curves going to the right (with respect to $p$) will never intersect, while the projected wave curves going to the left will intersect as $p$ decreases. If*

$$\frac{\partial}{\partial p} r(p_l, p_l, \gamma_1) > \frac{\partial}{\partial p} r(p_l, p_l, \gamma_2),$$

*then the projected wave curves going to the right will intersect, while the projected wave curves going to the left will not. If*

$$\frac{\partial}{\partial p} r(p_l, p_l, \gamma_1) = \frac{\partial}{\partial p} r(p_l, p_l, \gamma_2),$$

*then none of the projected wave curves will intersect.*

*(iv) The slope of a rarefaction wave in the plane $\gamma = \gamma_l$, $\partial r/\partial p$, only depends on $p$ and $\gamma_l$, not on $p_l$. Furthermore, there exist two constants $r'_{\min}$ and $r'_{\max}$ only depending on $p_{\min}$, $p_{\max}$ and $\overline{\gamma}$ so that*

$$r'_{\min} \leq \frac{\partial}{\partial p} r(p, p_l, \gamma_l) \leq r'_{\max}.$$

*(v) The slope of a shock wave in the plane $\gamma = \gamma_l$, $\partial s/\partial p$, depends on $p$, $\gamma_l$ and $p_l$. Furthermore, there exist two constants $s'_{\min}$ and $s'_{\max}$ only depending on $p_{\min}$, $p_{\max}$ and $\overline{\gamma}$ so that*

$$s'_{\min} \leq \frac{\partial}{\partial p} s(p, p_l, \gamma_l) \leq s'_{\max}.$$

*(vi) The wave curves have a continuous derivative at $U_l$,*

$$\lim_{p \to p_l} \frac{\partial}{\partial p} s(p, p_l, \gamma_l) = \frac{\partial}{\partial p} r(p_l, p_l, \gamma_l).$$

*Furthermore,*

$$\frac{\partial}{\partial p} s(p, p_l, \gamma_l) \geq \frac{\partial}{\partial p} r(p, p_l, \gamma_l),$$

*for all $p_l$. Hence, a shock wave is always steeper than a rarefaction wave at a given $p \neq p_l$ provided both waves lie in the plane $\gamma = \gamma_l$.*

*(vii) Rarefaction waves are additive; if a rarefaction wave connects $U_1$ to $U_2$ and another rarefaction wave of the same family connects $U_2$ to $U_3$, then the rarefaction wave connecting $U_1$ to $U_3$ equals the concatenation of the other two rarefaction waves.*

*(viii) Given two 1-shock waves starting at $(p_1, u, \gamma)$ and $(p_2, u, \gamma)$, respectively, and assume $p_1 < p_2$. Then the shock wave starting at $p_1$ is steeper than the shock wave starting at $p_2$ at any given point $p$, that is,*

$$\frac{\partial}{\partial p} s(p, p_2, \gamma) < \frac{\partial}{\partial p} s(p, p_1, \gamma),$$

*for all* $p \geq p_2 > p_1$.

*(ix) Given two 3-shock waves starting at* $(p_1, u, \gamma)$ *and* $(p_2, u, \gamma)$*, respectively, and assume* $p_1 < p_2$*. Then the shock wave starting at* $p_2$ *is steeper than the shock wave starting at* $p_1$ *at any given point* $p$*, that is,*

$$\frac{\partial}{\partial p} s(p, p_1, \gamma) < \frac{\partial}{\partial p} s(p, p_2, \gamma),$$

*for all* $p \leq p_1 < p_2$.

*Proof.* All the properties follows from differentiating the wave curves. □

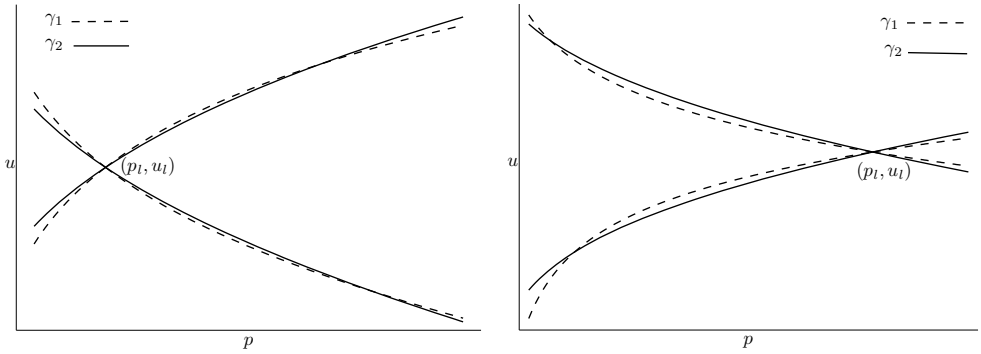


(a) Because $\frac{\partial}{\partial p} r(p_l, p_l, \gamma_l) > \frac{\partial}{\partial p} r(p_l, p_l, \gamma_2)$, the projected wave curves going to the right intersect.

(b) Because $\frac{\partial}{\partial p} r(p_l, p_l, \gamma_l) < \frac{\partial}{\partial p} r(p_l, p_l, \gamma_2)$, the projected wave curves going to the left intersect.

FIGURE 2. The wave curves through $U_1 = (p_l, u_l, \gamma_1)$ (dotted line) and $U_2 = (p_l, u_l, \gamma_2)$, where $\gamma_1 < \gamma_2$, projected onto the $(p, u)$-plane.

The projection onto the $(p, u)$-plane of two wave curves with different $\gamma$'s are shown in Figure 2. Note that the projected wave curves intersect, cf. property (iii), because the slopes of the projected wave curves depend on $\gamma$. The next lemma gives an estimate on how different two waves with different $\gamma$'s are.

**Lemma 2.2.** *Let* $\epsilon_1$ *and* $\epsilon_2$ *be 1-waves of the same type such that* $\epsilon_1$ *connects* $(p_0, u_0, \gamma_1)$ *to* $(p, u_1, \gamma_1)$ *and* $\epsilon_2$ *connects* $(p_0, u_0, \gamma_2)$ *to* $(p, u_2, \gamma_2)$*, or let* $\eta_1$ *and* $\eta_2$ *be 3-waves of the same type such that* $\eta_1$ *connects* $(p, u_1, \gamma_1)$ *to* $(p_0, u_0, \gamma_1)$ *and* $\eta_2$ *connects* $(p, u_2, \gamma_2)$ *to* $(p_0, u_0, \gamma_2)$*. Assume that all waves are contained in* $\mathcal{D}$ *and furthermore that* $u_1 < u_2$*. Then*

$$u_2 - u_1 \leq c_2 \left| p - p_0 \right| \left| \gamma_2 - \gamma_1 \right|, \tag{2.20}$$

*where* $c_2$ *only depends on* $p_{\min}$, $p_{\max}$ *and* $\overline{\gamma}$.

Note that for 1-waves we compare two waves where the projected waves start at the same point in the $(p, u)$-plane, while we for 3-waves compare two waves where the projected waves end at the same point. The proof of this lemma is given in [16] and is based on the techniques used in [28].

2.2. **The Riemann Problem.** We have the following fundamental definition.

**Definition 2.3.** The Riemann problem for (1.1) is the Cauchy problem with initial data

$$U(x,0) = \begin{cases} U_l, & \text{if } x < 0, \\ U_r, & \text{if } x > 0, \end{cases} \tag{2.21}$$

where $U = (v, u, \gamma)$ and $U_l, U_r \in \mathbb{R}$ are constants.

**Lemma 2.4.** *The Riemann problem for* (1.1) *where $U_l$ and $U_r$ are contained in $\mathcal{D}$, cf.* (2.16)*, has a unique solution without vacuum if*

$$u_r - u_l < r(p_r, 0, \gamma_r) - r(0, p_l, \gamma_l). \tag{2.22}$$

*Proof.* Note that if $\gamma_l = \gamma_r$, then the Riemann problem for (1.1) reduces to the Riemann problem for the $p$-system (1.3). The solution of this problem is described in detail in [24, Ch. 17, §A], and it is unique if (2.22) is satisfied with $\gamma_l = \gamma_r$.

A 2-wave takes us from one plane, $\gamma = \gamma_1$, to another plane, $\gamma = \gamma_2$, while $p$ and $u$ remain constant. Therefore, the Riemann problem has a unique solution if the projections onto the $(p, u)$-plane of the 1-wave curve, $\Phi_1(p, U_l)$, and the backward 3-wave curve, $\tilde{\Phi}_3(p, U_r)$, have a unique intersection point. From property (i) of Lemma 2.1 we have that the projection of $\Phi_1$ is strictly decreasing in $p$ and it follows that the projection of $\tilde{\Phi}_3$ is strictly increasing in $p$. Hence, the projected curves intersect at most once. The only case where the two curves do not intersect is if the projection of the backward 3-rarefaction wave from $U_r$ always lies above the projection of the 1-rarefaction wave from $U_l$. Thus, if

$$u_r - r(p_r, 0, \gamma_r) < u_l - r(0, p_l, \gamma_l),$$

then the projections of $\tilde{\Phi}_3(p, U_r)$ and $\Phi_1(p, U_l)$ onto the $(p, u)$-plane have a unique intersection point, and the Riemann problem has a unique solution. □

The solution of the Riemann problem $(U_l, U_r)$ is constructed as follows: Let $(\tilde{p}, \tilde{u})$ be the unique intersection between the projections of $\Phi_1(p, U_l)$ and $\tilde{\Phi}_3(p, U_r)$ onto the $(p, u)$-plane. We connect $U_l = (p_l, u_l, \gamma_l)$ to $\tilde{U}_1 = (\tilde{p}, \tilde{u}, \gamma_l)$ by a 1-curve, then we go from $\tilde{U}_1$ to $\tilde{U}_2 = (\tilde{p}, \tilde{u}, \gamma_r)$ along a contact discontinuity, and finally connect $\tilde{U}_2$ to $U_r = (p_r, u_r, \gamma_r)$ by a 3-wave.

2.3. **Invariant region and vacuum.** A region $\Omega$ is invariant for the Riemann problem if for any Riemann problem with initial data in $\Omega$, its solution is also in $\Omega$. For the $p$-system we know from [14, Ex. 3.5] that the convex region in the $(v, u)$-plane between the integral curves of the eigenvectors is invariant. This region bounds $v$ from below, but not from above, thus vacuum is included in the invariant region. In the $(p, u)$-plane this corresponds to the region bounded by $p = 0$ and the two integral curves. Since $\gamma$ cannot take any other values than those of the initial data, we find the invariant region for the $p$-system for each $\gamma$ and take the union of these. This gives us an invariant region for (1.1). Moreover, this gives us the upper bound on $p$, $p_{\max}$, which we need, but $p$ is still not bounded away from vacuum.

## 3. The Cauchy problem

We now turn to the Cauchy problem and use front tracking to obtain a sequence of approximate solutions. The goal of this section is to show that a subsequence converges to a weak solution of (1.1). In order to do this, we find a suitable Glimm functional and show

that it decreases in time. This requires detailed analysis of all possible interactions and most of this section is devoted to this. First of all we need some notation. We let

| | | |
|---|---|---|
| $\epsilon$ define a 1-wave, | $\alpha$ a 1-shock wave, | $\mu$ a 1-rarefaction wave, |
| $\eta$ a 3-wave, | $\beta$ a 3-shock wave, | $\nu$ a 3-rarefaction wave, |
| $\zeta$ a 2-wave, | $\theta$ a 1- or 3-wave. | |

Furthermore, we define *the strength of a* 1*-wave* or *a* 3*-wave* as the jump in $p$ across the wave and *the strength of a* 2*-wave* as the jump in $\gamma$ across the wave. The strength of a wave or a front is denoted by $|\theta|$. We are now ready to discuss front tracking and to define fronts. Note that we will use the above notation for fronts as well as waves. In addition, we will define non-physical fronts which will be denoted by $\theta^{\text{np}}$ and *the strength of a non-physical front* will be defined as its jump in $u$.

3.1. **Front tracking.** The first step of front tracking is to approximate the initial data (1.2) by a piecewise constant function $U_0^{\delta_{\text{init}}}$ so that

$$\lim_{\delta_{\text{init}}\to 0} \|U_0^{\delta_{\text{init}}} - U_0\|_{L^1} = 0,$$

where $U_0 = (p_0, u_0, \gamma_0)$ and $\delta_{\text{init}}$ is the distance between the discontinuities. Furthermore, the approximation has to satisfy (2.22) at every discontinuity so that all initial Riemann problems have a unique solution. Thus, no vacuum forms at $t = 0+$.

We then solve the Riemann problem defined by the discontinuities in $U_0^{\delta_{\text{init}}}$. All solutions of Riemann problems in front tracking have to be piecewise constant. Since shock waves and contact discontinuities are already piecewise constants, we use *an approximate Riemann solver* where the continuous rarefaction waves are approximated. We replace the rarefaction wave from the left state, $U_l$, to the right state, $U_r$, by a step function. Let $k := \lceil |p_r - p_l| / \delta \rceil$. Then we divide the rarefaction wave into $k$ jumps, each with strength $\hat{\delta} = |\theta|/k \le \delta$. The discontinuities move with the speed of their left state. Note that the jumps in the approximated rarefaction wave do not satisfy the Rankine–Hugoniot condition. It is obvious that this approximate solution of the Riemann problem converges to the exact solution a.e. when $\delta$ tends to zero.

Solving all Riemann problems present initially by the approximate solver, generates an approximate solution of the Cauchy problem for small $t > 0$. The solution is piecewise constant and a *front* is one discontinuity in the solution. Hence, a shock wave or a contact discontinuity is one front, while an approximated rarefaction wave consists of $k$ fronts where each front has strength less than or equal to $\delta$. Note that the two parameters $\delta_{\text{init}}$ and $\delta$ are chosen so that $\delta_{\text{init}} = \mathcal{O}(\delta)$. We denote the approximate solution $U^\delta$.

We track all fronts in $U^\delta$ until two or more fronts *interact*, that is, collide at a *collision point* $(x, \tau)$. The colliding fronts are called *incoming fronts*. Then we solve the Riemann problem defined by the states immediately to the left and right of the incoming fronts, and the fronts in this approximate solution are called *outgoing fronts* and are usually identifiable by a prime. We keep tracking all fronts and solving Riemann problems each time fronts collide.

In order to ensure that front tracking is well-defined for all times, we follow the approach of Bressan [4] and introduce non-physical fronts. Thus, an interaction is either solved by the standard approximate solver as described above, or by a *simplified Riemann solver*. Let $\rho > 0$ be a fixed threshold parameter. Interactions of the form $\zeta + \sum_i \epsilon_i$, or the symmetric

form $\sum_i \eta_i + \zeta$, are solved using the simplified Riemann solver if

$$|\zeta\,|\sum_i |\epsilon_i\,| \le \rho, \quad \text{or} \quad |\zeta\,|\sum_i |\eta_i\,| \le \rho, \tag{3.1}$$

respectively, otherwise the approximate Riemann solver is used. All other interactions are always solved using the approximate solver. The simplified Riemann solver introduces non-physical fronts which we denote $\theta^{\mathrm{np}}$. By construction, both $p$ and $\gamma$ are constant across a non-physical front and its strength equals the jump in $u$. In order to preserve the symmetry property of system (1.1), we introduce non-physical fronts traveling both to the left and to the right. In either case they travel with the absolute speed $\lambda_{\mathrm{np}} > \lambda_{\max}$, hence the name. Note that the Rankine–Hugoniot condition (2.6) is not satisfied for a non-physical front.

Let us first detail the solution of the interaction between one front and a contact discontinuity using the simplified solver. The solution consists of two physical fronts and a non-physical front:

$$\zeta + \epsilon \to \epsilon' + \zeta + \theta^{\mathrm{np}}.$$

The outgoing front $\epsilon'$ has the same strength and type as $\epsilon$, and connects $U_l = (p_l, u_l, \gamma_l)$ to $\tilde{U}_1 = (p_r, \tilde{u}, \gamma_l)$, as depicted in Figure 3(a). The contact discontinuity is, as always, unchanged, connecting $\tilde{U}_1$ to $\tilde{U}_2 = (p_r, \tilde{u}, \gamma_r)$. The non-physical front then connects $\tilde{U}_2$ to $U_r = (p_r, u_r, \gamma_r)$. Moreover, the non-physical front has positive speed traveling to the right. For the symmetric case,

$$\eta + \zeta \to \theta^{\mathrm{np}} + \zeta + \eta',$$

the non-physical front has negative speed.

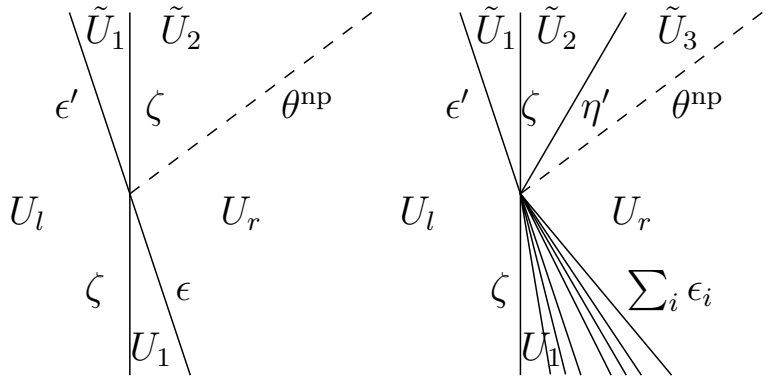


(a) Simplified solver for $\zeta + \epsilon$. (b) Simplified solver for $\zeta + \sum_i \epsilon_i$.

FIGURE 3. The simplified Riemann solver with non-physical fronts (dashed lines).

The solution we get using the simplified solver when two or more fronts of the same family interact with a contact discontinuity, consists of one physical front of each family, in addition to a non-physical front;

$$\zeta + \sum_i \epsilon_i \to \epsilon' + \zeta + \eta' + \theta^{\mathrm{np}},$$

see Figure 3(b). In order to determine the outgoing fronts, we introduce two auxiliary fronts, $\overline{\epsilon}$ and $\overline{\eta}$. These fronts are the solution of the Riemann problem $(U_1, U_r)$, thus, $\overline{\epsilon}$ connects $U_1$

to the intermediate state $\overline{U} = (\overline{p}, \overline{u}, \gamma_r)$, and $\overline{\eta}$ connects $\overline{U}$ to $U_r$. Let $\epsilon'$ be the front that has the same strength and type as $\bar{\epsilon}$, but with $\gamma = \gamma_l$, that is, connecting $U_l$ to $\tilde{U}_1 = (\overline{p}, \tilde{u}, \gamma_l)$. The contact discontinuity is unchanged, connecting $\tilde{U}_1$ to $\tilde{U}_2 = (\overline{p}, \tilde{u}, \gamma_r)$. Let $\eta'$ be $\overline{\eta}$ shifted in the $u$-direction so that $\eta'$ connects $\tilde{U}_2$ to $\tilde{U}_3 = (p_r, u_r + \tilde{u} - \overline{u}, \gamma_r)$. Finally, the non-physical front connects $\tilde{U}_3$ to $U_r$. The non-physical front has positive speed and changes only the value of $u$, as it is supposed to. This construction of the solution using the simplified Riemann solver is inspired by the formal tool of splitting an interaction into steps that we will introduce in the next section. More details on the process of finding the outgoing fronts using the simplified solver are included in the proof of Lemma 3.11 where we obtain estimates for these interactions. Note that $\epsilon' + \zeta + \eta'$ is the solution of the Riemann problem $(U_l, \tilde{U}_3)$, thus, the Rankine–Hugoniot condition (2.6) is satisfied for any shock or contact discontinuity. However, it is not satisfied for the non-physical front or any approximated rarefaction wave. We resolve the symmetric interaction in a similar manner, and get a non-physical front with negative speed;

$$\sum_i \eta_i + \zeta \to \theta^{\mathrm{np}} + \epsilon' + \zeta + \eta'.$$

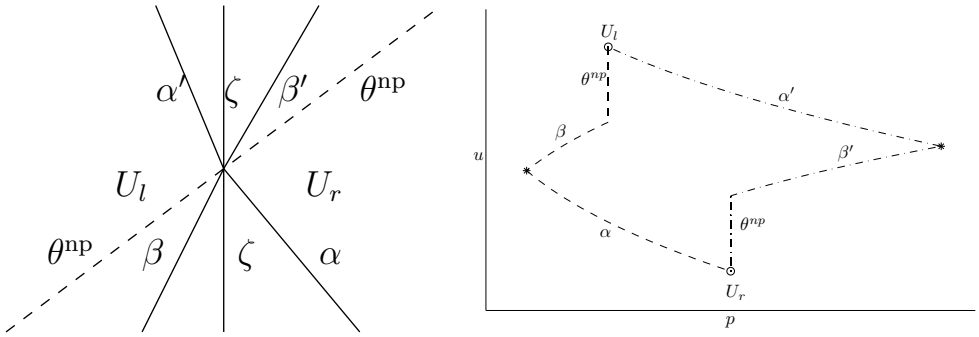


(a) in the $(x,t)$-plane. (b) Projected onto the $(p,u)$-plane.

FIGURE 4. The interaction $\theta^{\mathrm{np}} + \beta + \zeta + \alpha \to \alpha' + \zeta + \beta' + \theta^{\mathrm{np}}$.

Whenever we have an interaction with an incoming non-physical front, as in Figure 4, we first let the non-physical front pass through with its strength unchanged. Then we solve the remaining interaction, which is slightly shifted along the $u$-direction, using the approximate or simplified solver according to condition (3.1). Note that all wave curves are invariant in the $(p,u)$ plane under a translation in $u$.

Before we turn to the discussion of all possible interactions, we look at the error introduced using the simplified solver instead of the approximate solver. The lemma is given for the interactions involving 1-fronts, but we have the same results for the symmetric interactions involving 3-fronts.

**Lemma 3.1.** *Consider the interaction $\zeta + \sum_i^n \epsilon_i$ for $n \geq 1$. Let*

$$\zeta + \sum_i^n \epsilon_i \to \hat{\epsilon} + \zeta + \hat{\eta},$$

*be the solution, with intermediate states* $\hat{U}_i$, $i = 1, 2$, *obtained using the approximate solver, and let*

$$\zeta + \sum_i^n \epsilon_i \to \begin{cases} \epsilon' + \zeta + \theta^{np}, & \text{if } n = 1, \\ \epsilon' + \zeta + \eta' + \theta^{np}, & \text{if } n > 1, \end{cases}$$

*be the solution obtained using the simplified solver, with intermediate states* $\tilde{U}_i$, $i = 1, 2$ *and* $i = 1, 2, 3$, *respectively. Then,*

$$|\sigma_{\hat{\alpha}} - \sigma_{\alpha'}| = \mathcal{O}(1)\,|\theta^{np}|, \quad \text{if } \epsilon' = \alpha',$$
$$|\lambda_{\hat{\mu}} - \lambda_{\mu'}| = 0, \quad \text{if } \epsilon' = \mu',$$

*and, if* $\hat{\eta}$ *is of the same type as* $\eta'$ *for* $n > 1$,

$$\left|\sigma_{\hat{\beta}} - \sigma_{\beta'}\right| = \mathcal{O}(1)\,|\theta^{np}|, \quad \text{if } \eta' = \beta',$$
$$|\lambda_{\hat{\nu}} - \lambda_{\nu'}| = \mathcal{O}(1)\,|\theta^{np}|, \quad \text{if } \eta' = \nu'.$$

*Moreover,* $\left|\hat{U}_i - \tilde{U}_i\right| = \mathcal{O}(1)\,|\theta^{np}|$, $i = 1, 2$, *and* $\left|U_r - \tilde{U}_j\right| = \mathcal{O}(1)\,|\theta^{np}|$ *where* $j = 2$ *if* $n = 1$ *and* $j = 3$ *if* $n > 1$.

*Proof.* First note that $p$ and $u$ are equal for $\tilde{U}_1$ and $\tilde{U}_2$, and for $\hat{U}_1$ and $\hat{U}_2$, and we therefore omit the indices. Figure 5 shows the solutions of $\zeta + \epsilon$ for both solvers, and Figure 6 shows the solutions and the auxiliary fronts for an interaction of the type $\zeta + \sum_i \epsilon_i$. The rarefaction

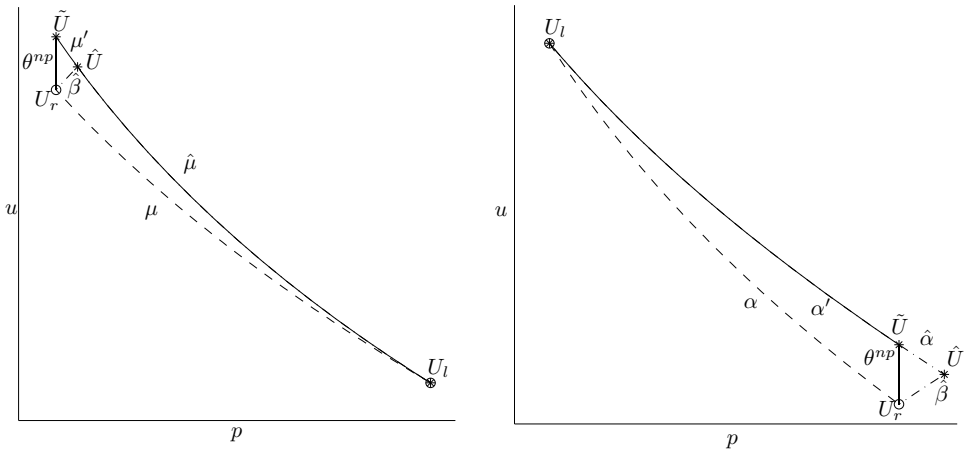


(a) $\zeta + \mu$. (b) $\zeta + \alpha$.

FIGURE 5. The interaction (dashed lines) solved by the approximate solver (dash-dotted lines) and by the simplified solver (solid lines).

fronts $\mu'$ and $\hat{\mu}$ have the same left state, and they therefore have the same speed. Likewise, the left state is the same for $\alpha'$ and $\hat{\alpha}$. However, the speed of a shock-front depends on the value of $p$ at the right state as well, where $p = \tilde{p}$ for $\alpha'$ and $p = \hat{p}$ for $\hat{\alpha}$. Since this difference in $p$ is less than a constant times the jump in $u$ across the non-physical front, that is, $|\tilde{p} - \hat{p}| = \mathcal{O}(1)\,|\theta^{\mathrm{np}}|$, we get

$$|\sigma_{\hat{\alpha}} - \sigma_{\alpha'}| = |\sigma_1(p_l, \hat{p}) - \sigma_1(p_l, \tilde{p})| \le |\sigma_1'(p_l, p^*)|\,|\tilde{p} - \hat{p}| = \mathcal{O}(1)\,|\theta^{\mathrm{np}}|,$$

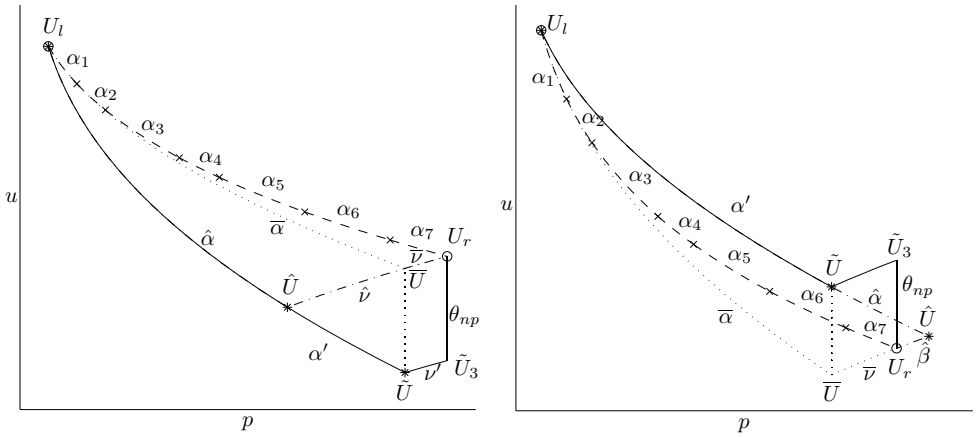


(a) When $\eta'$ and $\hat{\eta}$ are of the same type

(b) When $\eta'$ and $\hat{\eta}$ are not of the same type.

FIGURE 6. The interaction $\zeta + \sum_{i=1}^{7} \alpha_i$ (dashed lines), with the auxiliary curves (dotted lines), solved by the approximate solver (dash-dotted lines) and by the simplified solver (solid lines).

where $\sigma_1'$ is the derivative with respect to the second argument and $\hat{p} \le p^* \le \tilde{p}$.

If $n > 1$ and $\eta'$ is of the same type as $\hat{\eta}$, as for the interaction depicted in Figure 6(a), then $p = p_r$ at the right state for both fronts. However, at the left state we have $p = \tilde{p}$ for $\eta'$ and $p = \hat{p}$ for $\hat{\eta}$. This is the same difference in $p$ as above, thus,

$$\left|\sigma_{\hat{\beta}} - \sigma_{\beta'}\right| = |\sigma_3(\hat{p}, p_r) - \sigma_3(\tilde{p}, p_r)\,| \le |\sigma_3'(p^*, p_r)\,|\,|\tilde{p} - \hat{p}\,| = \mathcal{O}(1)\,|\theta^{\mathrm{np}}\,|,$$
$$|\lambda_{\hat{\nu}} - \lambda_{\nu'}\,| = |\lambda(\hat{p}) - \lambda(\tilde{p})\,| \le |\lambda_3'(p^*)\,|\,|\tilde{p} - \hat{p}\,| = \mathcal{O}(1)\,|\theta^{\mathrm{np}}\,|,$$

where $\sigma_3'$ is the derivative with respect to the first argument, $\lambda_3'$ the derivative with respect to $p$, and $\hat{p} \le p^* \le \tilde{p}$.

Moreover, $\gamma$ is equal for the two solutions and $|\tilde{u} - \hat{u}\,| \le |\theta^{\mathrm{np}}\,|$, thus, $\left|\hat{U}_i - \tilde{U}_i\right| = \mathcal{O}(1)\,|\theta^{\mathrm{np}}\,|$, $i = 1, 2$. Finally, let $j = 2$ for $n = 1$ and $j = 3$ for $n > 1$. Then, $\tilde{p}_j = p_r$ and $|\tilde{u}_j - u_r\,| = |\theta^{\mathrm{np}}\,|$, hence, $\left|U_r - \tilde{U}_j\right| = \mathcal{O}(1)\,|\theta^{\mathrm{np}}\,|$. □

In front tracking an interaction is a collision of arbitrarily many fronts at one point in space-time. However, in order to collide at the same point, their speeds must decrease from left to right. This observation has the immediate consequence.

**Lemma 3.2.** *All interactions between physical fronts in front tracking for system* (1.1) *is of the general form*

$$\sum_{i=1}^{m} \eta_i + \zeta + \sum_{j=1}^{n} \epsilon_j, \tag{3.2}$$

*where $\eta_i$ is a 3-front, $\zeta$ is a contact discontinuity, $\epsilon_j$ is a 1-front, and two adjacent fronts cannot both be rarefaction-fronts. All interactions with incoming non-physical fronts are of the same general form with a non-physical front as the leftmost and/or the rightmost incoming front. Furthermore, all wave families do not need to be present in an interaction.*

This is a major difference between front tracking and the Glimm scheme where at most four waves can interact. Furthermore, only the case with two interacting fronts or waves is the same in front tracking and in the Glimm scheme. Still, the following, simple symmetry property for system (1.1) proved in [16], is useful also for the interactions in front tracking.

**Lemma 3.3.** [16, Lemma 3.1] *Under the transformation $x \mapsto -x$, a 1-wave connecting $U_l$ to $U_r$ becomes a 3-wave connecting $U_r$ to $U_l$, and vice versa. A 2-wave is unchanged under this transformation, and a non-physical front becomes a non-physical front traveling in the opposite direction. Furthermore, the leftmost wave with respect to $x$ will become the rightmost wave with respect to $-x$, and so on.*

One of our main goals is to show that the approximate solution can be constructed at any time in a finite number of steps. Therefore we look at which interactions increase the number of fronts present. Firstly, recall that the solution of a Riemann problem consists of up to three waves, one from each family. Hence, the solution found by the approximate Riemann solver has four or more fronts if, and only if, a rarefaction wave splits into several fronts. For an interaction between three or more fronts solved by the approximate solver, the number of fronts can therefore only increase due to splitting of rarefaction waves.

Furthermore, an outgoing contact discontinuity is only present if there is an incoming contact discontinuity. Thus, the number of fronts for an interaction between two fronts, none of which are contact discontinuities, can only increase due to splitting of rarefaction waves.

Whenever the simplified solver is used for an interaction between two incoming fronts, we get two outgoing physical waves and one outgoing non-physical front. If there are three or more incoming fronts, the simplified solver gives three outgoing physical waves and one non-physical front. Hence, for an interaction solved by the simplified solver, the number of physical fronts can increase only due to splitting of rarefaction waves.

Except for split rarefaction waves, the number of fronts increases only for the interaction between a contact discontinuity and one other front solved by the approximate solver. These interactions have at least three outgoing fronts, and we refer to them as $\gamma$-collisions.

**Definition 3.4.** A *$\gamma$-collision* is the interaction between a contact discontinuity and a 1- or 3-front.

The four different $\gamma$-collisions, where symmetry reduces it to two distinct cases, are discussed discussed in the proof of Lemma 3.8 in Section 3.2.

If the strength of an outgoing rarefaction wave is larger than $\delta$, it splits into several fronts. The interactions where this might happen are either a new rarefaction-collision or an increasing rarefaction-collision as defined below.

**Definition 3.5.** A *new rarefaction-collision* is an interaction where there is an outgoing rarefaction wave of a family in which there are no incoming rarefaction-fronts.

**Definition 3.6.** An *increasing rarefaction-collision* is an interaction where the strength of an outgoing rarefaction wave is greater than the sum of the strengths of the incoming rarefaction-fronts of the same family.

Note that a $\gamma$-collision can also be a new rarefaction-collision, an increasing rarefaction-collision, or even both.

Summing up the front tracking construction, we have defined a piecewise constant function $U^\delta$, so that for all fixed $t$, $U^\delta(\cdot, t)$ is a piecewise constant function. Furthermore the construction gives a sequence of collision times $\tau_1 < \tau_2 < \dots$, and $U^\delta(\cdot, t)$ is defined for all

$t \le \lim_{n\to\infty} \tau_n$. We shall show that either $\{\tau_n\}$ is a finite sequence or $\lim_n \tau_n = \infty$, i.e., that $U^\delta(\cdot, t)$ can be constructed for any $t > 0$.

3.2. **The decreasing Glimm functional.** Set $t_n = (\tau_n + \tau_{n+1})/2$, where we have defined $\tau_0 = 0$, and define the functional

$$G(t_n) := F(t_n) + 3C_1(\overline{\gamma} - 1)Q_1(t_n) + 3C_2Q_2(t_n), \tag{3.3}$$

where $C_1$ is the constant appearing in the estimates given by (3.16) for the interaction of Type Bbii, cf. the proof of Lemma 3.8,

$$C_2 := \frac{c_2}{\min\{r'_{\min}, s'_{\min}\}} = kc_2, \tag{3.4}$$

where $c_2$ is the constant from Lemma 2.2 and

$$k := \frac{1}{\min\{r'_{\min}, s'_{\min}\}}. \tag{3.5}$$

Note that both $C_1$ and $C_2$ are constants only depending on $p_{\min}$, $p_{\max}$ and $\overline{\gamma}$. This is the same functional as the Glimm functional defined in [16], and the two first terms are similar to the Glimm functional used in [21]. The linear functional $F$ and the two quadratic functionals $Q_1$ and $Q_2$ are defined by

$$F(t_n) := \sum\{|\theta| \mid \text{all shock-fronts } \theta \text{ at } t = t_n\}, \tag{3.6}$$

$$Q_1(t_n) := \sum\{|\alpha|\,|\beta| \mid \text{all approaching 1- and 3-shock-fronts at } t = t_n\}, \tag{3.7}$$

$$Q_2(t_n) := \sum\{|\zeta|\,|\theta| \mid \text{all approaching pairs of } \zeta \text{ and } \theta \text{ at } t = t_n\}, \tag{3.8}$$

where two fronts of different families are approaching if the front of the lowest family is to the right of the other. Note that $F$ and $Q_1$ only sum over shock-fronts, while $Q_2$ also sums over rarefaction-fronts. Furthermore, none of the terms involve the strength of non-physical fronts.

We call the lines $t = t_n$ *time lines*. The only difference between the functionals above and the functionals used for the Glimm scheme in [16] is that the above ones are defined on time lines, while the functionals in [16] are defined on mesh curves.

We need two more functionals, one summing over all shock- and rarefaction-fronts at $t = t_n$ and one summing over the contact discontinuities at $t = t_n$. Note that the sum of all contact discontinuities is constant for all time lines. We define

$$L(t_n) := \sum\{|\theta| \mid \text{all } \theta \text{ at } t = t_n\}, \tag{3.9}$$

$$F_\gamma := \sum\{|\zeta| \mid \text{all } \zeta\}. \tag{3.10}$$

We will show that $G$ is a decreasing functional in time. Let

$$C = \min\{\tilde{C}, 1\}, \tag{3.11}$$

where the minimum is taken over all the constants $\tilde{C}$ appearing in the estimates for interactions of Type Ba discussed in the proof of Lemma 3.8. Note that $0 < C \le 1$ depends only on $p_{\min}$, $p_{\max}$ and $\overline{\gamma}$. The rest of this subsection will be devoted to proving the following result:

**Proposition 3.7.** *If*

$$3C_1(\overline{\gamma} - 1)L(t_0) \le \frac{C}{3} \qquad \text{and} \qquad 3C_2F_\gamma \le \frac{C}{3}. \tag{3.12}$$

*then $G$ defined by* (3.3) *is decreasing and $F(t_n) \le \frac{5}{3}L(t_0)$. In particular, $G$ decreases by at least $\frac{2}{3}q$ across an increasing rarefaction-collision where the strength of the rarefaction*

*wave increases by $q > 0$, by at least $\frac{2}{3}|\theta'|$ across a new rarefaction-collision where $\theta'$ denotes the new outgoing rarefaction wave, and by at least $3k|\theta^{np}|$ for an interaction where a non-physical front is generated.*

We prove this proposition through a series of lemmas where we start by considering interactions between two fronts, then gradually build up to interactions of the general form given by (3.2), including incoming non-physical fronts. For all possible interactions in front tracking we show that $G$ is decreasing and, in particular, we identify all new or increasing rarefaction-collisions and all interactions generating a non-physical front.

Before we state and prove the different lemmas, we present the general idea based on induction on successive time lines: First we show that $G(t_1) - G(t_0) \leq 0$. Then we assume $G(t_n) \leq G(t_{n-1}) \leq \cdots \leq G(t_0)$. The induction step is to show that $\Delta G := G(t_{n+1}) - G(t_n) \leq 0$. Note that if $G$ is decreasing up to $t = t_n$, then we have

$$\begin{aligned} F(t_n) &\leq G(t_n) \leq \cdots \leq G(t_0) = F(t_0) + 3C_1(\overline{\gamma} - 1)Q_1(t_0) + 3C_2Q_2(t_0) \\ &\leq F(t_0) + 3C_1(\overline{\gamma} - 1)(F(t_0))^2 + 3C_2L(t_0)F_\gamma \\ &\leq (1 + 3C_1(\overline{\gamma} - 1)F(t_0) + 3C_2F_\gamma)L(t_0) \\ &\leq (1 + 3C_1(\overline{\gamma} - 1)L(t_0) + 3C_2F_\gamma)L(t_0) \\ &\leq \left(1 + \frac{C}{3} + \frac{C}{3}\right)L(t_0) \leq \frac{5}{3}L(t_0). \end{aligned} \tag{3.13}$$

We only give the estimates for $\Delta G$ here. Estimating $G(t_1) - G(t_0)$ is very similar, giving terms involving $F(t_0)$ where the estimate for $\Delta G$ has terms involving $F(t_n)$.

For the more involved interactions we use a computational trick where we divide the interaction into steps where only a part of the fronts interact at each step. It is important to note that in the front tracking algorithm all fronts in an interaction meet at the same point and that no speeds are altered. It is just in the estimation of $\Delta G$ we do this step procedure as a formal trick to go from the incoming fronts to a set of fronts which are comparable to the outgoing fronts. Note also that the outgoing fronts are not altered in this process. This method corresponds to the use of inner diamonds for the Glimm scheme in [16]. DiPerna [10] constructs the outgoing solution by resolving the interaction into a composition of binary interactions. This method of decomposition is similar to our formal method of dividing an interaction into steps.

Thus, we divide the interaction into $l$ steps where only some of the fronts interact at each step, the rest is left unchanged. As long as the interaction at one step is an interaction already analyzed, we know that $G$ decreases across that step. We continue this until we at some point directly can show that $G$ is decreasing across the last step, where the last step is going from some collection of fronts to the outgoing fronts. Formally, the steps are obtained by shifting the speeds of the incoming fronts slightly, so that only the intended fronts meet at a shifted collision point. This is done for each step and we introduce intermediate time lines, $t = t_i^*$, so that the interaction at the $i$th step lies between $t_{i-1}^*$ and $t_i^*$ where $t_0^* = t_n$ and $t_l^* = t_{n+1}$. As long as we have $\Delta G_i := G(t_i^*) - G(t_{i-1}^*) \leq 0$ for $i = 1, \ldots, l$, it follows that $\Delta G \leq 0$. Note again that this step procedure is only a computational trick, and that the front-tracking algorithm as such involves no shifting of speeds.

Figure 7 shows how a typical interaction of the type $\sum_i \eta_i + \sum_j \epsilon_j$ is divided into two additional steps. First we let all 3-fronts interact at one collision point whereas all 1-fronts interact at a different point. Both interactions result in a 1-wave and a 3-wave. At the second step we let the approaching 3- and 1-wave interact. Thus, at $t = t_2^*$ we have a collection of

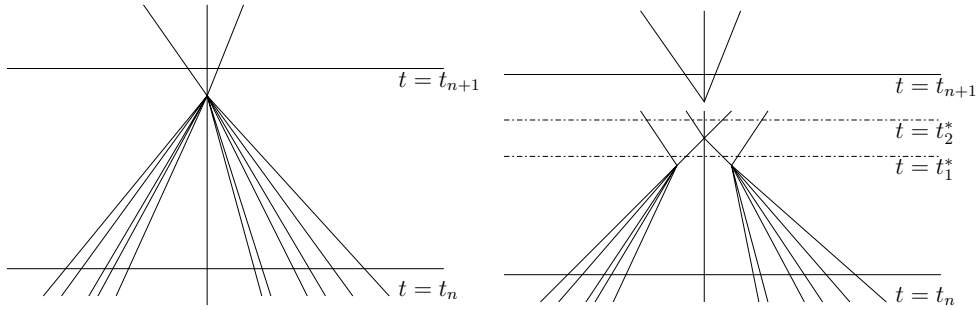


(a) The original interaction. (b) The interaction divided into steps.

FIGURE 7. A typical interaction of the form $\sum_i \eta_i + \sum_j \epsilon_j$.

four waves and we compare these to the outgoing fronts. Note that we have not shifted or altered the outgoing fronts at any point in this step procedure.

For some cases we use an additional trick to avoid getting too many steps. Instead of letting some fronts interact at a shifted collision point, we replace the fronts with new fronts connecting the same left and right state. Since this is not a valid interaction, we need to show that $\Delta G_i \leq 0$ for this step, and we do that by comparing the new fronts with the replaced fronts. Still this is just a formal trick and the outgoing fronts are not altered.

In Lemma 3.8 through Lemma 3.14 we cover all possible interactions, and we start by the cases with two interacting fronts. Recall that these are the same interactions as for the Glimm scheme, cf. [16], and they are labeled in the same manner as in [16].

**Lemma 3.8.** *For all interactions between two fronts we have $\Delta G \leq 0$. In particular, $\Delta G \leq -\frac{2}{3}q$ for all increasing rarefaction-collisions where the strength of the rarefaction wave has increased by $q > 0$ and $\Delta G \leq -\frac{2}{3}|\theta'|$ for new rarefaction-collisions where $\theta'$ denotes the new rarefaction wave. Moreover, $\Delta G \leq -\frac{1}{9}C_2|\zeta||\theta|$ for all $\gamma$-collisions where $\theta$ is the incoming front, and $\Delta G \leq -3k|\theta^{np}|$ for interactions generating a non-physical front.*

*Proof.* The possible interactions between two fronts are the same as the interactions of Type B considered when using the Glimm scheme, cf. [16]. Therefore, we here give the estimates without proofs. All the estimates for interactions without a contact discontinuity are obtained from the estimates by Nishida and Smoller in [21], while the estimates for interactions with a contact discontinuity are found using Lemma 2.2. The estimates for the interactions between a contact discontinuity and another front solved by the simplified solver are also obtained using Lemma 2.2.

Type Ba: Two waves of the same family.

(i) $\alpha_1 + \alpha_2 \to \alpha' + \nu'$, symmetric to $\beta_1 + \beta_2 \to \mu' + \beta'$: This is a new rarefaction-collision and we have

$$|\alpha'| - |\alpha_1| - |\alpha_2| = -|\nu'| \;\Rightarrow\; \Delta G \leq -\frac{2}{3}|\nu'|.$$

(ii) $\alpha + \mu$, symmetric to $\nu + \beta$. There are two possible outcomes:

- $\alpha + \mu \to \mu' + \beta'$: For this case we have

$$|\mu'| \leq |\mu|, \quad |\beta'| - |\alpha| \leq -\tilde{C}|\beta'| \;\Rightarrow\; \Delta G \leq 0.$$

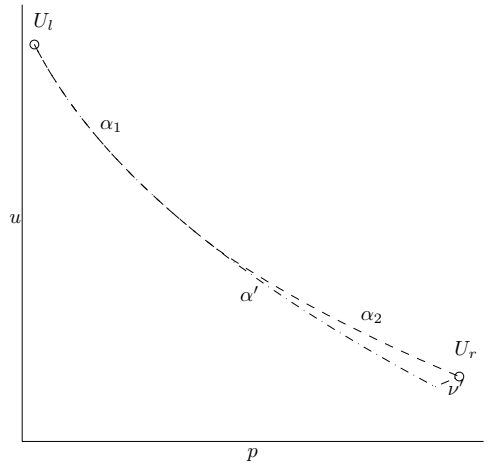


FIGURE 8. The interaction $\alpha_1 + \alpha_2 \to \alpha' + \nu'$.

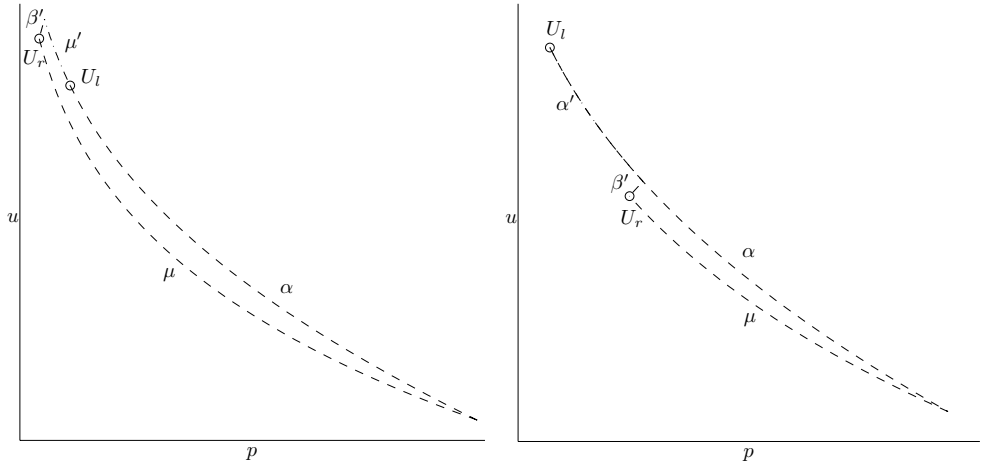


(a) $\alpha + \mu \to \mu' + \beta'$. (b) $\alpha + \mu \to \alpha' + \beta'$.

FIGURE 9. The interaction $\alpha + \mu$.

- $\alpha + \mu \to \alpha' + \beta'$: We have

$$|\alpha'| + |\beta'| - |\alpha| \le -\tilde{C}\,|\beta'| \;\Rightarrow\; \Delta G \le 0.$$

(iii) $\mu + \alpha$, symmetric to $\beta + \nu$: There are two possible outcomes:

- $\mu + \alpha \to \mu' + \beta'$: For this case

$$|\mu'| \le |\mu|, \quad |\beta'| - |\alpha| \le -\tilde{C}\,|\beta'| \;\Rightarrow\; \Delta G \le 0.$$

- $\mu + \alpha \to \alpha' + \beta'$. In this case, the interaction is replaced by a new one,

$$\mu + \alpha \xrightarrow{\Delta G_1} \overline{\beta} + \overline{\alpha} \xrightarrow{\Delta G_2} \alpha' + \beta', \tag{3.14}$$

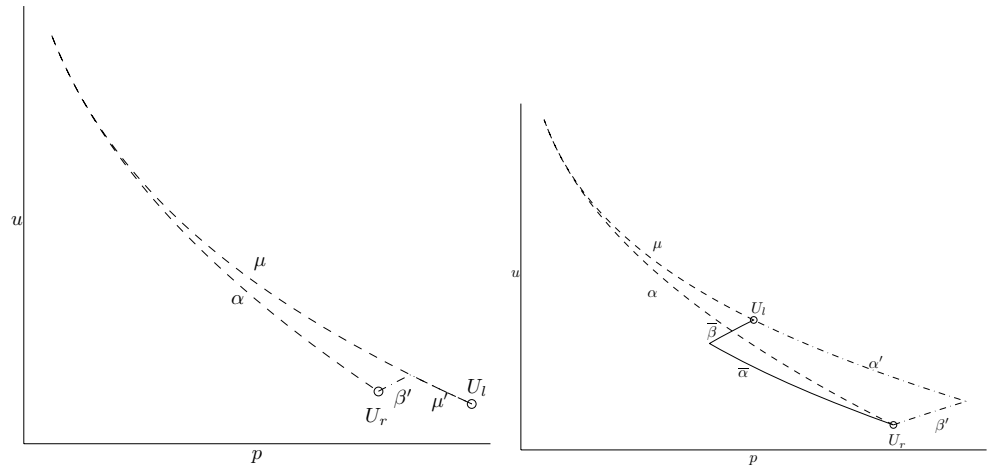


(a) $\mu+\alpha\to\mu'+\beta'$. (b) $\mu+\alpha\to\alpha'+\beta'$.

FIGURE 10. The interaction $\mu+\alpha$.

for which we have the estimate

$$|\overline{\alpha}\,|+\left|\overline{\beta}\,\right|-|\alpha\,|\le-\tilde{C}\left|\overline{\beta}\,\right|\ \Rightarrow\ \Delta G_1\le 0.$$

Furthermore, we have $\Delta G_2\le 0$ by estimate (3.16) for $\beta+\alpha$ below, cf. Type Bbii. Hence, $\Delta G\le 0$.

Type Bb: Different families, no contact discontinuity.

(i) $\nu+\mu\to\nu'+\mu'$. None of the rarefaction-fronts increase, and we have

$$|\mu'\,|\le|\mu\,|,\quad |\nu'\,|\le|\nu\,|\ \Rightarrow\ \Delta G_1\le 0. \tag{3.15}$$

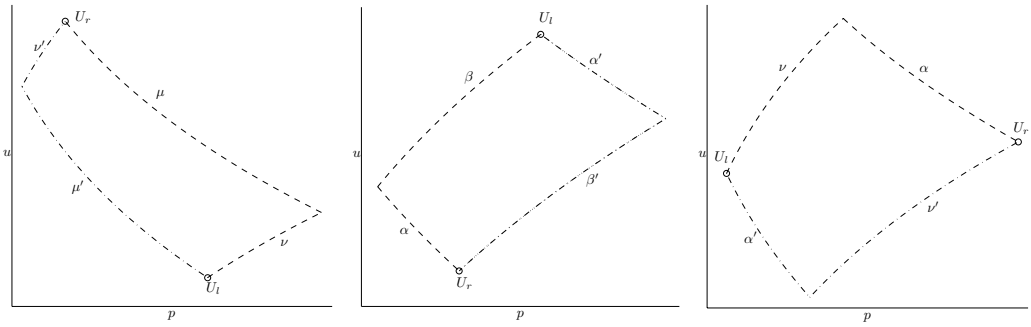


(a) $\nu+\mu\to\mu'+\nu'$. (b) $\beta+\alpha\to\alpha'+\beta'$. (c) $\nu+\alpha\to\alpha'+\nu'$.

FIGURE 11. The interactions of Type Bb

(ii) $\beta+\alpha\to\alpha'+\beta'$. We have

$$|\alpha'\,|-|\alpha\,|\le(\overline{\gamma}-1)C_1\,|\alpha\,|\,|\beta\,|,\quad |\beta'\,|-|\beta\,|\le(\overline{\gamma}-1)C_1\,|\alpha\,|\,|\beta\,|, \tag{3.16}$$

thus

$$\Delta G \le -\frac{1}{9}(\overline{\gamma}-1)C_1\,|\alpha\,|\,|\beta\,|\,.$$

(iii) $\nu+\alpha \to \alpha'+\nu'$, symmetric to $\beta+\mu \to \mu'+\beta'$. This is an increasing rarefaction-collision where we for $q>0$ have

$$|\alpha'\,|-|\alpha\,|=-q, \quad |\nu'\,|-|\nu\,|=q \;\Rightarrow\; \Delta G \le -\frac{2}{3}q.$$

Type Bc: With a contact discontinuity: These are the four possible $\gamma$-collisions.

(i) $\zeta+\mu$, symmetric to $\nu+\zeta$: There are two possible outcomes for this $\gamma$-collision, and, in addition, we have the case where the simplified Riemann solver is used, introducing a non-physical front.

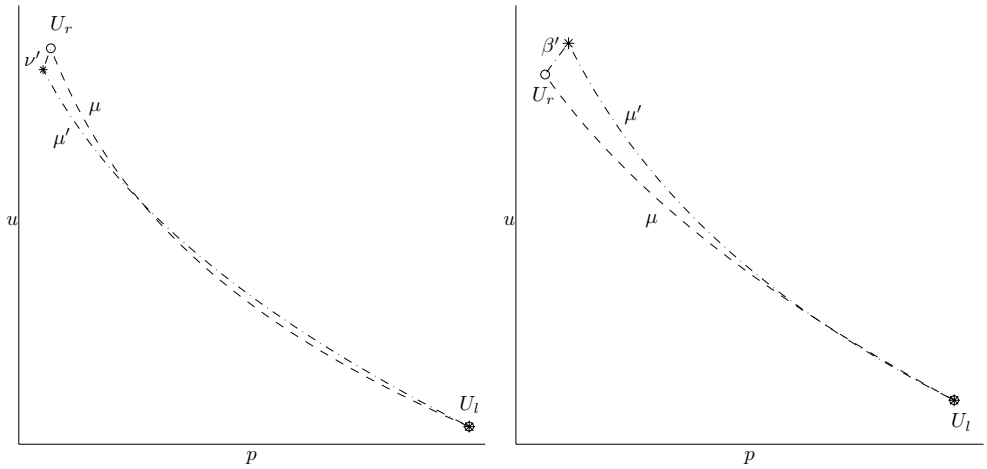


(a) $\zeta+\mu \to \mu'+\zeta+\nu'$. (b) $\zeta+\mu \to \mu'+\zeta+\beta'$.

FIGURE 12. The interaction $\zeta+\mu$.

- $\zeta+\mu \to \mu'+\zeta+\nu'$: This interaction is a new rarefaction-collision and an increasing rarefaction-collision with $q=|\nu'\,|$. We have

$$|\mu'\,|-|\mu\,|=|\nu'\,|\le C_2\,|\mu\,|\,|\zeta\,|\,,$$

from which we find

$$\Delta G \le -\frac{8}{3}C_2\,|\mu\,|\,|\zeta\,| \le -\frac{2}{3}\,|\nu'\,|-\frac{2}{3}q.$$

- $\zeta+\mu \to \mu'+\zeta+\beta'$: The rarefaction-front does not increase and

$$|\mu'\,|-|\mu\,|\le 0, \quad |\beta'\,|\le C_2\,|\mu\,|\,|\zeta\,| \;\Rightarrow\; \Delta G \le -\frac{10}{9}C_2\,|\mu\,|\,|\zeta\,|\,.$$

- $\zeta+\mu \to \mu'+\zeta+\theta^{\mathrm{np}}$: By construction, $|\mu'\,|=|\mu\,|$. Using Lemma 2.2, we find

$$|\theta^{\mathrm{np}}\,|\le c_2\,|\mu\,|\,|\zeta\,|\,, \tag{3.17}$$

from which we get

$$\Delta G \le -3C_2\,|\mu\,|\,|\zeta\,| \le -3k\,|\theta^{\mathrm{np}}\,|\,,$$

where $k$ given by (3.5) depends only on $p_{\min}$, $p_{\max}$ and $\overline{\gamma}$.

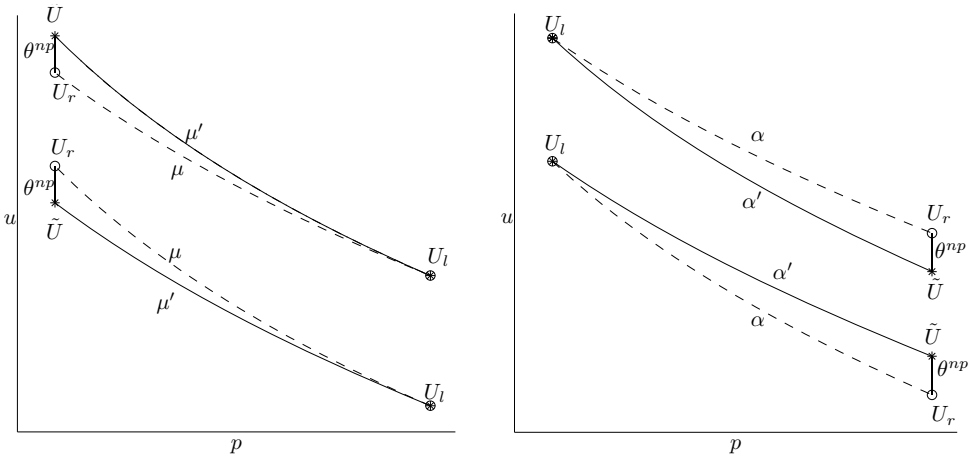


(a) $\zeta + \mu \to \mu' + \zeta + \theta^{\mathrm{np}}$. (b) $\zeta + \alpha \to \alpha' + \zeta + \theta^{\mathrm{np}}$.

FIGURE 13. The interaction $\zeta + \epsilon$ solved using the simplified solver.

(ii) $\zeta + \alpha$, symmetric to $\beta + \zeta$. This $\gamma$-collision has two possible outcomes, in addition to the case with a non-physical front.

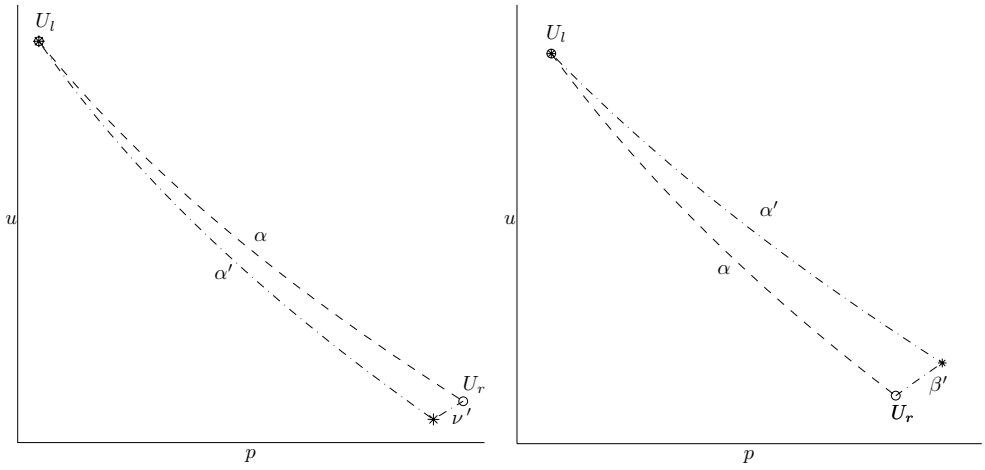


(a) $\zeta + \alpha \to \alpha' + \zeta + \nu'$. (b) $\zeta + \alpha \to \alpha' + \zeta + \beta'$.

FIGURE 14. The interaction $\zeta + \alpha$.

- $\zeta + \alpha \to \alpha' + \zeta + \nu'$: For this new rarefaction-collision we have

$$|\alpha'| - |\alpha| \le 0, \quad |\nu'| \le C_2 |\alpha| |\zeta|,$$

thus,

$$\Delta G \le -\frac{2}{3} C_2 |\alpha| |\zeta| \le -\frac{2}{3} |\nu'|.$$

- $\zeta + \alpha \to \alpha' + \zeta + \beta'$: For this case we have

$$|\alpha'| - |\alpha| = |\beta'| \leq C_2 |\alpha| |\zeta| \;\Rightarrow\; \Delta G \leq -\frac{1}{9} C_2 |\zeta| |\beta|.$$

- $\zeta + \alpha \to \alpha' + \zeta + \theta^{\text{np}}$: By construction, $|\alpha'| = |\alpha|$ and by Lemma 2.2

$$|\theta^{\text{np}}| \leq c_2 |\mu| |\zeta|. \tag{3.18}$$

Thus,

$$\Delta G \leq -3C_2 |\alpha| |\zeta| \leq -3k |\theta^{\text{np}}|,$$

where $k$ only depends on $p_{\min}$, $p_{\max}$ and $\overline{\gamma}$.

□

With the basic interactions between two fronts covered, we are able to consider more involved interactions. First interactions between arbitrary many fronts of the same family are studied. Two interactions of this kind are given in Figure 15, see also Example 3.10 below. Note that no interaction of this form can be an increasing rarefaction-collision.

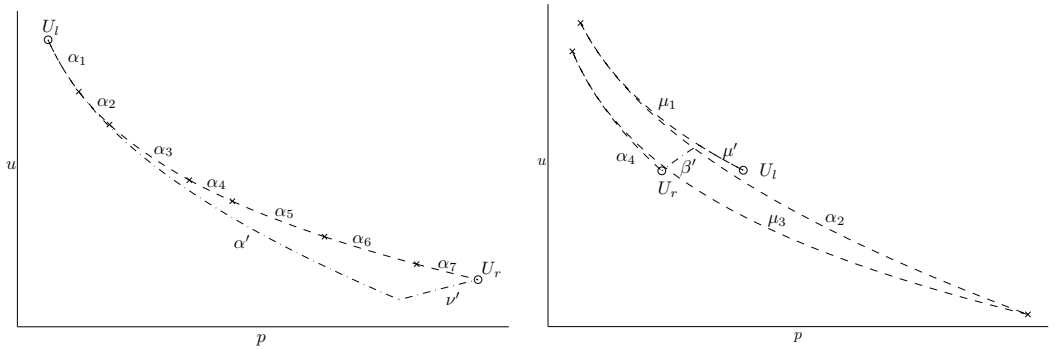


(a) $\sum_{i=1}^{7} \alpha_i \to \alpha' + \nu'$. (b) $\mu_1 + \alpha_2 + \mu_3 + \alpha_4 \to \mu' + \beta'$.

FIGURE 15. Some interactions of the form (3.19).

**Lemma 3.9.** *For all interactions between arbitrary many fronts of the same family where two adjacent fronts cannot both be rarefaction-fronts, we have $\Delta G \leq 0$, and in particular, $\Delta G \leq -\frac{2}{3}|\theta'|$ for new rarefaction-collisions where $\theta'$ denotes the new rarefaction wave. Furthermore, there are three possible outcomes for these interactions;*

$$\sum_{i=1}^{n} \epsilon_i \to \begin{cases} \mu' + \beta', \\ \alpha' + \nu', \\ \alpha' + \beta', \end{cases} \quad \textit{symmetric to} \quad \sum_{i=1}^{n} \eta_i \to \begin{cases} \alpha' + \nu', \\ \mu' + \beta', \\ \alpha' + \beta'. \end{cases} \tag{3.19}$$

*Proof.* We prove the lemma for interactions between three or more 1-fronts, the interactions with $n = 2$ are already covered by Lemma 3.8. None of the interactions can have two rarefaction waves as outgoing waves due to property (i) of Lemma 2.1. Recall also that $p$ increases along a 1-shock wave and decreases along a 1-rarefaction wave.

Consider first the case $\alpha' + \nu'$. Then the interaction is a new rarefaction-collision where $U_r$ is to the right of $U_l$ and above the 1-shock wave starting at $U_l$. Since only the $\alpha_i$-fronts

among the incoming fronts bring us to the right, we have

$$|\alpha'| - \sum_{i=1}^{n} |\alpha_i| \le -|\nu'| \;\Rightarrow\; \Delta G \le -\frac{2}{3}|\nu'|.$$

For the case $\mu' + \beta'$, $U_r$ is to the left of $U_l$. The only incoming fronts bringing us to the left are the $\mu_i$-fronts, thus

$$|\mu'| \le \sum_{i=1}^{n} |\mu_i|.$$

Hence, no interaction between fronts of the same family is an increasing rarefaction-collision.

Therefore we consider the last two cases together, that is, $\epsilon' + \beta'$ where $\epsilon'$ is either a shock or a rarefaction wave. We divide the interaction into several steps where two fronts interact at each step, hence, $\Delta G_j \le 0$ by Lemma 3.8. Recall that two adjacent fronts in the interaction cannot both be rarefaction-fronts. The strategy is as follows: Start with the rightmost front and search for the first place where two adjacent fronts are of different types, i.e., $\alpha_i + \mu_{i+1}$ or $\mu_i + \alpha_{i+1}$. Let these fronts interact with outcome $\tilde{\epsilon}_k + \tilde{\beta}_k$. Whenever there is a 1-shock to the right of $\tilde{\beta}_k$, we proceed by letting them interact; $\tilde{\beta}_k + \alpha \to \tilde{\alpha}_{k+1} + \tilde{\beta}_{k+1}$, and we repeat this as long as there is a 1-shock to the right of the 3-shock. Thus, we end up with a collection of $\beta$-waves as the rightmost waves. Furthermore, whenever this process results in two adjacent rarefaction waves, we recall from property (vii) of Lemma 2.1 that rarefaction waves (and fronts) are additive and we add them up to a new rarefaction wave. We continue this process until all 1-fronts of different types have interacted, and we are left with either $\tilde{\mu} + \sum \tilde{\beta}_k$ or $\sum \tilde{\alpha}_k + \sum \tilde{\beta}_k$. For the first case we have

$$\sum_{i=1}^{n} \epsilon_i \xrightarrow{\Delta G_1} \tilde{\mu} + \sum_k \tilde{\beta}_k \xrightarrow{\Delta G_2} \mu' + \beta', \tag{3.20}$$

where we already know that $\Delta G_1 \le 0$. By property (ix) of Lemma 2.1 it follows that $\sum_k \left|\tilde{\beta}_k\right| > |\beta'|$, thus, there is a $q > 0$ so that

$$|\mu'| - |\tilde{\mu}| = q, \quad |\beta'| - \sum_k \left|\tilde{\beta}_k\right| = -q \;\Rightarrow\; \Delta G_2 \le 0.$$

For the latter case we have

$$\sum_{i=1}^{n} \epsilon_i \xrightarrow{\Delta G_1} \sum_k \tilde{\alpha}_k + \sum_k \tilde{\beta}_k \xrightarrow{\Delta G_2} \alpha' + \beta',$$

where we already know that $\Delta G_1 \le 0$. Furthermore, it follows from the properties (viii) and (ix) of Lemma 2.1 that

$$|\alpha'| - \sum_k |\tilde{\alpha}_k| \le 0, \quad |\beta'| - \sum_k \left|\tilde{\beta}_k\right| \le 0 \;\Rightarrow\; \Delta G_2 \le 0.$$

This proves the lemma for the interaction $\sum_i \epsilon_i$, and the results for $\sum_i \eta_i$ follows by symmetry. However, we include another estimate for the last case discussed above, which will prove useful later. The number of $\tilde{\alpha}_k$-fronts is less than or equal to the number of incoming $\alpha_i$-fronts. Going carefully through each steps, we find that each $\tilde{\alpha}_k$ has a corresponding incoming $\alpha_i$ so that

$$|\tilde{\alpha}_k| \le \prod_{j \ne i} (1 + C_1(\overline{\gamma} - 1)|\epsilon_j|)\,|\alpha_i| \le \frac{4}{3}|\alpha_i|, \tag{3.21}$$

because

$$\begin{aligned}\prod_{j\neq i}(1+C_1(\overline{\gamma}-1)\,|\epsilon_j\,|) &\leq 1+\frac{3}{2}\sum_j C_1(\overline{\gamma}-1)\,|\epsilon_j\,|\\ &\leq 1+\frac{3}{2}C_1(\overline{\gamma}-1)F(t_{n-1})\\ &\leq 1+\frac{3}{2}C_1(\overline{\gamma}-1)\frac{5}{3}L(t_0)\leq\frac{4}{3}.\end{aligned}$$

Here we have used that

$$\prod_i(1+x_i)\leq\exp\left(\sum_i x_i\right)\leq 1+\frac{3}{2}\sum_i x_i,\quad\text{for}\quad\sum_i x_i\leq\frac{1}{2}.$$

□

Before we continue to the more complicated interactions, we give an example to illustrate how we divide an interaction of the form (3.19) into smaller steps.

**Example 3.10.** Consider the interaction $\mu_1+\alpha_2+\mu_3+\alpha_4\to\alpha'+\beta'$ as depicted in Figure 16(a). Dividing this interaction according to the strategy we discussed in the previous proof, see Figure 16(b), we get

$$\begin{aligned}\mu_1+\alpha_2+[\mu_3+\alpha_4]&\xrightarrow{\Delta G_1}[\mu_1+\alpha_2]+\tilde{\alpha}_1+\tilde{\beta}_1\xrightarrow{\Delta G_2}\tilde{\alpha}_2+[\tilde{\beta}_2+\tilde{\alpha}_1]+\tilde{\beta}_1\\ &\xrightarrow{\Delta G_3}\tilde{\alpha}_2+\tilde{\alpha}_3+\tilde{\beta}_3+\tilde{\beta}_1\xrightarrow{\Delta G_4}\alpha'+\beta',\end{aligned}$$

where $\Delta G_i\leq 0$, $i=1,2,3$, by Lemma 3.8. By the properties of shock waves, we have

$$|\alpha'\,|-|\tilde{\alpha}_2\,|-|\tilde{\alpha}_3\,|\leq 0,\quad |\beta'\,|-\left|\tilde{\beta}_1\right|-\left|\tilde{\beta}_3\right|\leq 0,\quad\Rightarrow\quad\Delta G_4\leq 0.$$

Note that $\mu+\alpha$ as above is the second case of the interaction of Type Baiii discussed in Lemma 3.8, where we introduced an extra step to solve it. This is given in (3.14) where $\left|\overline{\beta}\right|\leq|\mu\,|$ and $|\overline{\alpha}\,|\leq|\alpha\,|$. Using this, and the estimates given by (3.16) for $\overline{\beta}+\overline{\alpha}$, we find

$$\begin{aligned}|\tilde{\alpha}_2\,|&\leq(1+(\overline{\gamma}-1)C_1\left|\overline{\beta}_2\right|)\,|\overline{\alpha}_2\,|\leq(1+(\overline{\gamma}-1)C_1\,|\mu_1\,|)\,|\alpha_2\,|\,,\\ |\tilde{\alpha}_3\,|&\leq(1+(\overline{\gamma}-1)C_1\left|\tilde{\beta}_2\right|)\,|\tilde{\alpha}_1\,|\\ &\leq(1+(\overline{\gamma}-1)C_1(1+(\overline{\gamma}-1)C_1\,|\overline{\alpha}_2\,|)\left|\overline{\beta}_2\right|)(1+(\overline{\gamma}-1)C_1\left|\overline{\beta}_1\right|)\,|\overline{\alpha}_2\,|\\ &\leq(1+(\overline{\gamma}-1)C_1\,|\mu_1\,|)(1+(\overline{\gamma}-1)C_1\,|\alpha_2\,|)(1+(\overline{\gamma}-1)C_1\,|\mu_3\,|)\,|\alpha_4\,|\,,\end{aligned}$$

showing that estimate (3.21) holds for $\tilde{\alpha}_2$ and $\tilde{\alpha}_3$.

Using Lemma 3.9 we are now able to divide the more involved interactions into smaller steps and through this show that $G$ decreases. We start by adding a contact discontinuity to the interactions.

**Lemma 3.11.** *The functional $G$ decreases for all interactions of the form*

$$\zeta+\sum_{i=1}^n\epsilon_i\ \textit{and the symmetric form}\ \sum_{i=1}^n\eta_i+\zeta. \tag{3.22}$$

*Furthermore, $\Delta G\leq-\frac{2}{3}\,|\theta'\,|$ for new rarefaction-collisions where $\theta'$ is the new wave, $\Delta G\leq-\frac{2}{3}q$ for increasing rarefaction-collisions where the strength of the rarefaction wave increases by $q>0$, and $\Delta G\leq-3k\,|\theta^{np}\,|$ for interactions generating a non-physical front.*

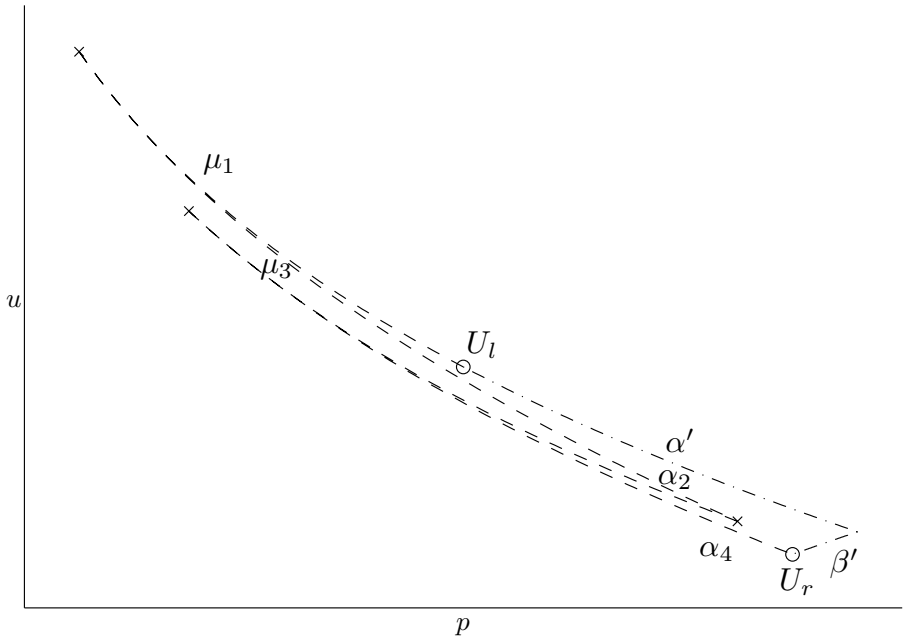


(a) The original interaction

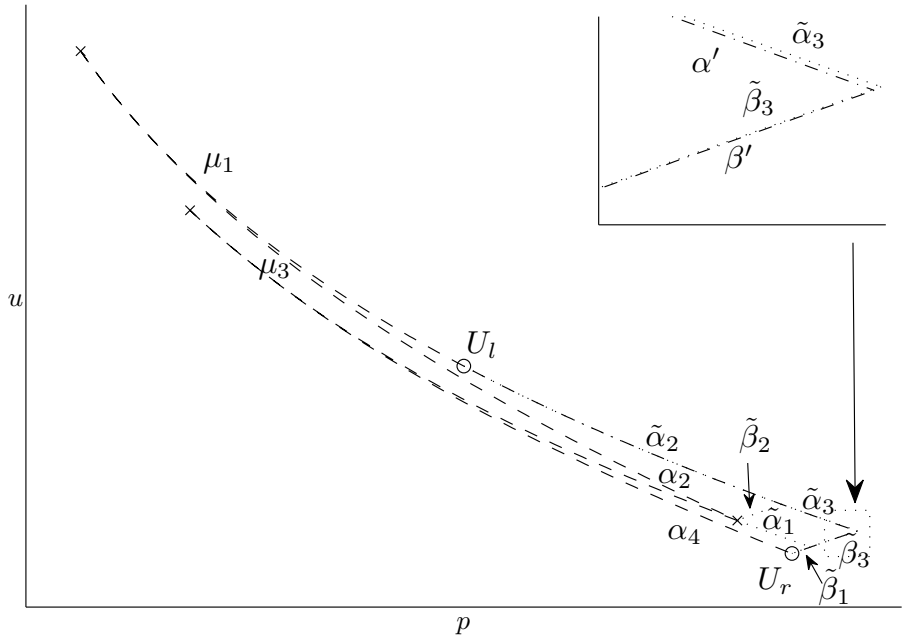


(b) Divided into smaller steps

FIGURE 16. The interaction $\mu_1 + \alpha_2 + \mu_3 + \alpha_4 \to \alpha' + \beta'$ of Example 3.10.

*Proof.* Let us first consider when $|\zeta\,|\sum_i|\epsilon\,|>\rho$, so that the approximate solver is used. We then divide interaction $\zeta+\sum_{i=1}^n\epsilon_i$ into two steps where we let $\sum_{i=1}^n\epsilon_i$ interact at the first step. By Lemma 3.9 we know that $G$ is decreasing for this interaction and that there are three possible cases. We write this

$$\zeta+\sum_{i=1}^n\epsilon_i\xrightarrow{\Delta G_1}\zeta+\begin{cases}\mu+\beta\\ \alpha+\nu\\ \alpha+\beta\end{cases}\xrightarrow{\Delta G_2}\epsilon'+\zeta+\eta',$$

where $\Delta G_1\le 0$. At the second step there are three possible interactions of the form $\zeta+\epsilon+\eta\to\epsilon'+\zeta+\eta'$. The outgoing 1-wave is of the same type as the incoming 1-wave for all of these interactions, while the type of the 3-wave depends on the different $\gamma$-values, giving two possible cases for each interaction.

Consider first the case where the incoming and outgoing 3-waves are of the same type. If the intersection between $\epsilon'$ and $\eta'$ is below the intersection between $\epsilon$ and $\eta$ when viewed in the $(p,u)$-plane, we have

$$\begin{aligned}|\mu'\,|-|\mu\,|=q,\quad |\beta'\,|-|\beta\,|=-q\ &\Rightarrow\Delta G_2\le-\frac{2}{3}|\mu'\,|,\\ |\alpha'\,|-|\alpha\,|=-q,\quad |\nu'\,|-|\nu\,|=q\ &\Rightarrow\Delta G_2\le-\frac{2}{3}|\nu'\,|,\\ |\alpha'\,|-|\alpha\,|\le 0,\quad |\beta'\,|-|\beta\,|\le 0\ &\Rightarrow\Delta G_2\le 0,\end{aligned}$$

for the three interactions, respectively. The two first are increasing rarefaction-collisions, however, the overall interactions are not increasing rarefaction-collisions because property (i) of Lemma 2.1 yields that $|\epsilon'\,|$ is less than the sum of the strengths of the incoming 1-fronts of the same type. If the intersection in the $(p,u)$-plane between $\epsilon'$ and $\eta'$ is above the intersection between $\epsilon$ and $\eta$, we apply Lemma 2.2 to $\epsilon$ and $\epsilon'$ and find that

$$\begin{aligned}0\le|\beta'\,|-|\beta\,|\le|\mu\,|-|\mu'\,|\le C_2\,|\mu'\,|\,|\zeta\,|\le C_2\,|\mu\,|\,|\zeta\,|\ &\Rightarrow\Delta G_2\le 0,\\ |\alpha'\,|-|\alpha\,|\le C_2\,|\alpha\,|\,|\zeta\,|,\quad |\nu'\,|-|\nu\,|\le 0\ &\Rightarrow\Delta G_2\le 0,\\ |\beta'\,|-|\beta\,|=|\alpha'\,|-|\alpha\,|\le C_2\,|\alpha\,|\,|\zeta\,|\ &\Rightarrow\Delta G_2\le 0,\end{aligned}$$

for the three interactions, respectively.

Consider now the case where the 3-waves are of different types. The interactions with $\eta'=\nu'$ are new rarefaction-collisions, and the interaction with $\epsilon'=\mu'$ is also an increasing rarefaction-collision with $|\nu'\,|\le|\mu'\,|-|\mu\,|=q$. We obtain the following estimates;

$$\begin{aligned}|\nu'\,|\le q=|\mu'\,|-|\mu\,|\le C_2\,|\mu\,|\,|\zeta\,|\ &\Rightarrow\Delta G_2\le-\frac{2}{3}|\nu'\,|-\frac{2}{3}q,\\ |\beta'\,|-|\beta\,|=|\alpha'\,|-|\alpha\,|\le C_2\,|\alpha\,|\,|\zeta\,|\ &\Rightarrow\Delta G_2\le 0,\\ |\alpha'\,|-|\alpha\,|=-|\nu'\,|-|\beta\,|\le-|\nu'\,|\ &\Rightarrow\Delta G_2\le-\frac{2}{3}|\nu'\,|,\end{aligned}$$

where we used Lemma 2.2 on $\epsilon$ and $\epsilon'$ for the two first interactions.

Next, we consider the case where the simplified solver is used to solve $\zeta+\sum_{j=1}^n\epsilon_j$ with $n\ge 2$. The construction of the solution, as described in Section 3.1, can be viewed as dividing the interaction into three steps. First we let $\sum_i\epsilon_i$ interact, resulting in $\overline{\epsilon}+\overline{\eta}$, then we solve the interaction between $\zeta+\overline{\epsilon}$ using the simplified solver. Finally, the non-physical front interact with $\overline{\eta}$. Since the non-physical front just passes through without changing its

strength, $\eta'$ is just $\overline{\eta}$ shifted in the $u$-direction. We write this

$$\zeta + \sum_{j=1}^{n} \epsilon_j \xrightarrow{\Delta G_1} \begin{cases} [\zeta + \overline{\mu}] + \overline{\beta} \xrightarrow{\Delta G_2} \mu' + \zeta + [\theta^{\mathrm{np}} + \overline{\beta}] \xrightarrow{\Delta G_3} \mu' + \zeta + \beta' + \theta^{\mathrm{np}}, \\ [\zeta + \overline{\alpha}] + \overline{\nu} \xrightarrow{\Delta G_2} \alpha' + \zeta + [\theta^{\mathrm{np}} + \overline{\nu}] \xrightarrow{\Delta G_3} \alpha' + \zeta + \nu' + \theta^{\mathrm{np}}, \\ [\zeta + \overline{\alpha}] + \overline{\beta} \xrightarrow{\Delta G_2} \alpha' + \zeta + [\theta^{\mathrm{np}} + \overline{\beta}] \xrightarrow{\Delta G_3} \alpha' + \zeta + \beta' + \theta^{\mathrm{np}}. \end{cases}$$

Figure 6 shows the intermediate fronts for the second interaction, in addition to the solution using the approximate solver. For the first step we have $\Delta G_1 \leq 0$ by Lemma 3.9, and, from the proof of the lemma, we have

$$|\overline{\mu}| \leq \sum_i |\mu_i|, \quad |\overline{\alpha}| \leq \sum_i |\alpha_i|, \quad |\overline{\alpha}| \leq \sum_k |\tilde{\alpha}_k| \leq \frac{4}{3} \sum_i |\alpha_i|,$$

respectively, where the last inequality follows from estimate (3.21). For the second step, we have from the proof of Lemma 3.8 and the above estimate that

$$|\theta^{\mathrm{np}}| \leq c_2 |\overline{\epsilon}| |\zeta| \leq \frac{4}{3} c_2 |\zeta| \sum_i |\epsilon_i|, \text{ and } \Delta G_2 \leq -3k |\theta^{\mathrm{np}}|. \tag{3.23}$$

Finally, since $|\overline{\eta}| = |\eta'|$, it follows that $\Delta G_3 = 0$. Hence, $\Delta G \leq \Delta G_1 + \Delta G_2 + \Delta G_3 \leq -3k |\theta^{\mathrm{np}}|$, and we have covered the case where non-physical fronts are generated.

Thus, $G$ decreases for all interactions of the form $\zeta + \sum_{j=1}^{n} \epsilon_j$ where the case $n = 1$ is covered by Lemma 3.8. The result for $\sum_{i=1}^{n} \eta_i + \zeta$ follows by symmetry. □

Next, we consider interactions between arbitrary many fronts of the first and third family.

**Lemma 3.12.** *The functional $G$ is decreasing for all interactions of the form*

$$\sum_{i=1}^{n} \eta_i + \sum_{j=1}^{m} \epsilon_j. \tag{3.24}$$

*Furthermore, $\Delta G \leq -\frac{2}{3} q$ for increasing rarefaction-collisions where $q > 0$ is the increase in the strength of the rarefaction wave, and $\Delta G \leq -\frac{2}{3} |\theta'|$ for new rarefaction-collisions where $\theta'$ is the new rarefaction wave.*

*Proof.* If $n > 1$ and $m > 1$, we divide these interactions into steps as follows;

$$\sum_{i=1}^{n} \eta_i + \sum_{j=1}^{m} \epsilon_j \xrightarrow{\Delta G_1} \begin{cases} \mu_1 + \beta_1 \\ \alpha_1 + \nu_1 \\ \alpha_1 + \beta_1 \end{cases} + \begin{cases} \mu_2 + \beta_2 \\ \alpha_2 + \nu_2 \\ \alpha_2 + \beta_2 \end{cases} \xrightarrow{\Delta G_n} \epsilon' + \eta',$$

where $\Delta G_1 \leq 0$ by Lemma 3.9. There are nine possible interactions at the third step, but three of these are symmetric to one of the other, leaving us with six interactions to consider. If $n = 1$ and $m > 1$ (symmetric to $n > 1$ and $m = 1$), the interactions are divided as follows;

$$\eta + \sum_{j=1}^{n} \epsilon_j \xrightarrow{\Delta G_1} \begin{cases} \beta_1 \\ \nu_1 \end{cases} + \begin{cases} \mu_2 + \beta_2 \\ \alpha_2 + \nu_2 \\ \alpha_2 + \beta_2 \end{cases} \xrightarrow{\Delta G_n} \epsilon' + \eta',$$

where $\Delta G_1 \leq 0$ by Lemma 3.9. This gives us six interactions to consider for the second step. The interactions with $n = m = 1$ are already covered by Lemma 3.8.

We consider first the interactions with only one combination of outgoing waves, that is,

$$\alpha_1 + \beta_1 + \alpha_2 + \beta_2 \to \alpha' + \beta' \text{ and } \mu_1 + \beta_1 + \mu_2 + \beta_2 \to \mu' + \beta',$$

where the last one is symmetric to $\alpha_1+\nu_1+\alpha_2+\nu_2\to\alpha'+\nu'$. We divide these into one extra step;

$$\epsilon_1+[\beta_1+\epsilon_2]+\beta_2\xrightarrow{\Delta G_2}\epsilon_1+\overline{\epsilon}+\overline{\beta}+\beta_2\xrightarrow{\Delta G_3}\epsilon'+\beta',$$

where all $\epsilon$-fronts are of the same type. From Lemma 3.8 we have the necessary estimate on $\Delta G_2$. For the interactions at the last step, the latter one being an increasing rarefaction-collision, we obtain from the properties of the shock waves that

$$|\alpha'|-|\alpha_1|-|\overline{\alpha}|\le 0,\quad |\beta'|-|\beta_2|-\left|\overline{\beta}\right|\le 0\ \Rightarrow\ \Delta G_3\le 0,$$
$$|\mu'|-|\mu_1|-|\overline{\mu}|=q_3,\quad |\beta'|-|\beta_2|-\left|\overline{\beta}\right|=-q_3\ \Rightarrow\ \Delta G_3\le -\frac{2}{3}q_3,$$

for a $q_3\ge 0$. This also applies to the interactions $\beta_1+\alpha_2+\beta_2$, $\beta_1+\mu_2+\beta_2$ and $\nu_1+\alpha_2+\nu_2$ which all have only one combination of outgoing waves and where the last two are increasing rarefaction-collisions.

We now turn to the interactions

$$\alpha_1+\beta+\alpha_2+\nu,\quad \text{which is symmetric to}\quad \mu+\beta_1+\alpha+\beta_2,$$
$$\alpha_1+\nu+\alpha_2+\beta,\quad \text{which is symmetric to}\quad \alpha+\beta_1+\mu+\beta_2.$$

These have two combination of outgoing waves, $\alpha'+\nu'$ and $\alpha'+\beta'$, and are divided into smaller steps;

$$\begin{aligned}\alpha_1+[\eta_1+\alpha_2]+\eta_2&\xrightarrow{\Delta G_2}\alpha_1+\overline{\alpha}+[\overline{\eta}_1+\eta_2]\\&\xrightarrow{\Delta G_3}\alpha_1+\overline{\alpha}+\tilde{\alpha}+\tilde{\eta}\xrightarrow{\Delta G_4}\alpha'+\eta',\end{aligned}$$

where $\eta_1$ and $\overline{\eta}_1$ are of the same type, whereas $\eta_2$ is not, and where $\tilde{\eta}$ and $\eta'$ are of the same type. From Lemma 3.8 we have the needed estimates on $\Delta G_2$ and $\Delta G_3$. Due to property (viii) of Lemma 2.1 we find for $q_4>0$ that

$$|\alpha'|-|\tilde{\alpha}|-|\overline{\alpha}|-|\alpha_1|=-q_4,\quad |\nu'|-|\tilde{\nu}|\le q_4\quad\Rightarrow\quad \Delta G_4\le -\frac{2}{3}q_4,$$
$$|\alpha'|-|\tilde{\alpha}|-|\overline{\alpha}|-|\alpha_1|\le 0,\quad |\beta'|-\left|\tilde{\beta}\right|\le 0\quad\Rightarrow\quad \Delta G_4\le 0.$$

This also covers the special cases $\beta_1+\alpha_2+\nu_2$ and $\nu_1+\alpha_2+\beta_2$. Note that if $\eta_1=\beta_1$, then $|\nu'|\le|\nu|$ by construction, so these interactions are actually not increasing rarefaction-collisions.

Then we are left with two interactions, each having four subcases,

$$\mu+\beta+\alpha+\nu,\quad\text{and}\quad \alpha+\mu+\nu+\beta.$$

In the case with $\mu'+\nu'$ we divide the first interaction into smaller steps

$$\alpha+[\nu+\mu]+\beta\xrightarrow{\Delta G_2}\alpha+\overline{\mu}+\overline{\nu}+\beta\xrightarrow{\Delta G_3}\mu'+\nu',$$

where $\Delta G_2\le 0$ by Lemma 3.8 and

$$|\mu'|\le|\overline{\mu}|\le|\mu|,\quad |\nu'|\le|\overline{\nu}|\le|\nu|\quad\Rightarrow\quad \Delta G_3\le 0,$$

follows from the properties of wave curves and estimate (3.15). For the second interaction it follows by construction that

$$|\mu'|-|\mu|\le 0,\quad |\nu'|-|\nu|\le 0\ \Rightarrow\quad \Delta G\le 0.$$

In the case with $\alpha'+\nu'$, it follows by construction that the first interaction is an increasing rarefaction-collision where

$$|\alpha'|-|\alpha|=-q,\quad |\nu'|-|\nu|\le q\ \Rightarrow\ \Delta G\le -\frac{2}{3}q.$$

For the second interaction we have $|\nu'| \le |\nu|$. We divide the interaction into smaller steps,

$$\mu + [\beta + \alpha] + \nu \xrightarrow{\Delta G_2} [\mu + \overline{\alpha}] + \overline{\beta} + \nu \xrightarrow{\Delta G_3} \tilde{\alpha} + [\tilde{\beta} + \overline{\beta} + \nu] \xrightarrow{\Delta G_4} \tilde{\alpha} + \hat{\alpha} + \hat{\nu} \xrightarrow{\Delta G_5} \alpha' + \nu',$$

where we have the necessary estimates on $\Delta G_2$ and $\Delta G_3$ from Lemma 3.8 and for $\Delta G_4$ by Lemma 3.9. By property (viii) of Lemma 2.1 we find for a $q > 0$ that

$$|\alpha'| - |\tilde{\alpha}| - |\hat{\alpha}| = -q, \quad |\nu'| - |\hat{\nu}| = q \;\Rightarrow\; \Delta G_5 \le 0.$$

The last two cases can be considered together. Note that for either interaction we obtain $|\nu'| \le |\nu|$ so that none of them are increasing rarefaction-collisions. We divide the interactions as follows;

$$\epsilon_1 + [\eta_1 + \epsilon_2] + \eta_2 \xrightarrow{\Delta G_2} \epsilon_1 + \overline{\epsilon} + [\overline{\eta} + \eta_2] \xrightarrow{\Delta G_3} [\epsilon_1 + \overline{\epsilon} + \tilde{\alpha}] + \tilde{\beta} \xrightarrow{\Delta G_4} \hat{\epsilon} + \hat{\beta} + \tilde{\beta} \xrightarrow{\Delta G_5} \epsilon' + \beta',$$

where $\overline{\epsilon}$ is of the same type as $\epsilon_2$, $\overline{\eta}$ of same type as $\eta_1$, and $\hat{\epsilon}$ of the same type as $\epsilon'$. From Lemma 3.8 and Lemma 3.9 we have estimates on $\Delta G_2$, $\Delta G_3$ and $\Delta G_4$, and by properties (viii) and (ix) of Lemma 2.1 we find

$$|\mu'| - |\hat{\mu}| = q, \quad |\beta'| - \left|\hat{\beta}\right| - \left|\tilde{\beta}\right| = -q \;\Rightarrow\; \Delta G \le 0,$$
$$|\alpha'| - |\hat{\alpha}| \le 0, \; |\beta'| - \left|\hat{\beta}\right| - \left|\tilde{\beta}\right| \le 0 \;\Rightarrow\; \Delta G \le 0.$$

The interaction $\nu_1 + \alpha_2 + \beta_2$ has also four cases, and for all but one case, the above analysis apply. In the case $\alpha' + \nu'$, $\beta_2$ must cross $\nu$, and therefore there exist a $\hat{\nu}$ and a $\hat{\beta}$ so that $\hat{\nu} + \hat{\beta}$ connects $U_l$ to $U_r$ and

$$|\hat{\nu}| \le |\nu|, \quad \left|\hat{\beta}\right| \le |\beta|. \tag{3.25}$$

Then the interaction can be divided into the following steps,

$$\nu_1 + \mu_2 + \beta_2 \xrightarrow{\Delta G_2} [\hat{\nu} + \hat{\beta}] \xrightarrow{\Delta G_3} \alpha' + \nu',$$

where $\Delta G_2 \le 0$ follows from (3.25) and $\Delta G_3 \le 0$ from Lemma 3.8. Note that $|\nu'| \le |\nu|$ by construction, so this is not an increasing rarefaction-collision.

This completes the discussion of all possible interactions at the second step, and thereby completes the proof. □

**Lemma 3.13.** *The functional $G$ decreases for all interactions of the form*

$$\sum_{i=1}^{n} \eta_i + \zeta + \sum_{i=1}^{m} \epsilon_i. \tag{3.26}$$

*Furthermore, $\Delta G \le -\frac{2}{3} q$ for all increasing rarefaction-collisions where the strength of the outgoing rarefaction wave increases by $q > 0$, and $\Delta G \le -\frac{2}{3} |\theta'|$ for new rarefaction-collisions where $\theta'$ denotes the new outgoing rarefaction wave.*

*Proof.* This is the general form for interactions possible in front tracking. All interactions without $\zeta$ are already covered by Lemma 3.12. Furthermore, Lemma 3.11 covers the interaction where $m = 0$ (or $n = 0$).

If $n > 1$ and $m > 1$, then we divide the interactions into smaller steps as follows

$$\sum_{i=1}^{n} \eta_i + \zeta + \sum_{j=1}^{m} \epsilon_j \xrightarrow{\Delta G_1} \begin{cases} \mu_1 + \beta_1 \\ \alpha_1 + \nu_1 \\ \alpha_1 + \beta_1 \end{cases} + \zeta + \begin{cases} \mu_2 + \beta_2 \\ \alpha_2 + \nu_2 \\ \alpha_2 + \beta_2 \end{cases} \xrightarrow{\Delta G_n} \epsilon' + \zeta + \eta', \tag{3.27}$$

where three of the nine possible combinations at the last step are symmetric to one of the other, thus, we have six different interactions to consider. If $n = 1$ and $m > 1$ (symmetric to $n > 1$ and $m = 1$), we get

$$\eta_1 + \zeta + \sum_{j=1}^{m} \epsilon_j \xrightarrow{\Delta G_1} \eta_1 + \zeta + \begin{cases} \mu_2 + \beta_2 \\ \alpha_2 + \nu_2 \\ \alpha_2 + \beta_2 \end{cases} \xrightarrow{\Delta G_n} \epsilon' + \zeta + \eta', \tag{3.28}$$

with six different interactions at the second step. In addition, we have the four interactions where $m = n = 1$,

$$\eta_1 + \zeta + \epsilon_2 \xrightarrow{\Delta G_n} \epsilon' + \zeta + \eta', \tag{3.29}$$

where one is symmetric to one of the others.

An interaction that is symmetric to itself is referred to as a self-symmetric interaction. Three of the interactions given by (3.27) are self-symmetric. The other interactions have a symmetric interaction, and we choose to discuss the interactions starting with $\alpha_1 + \nu_1$ over the ones starting with $\epsilon_1 + \beta_1$, and the interaction starting with $\alpha_1 + \beta_1$ over the one starting with $\mu_1 + \beta_1$. None of the interactions given by (3.28) are symmetric to itself or to one of the other interactions. For the two interactions of the form $\epsilon + \zeta + \mu_2 + \beta_2$, we will throughout this proof consider their symmetric interactions, $\alpha_1 + \nu_1 + \zeta + \eta_2$ instead. There are two self-symmetric interactions given by (3.29). The remaining two interactions are symmetric, and we choose to discuss the one with $\eta_1 = \nu_1$.

We write the six interactions given by (3.27) of the general form

$$\epsilon_1 + \eta_1 + \zeta + \epsilon_2 + \eta_2 \xrightarrow{\Delta G_n} \epsilon' + \zeta + \eta'. \tag{3.30}$$

If $\epsilon_1$ is of the same type as $\epsilon_2$ and $\eta_1$ is of the same type as $\eta_2$, then the interaction has only three possible combinations of outgoing fronts. Thus, two of the interactions given by (3.30) have three possible combination of outgoing fronts, while the remaining four interactions have four possible combination of outgoing waves

First, we consider the case where the outgoing fronts are $\mu' + \zeta + \nu'$. This is not a case for the interaction where all incoming fronts are shock-fronts. For the two interactions where $\epsilon_1 + \eta_1$ is not equal to $\alpha_1 + \nu_1$, one of the following estimates holds;

$$\begin{aligned} |\mu'| - |\mu| \le 0, \quad |\nu'| - |\nu| \le 0 \;&\Rightarrow\; \Delta G \le 0, \\ |\mu'| - |\mu| \le |\beta| = q, \quad |\nu'| - |\nu| \le 0 \;&\Rightarrow\; \Delta G \le -\frac{2}{3}q, \\ |\mu'| - |\mu| \le 0, \quad |\nu'| - |\nu| \le |\alpha| = q \;&\Rightarrow\; \Delta G \le -\frac{2}{3}q. \end{aligned} \tag{3.31}$$

For the three interactions where $\epsilon_1 + \eta_1 = \alpha_1 + \nu_1$, we need to divide the interactions into smaller steps;

$$\begin{aligned} +\epsilon_2 + \eta_2 &\xrightarrow{\Delta G_2} \overline{\epsilon} + \zeta + [\overline{\nu} + \epsilon_2] + \eta_2 \xrightarrow{\Delta G_3} \overline{\epsilon} + [\zeta + \tilde{\epsilon} + \tilde{\nu}] + \eta_2 \\ &\xrightarrow{\Delta G_4} \overline{\epsilon} + \hat{\epsilon} + \zeta + \hat{\nu} + \eta_2 \xrightarrow{\Delta G_5} \mu' + \zeta + \nu', \end{aligned} \tag{3.32}$$

where $\tilde{\epsilon}$ and $\hat{\epsilon}$ are of the same type as $\epsilon_2$. If $\epsilon_2$ is a shock-front, then $\overline{\epsilon}$ is a rarefaction-front, otherwise, $\overline{\epsilon}$ can be of either type. From Lemma 3.8 and Lemma 3.9 we have estimates for $\Delta G_i$ for $i = 2, 3, 4$. Furthermore, we have

$$|\mu'| - |\overline{\mu}| - |\hat{\mu}| \leq 0, \quad |\nu'| - |\hat{\nu}| \leq 0 \;\Rightarrow\; \Delta G_5 \leq 0,$$

where $|\overline{\mu}|$ is only included if $\overline{\epsilon}$ is a rarefaction-front, and $|\hat{\nu}|$ only if $\hat{\epsilon}$ is a rarefaction-front.

Next, we consider interactions given by (3.28) and (3.29). If all incoming fronts are shock-fronts, then $\mu' + \zeta + \nu'$ is not a possible combination of outgoing fronts. All interactions with $\eta_1 = \nu_1$ can be divided into smaller steps similar to (3.32), giving us the the same estimates for the last step. For the interactions with $\eta_1 = \beta_1$, one of the estimates given by (3.31) holds. Hence, the case $\mu' + \zeta + \nu'$ is covered for all interactions given by (3.28) and (3.29).

Let us now consider the case where the outgoing waves are $\mu' + \zeta + \beta'$. This combination is not possible for the interaction where the incoming 1-fronts are shock-fronts and the 3-fronts are rarefaction-fronts. The other three interactions where the incoming 1-fronts are shock-fronts, have at least one incoming 3-shock and we have

$$|\beta'| - \sum_{\eta=\beta} |\eta_i| \leq -|\mu'| \quad \Rightarrow\; \Delta G \leq 0, \tag{3.33}$$

where we sum over the strength of the incoming 3-shocks. Thus, we are left with the interactions $\alpha + \nu + \zeta + \mu + \beta$ and $\mu + \beta + \zeta + \alpha + \nu$. First, note that if neither $\alpha$ nor $\mu'$ intersects $\mu$ for the first interaction, or if $\nu$ or $\beta'$ does intersect $\beta$ for the second, we have for a $q > 0$ that

$$|\mu'| - |\mu| \leq q, \quad |\beta'| - |\beta| = -q \;\Rightarrow\; \Delta G \leq -\frac{2}{3}q.$$

If $\alpha$ intersects $\mu$ for the first interaction, we can replace the interaction with a new one, still connecting the left state to the right state, as follows;

$$\begin{aligned}\alpha + \nu + \zeta + \mu + \beta &\xrightarrow{\Delta G_2} \hat{\alpha} + [\zeta + \hat{\mu} + \beta] \xrightarrow{\Delta G_3} \hat{\alpha} + \overline{\mu} + \zeta + \overline{\beta} \\ &\xrightarrow{\Delta G_4} \tilde{\mu} + \zeta + \tilde{\beta} + \overline{\beta} \xrightarrow{\Delta G_5} \mu' + \zeta + \beta'.\end{aligned}$$

From Lemma 3.9 we have estimates for $\Delta G_3$ and $\Delta G_4$. Moreover, we have for a $q_5 > 0$ that

$$\begin{aligned}|\hat{\alpha}| - |\alpha| \leq 0,\ |\hat{\mu}| - |\mu| \leq 0 \;&\Rightarrow\; \Delta G_2 \leq 0, \\ |\mu'| - |\tilde{\mu}| \leq q_5, \quad |\beta'| - \left|\tilde{\beta}\right| - \left|\overline{\beta}\right| = -q_5 \;&\Rightarrow\; \Delta G_5 \leq -\frac{2}{3}q_5.\end{aligned}$$

If $\mu'$ intersects $\mu$, we use a similar approach and replace the interaction with a new one,

$$\begin{aligned}\alpha + \nu + \zeta + \mu + \beta &\xrightarrow{\Delta G_2} \hat{\mu}_1 + [\zeta + \hat{\mu}_2 + \beta] \\ &\xrightarrow{\Delta G_3} \hat{\mu}_1 + \overline{\mu} + \zeta + \overline{\beta} \xrightarrow{\Delta G_4} \mu' + \zeta + \beta',\end{aligned}$$

where we have estimate for $\Delta G_3$ due to Lemma 3.9. Moreover,

$$\begin{aligned}|\hat{\mu}_1| + |\hat{\mu}_2| - |\mu| \leq 0 \;&\Rightarrow\; \Delta G_2 \leq 0, \\ |\mu'| - |\overline{\mu}| - |\hat{\mu}_1| = 0, \quad |\beta'| - \left|\overline{\beta}\right| = 0 \;&\Rightarrow\; \Delta G_5 \leq 0.\end{aligned}$$

If no fronts intersect for the second interaction, we cannot apply a clever replacement. Thus, we divide the interaction into several smaller steps,

$$\begin{aligned}[\mu+\beta+\zeta]+\alpha+\nu &\xrightarrow{\Delta G_2} \overline{\mu}+\zeta+[\overline{\beta}+\alpha]+\nu \xrightarrow{\Delta G_3} \overline{\mu}+[\zeta+\tilde{\alpha}+\tilde{\beta}]+\nu\\ &\xrightarrow{\Delta G_4} \overline{\mu}+\hat{\alpha}+[\zeta+\hat{\beta}+\nu] \xrightarrow{\Delta G_5} [\overline{\mu}+\hat{\alpha}+\overline{\overline{\alpha}}+\zeta]+\overline{\overline{\beta}}\\ &\xrightarrow{\Delta G_6} \check{\mu}+\zeta+\check{\beta}+\overline{\overline{\beta}} \xrightarrow{\Delta G_7} \mu'+\zeta+\beta',\end{aligned}$$

where we have estimates for $\Delta G_i$, $i=2,\dots,6$, from Lemma 3.8 and Lemma 3.9. Furthermore, we have for a $q_7>0$ that

$$|\mu'|-|\check{\mu}|\le q_7,\quad |\beta'|-\left|\check{\beta}\right|-\left|\overline{\overline{\beta}}\right|=q_7 \;\Rightarrow\; \Delta G_7\le -\frac{2}{3}q_7.$$

Similarly, $\mu'+\zeta'+\beta'$ is not a case for interactions given by (3.28) and (3.29) where the incoming 1-fronts are shock-fronts and the incoming 3-fronts are rarefaction-fronts. Moreover, all interactions where $\epsilon_2=\alpha_2$ have estimate given by (3.33). The remaining two interactions are special cases of $\alpha_1+\nu_1+\zeta+\mu_2+\beta_2$ where either $\alpha_1$ or $\beta_2$ is missing, and they are covered by the above discussion.

Observe that for the self-symmetric interactions the case where the outgoing waves are $\mu'+\zeta+\beta'$ is symmetric to the case where the outgoing waves are $\alpha'+\zeta+\nu'$. Thus, only one case is left for these three interactions, the case where we have $\alpha'+\zeta+\beta'$. Some configurations of fronts gives us

$$|\alpha'|-|\alpha|\le 0,\quad |\beta'|-|\beta|\le 0 \;\Rightarrow\; \Delta G\le 0,$$

directly. Otherwise, we have to divide the interactions into smaller steps as follows

$$\begin{aligned}\epsilon_1+\eta_1+[\zeta+\epsilon_2+\eta_2] &\xrightarrow{\Delta G_2} \epsilon_1+[\eta_1+\overline{\epsilon}]+\zeta+\overline{\eta} \xrightarrow{\Delta G_3} \epsilon_1+[\tilde{\epsilon}+\tilde{\eta}+\zeta]+\overline{\eta}\\ &\xrightarrow{\Delta G_4} [\epsilon_1+\hat{\epsilon}+\zeta]+\hat{\eta}+\overline{\eta} \xrightarrow{\Delta G_5} \overline{\overline{\alpha}}+[\zeta+\overline{\overline{\eta}}+\hat{\eta}+\overline{\eta}]\\ &\xrightarrow{\Delta G_6} \overline{\overline{\alpha}}+\check{\epsilon}+\zeta+\check{\beta} \xrightarrow{\Delta G_7} \alpha'+\zeta+\beta',\end{aligned}$$

where $\overline{\epsilon}$ and $\tilde{\epsilon}$ are of the same type as $\epsilon_2$, and $\tilde{\eta}$ is of the same type as $\eta_1$. If $\eta_1$ is a rarefaction-front, then $\overline{\eta}$ is a shock-front, $\hat{\epsilon}$ can be of either type, and $\overline{\overline{\eta}}$ will be of the opposite type of $\hat{\epsilon}$. If $\eta_1$ is a shock-front, then $\overline{\eta}$ can be of either type, $\hat{\epsilon}=\hat{\alpha}$, and $\overline{\overline{\eta}}$ is of the opposite type as $\epsilon_1$. Moreover, if $\overline{\overline{\eta}}$ and $\hat{\eta}$ are both rarefaction-fronts, we add them together to one 3-rarefaction wave according to property (i) of Lemma 2.1. If all 3-fronts at step six are shock-fronts, then $\check{\epsilon}=\check{\mu}$ and does not take part in the estimate below, otherwise $\check{\epsilon}=\check{\alpha}$. We have estimates for $\Delta G_i$, $i=2,\dots,6$, due to Lemma 3.8 and 3.9. Moreover,

$$|\alpha'|-\left|\overline{\overline{\alpha}}\right|-|\check{\alpha}|\le 0,\quad |\beta'|-\left|\check{\beta}\right|\le 0 \;\Rightarrow\; \Delta G_7\le 0.$$

None of the interactions given by (3.28) are self-symmetric. For interactions given by (3.29), one of the self-symmetric interactions involve only rarefaction-fronts and $\alpha'+\zeta+\beta'$ is therefore not a possible case. The other self-symmetric interaction, $\beta+\zeta+\alpha$, can be divided into smaller steps as above and is thus covered by the estimates just given. Here, step four is redundant.

Finally, we consider the last two cases, when the outgoing waves are $\alpha'+\zeta+\nu'$ or $\alpha'+\zeta+\beta'$, for the three interactions that are not self-symmetric. These interactions all have two incoming shock-fronts of the first family, and we observe that

$$\text{if } |\alpha'|-|\alpha_1|-|\alpha_2|=-q\le 0, \text{ then } \begin{cases}|\nu'|-|\nu|\le q & \Rightarrow\ \Delta G\le -\frac{2}{3}q,\\ |\beta'|-|\beta|\le 0 & \Rightarrow\ \Delta G\le 0.\end{cases}$$

If this condition of the 1-shocks does not hold, we divide the interactions into smaller steps as follows;

$$\begin{aligned}\alpha_1+\eta_1+[\zeta+\alpha_2+\eta_2] &\xrightarrow{\Delta G_2} \alpha_1+[\eta_1+\overline{\alpha}]+\zeta+\overline{\eta} \xrightarrow{\Delta G_3} \alpha_1+[\tilde{\alpha}+\tilde{\eta}+\zeta]+\overline{\eta}\\ &\xrightarrow{\Delta G_4} [\alpha_1+\hat{\epsilon}+\zeta]+\hat{\eta}+\overline{\eta} \xrightarrow{\Delta G_5} \overline{\overline{\alpha}}+[\zeta+\overline{\overline{\eta}}+\hat{\eta}+\overline{\eta}]\\ &\xrightarrow{\Delta G_6} \overline{\overline{\alpha}}+\check{\alpha}+\zeta+\check{\eta} \xrightarrow{\Delta G_7} \alpha'+\zeta+\eta',\end{aligned}$$

where $\tilde{\eta}$ and $\hat{\eta}$ are of the same type as $\eta_1$, and $\check{\eta}$ is of the same type as $\eta'$. Furthermore, if $\eta_1$ and $\eta_2$ are rarefaction-fronts and $\eta'$ is a shock-front, then $\overline{\eta}$ is also a shock-front. If $\eta_2$ and $\eta'$ are of the same type, while $\eta_1$ is not, then $\overline{\eta}$ is of the same type as $\eta_2$. Otherwise, $\overline{\eta}$ can be of either type. Likewise, $\hat{\epsilon}$ can be of either type, and we therefore have to include step five, where $\overline{\overline{\eta}}$ is not of the same type as $\hat{\epsilon}$. Moreover, if at some point, two adjacent 3-fronts are both rarefaction-fronts, then we add them together to one 3-rarefaction wave according to property (i) of Lemma 2.1. Finally, if all 3-fronts at step six, that is, $\overline{\overline{\eta}}$, $\hat{\eta}$ and $\overline{\eta}$, are all of the same type as $\eta'$, then we skip step six and replace the strength of $\check{\eta}$ in the estimates below by the sum of the strength of these 3-fronts. From Lemma 3.8 and 3.9 we have estimates for $\Delta G_i$, $i=2,\dots,6$. Finally, we have

$$\begin{aligned}|\alpha'|-\left|\overline{\overline{\alpha}}\right|-|\check{\alpha}|=q_7, \quad |\nu'|-|\check{\nu}|\le q_7 \;\Rightarrow\; \Delta G_7\le -\frac{2}{3}q_7,\\ |\alpha'|-\left|\overline{\overline{\alpha}}\right|-|\check{\alpha}|\le 0, \quad |\beta'|-\left|\check{\beta}\right|\le 0 \;\Rightarrow\; \Delta G_7\le 0,\end{aligned}$$

for the two cases, respectively.

The interactions given by (3.28) and (3.29) can be divided into smaller steps in the same way. For interactions with no $\epsilon_1$, we in general only need six steps because step four is not needed. However, if $\hat{\epsilon}=\hat{\mu}$, we may have to interchange step four and five, so that we still have seven steps. Moreover, if

$$|\alpha'|-|\alpha|\le -|\nu'|, \text{ then } \Delta G\le 0,$$

without dividing the interaction into smaller steps.

All cases for all interactions are now considered, thus, we have proved the lemma. □

This concludes the discussion of all interactions between physical fronts. For interactions generating non-physical fronts and interactions where one of the incoming fronts is non-physical, we have:

**Lemma 3.14.** *For an interaction where a non-physical front is generated, we have*

$$\Delta G\le -3k|\theta^{np}|, \text{ and } |\theta^{np}|\le \frac{4}{3}c_2\rho, \tag{3.34}$$

*where the positive constants $k$ and $c_2$ depend only on $p_{\min}$, $p_{\max}$, and $\overline{\gamma}$. Moreover, $\Delta G\le 0$ for all interactions with incoming non-physical fronts, and the strength of a non-physical front does not change in interactions.*

*Proof.* The simplified Riemann solver is used for interactions of the type $\zeta+\sum_{i=1}^n\epsilon_i$, and the symmetric interactions, where condition (3.1) holds, that is, where $|\zeta|\sum_i|\epsilon_i|\le\rho$. Since non-physical fronts cannot be generated in any other interactions, it follows from Lemma 3.8 and Lemma 3.11 that $\Delta G\le -3k|\theta^{\mathrm{np}}|$. By estimates (3.17), (3.18), and (3.23) established in the proofs of these lemmas, we have

$$|\theta^{\mathrm{np}}|\le\frac{4}{3}c_2|\zeta|\sum_i|\epsilon_i|\le\frac{4}{3}c_2\rho.$$

Whenever a non-physical front is involved in an interaction, we let the non-physical front pass through the interaction without changing its strength. Then we solve the remaining interaction. The non-physical front only introduces a shift in the $u$-variable, and since all wave curves are invariant under a transformation in $u$, the interaction and all its estimates are the same as if it was not shifted. Hence, by Lemma 3.8 through Lemma 3.13, and the fact that the non-physical front plays no role in $G$, we have $\Delta G \leq 0$ for all interactions with an incoming non-physical front. This also applies to interactions having two incoming non-physical fronts, one with negative and one with positive speed. In particular we have $\Delta G = 0$ when a non-physical front collides with one other front, physical or non-physical; they just pass through each other, continuing with the same strength. □

We have now established that $\Delta G \leq 0$ for all possible interactions and can finally prove that $G$ is decreasing in time.

*Proof of Proposition* 3.7. By Lemma 3.8 through Lemma 3.14 it follows that $G$ decreases for all possible interactions, and, in particular, that $\Delta G \leq -\frac{2}{3}q$ for all increasing rarefaction-collisions where the strength of the rarefaction wave increases by $q$, $\Delta G \leq -\frac{2}{3}|\theta'|$ for all new rarefaction-collisions where $\theta'$ denotes the new rarefaction wave, and $\Delta G \leq -3k|\theta^{\text{np}}|$ for all interactions generating a non-physical front. Finally, since $G$ decreases, it follows from (3.13) that $F(t_n) \leq \frac{5}{3}L(t_0)$. □

3.3. **Finite number of interactions.** The next step is to show that the front-tracking algorithm generates an approximate solution in a finite number of steps. We do this by proving that there is a finite number of physical and non-physical fronts, and, hence, a finite number of interactions.

As discussed in Subsection 3.1, the number of fronts increases when we have a $\gamma$-collision solved by the approximate solver, or when a rarefaction wave splits. Moreover, splitting of rarefaction waves can only be caused by new rarefaction-collisions or increasing rarefaction-collisions, and we now show that the number of such interactions is finite.

**Lemma 3.15.** *For a fixed $\delta$, there is only a finite number of new rarefaction-collisions where the new rarefaction wave splits into two or more fronts.*

*Proof.* From Proposition 3.7 we have $\Delta G \leq -\frac{2}{3}|\theta|$ for all new rarefaction-collisions, where $\theta$ is the new outgoing rarefaction wave. This was proved in Subsection 3.2 where all interactions of this type were identified. The new rarefaction wave splits into two or more fronts only if its strength, $|\theta|$, is larger than $\delta$. Hence, $\Delta G \leq -\frac{2}{3}\delta$ across a new rarefaction-collision where the new rarefaction wave splits. Since $G$ is a decreasing, non-negative functional, there can only be a finite number of interactions where $G$ decreases by at least $\frac{2}{3}\delta$. This proves the lemma. □

We next consider the increasing rarefaction-collisions and look at the change in $G$ from a split rarefaction-front appears until it has gained enough strength to split again. That is, consider an increasing rarefaction-collision at $t = \tau_1$ where the outgoing rarefaction wave splits into several fronts. Let $\tau_n$ be the collision time when the first of the split rarefaction-fronts splits again after gaining strength through increasing rarefaction-collisions. Fix two time lines, $t_i$ and $t_j$, so that $t_i < \tau_1 < \tau_n < t_j$. Assume that the only rarefaction-front crossing $t = t_i$ that results in a split rarefaction wave (through increasing rarefaction-collisions) before $t = t_j$, is the rarefaction-front colliding at $t = \tau_1$. Define $\Delta G_{\text{split}} := G(t_j) - G(t_i)$.

**Lemma 3.16.** *Let $t_i < \tau_1 < \tau_n < t_j$ and $\Delta G_{\text{split}}$ be as defined above. Then, for a fixed $\delta$,*

$$\Delta G_{\text{split}} \leq -\frac{1}{3}\delta. \tag{3.35}$$

*Furthermore, there is only a finite number of increasing rarefaction-collisions where the increasing rarefaction wave splits into two or more fronts.*

*Proof.* From Proposition 3.7 we have $\Delta G \leq -\frac{2}{3}q$ for all increasing rarefaction-collisions where $q > 0$ bounds the increase of the strength of the rarefaction wave, that is, the strength of the outgoing rarefaction wave is less than or equal to $q$ plus (the sum of) the strength(s) of the incoming rarefaction-front(s) of the same family.

Let $\theta'$ be the outgoing rarefaction wave of the increasing rarefaction collision at $t = \tau_1$, thus, $\theta'$ splits, and let furthermore $\theta_0$ be the incoming rarefaction-front of the same family. By the assumptions, $|\theta_0| = a\delta$ for $0 < a \leq 1$, and

$$\delta < |\theta'| \leq |\theta_0| + q_1.$$

Furthermore, $\Delta G_1 \leq -\frac{2}{3}q_1$ across this interaction. Let $m$ be the number of fronts $\theta'$ splits into and let furthermore $\theta_1$ denote the first of these split fronts that gain enough strength to split again. Thus,

$$|\theta_1| = \frac{1}{m}|\theta'| \leq \frac{|\theta_0| + q_1}{m} = \frac{a\delta + q_1}{m}.$$

We follow this rarefaction-front until it splits again after an interaction at $t = \tau_n$, and in

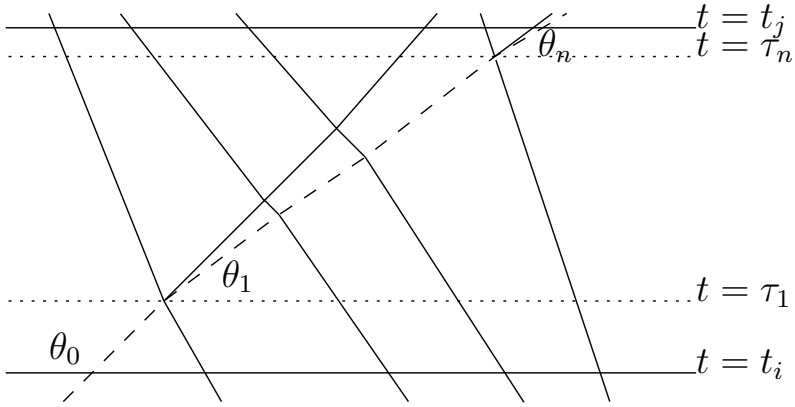


FIGURE 17. An illustration of several increasing rarefaction-collision where a rarefaction wave splits at $t = \tau_1$ and $t = \tau_n$.

Figure 17, where $m = 2$, this front is drawn by dashed lines. The only way for the rarefaction-front to gain strength is through increasing rarefaction-collisions, all other interactions only weaken the rarefaction-front. We can therefore assume that the rarefaction-front we follow is only involved in increasing rarefaction-collisions up to $t = t_j$. For each interaction the strength of the rarefaction-front increases by at most $q_i$, thus,

$$|\theta_n| \leq |\theta_{n-1}| + q_n \leq |\theta_1| + \sum_2^n q_k \leq \frac{a\delta + q_1}{m} + \sum_2^n q_k \leq \frac{a}{m}\delta + \sum_1^n q_k, \tag{3.36}$$

and $\Delta G_k \leq -\frac{2}{3}q_k$ for $k = 1, \ldots, n$. By definition, $\tau_n$ is the first collision time after $\tau_1$ where a rarefaction wave splits, thus,

$$|\theta_{n-1}| \leq \delta < |\theta_n|. \tag{3.37}$$

All interactions taking place between $t_i$ and $t_j$ have $\Delta G \leq 0$ by Proposition 3.7. Combining (3.36) and (3.37) we get

$$\begin{aligned}\Delta G_{\text{split}} &= \sum_{\tau_k} \Delta G(\tau_k) + \sum_{\tau \neq \tau_k} \Delta G(\tau) \leq \sum_{\tau_k} \Delta G(\tau_k) \\ &\leq \sum_{i=1}^{n} -\frac{2}{3} q_k \leq -\frac{2}{3}\left(1 - \frac{a}{m}\right)\delta \leq -\frac{1}{3}\delta,\end{aligned}$$

where we have used that $0 < a \leq 1$ and $m \geq 2$. This proves (3.35).

Furthermore, $G$ is non-negative and decreases by at least $\frac{1}{3}\delta$ from the time when a rarefaction wave splits due to an increasing rarefaction-collision until the time when the first of the split fronts has gained enough strength to split again. Hence, this can only happen a finite number of times, and therefore, there can only be a finite number of increasing rarefaction-collisions where the rarefaction wave splits. □

Thus, by Lemma 3.15 and Lemma 3.16, there is a finite number of interactions resulting in split rarefaction waves. That is, there is only a finite number of interactions with more than one outgoing front of each family.

The only other interactions with more outgoing physical fronts than incoming fronts, are $\gamma$-collisions solved by the approximate solver. These interaction are solved by the approximate solver if $|\theta|\,|\zeta| > \rho$, where $\theta$ is the incoming 1- or 3-front. By Proposition 3.7, $G$ decreases and, and in particular, $\Delta G \leq 0$ for all interactions. Therefore,

$$0 < G(t_n) \leq G(t_0) + \sum_{\tau < t_n} \Delta G(\tau) \leq G(t_0) + \sum_{\tau_\gamma < t_n} \Delta G(\tau_\gamma),$$

where $\tau$ is any collision time and $\tau_\gamma$ is the collision time of a $\gamma$-collision solved by the approximate solver. Furthermore, Lemma 3.8 states that $\Delta G \leq -\frac{1}{9}|\theta|\,|\zeta|$ for all $\gamma$-collisions, thus,

$$\sum_{\tau_\gamma < t_n} |\theta|\,|\zeta| \leq -9 \sum_{\tau_\gamma < t_n} \Delta G(\tau_\gamma) \leq 9G(t_0).$$

This estimate is true for all $t_n < \infty$, hence, there is at most $9G(t_0)/\rho$ number of $\gamma$-collisions where $|\theta|\,|\zeta| > \rho$, that is, where a $\gamma$-collision is solved by the approximate solver. These are the only interactions creating more physical fronts in addition to the finite number of split rarefaction waves. Thus, the number of physical fronts remains finite for all times. Moreover, non-physical fronts are only generated when physical fronts interact with a contact discontinuity. Each physical front can only interact once with a given contact discontinuity, and there is a finite number of contact discontinuities, hence, there is a finite number of interactions generating non-physical fronts.

In other words, there is a finite number of physical and non-physical fronts for any given time, and these fronts can only interact a finite number of times. Thus, front tracking gives us an approximate solution in a finite number of steps for any $t \in (0, \infty)$.

3.4. **The total amount of non-physical fronts.** In order to prove that the sequence of approximate solutions converges to a weak solution, we need to estimate the total amount of non-physical fronts introduced. First of all, we assign a *generation* to all fronts except the contact discontinuities.

All initial 1- and 3-fronts are of generation one. The outgoing front of an interaction has the lowest generation of the incoming fronts of the same family. If there is no incoming front of the same family, the outgoing front has a generation one higher than the highest generation of the incoming fronts. If there is a non-physical front generated in an interaction, its generation is also one higher than the highest generation of the incoming fronts. If an interaction has an incoming non-physical front, the outgoing non-physical front has the same generation as the incoming, thus, the generation of a non-physical front never changes once it is created. Furthermore, all fronts part of a split rarefaction wave have the same generation as the rarefaction wave.

From the results in Proposition 3.7 we have

$$0 < G(t_n) = G(t_0) + \sum_{\tau \le t_n} \Delta G(\tau) \le G(t_0) + \sum_{\tau_{\rm np} \le t_n} \Delta G(\tau_{\rm np}),$$

where $\tau_{\rm np}$ is a collision time when a non-physical front is generated. Moreover, by Lemma 3.14 we have $\Delta G \le -3k\,|\theta^{\rm np}\,|$ for all interactions where a non-physical front is generated. Let $\theta_i^{\rm np}$ denote a non-physical front of generation $i$. Since neither the strength of a non-physical front, nor its generation, changes due to interactions, we get

$$\sum_i \sum_{t=t_n} |\theta_i^{\rm np}\,| = \sum_{\tau_{\rm np} \le t_n} |\theta^{\rm np}\,| \le -\frac{1}{3k} \sum_{\tau_{\rm np} \le t_n} \Delta G(\tau_{\rm np}) \le \frac{G(t_0)}{3k}. \tag{3.38}$$

Thus, there exists a $j$ so that

$$\sum_{i>j} \sum_{t=t_n} |\theta_i^{\rm np}\,| = \mathcal{O}(1)\,\delta_{\rm init}. \tag{3.39}$$

Let $N_j$ be the number of fronts of generation less than or equal to $j$. From the previous section we know that $N_j$ is finite. and according to [4, Ch. 7.3],

$$N_j \le P_j(N_0, \delta^{-1}),$$

where $P_j$ is a polynomial function of $\delta^{-1}$ and the number of initial fronts, $N_0$. Using this, we can now prove the following:

**Lemma 3.17.** *For any given $\delta_{\rm init} > 0$ there exists a $\rho > 0$ so that*

$$\sum_{t=t_n} |\theta^{np}\,| = \mathcal{O}\left(\delta_{\rm init}\right).$$

*Proof.* Fix a $j = j_0$ so that (3.39) holds. The number of non-physical fronts of generation less than or equal to $j_0$ is less than $N_{j_0}$, which again is bounded by $P_{j_0}(N_0, \delta^{-1})$. We therefore get

$$\begin{aligned}\sum_{t=t_n} |\theta^{\rm np}\,| &\le \sum_{i \le j_0} \sum_{t=t_n} |\theta_i^{\rm np}\,| + \sum_{i>j_0} \sum_{t=t_n} |\theta_i^{\rm np}\,| \\ &\le \frac{4}{3} c_2 \rho P_{j_0}(N_0, \delta^{-1}) + \mathcal{O}(1)\delta_{\rm init} = \mathcal{O}\left(\delta_{\rm init}\right),\end{aligned}$$

by choosing $\rho$ so that $\frac{4}{3} c_2 \rho P_{j_0}(N_0, \delta^{-1}) = \mathcal{O}(\delta_{\rm init})t$. □

Recall that $\delta_{\rm init} = \mathcal{O}(\delta)$, so that $\delta_{\rm init} \to 0$ when $\delta \to 0$.

3.5. **Bounded total variation.** We have established that if condition (3.12) is satisfied, then $G$ is decreasing and $U^\delta$ can be defined up to any time. The next step is to bound the total variation of $U^\delta$.

From Section 3.2 we recall that $C_1$ is the constant appearing in estimate (3.16), $C_2$ is given by (3.4), $k$ by (3.5), and $C$ by (3.11). Define the constant

$$\kappa := 1 + \frac{10}{9}\left(3s'_{\max}k + 1\right),$$

where $s'_{\max}$ is the upper bound of $\partial s/\partial p$, cf. property (v) of Lemma 2.1. Given these constants, that only depend on $p_{\min}$, $p_{\max}$ and $\overline{\gamma}$, we can state the following result.

**Lemma 3.18.** *If the initial data satisfy*

$$(\overline{\gamma}-1)\mathrm{T.V.}(p_0,u_0) \le \frac{C}{9kC_1} \text{ and } \mathrm{T.V.}(\gamma_0) \le \frac{C}{9C_2}, \tag{3.40}$$

*and the approximate solution $U^\delta(x,t) = (p^\delta(x,t), u^\delta(x,t), \gamma^\delta(x,t))$ obtained using front tracking is bounded away from vacuum, then*

$$\mathrm{T.V.}(p^\delta(\,\cdot\,,t), u^\delta(\,\cdot\,,t)) \le 2\kappa k \mathrm{T.V.}(p_0,u_0), \tag{3.41}$$

$$\mathrm{T.V.}(\gamma^\delta(\,\cdot\,,t)) \le \mathrm{T.V.}(\gamma_0). \tag{3.42}$$

*Proof.* First, (3.42) is obvious since $\gamma$ only changes along contact discontinuities, thus,

$$\mathrm{T.V.}(\gamma^\delta(\,\cdot\,,t_n)) = F_\gamma = \mathrm{T.V.}(\gamma^\delta(\cdot,0)) \le \mathrm{T.V.}(\gamma_0),$$

for any time line $t = t_n$. Furthermore,

$$L(t_0) \le \mathrm{T.V.}(p^\delta(\,\cdot\,,0)) + k\mathrm{T.V.}(u^\delta(\,\cdot\,,0)) \le k\mathrm{T.V.}(p^\delta(\,\cdot\,,0), u^\delta(\,\cdot\,,0)),$$

for $t_0 = 0+$. Whenever (3.40) is satisfied, we therefore have

$$L(t_0) \le k\mathrm{T.V.}(p^\delta(\,\cdot\,,0), u^\delta(\,\cdot\,,0)) \le k\mathrm{T.V.}(p_0,u_0) \le \frac{C}{9C_1(\overline{\gamma}-1)},$$

$$F_\gamma = \mathrm{T.V.}(\gamma^\delta(\,\cdot\,,0)) \le \mathrm{T.V.}(\gamma_0) \le \frac{C}{9C_2},$$

thus, by Proposition 3.7 the Glimm functional is decreasing and $F(t_n) \le \frac{5}{3}L(t_0)$. We use this to bound $\mathrm{T.V.}(u^\delta(\,\cdot\,,t_n))$. If there were no non-physical fronts, we would have

$$\sum_{\mathrm{rf}} [\![u]\!] = \sum_{\mathrm{shock}} [\![u]\!] + u(\infty,\,\cdot\,) - u(-\infty,\,\cdot\,),$$

because $u$ is increasing along all rarefaction waves and decreasing along all shock waves. Here $[\![u]\!] := |u_r - u_l\,|$ for a wave connecting $U_l$ to $U_r$, and rf is short for rarefaction wave. Let $u_\pm = u_0(\pm\infty)$ and define

$$c_0 := |u(\infty,\,\cdot\,) - u(-\infty,\,\cdot\,)\,| = |u_+ - u_-\,|, \tag{3.43}$$

since $u(\pm\infty,\,\cdot\,) = u_0(\pm\infty)$. Including the non-physical fronts, we have

$$\sum_{\mathrm{rf}} [\![u]\!] \le \sum_{\mathrm{shock}} [\![u]\!] + \sum_{\mathrm{np}} [\![u]\!] + c_0,$$

where "np" is short for non-physical front. Thus,

$$\mathrm{T.V.}(u^\delta(\,\cdot\,,t_n)) = \sum_{\mathrm{rf}} [\![u]\!] + \sum_{\mathrm{shock}} [\![u]\!] + \sum_{\mathrm{np}} [\![u]\!] \le 2\sum_{\mathrm{shock}} [\![u]\!] + 2\sum_{\mathrm{np}} [\![u]\!] + c_0$$

$$
\begin{aligned}
&\le 2\sum_{\text{shock}} |s'(\tilde{p},p_l,\gamma_l)\,|\,[\![p]\!] + \frac{2}{3k}G(t_0) + c_0\\
&\le 2s'_{\max}\sum_{\text{shock}}[\![p]\!] + \frac{10}{9k}L(t_0) + c_0 = 2s'_{\max}F(t_n) + \frac{10}{9k}L(t_0) + c_0\\
&\le 2s'_{\max}\frac{5}{3}L(t_0) + \frac{10}{9k}L(t_0) + c_0 \le \frac{10}{9}\left(3s'_{\max}k+1\right)\text{T.V.}(p_0,u_0) + c_0\\
&\le \kappa\text{T.V.}(p_0,u_0),
\end{aligned}
$$

where we have used that $c_0 \le \text{T.V.}(u_0)$ and $\sum_{\text{np}}[\![u]\!] = \sum|\theta^{\text{np}}\,| \le G(t_0)/3k$, cf. (3.38). For $\text{T.V.}(p^\delta(\,\cdot\,,t_n))$ we find

$$
\begin{aligned}
\text{T.V.}(p^\delta(\,\cdot\,,t_n)) &= \sum_{\text{rf}}[\![p]\!] + \sum_{\text{shock}}[\![p]\!] \le k\left(\sum_{\text{rf}}[\![u]\!] + \sum_{\text{shock}}[\![u]\!]\right)\\
&\le k\text{T.V.}(u^\delta(\,\cdot\,,t_n)) \le \kappa k\text{T.V.}(p_0,u_0).
\end{aligned}
$$

This proves (3.41) because

$$
\begin{aligned}
\text{T.V.}(p^\delta(\,\cdot\,,t_n),u^\delta(\,\cdot\,,t_n)) &= \text{T.V.}(p^\delta(\,\cdot\,,t_n)) + \text{T.V.}(u^\delta(\,\cdot\,,t_n))\\
&\le 2\kappa k\text{T.V.}(p_0,u_0).
\end{aligned}
$$

□

We also have to bound the approximate solution away from vacuum. From

$$
\sup(y) \le |y(\infty)\,| + |y(-\infty)\,| + \text{T.V.}(y),
$$

and the fact that $p^\delta(\pm\infty,\,\cdot\,) = p_0(\pm\infty) := p_\pm$, it follows that

$$
\begin{aligned}
\sup(p^\delta - p_+) &\le \left|p^\delta(\infty) - p_+\,\right| + \left|p^\delta(-\infty) - p_+)\,\right| + \text{T.V.}(p^\delta)\\
&= |p_+ - p_-)\,| + \text{T.V.}(p^\delta)\\
&\le 2\text{T.V.}(p^\delta) \le 2\kappa k\text{T.V.}(p_0,u_0).
\end{aligned}
$$

Similarly, we obtain

$$
\begin{aligned}
\sup(p^\delta - p_-) &\le 2\kappa k\text{T.V.}(p_0,u_0),\\
\sup(u^\delta - u_+) &\le 2\kappa\text{T.V.}(p_0,u_0),\\
\sup(u^\delta - u_-) &\le 2\kappa\text{T.V.}(p_0,u_0).
\end{aligned}
$$

Furthermore, $\gamma^\delta(\,\cdot\,,t)$ always lies between 1 and $\overline{\gamma}$. Thus, the approximate solution obtained by front tracking will always be contained in the domain

$$
\begin{aligned}
\mathcal{U} = \Big\{(p,u,\gamma)\,|\,&\max\{|p-p_-\,|\,,|p-p_+\,|\} \le 2\kappa k\text{T.V.}(p_0,u_0),\\
&\max\{|u-u_-\,|\,,|u-u_+\,|\} \le 2\kappa\text{T.V.}(p_0,u_0), \gamma\in(1,\overline{\gamma}]\Big\},
\end{aligned}
\tag{3.44}
$$

where $p_\pm = p_0(\pm\infty)$ and $u_\pm = u_0(\pm\infty)$. We are now able to bound $U^\delta$ away from vacuum.

**Lemma 3.19.** *If the initial data satisfy*

$$
2\kappa k\text{T.V.}(p_0,u_0) \le \tilde{p} - p_{\min}, \tag{3.45}
$$

*for a $p_{\min} > 0$ and $\tilde{p} = \max\{p_-,p_+\}$, or the stronger condition*

$$
(\overline{\gamma}-1)\text{T.V.}(p_0,u_0) \le C_3, \tag{3.46}
$$

*where*

$$C_3 := \frac{\overline{\gamma}^{1/2}}{\kappa k r'_{\max}} \left( \tilde{p}^{(\overline{\gamma}-1)/(2\overline{\gamma})} - p_{\min}^{(\overline{\gamma}-1)/(2\overline{\gamma})} \right), \tag{3.47}$$

*then $p \geq p_{\min}$ for all $U \in \mathcal{U}$. Moreover, the approximate solution obtained using front tracking is bounded and, in particular, satisfies $0 < p_{\min} \leq p^\delta(x,t) \leq p_{\max}$.*

*Proof.* For a $p < \min(p_0(x))$ we have

$$\max\{|p - p(\infty, \cdot)|, |p - p(-\infty, \cdot)|\} = \max\{p_-, p_+\} - p = \tilde{p} - p,$$

hence, $p$ is in $\mathcal{U}$ if $\tilde{p} - p \leq 2\kappa k \text{T.V.}(p_0, u_0)$. Thus, if

$$2\kappa k \text{T.V.}(p_0, u_0) \leq \tilde{p} - p_{\min},$$

for a given $p_{\min}$ so that $0 < p_{\min} \leq \min(p_0)$, then $p \geq p_{\min}$ for all $U \in \mathcal{U}$.

Since condition (3.40) imposes a restriction on $(\overline{\gamma} - 1)\text{T.V.}(p_0, u_0)$, we reformulate condition (3.45) to do the same. For a $p_* \geq \tilde{p} \geq p_{\min}$ there is a constant $u_*$ so that we can write

$$u(p) = u_* - r(p, p_*, \overline{\gamma}).$$

From the mean value theorem we get that

$$|\tilde{p} - p_{\min}| = \frac{1}{|u'(\hat{p})|} |u(\tilde{p}) - u(p_{\min})| \geq \frac{1}{r'_{\max}} (u(p_{\min}) - u(\tilde{p})),$$

for $p_{\min} \leq \hat{p} \leq \tilde{p}$. Furthermore,

$$\begin{aligned} u(p_{\min}) - u(\tilde{p}) &= u_* - \frac{2\overline{\gamma}^{\frac{1}{2}}}{\overline{\gamma} - 1} \left( p_{\min}^{\frac{\overline{\gamma}-1}{2\overline{\gamma}}} - p_*^{\frac{\overline{\gamma}-1}{2\overline{\gamma}}} \right) - u_* + \frac{2\overline{\gamma}^{\frac{1}{2}}}{\overline{\gamma} - 1} \left( \tilde{p}^{\frac{\overline{\gamma}-1}{2\overline{\gamma}}} - p_*^{\frac{\overline{\gamma}-1}{2\overline{\gamma}}} \right) \\ &= \frac{2\overline{\gamma}^{\frac{1}{2}}}{\overline{\gamma} - 1} \left( \tilde{p}^{\frac{\overline{\gamma}-1}{2\overline{\gamma}}} - p_{\min}^{\frac{\overline{\gamma}-1}{2\overline{\gamma}}} \right), \end{aligned}$$

so that

$$\tilde{p} - p_{\min} \geq \frac{2\overline{\gamma}^{1/2}}{(\overline{\gamma} - 1) r'_{\max}} \left( \tilde{p}^{\frac{\overline{\gamma}-1}{2\overline{\gamma}}} - p_{\min}^{\frac{\overline{\gamma}-1}{2\overline{\gamma}}} \right).$$

Therefore, we have that $p \geq p_{\min} > 0$ for all $p \in \mathcal{U}$ if

$$2\kappa k \text{T.V.}(p_0, u_0) \leq \frac{2\overline{\gamma}^{1/2}}{(\overline{\gamma} - 1) r'_{\max}} \left( \tilde{p}^{\frac{\overline{\gamma}-1}{2\overline{\gamma}}} - p_{\min}^{\frac{\overline{\gamma}-1}{2\overline{\gamma}}} \right),$$

which proves the lemma. □

3.6. **Convergence to a weak solution.** The approximate solution, $U^\delta$, is bounded and, in particular, bounded away from vacuum. Furthermore, the total variation of $U^\delta$ is bounded independent of $\delta$, as shown in the previous section. Since $v = p^{-1/\gamma}$, we furthermore have that $v^\delta$ is bounded and have bounded total variation independent of $\delta$. Thus, the approximate solution given in the conservative variables, $\tilde{U}^\delta = (v^\delta, u^\delta, \gamma^\delta)$, is bounded, and

$$\text{T.V.}(\tilde{U}^\delta(\cdot, t)) \leq M_0, \tag{3.48}$$

for a constant $M_0$ independent of $\delta$.

We first use Kolmogorov's compactness theorem [15, Thm. A.5] to show that there is a subsequence of $\{\tilde{U}^\delta\}_{\delta>0}$ that converges in $L^1_{\text{loc}}(\mathbb{R} \times [0,T])$. To that end we observe that

$$\int_{\mathbb{R}} \left| \tilde{U}^\delta(x + \omega, t) - \tilde{U}^\delta(x, t) \right| \mathrm{d}x \leq \omega \text{T.V.}(\tilde{U}^\delta(\cdot, t)) \leq M_0 \omega. \tag{3.49}$$

Thus, it remains to show that for any $R > 0$,

$$\int_{-R}^{R} \left| \tilde{U}^\delta(x,t) - \tilde{U}^\delta(x,s) \right| \mathrm{d}x \le M_1(t-s), \tag{3.50}$$

where $t \ge s \ge 0$ and $M_1$ is independent of $\delta$. See Theorem A.8 in [15] for a detailed proof of why (3.48)-(3.50) yield a convergent subsequence using Kolmogorov's compactness theorem. Here we proceed by showing that (3.50) holds for our system.

For $t \in (\tau_j, \tau_{j+1}]$, where $\tau_j$ and $\tau_{j+1}$ are two consecutive collision times, we can write $\tilde{U}^\delta$ as

$$\tilde{U}^\delta(x,t) = \sum_{k=1}^{N_{\tau_j}} (U_{k-1}^j - U_k^j) H(x - x_k^j(t)) + U_{N\tau_j},$$

where $x_k^j$ is the position of the $k$th front from the left, $H$ is the Heaviside function, $N_{\tau_j}$ is the number of fronts after the collision at $\tau_j$, and $\tilde{U}^\delta(x,t) = U_k^j$ for $x \in (x_k^j, x_{k+1}^j)$. Assume now that $t \in [\tau_j, \tau_{j+1}]$ and $s \in [\tau_j, \tau_{j+1}]$ where $j \le i$ and $s \le t$. Then

$$\begin{aligned}
\int_{\mathbb{R}} \left| \tilde{U}^\delta(x,t) - \tilde{U}^\delta(x,\tau_j) \right| \mathrm{d}x &= \int_{\mathbb{R}} \left| \int_{\tau_j}^{t} \frac{\mathrm{d}}{\mathrm{d}\hat{t}} \tilde{U}^\delta(x,\hat{t}) \mathrm{d}\hat{t} \right| \mathrm{d}x \\
&\le \int_{\mathbb{R}} \int_{\tau_j}^{t} \sum_{k=1}^{N_{\tau_j}} \left| U_{k-1}^j - U_k^j \right| \left| \frac{\mathrm{d}}{\mathrm{d}\hat{t}} x_k^j(\hat{t}) \right| \left| H'(x - x_k^j(\hat{t})) \right| \mathrm{d}\hat{t}\mathrm{d}x \\
&\le \lambda_{\mathrm{np}} \int_{\tau_j}^{t} \sum_{k=1}^{N_{\tau_j}} \left| U_{k-1}^j - U_k^j \right| \int_{\mathbb{R}} \left| H'(x - x_k^j(\hat{t})) \right| \mathrm{d}x \mathrm{d}\hat{t} \\
&\le \lambda_{\mathrm{np}} (t - \tau_j) \mathrm{T.V.}(\tilde{U}^\delta(\cdot,t)) \le \lambda_{\mathrm{np}} M_0 (t - \tau_j),
\end{aligned}$$

where we have used that $\left| \frac{\mathrm{d}}{\mathrm{d}\hat{t}} x_k^j(\hat{t}\,) \right| \le \lambda_{\mathrm{np}}$. By similar arguments we get

$$\begin{aligned}
\int_{\mathbb{R}} \left| \tilde{U}^\delta(x,\tau_j) - \tilde{U}^\delta(x,\tau_{j+1}) \right| \mathrm{d}x &\le \lambda_{\mathrm{np}} M_0 (\tau_j - \tau_{j+1}), \quad \text{if } j+1 < i, \\
\int_{\mathbb{R}} \left| \tilde{U}^\delta(x,\tau_{j+1}) - \tilde{U}^\delta(x,s) \right| \mathrm{d}x &\le \lambda_{\mathrm{np}} M_0 (\tau_{j+1} - s).
\end{aligned}$$

Hence,

$$\begin{aligned}
\int_{\mathbb{R}} \left| \tilde{U}^\delta(x,t) - \tilde{U}^\delta(x,s) \right| \mathrm{d}x &\le \int_{\mathbb{R}} \left| \tilde{U}^\delta(x,t) - \tilde{U}^\delta(x,\tau_j) \right| \mathrm{d}x \\
&\quad + \int_{\mathbb{R}} \left| \tilde{U}^\delta(x,\tau_j) - \tilde{U}^\delta(x,\tau_{j+1}) \right| \mathrm{d}x + \int_{\mathbb{R}} \left| \tilde{U}^\delta(x,\tau_{j+1}) - \tilde{U}^\delta(x,s) \right| \mathrm{d}x \\
&\le \lambda_{\mathrm{np}} M_0 (t - s),
\end{aligned}$$

where the middle integral is only included if $j+1 < i$. Since $\lambda_{\mathrm{np}} M_0$ is a constant independent of $\delta$, we have now established (3.50). Hence, there exists a function $U(x,t)$ and a subsequence $\{\delta_j\} \subset \{\delta\}$ so that $\tilde{U}^{\delta_j} \to U$ in $L^1_{\mathrm{loc}}(\mathbb{R} \times [0,T])$ as $j \to \infty$.

We still have to show that the limit is a weak solution. Recall from equation (2.1) that $U = (v,u,\gamma)$ is a weak solution on a strip $[t,s]$ if

$$\mathcal{I}_t^s(U) := \int_t^s \int_{\mathbb{R}} U\phi_t + f(U)\phi_x \mathrm{d}x\mathrm{d}t \tag{3.51}$$

$$-\int_{\mathbb{R}} U(x,s)\phi(x,s)\mathrm{d}x + \int_{\mathbb{R}} U(x,t)\phi(x,t)\mathrm{d}x = 0,$$

for all test functions $\phi$. Fix two successive collision times, $\tau_j$ and $\tau_{j+1}$, and let $\tilde{U}^\delta$ be the approximate solution found using front tracking. The approximate solution $\tilde{U}^\delta$ is not a weak solution because we have introduced non-physical fronts and approximate rarefaction waves. Therefore, we need to estimate how far $\tilde{U}^\delta$ is from the weak solution.

Let $s_1 = \tau_j$ and let $V_i(x,s)$ be the weak solution of

$$V_t + f(V)_x = 0, \quad V(x,s_i) = \tilde{U}^\delta(x,s_i). \tag{3.52}$$

We find $V_1$ fot $t$ close to $s_1$ by solving exactly the Riemann problems at the jumps of $\tilde{U}^\delta(x,s_1)$. This solution is defined up to the time $s_2 > s_1$ when the first waves interact. If no waves in $V_1$ collide before $\tau_{j+1}$, we have $s_2 = \tau_{j+1}$. Otherwise, we let $V_2$ be the solution for $s \geq s_2$ of (3.52) with $i = 2$ and $\tilde{U}^\delta(x,s_2)$ as initial data. In this way we fill $[\tau_j, \tau_{j+1})$ with small strips $[s_i, s_{i+1})$ on which we have defined $V_i$. Let $V$ denote the function that equals $V_i$ at each interval $[s_i, s_{i+1})$, thus, $V(x,s_i) = \tilde{U}^\delta(x,s_i)$ for each $i$. Figure 18(a) shows this construction when a non-physical front is present in $\tilde{U}^\delta$, while Figure 18(b) shows the first steps in the construction when a rarefaction front interacts with a front of the same family at $\tau_{j+1}$.

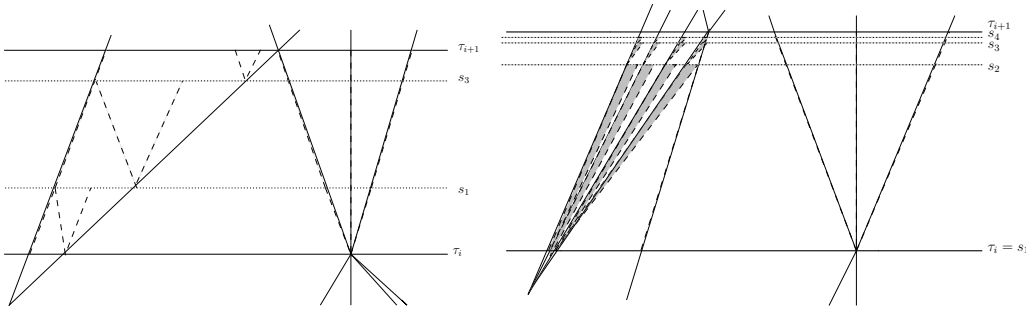


(a) When $\tilde{U}^\delta$ contains a non-physical front

(b) The first steps when a rarefaction front interacts with a front of the same family at $\tau_{j+1}$.

FIGURE 18. The approximate solution $\tilde{U}^\delta$ (solid lines) and the exact solution $V_i$ (dashed line) at each interval $[s_i, s_{i+1})$.

Let furthermore $V^\delta$ be the approximation of $V$ found by solving (3.52) using front tracking without non-physical fronts. That is, we solve all Riemann problems using the approximate solver and never use the simplified solver. No front in $V^\delta$ will interact in one strip, thus, $V^\delta$ only differs from $V$ for rarefaction waves. From the approximation of rarefaction waves by fronts, we have that $\left|V_i(x,t) - V^\delta(x,t)\right| = \mathcal{O}(\delta)$ for $(x,t)$ in a rarefaction fan. Thus, for $t \in [s_i, s_{i+1}]$ the integral

$$\int_{\mathbb{R}} \left|V(x,t) - V^\delta(x,t)\right| \mathrm{d}x,$$

will be the sum of the integrals across the rarefaction fans of $V$. Let $V_l$ and $V_r$ be the left and right state of such a fan. The integral over this fan will be the sum of the integrals across each step in $V^\delta$, and there are $|p_r - p_l|/\mathcal{O}(\delta)$ steps, each with the width $(t - s_i)\Delta\lambda = (t - s_i)\mathcal{O}(\delta)$, where $\Delta\lambda$ is the difference in the characteristic speed across a rarefaction-front in $V^\delta$. We

sum over $j$, that is, over all rarefaction fans in $V$, and find that

$$\int_{\mathbb{R}} \left| V(x,t) - V^\delta(x,t) \right| \mathrm{d}x = \sum_j \frac{\left| p_r^j - p_l^j \right|}{\mathcal{O}(\delta)} \mathcal{O}(\delta)(t-s_i)\mathcal{O}(\delta) \\ \leq (t-s_i)\mathrm{T.V.}(p^\delta)\mathcal{O}(\delta) \leq (t-s_i)\mathcal{O}(\delta), \tag{3.53}$$

since $\sum_j \left| p_r^j - p_l^j \right| \leq \mathrm{T.V.}(p^\delta) \leq M_0$.

Next, we compare $V^\delta$ to $U^\delta$. Since $U^\delta(x,s_i)$ is used as initial data solving (3.52) for each strip, the two solutions only differs where $U^\delta$ have Riemann problems solved by the simplified solver. Thus, in order to estimate the integral

$$\int_{\mathbb{R}} \left| U^\delta(x,t) - V^\delta(x,t) \right| \mathrm{d}x, \tag{3.54}$$

for a $t \in [s_i, s_{i+1})$, we need to take a closer look at the approximation done using the simplified Riemann solver defined in Section 3.1. Consider the interaction $\zeta + \sum_i^n \epsilon_i$ and note that the arguments are similar for the symmetric case. As in Lemma 3.1, we let $\hat{\epsilon} + \zeta + \hat{\eta}$ with intermediate states $\hat{U}_i$, $i = 1, 2$, be the solution using the approximate solver, and $\epsilon' + \zeta + \theta^{\mathrm{np}}$ and $\epsilon' + \zeta + \eta' + \theta^{\mathrm{np}}$ with intermediate states $\tilde{U}_i$, $i = 1, 2$ and $i = 1, 2, 3$, be the solution using the simplified solver for $n = 1$ and $n > 1$, respectively. If $\epsilon'$ is a shock-front, then $\alpha'$ and $\hat{\alpha}$ have slightly different speeds giving rise to a jump in $\left| U^\delta - V^\delta \right|$ of the width $|\sigma_{\hat{\alpha}} - \sigma_{\alpha'}|\,(t-s_i) = \mathcal{O}(1)\,|\theta^{\mathrm{np}}|\,(t-s_i)$, cf. Lemma 3.1. If $\epsilon'$ is a rarefaction-front, the speeds are equal. If $n > 1$ and $\hat{\eta}$ is of the same type as $\eta'$, we also get a jump in $\left| U^\delta - V^\delta \right|$ due to different speeds. The width of this jump is $|\sigma_{\hat{\eta}} - \sigma_{\eta'}|\,(t-s_i) = \mathcal{O}(1)\,|\theta^{\mathrm{np}}|\,(t-s_i)$, where we let $\sigma$ denote the speed for both shock- and rarefaction-fronts. If $\hat{\eta}$ and $\eta'$ are of different types, the height of the jump due to different speeds is less than $\left| U_r - \tilde{U}_3 \right|$. The remaining jumps in $\left| U^\delta - V^\delta \right|$ over this interaction are $\left| \hat{U}_1 - \tilde{U}_1 \right|$, $\left| \hat{U}_2 - \tilde{U}_2 \right|$, and $\left| U_r - \tilde{U}_j \right|$ where $j = 2$ if $n = 1$, and $j = 3$ if $n > 1$. From Lemma 3.1 we have that the heights of these jumps are all bounded by $\mathcal{O}(1)\,|\theta^{\mathrm{np}}|$. Thus,

$$\int_{\mathbb{R}} \left| U^\delta(x,t) - V^\delta(x,t) \right| \mathrm{d}x \leq \sum_{\mathrm{np}} \mathcal{O}(1)\,|\theta^{\mathrm{np}}|\,(t-s_i) = \mathcal{O}(\delta)(t-s_i), \tag{3.55}$$

using that $\sum |\theta^{\mathrm{np}}| \leq \mathcal{O}(1)\delta_{\mathrm{init}} = \mathcal{O}(\delta)$ according to Lemma 3.17.

Combining (3.53) and (3.55), we finally get

$$\int_{\mathbb{R}} \left| U^\delta(x,t) - V(x,t) \right| \mathrm{d}x \leq \int_{\mathbb{R}} \left| U^\delta(x,t) - V^\delta(x,t) \right| + \int_{\mathbb{R}} \left| V(x,t) - V^\delta(x,t) \right| \\ = \mathcal{O}(\delta)(t-s_i).$$

Our goal is to show that $\left| \mathcal{I}_0^T(U) \right| = 0$ where $U(x,t)$ is the limit of $\tilde{U}^{\delta_j}(x,t)$. We start by estimating $\left| \mathcal{I}_{s_i}^{s_{i+1}}(\tilde{U}^\delta) \right|$. Recall that $V_i(x,s_i) = \tilde{U}^\delta(x,s_i)$ and that $V_i$ is a weak solution on each strip, thus, $\mathcal{I}_{s_i}^{s_{i+1}}(V_i) = 0$. We start with $v^\delta$;

$$\begin{aligned} \left| \mathcal{I}_{s_i}^{s_{i+1}}(v^\delta) \right| &= \left| \mathcal{I}_{s_i}^{s_{i+1}}(v^\delta) - \mathcal{I}_{s_i}^{s_{i+1}}(v_i) \right| \\ &= \left| \int_{s_i}^{s_{i+1}} \int_{\mathbb{R}} (v^\delta - v_i)\phi_t + (-u^\delta + u_i)\phi_x \mathrm{d}x\mathrm{d}t \right. \\ &\qquad \left. - \int_{\mathbb{R}} (v^\delta(x,s_{i+1}) - v_i(x,s_{i+1}))\phi(x,s_{i+1})\mathrm{d}x \right| \end{aligned}$$

$$\begin{aligned}
&\leq M_2\Big( \int_{s_i}^{s_{i+1}} \int_{\mathbb{R}} \big| v^\delta - v_i \big| + \big| u^\delta - u_i \big| \,\mathrm{d}x\mathrm{d}t \\
&\qquad + \int_{\mathbb{R}} \big| v^\delta(x, s_{i+1}) - v_i(x, s_{i+1}) \big| \,\mathrm{d}x \Big) \\
&\leq \mathcal{O}(\delta) \left( (s_{i+1} - s_i)^2 + (s_{i+1} - s_i) \right),
\end{aligned}$$

where $M_2$ bounds $|\phi_x|$ and $|\phi_t|$. For $u^\delta$ we get

$$\begin{aligned}
\big| \mathcal{I}_{s_i}^{s_{i+1}}(u^\delta) \big| &= \big| \mathcal{I}_{s_i}^{s_{i+1}}(u^\delta) - \mathcal{I}_{s_i}^{s_{i+1}}(u_i) \big| \\
&= \Big| \int_{s_i}^{s_{i+1}} \int_{\mathbb{R}} (u^\delta - u_i)\phi_t + (p^\delta - p_i)\phi_x \mathrm{d}x\mathrm{d}t \\
&\qquad - \int_{\mathbb{R}} (u^\delta(x, s_{i+1}) - u_i(x, s_{i+1}))\phi(x, s_{i+1}) \mathrm{d}x \Big| \\
&\leq M_2\Big( \int_{s_i}^{s_{i+1}} \int_{\mathbb{R}} \big| u^\delta - u_i \big| + \big| p^\delta - p_i \big| \,\mathrm{d}x\mathrm{d}t \\
&\qquad + \int_{\mathbb{R}} \big| u^\delta(x, s_{i+1}) - u_i(x, s_{i+1}) \big| \,\mathrm{d}x \Big) \\
&\leq \mathcal{O}(\delta) \left( (s_{i+1} - s_i)^2 + (s_{i+1} - s_i) \right),
\end{aligned}$$

where we have used that

$$\int_{\mathbb{R}} \big| p_i(x,t) - p^\delta(x,t) \big| \,\mathrm{d}x \leq (t - s_i)\mathcal{O}(\delta),$$

by the same arguments as above. Since $\gamma$ only changes along contact discontinuities and these are solved exactly both by the approximate and the simplified solver, we actually have $\gamma_i(x,t) = \gamma^\delta(x,t)$, thus

$$\big| \mathcal{I}_{s_i}^{s_{i+1}}(\gamma^\delta) \big| = \big| \mathcal{I}_{s_i}^{s_{i+1}}(\gamma_i) \big| = 0.$$

Let $\tau_j$ and $\tau_{j+1}$ still be two successive collision times and recall that $\tau_{j+1} - \tau_j = \sum_{i=1}^{\infty}(s_{i+1} - s_i)$. Thus,

$$\begin{aligned}
\Big| \mathcal{I}_{\tau_j}^{\tau_{j+1}}(\tilde{U}^\delta) \Big| &\leq \sum_{i=1}^{\infty} \Big| \mathcal{I}_{s_i}^{s_{i+1}}(\tilde{U}^\delta) \Big| \\
&\leq \sum_{i=1}^{\infty} \mathcal{O}(\delta) \left( (s_{i+1} - s_i)^2 + (s_{i+1} - s_i) \right) \\
&\leq \mathcal{O}(\delta) \left( (\tau_{j+1} - \tau_j)^2 + (\tau_{j+1} - \tau_j) \right).
\end{aligned}$$

Since $\tilde{U}^\delta$ is bounded and $\tilde{U}^{\delta_j}(x,t) \to U(x,t)$ in $L^1_{\mathrm{loc}}$ where $U = (v, u, \gamma)$, $p^\delta$ will converge to $p = v^{-1/\gamma}$ in $L^1_{\mathrm{loc}}$. Thus, for any time $T < \infty$,

$$\begin{aligned}
\big| \mathcal{I}_0^T(U) \big| &= \lim_{\delta \to 0} \Big| \mathcal{I}_0^T(\tilde{U}^\delta) \Big| = \lim_{\delta \to 0} \sum_j \Big| \mathcal{I}_{\tau_j}^{\tau_{j+1}}(\tilde{U}^\delta) \Big| \\
&= \lim_{\delta \to 0} \sum_j \mathcal{O}(\delta) \left( (\tau_{j+1} - \tau_j)^2 + (\tau_{j+1} - \tau_j) \right) \\
&\leq \lim_{\delta \to 0} \mathcal{O}(\delta)(T + T^2) = 0,
\end{aligned}$$

which proves that $\tilde{U}^\delta$ converges to a weak solution of (1.1) as $\delta \to 0$.

Thus, we have finally proved the main theorem:

**Theorem 3.20.** *Consider the Cauchy problem for system* (1.1) *with initial data* (1.2) *where* $\inf(p_0(x)) > 0$ *and* $1 < \gamma_0(x) \le \overline{\gamma}$. *Assume that the initial data* $(u_0, p_0)$ *and* $\gamma(x)$ *satisfy*

$$(\overline{\gamma} - 1)\text{T.V.}(p_0, u_0) \le \min\left\{\frac{C}{9kC_1}, C_3\right\}, \tag{3.56}$$

$$\text{T.V.}(\gamma(x)) \le \frac{C}{9C_2}. \tag{3.57}$$

*Then the front tracking algorithm produces a sequence of approximate solutions which converges to a global weak solution of the system* (1.1).

Note that all constants only depend on $p_{\min}$, $p_{\max}$ and $\overline{\gamma}$. Thus, by reducing $\overline{\gamma}$, we may allow arbitrary large total variation for $p_0$ and $u_0$.

By the results of Wagner [27], there is a one-to-one correspondence between a weak solution of (1.1) and a weak solution of the system given in Eulerian coordinates,

$$\begin{aligned} \rho_t + (\rho u)_x &= 0, \\ (\rho u)_t + (\rho u^2 + p(\rho, \gamma))_x &= 0, \\ (\rho\gamma)_t + (\rho u \gamma)_x &= 0, \end{aligned} \tag{3.58}$$

where $x \in \mathbb{R}$ is the physical space variable and $t \in (0, \infty)$ denotes time.

## 4. Numerical examples

We have implemented an approximate and a simplified Riemann solver as described in Subsection 3.1 using MATLAB. These are used together with the front-tracking code at the web page of [15][1]. The threshold parameter $\rho$, which determines when to invoke the simplified Riemann solver, is set to $\delta^3$ for all examples. Furthermore, we let $\lambda_{\text{np}} = 2\lceil\lambda_{\max}\rceil$. The front-tracking code is slightly adjusted so that $G(t)$ is computed for all times.

We find $p_{\max}$ as described in Subsection 2.3. Instead of using (3.46) to find $p_{\min}$, we choose a suitable candidate for $p_{\min}$ and then check that this candidate indeed satisfies $p_{\min} \le p^\delta(x,t)$ for all $x$ and $t$. For the two first examples

$$p_{\min} = \min(p_0(x)) - (p_{\max} - \max(p_0(x))), \tag{4.1}$$

is used as our candidate.

**Example 4.1.** The initial data in this example are piecewise constant and symmetric. We have one gas with $p = 1.26$, $u = 3.00$ and $\gamma = 1.051$ which initially is trapped by another gas with $p = 1.30$, $u = 2.99$ and $\gamma = 1.010$. This is the same initial data as used in Example 1 in [16] where we solved the problem using the Glimm scheme. The constants calculated for

| $p_{\max}$ | $p_{\min}$ | $\overline{\gamma}$ | $C_1$ | $C_2$ | $C$ | $k$ |
|---|---|---|---|---|---|---|
| 1.3067 | 1.2534 | 1.051 | 15.9703 | 1.3309 | 1 | 1.3309 |

TABLE 1. The constants for Example 4.1.

this example are listed in Table 1, and (3.40) is satisfied since

$$\text{T.V.}(p_0, u_0) = 0.1 \le 0.1025 = C/(9kC_1(\overline{\gamma} - 1)), \tag{4.2}$$

$$\text{T.V.}(\gamma_0) = 0.082 \le 0.0835 = C/(9C_2). \tag{4.3}$$

Figure 19 shows $U^\delta(\cdot, t)$ at some different times. In Figure 20 the solution is compared

[1] http://www.math.ntnu.no/~holden/FrontBook/matlabcode.html

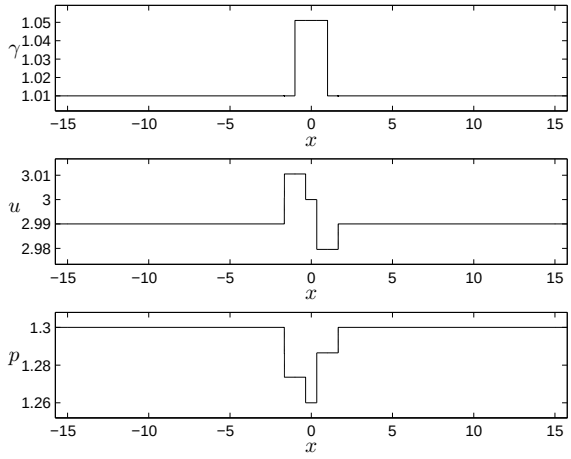


(a) $t = 0.507$.

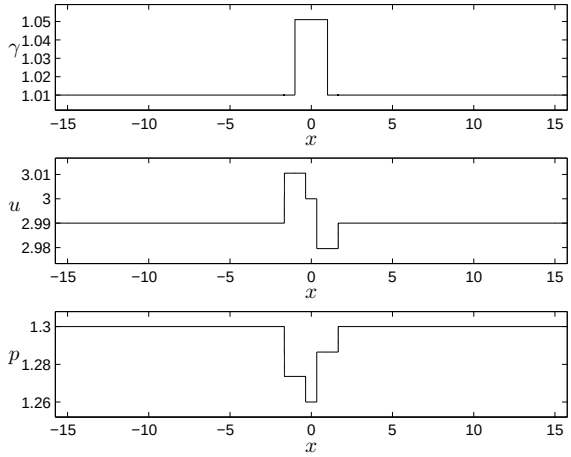


(b) $t = 2.039$.

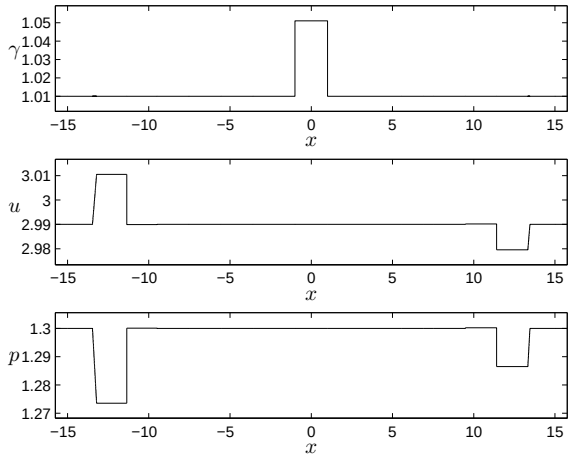


(c) $t = 9.55$.

FIGURE 19. The solution $U^\delta(\,\cdot\,, t)$ at different times $t$ for Example 4.1.

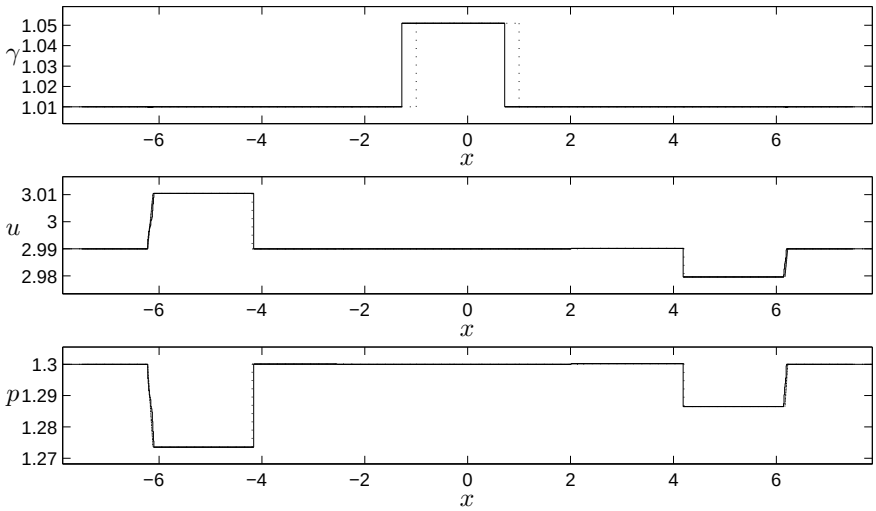


FIGURE 20. The solution of Example 4.1 at $t = 4.002$ using front tracking (dotted line) and the Glimm scheme (solid line).

with the solution found using the Glimm scheme, cf. [16]. The solution obtained using the two methods are very similar, except that the contact discontinuities move back and forth due to the randomness of the Glimm scheme whereas they in front tracking always stay at $\pm 1$. Note that no non-physical fronts has been generated at this point.

The front-tracking solution in the $(x, t)$-plane is shown in Figure 21. Here $\delta = 0.0005$, thus, the rarefaction fronts are very close and look like rarefaction fans. Note furthermore that one front is one line regardless of its strength, thus, in Figure 21 one does not distinguish between strong and weak shock-fronts. Therefore, Figure 21 picks up the interaction of small fronts which is very hard to do using the Glimm scheme, cf. [16]. In this example we see that after some time, one non-physical front is generated, and from then on, there is no more interactions with a contact discontinuity. Finally, Figure 22 shows $G(t)$ for this example.

**Example 4.2.** The initial data in this example are also piecewise constant. For $-1 < x < 1$ we have $p = 2.5$ and $u = 3.0$, while we outside the unit interval have $p = 1.5$ and $u = 2.0$. Furthermore, $\gamma = 1.5$ for $x < -1$ and $0 < x < 1$ while $\gamma = 2.0$ for $-1 < x < 0$ and $x > 1$.

These initial data are far from satisfying condition (3.40), and are therefore not covered by Theorem 3.20. However, as shown in Figure 25, $G(t)$ does decrease for this example, which is enough to ensure convergence to a weak solution.

In Figure 23 we see $U^\delta(\,\cdot\,, t)$ at some different times, while Figure 24 shows the solution in the $(x, t)$-plane. The split rarefaction waves are more visible here, because we have used $\delta = 0.1$. Initially we have three Riemann problems. The solution of the one situated at $x = -1$ is a 1-shock wave, a contact discontinuity and a 3-rarefaction wave, the one situated at $x = 1$ is almost symmetric with a solution consisting of a 1-rarefaction wave, a contact discontinuity and a 3-shock wave, while at $x = 0$ we have only a jump in $\gamma$, hence, the solution is a single contact discontinuity. We see that the first non-physical fronts are generated when reflected fronts of a $\gamma$-collision interacts with another contact discontinuity. The reflected fronts become weaker for each $\gamma$-collision, thus, after some time, all fronts present between the contact discontinuities are non-physical fronts. These non-physical fronts just pass through

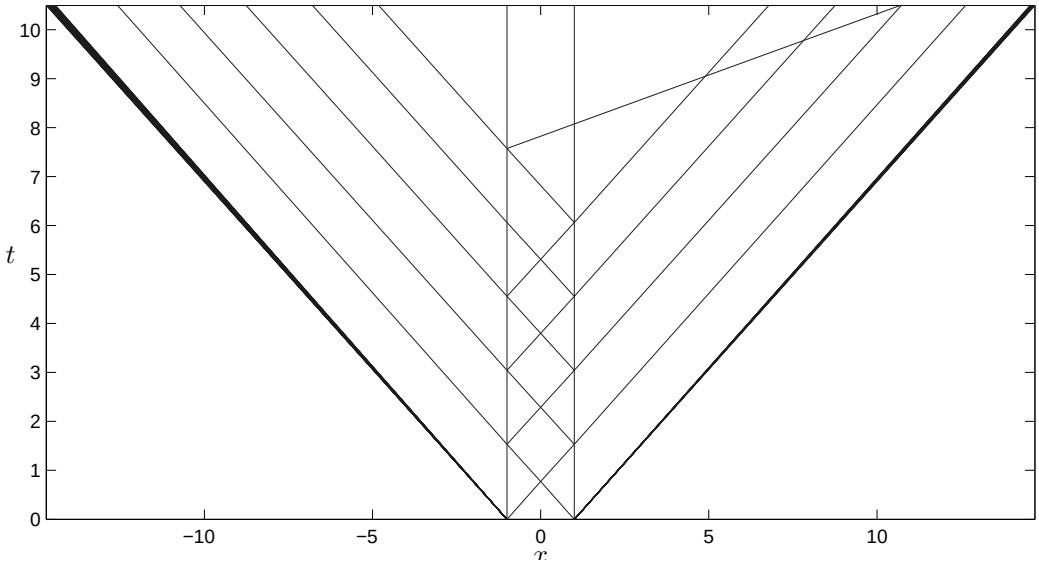


FIGURE 21. The solution $U^\delta(x,t)$ in the $(x,t)$-plane for Example 4.1.

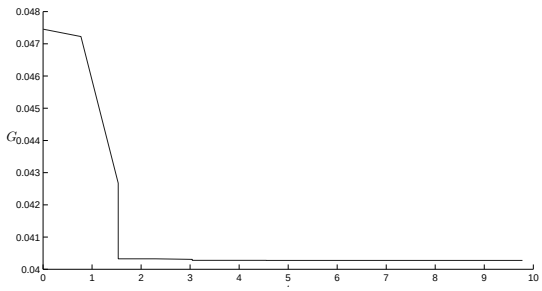


FIGURE 22. $G(t)$ for Example 4.1.

the contact discontinuities without generating more reflected fronts. Recall that $p$ and $\gamma$ are constant across non-physical fronts, thus, comparing the plots for $p$ and $u$ in Figure 23 we see that the non-physical fronts are small compared to the physical fronts.

**Example 4.3.** In this example $\gamma_0$ is a continuous function where $\gamma_0 = 1.7406$ for $x \le -0.4$, $\gamma_0 = 2.6994$ for $x \ge 0.6$ and increases smoothly from 1.7406 to 2.6994 by a sine function in the region $-0.4 \le x \le 0.6$. In the same region we have a high initial pressure, $p_0 = 8$, while $p_0 = 3$ outside. The velocity is piecewise constant and decaying; $u_0 = 3$ for $x \le -0.4$, $u_0 = 2$ for $-0.4 \le x \le 0.6$ and $u_0 = 1$ for $x \ge 0.6$. The initial data are made piecewise constant with $\delta_{\text{init}} = \Delta x = 0.2$. Furthermore, we have chosen $\delta = 0.2$.

These initial data are far from satisfying condition (3.40), but $G$ is still decreasing as shown in in Figure 28. For this example we have that $p^\delta(x,t) \ge 3$, and therefore $p_{\min}$ is set to 3.

In Figure 26 we see $U^\delta(\cdot,t)$ at some different times, while Figure 27 shows the solution in the $(x,t)$-plane. In Figure 27 we observe many fronts interacting, but Figure 26 reveals that

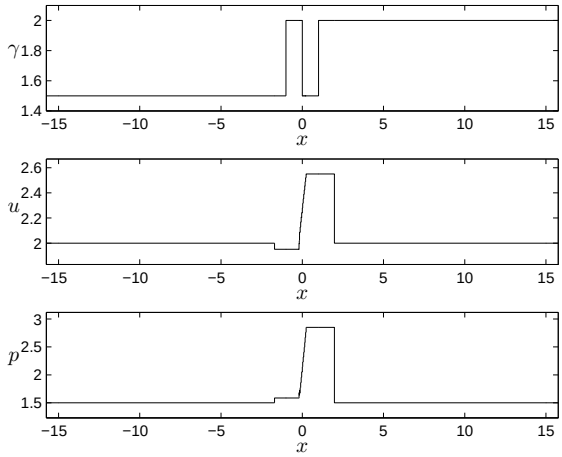


(a) $t = 0.4$.

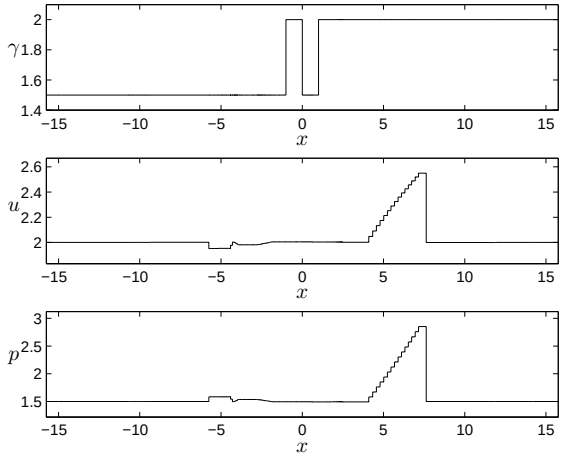


(b) $t = 2.7$.

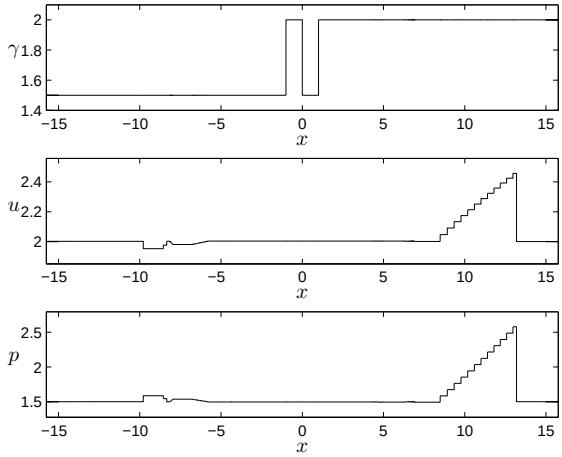


(c) $t = 5$.

FIGURE 23. $U^\delta(\,\cdot\,, t)$ at different times $t$ for Example 4.2.

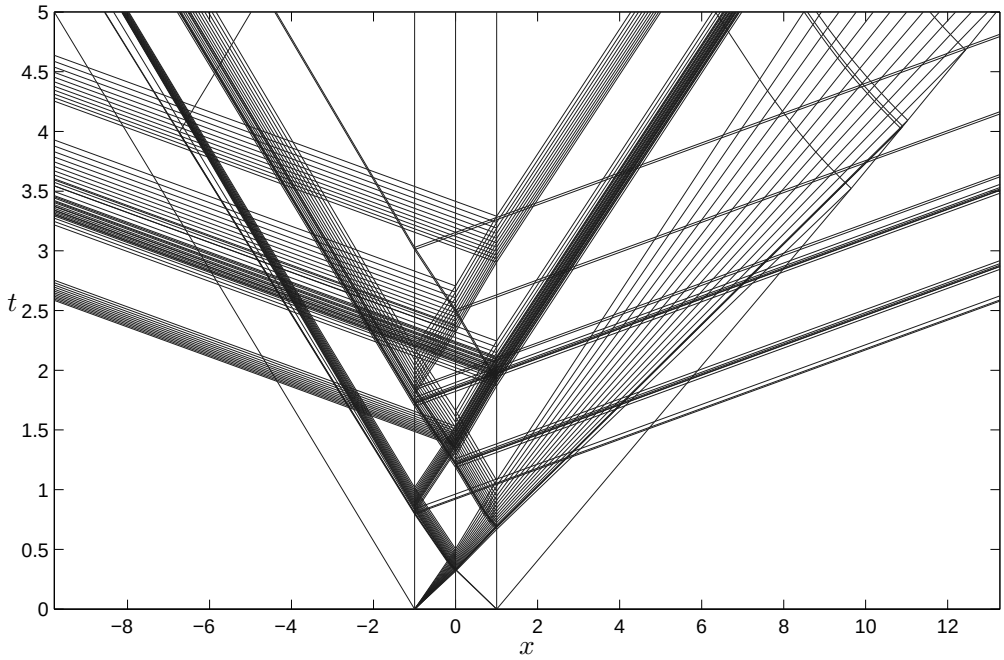


FIGURE 24. The solution $U^\delta(x,t)$ in the $(x,t)$-plane for Example 4.2.

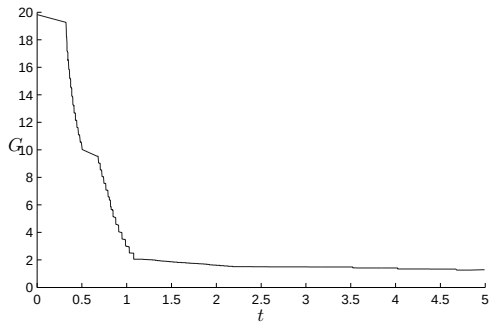


FIGURE 25. $G$ for Example 4.2.

after a short time, all fronts except the leftmost and rightmost shocks are very weak fronts, including the non-physical fronts. This is also in accordance with Figure 28 where we after a short time have only very small changes in $G$.

## ACKNOWLEDGEMENT

This paper was written as part of the international research program on Nonlinear Partial Differential Equations at the Centre for Advanced Study at the Norwegian Academy of Science and Letters in Oslo during the academic year 2008–09.

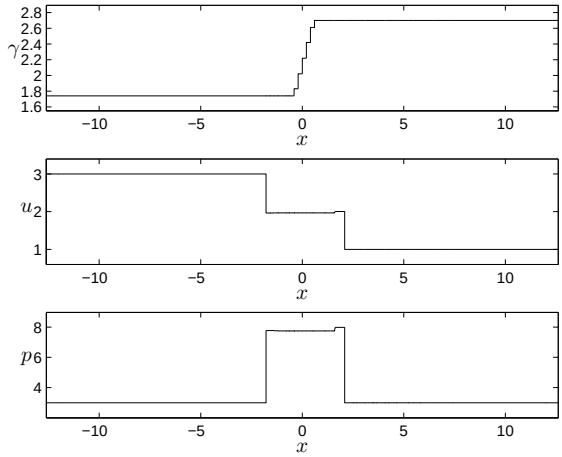


(a) $t = 0.3$.

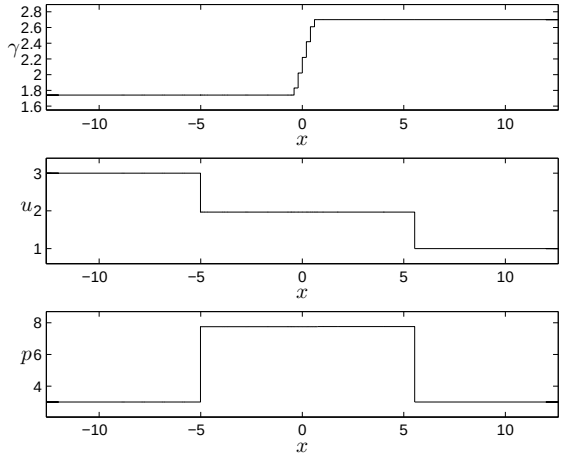


(b) $t = 1$.

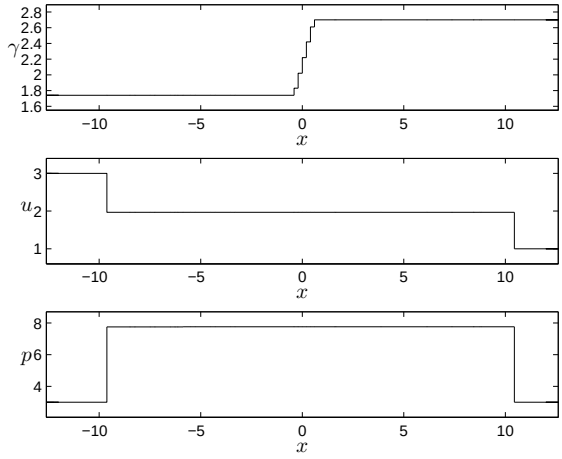


(c) $t = 2$.

FIGURE 26. $U^\delta(\cdot, t)$ at different times $t$ for Example 4.3.

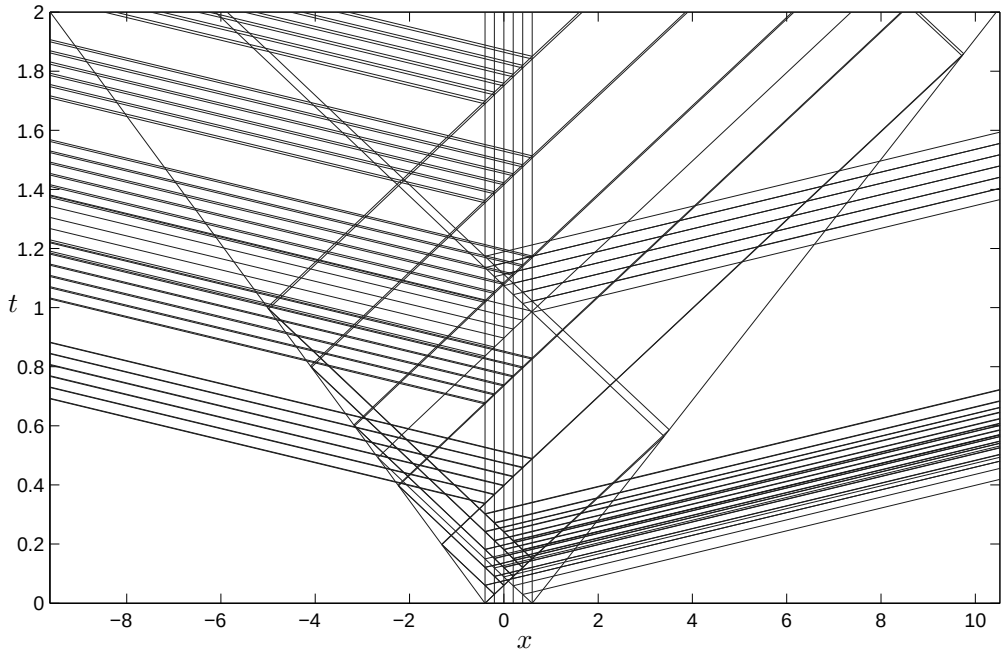


FIGURE 27. The solution $U^\delta(x,t)$ in the $(x,t)$-plane for Example 4.3.

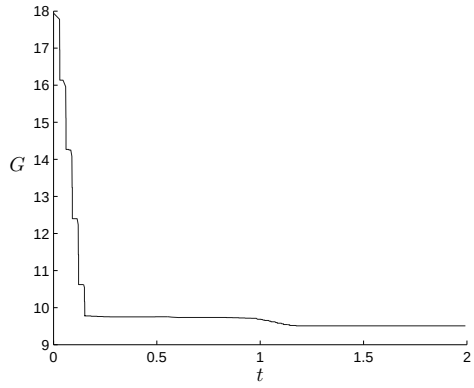


FIGURE 28. $G$ for Example 4.3.

## REFERENCES

[1] D. Amadori and A. Corli. On a model of multiphase flow. *SIAM J. Math. Anal*, 40(1):134–166, 2008.
[2] F. Asakura. Wave-front tracking for the equation of non-isentropic gas dynamics. *RIMS Kokyuroku*, 1495:78–91, 2006.
[3] F. Asakura. Wave-front tracking for the equation of isentropic gas dynamics. *Quart. Appl. Math.*, 63(1):20–33, 2005.
[4] A. Bressan. *Hyperbolic Systems of Conservation Laws.* Oxford University Press, 2000.

[5] A. Bressan and R. M. Colombo. Unique solutions of $2 \times 2$ conservation laws with large data. *Indiana Univ. Math. J.*, 44(3):677–725, 1993.
[6] C. Chalons and F. Coquel. Navier–Stokes equations with several independent pressure laws and explicit predictor-corrector schemes. *Numer. Math.* 101:451–478, 2005.
[7] G.-Q. Chen, C. Christoforou, and Y. Zhang. Dependence of entropy solutions in the large for the Euler equations on nonlinear flux functions. *Indiana Univ. Math. J.* 56(5):2535–2567, 2007.
[8] G.-Q. Chen, C. Christoforou, and Y. Zhang. Continuous dependence of entropy solutions to the Euler equations on the adiabatic exponent and Mach number *Arch. Ration. Mech. Anal.* 189:97–130, 2008.
[9] R. J. DiPerna. Existence in the large for quasilinear hyperbolic conservation laws. *Arch. Rational Mech. Anal.*, 52:244–257, 1973.
[10] R. J. DiPerna. Global existence of solutions to nonlinear hyperbolic systems of conservation laws. *J. Differential Equations*, 20:187–212, 1976.
[11] S. Evje and K. H. Karlsen. Global existence of weak solutions for a viscous two-phase model. *J. Differential Equations*, to appear.
[12] H. Fan. On a model of the dynamics of liquid/vapor phase transitions. *SIAM J. Appl. Math.*, 60(4):1270–1301. 2000.
[13] J. Glimm. Solution in the large for nonlinear hyperbolic systems of equations. *Comm. Pure Appl. Math.*, 18:697–715, 1965.
[14] D. Hoff. Invariant regions for systems of conservations laws. *Trans. Amer. Math. Soc.*, 289(2):591–610, 1985.
[15] H. Holden and N. H. Risebro. *Front Tracking for Hyperbolic Conservation Laws*. Springer-Verlag, 2002.
[16] H. Holden, N. H. Risebro and H. Sande. The solution of the Cauchy problem with large data for a model of a mixture of gases. To appear in *J. Hyperbolic Differ. Eq.*
[17] T.-P. Liu. Solutions in the large for the equations of nonisentropic gas dynamics. *Indiana Univ. Math. J*-, 26(1):147–177, 1977.
[18] T. P. Liu and J. A. Smoller. On the vacuum state for the isentropic gas dynamics equations. *Adv. in Appl. Math.*, 1(4):345–359, 1980.
[19] Y. Lu. *Hyperbolic Conservation Laws and the Compensated Compactness Method*. Shapman&Hall/CRC, 2003.
[20] T. Nishida. Global solution for an initial boundary value problem for a quasilinear hyperbolic system. *Proc. Japan Acad.*, 44:642–646, 1968.
[21] T. Nishida and J. A. Smoller. Solution in the large for some nonlinear hyperbolic conservation laws. *Comm. Pure Appl. Math.*, 26:183–200, 1973.
[22] Y.-J. Peng. Solutions faibles globales pour l'quation d'Euler d'un fluide compressible avec de grandes donnees initales. *Comm. Partial Differential Equations*, 17(1-2):161–187, 1992.
[23] Y.-J. Peng. Solutions faibles globales pour un modèle d'écoulements diphasiques. *Ann. Scuola Norm. Sup. Pisa Cl. Sci. (4)*, 21(4):523–540, 1994.
[24] J. Smoller. *Shock Waves and Reaction-Diffusion Equations*. Springer-Verlag, second edition, 1994.
[25] J. B. Temple. Solution in the large for the nonlinear hyperbolic concervation laws of gas dynamics. *J. Differential Equations*, 41:96–161, 1981.
[26] B. Temple and R. Young. The large time stability of sound waves. *Comm. Math. Phys.*, 179(2):417–466, 1996.
[27] D. H. Wagner. Equivalence of the Euler and Lagrangian equations of gas dynamics for weak solutions. *J. Differential Equations*, 68(1):118–136, 1987.
[28] W.-A. Yong. A simple approach to Glimm's interaction estimates. *Appl. Math. Lett.*, 12(2):29–34, 1999.
[29] B. D. Wissmann. Global soutions to the ultra-relativistic Euler equations. arXiv:0705.1333v1 [math.AP] 9 May 2007.

(Holden)
Department of Mathematical Sciences, Norwegian University of Science and Technology, NO–7491 Trondheim, Norway, and
Centre of Mathematics for Applications, University of Oslo, P.O. Box 1053, Blindern, NO–0316 Oslo, Norway
*E-mail address*: holden@math.ntnu.no
*URL*: www.math.ntnu.no/~holden/

(Risebro)
Centre of Mathematics for Applications, University of Oslo, P.O. Box 1053, Blindern, NO–0316 Oslo, Norway
*E-mail address*: nilshr@math.uio.no
*URL*: folk.uio.no/nilshr/

(Sande)
Department of Mathematical Sciences, Norwegian University of Science and Technology, NO–7491 Trondheim, Norway
*E-mail address*: hildes@math.ntnu.no
*URL*: www.math.ntnu.no/~hildes/

# Appendix

# APPENDIX

## Appendix A. Some properties of the system

In this appendix we take a closer look at some properties of the system given in Lagrangian coordinates as

$$\begin{aligned} v_t - u_x &= 0, \\ u_t + p(v,\gamma)_x &= 0, \\ \gamma_t &= 0, \end{aligned} \tag{A.1}$$

for $x \in \mathbb{R}$ and $t \in (0,\infty)$. Recall that this system models one dimensional, immiscible flow of several isentropic gases where $v = 1/\rho$ is the specific volume, $u$ is the velocity, $\gamma > 1$ is the adiabatic gas constant for each gas, and the pressure $p$ is given by a $\gamma$-law, $p(v,\gamma) = v^{-\gamma}$. Note also that we only consider the system away from vacuum, that is, for $v < \infty$, or equivalently, $p > 0$.

A.1. **Riemann invariants.** First, we discuss the Riemann invariants and prove that system (A.1) does not have a coordinate system of Riemann invariants, only a 2-Riemann coordinate. For the general theory on Riemann invariants, see, e.g., [1]. Let us start with some definitions.

**Definition A.1.** An *$i$-Riemann invariant* is a function $w$ such that

$$\nabla w \cdot r_i = 0, \tag{A.2}$$

where $r_i$ is the $i$th eigenvector. Furthermore, if $w_j$ is an $i$-Riemann invariant for all $i \neq j$, $i = 1,\dots,n$, then $w_j$ is a *Riemann coordinate* for the $j$th family.

**Definition A.2.** An $n \times n$ system of hyperbolic conservation laws has *a coordinate system of Riemann invariants* if there exist $n$ scalar functions $w_i$, $i = 1,\dots,n$, so that, for any $i,j = 1,\dots,n$, where $i \neq j$, we have that $w_j$ is an $i$-Riemann invariant for the system.

Note that Definition A.2 implies that all $2 \times 2$ systems of strictly hyperbolic conservation laws have a coordinate system of Riemann invariants. By rewriting Definition A.2 using Lie brackets, as shown in [1, p. 185], it becomes easier to verify whether or not an $n \times n$ system, $n > 2$, has a coordinate system of Riemann invariants. We state this as a corollary.

**Corollary A.3.** *An $n \times n$ system of hyperbolic conservation laws has a coordinate system of Riemann invariants if, and only if,*

$$[r_j, r_k] = \alpha_j^k r_j - \alpha_k^j r_k, \tag{A.3}$$

*for $j,k = 1,\dots,n$, where $j \neq k$, $\alpha_j^k$ are scalar fields, and $[r_j,r_k] := \nabla r_j \cdot r_k - \nabla r_k \cdot r_j$.*

The functions

$$\begin{cases} \gamma,\ u + \frac{2\sqrt{\gamma}}{\gamma-1} v^{(1-\gamma)/2}, \\ u,\ v^{-\gamma}, \\ \gamma,\ u - \frac{2\sqrt{\gamma}}{\gamma-1} v^{(1-\gamma)/2}, \end{cases} \tag{A.4}$$

are, respectively, 1-, 2-, and 3-Riemann invariants for system (A.1). Furthermore, we have the following result:

**Lemma A.4.** *System* (A.1) *does not have a coordinate system of Riemann invariants. However, $\gamma$ is a Riemann coordinate for the second family.*

*Proof.* It follows directly from Definition A.1 that $\gamma$ is a Riemann coordinate for the second family because $\gamma$ is both a 1- and a 3-Riemann invariant for system (A.1).

Recall that the eigenvectors are given as

$$r_1 = (1, \lambda, 0)^t, \quad r_2 = (-p_\gamma, 0, p_v)^t, \quad r_3 = (1, -\lambda, 0)^t,$$

where $\lambda = \sqrt{-p_v}$, thus,

$$\nabla r_1 = \begin{pmatrix} 0 & 0 & 0 \\ \lambda_v & 0 & \lambda_\gamma \\ 0 & 0 & 0 \end{pmatrix} = -\nabla r_3 \qquad \text{and} \qquad \nabla r_2 \qquad = \begin{pmatrix} -p_{\gamma v} & 0 & -p_{\gamma\gamma} \\ 0 & 0 & 0 \\ p_{vv} & 0 & p_{v\gamma} \end{pmatrix}.$$

For $j = 1$ and $k = 3$, condition (A.3) is satisfied because

$$[r_1, r_3] = \nabla r_1 \cdot r_3 - \nabla r_3 \cdot r_1 = (0, 2\lambda_v, 0)^t = \alpha_1^3 r_1 - \alpha_3^1 r_3,$$

for $\alpha_1^3 = \alpha_3^1 = \lambda_v/\lambda$. This confirms that system (A.1) has a Riemann coordinate for the second family. However, for $j = 1$ and $k = 2$, condition (A.3) is not satisfied because

$$[r_1, r_2] = \nabla r_1 \cdot r_2 - \nabla r_2 \cdot r_1 = (p_{\gamma v}, -\lambda_v p_\gamma + \lambda_\gamma p_v, -p_{vv})^t,$$

and there are no scalar fields, $\alpha_1^2$ and $\alpha_2^1$, so that $[r_1, r_2] = \alpha_1^2 r_1 - \alpha_2^1 r_2$. Thus, condition (A.3) is not satisfied for all $j, k = 1, 2, 3$, where $j \neq k$, thus, system (A.1) does not have a coordinate system of Riemann invariants. □

A.2. **Entropy/entropy flux pairs.** Consider an $n \times n$ system of hyperbolic conservation laws on the form $U_t + f(U)_x = 0$, and let $\eta$ and $q$ be scalar functions of $U$. If

$$\nabla q = \nabla \eta \, \mathrm{d}f(U), \tag{A.5}$$

then $(\eta, q)$ form *an entropy/entropy flux pair* for the system. For system (A.1) we have the following entropy/entropy flux pair:

**Lemma A.5.** *The scalar functions defined by*

$$\begin{aligned} \eta(v, u, \gamma) &= \frac{1}{2}u^2 - \int_0^v p(\tau, \gamma)\mathrm{d}\tau + h(\gamma), \\ q(v, u, \gamma) &= up(v, \gamma), \end{aligned} \tag{A.6}$$

*where $h(\gamma)$ is an arbitrary function of $\gamma$, form an entropy/entropy flux pair for system* (A.1).

*Proof.* We have to show that (A.6) satisfies (A.5) where $f = (-u, p(v, \gamma), 0)^t$ so that the right hand side reads

$$(\eta_v, \eta_u, \eta_\gamma) \begin{pmatrix} 0 & -1 & 0 \\ p_v & 0 & p_\gamma \\ 0 & 0 & 0 \end{pmatrix} = (p_v \eta_u, -\eta_v, p_\gamma \eta_u).$$

Differentiating (A.6) gives us

$$\begin{aligned} q_v &= up_v, & q_u &= p, & q_\gamma &= up_\gamma, \\ \eta_v &= -p, & \eta_u &= u, & \eta_\gamma &= -\frac{\mathrm{d}}{\mathrm{d}\gamma}\int_0^v p(\tau, \gamma)\mathrm{d}\tau + h_\gamma, \end{aligned}$$

thus,

$$(q_v, q_u, q_\gamma) = (p_v \eta_u, -\eta_v, p_\gamma \eta_u),$$

and (A.5) is satisfied for any function $h(\gamma)$. □

## Appendix B. Interactions between two waves or fronts with constant $\gamma$

An interaction has constant $\gamma$ if there is no contact discontinuity among the incoming waves or fronts. Moreover, the interactions with constant $\gamma$ are equal to the interactions of the corresponding $p$-system, and our estimates are based on the estimates for the $p$-system given by Nishida and Smoller in [2, Lemma 4]. This transformation of the interaction estimates were left out of the papers due to space limitations and is therefore discussed in this appendix.

B.1. **The $p$-system.** First, we discuss some properties of the $p$-system, which is a $2 \times 2$ system describing the flow of one isentropic gas. In Lagrangian coordinates the system reads

$$\begin{aligned} v_t - u_x &= 0, \\ u_t + p(v)_x &= 0, \end{aligned} \tag{B.1}$$

where $v = 1/\rho$ is the specific volume, $u$ is the velocity, and the pressure $p$ is given by a $\gamma$-law, $p(v) = v^{-\gamma}$, where $\gamma > 1$ is the adiabatic gas constant. We only consider system (B.1) away from vacuum, that is, for $v < \infty$, or equivalently, for $p > 0$. The functions

$$r = u - \frac{2\sqrt{\gamma}}{\gamma - 1}\left(p^{(\gamma-1)/2\gamma} - 1\right) \quad \text{and} \quad s = u + \frac{2\sqrt{\gamma}}{\gamma - 1}\left(p^{(\gamma-1)/2\gamma} - 1\right),$$

are 1- and 2-Riemann invariants for (B.1), respectively.[1] As noted in Section A.1, all $2 \times 2$ systems have a coordinate system of Riemann invariants, thus, $(r, s)$ forms a coordinate system for (B.1). Moreover, the mapping from $(p, u)$ to $(r, s)$ is one-to-one and onto for all $p > 0$.

As noted in the papers, the rarefaction and shock curves for system (A.1) have constant $\gamma$ and are equal to the wave curves for the corresponding $p$-systems (B.1). Let us therefore consider the wave curves for the $p$-system given by $r$ and $s$ as shown in Figure 1. For a wave connecting $(r_1, s_1)$ to $(r_2, s_2)$ one of the following holds,

| | | | | |
|---|---|---|---|---|
| 1-rarefaction: | $r_1 < r_2$, | $s_1 = s_2$, | | |
| 3-rarefaction: | $r_1 = r_2$, | $s_1 < s_2$, | | |
| 1-shock: | $r_1 > r_2$, | $s_1 > s_2$, | $\lvert s_1 - s_2 \rvert = q_1 \lvert r_1 - r_2 \rvert$ | for $0 < q_1 < 1$, |
| 3-shock: | $r_1 > r_2$, | $s_1 > s_2$, | $\lvert r_1 - r_2 \rvert = q_3 \lvert s_1 - s_2 \rvert$ | for $0 < q_3 < 1$, |

depending on the type and family of the wave.

In addition to the above properties of the wave curves, we need estimates on the transformation between $(r, s)$ and $(p, u)$. First of all,

$$\begin{aligned} s + r &= 2u, \\ s - r &= \frac{4\gamma^{1/2}}{\gamma - 1}\left(p^{(\gamma-1)/2\gamma} - 1\right) := f(p). \end{aligned}$$

Furthermore,

$$\lvert f(p_2) - f(p_1) \rvert = \lvert f'(\tilde{p}) \rvert \lvert p_2 - p_1 \rvert,$$

where $f'(\tilde{p}) = 2\gamma^{-\frac{1}{2}}\tilde{p}^{-(\gamma+1)/2\gamma}$ for a $\tilde{p}$ between $p_1$ and $p_2$. For $p_1 < p_2$, we therefore have

$$\lvert f'(p_2) \rvert \lvert p_2 - p_1 \rvert \le \lvert f(p_2) - f(p_1) \rvert \le \lvert f'(p_1) \rvert \lvert p_2 - p_1 \rvert. \tag{B.2}$$

As in the papers, we only consider interactions between waves or fronts that are contained in the domain

$$\mathcal{D} = \{(p, u, \gamma) \mid p \in [p_{\min}, p_{\max}], \lvert u \rvert < \infty, \gamma \in (1, \overline{\gamma}]\},$$

[1] This is the same Riemann invariants as used in [2] letting the constant $k$ be equal to one.

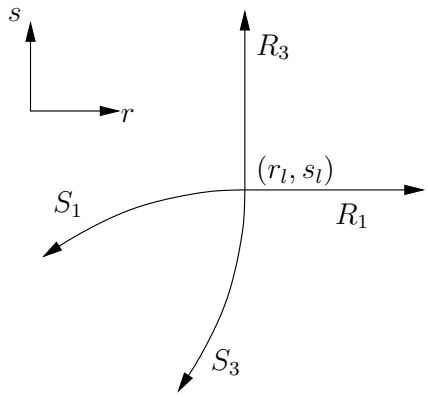


FIGURE 1. The rarefaction waves, $R_1$ and $R_3$, and the shock waves, $S_1$ and $S_3$, through the point $(r_l, s_l)$.

where $0 < p_{\min} \leq p_{\max} < \infty$ and $\overline{\gamma} := \sup(\gamma_0) \in (1, \infty)$ are constants. Thus, we have upper and lower bounds on $p$, and can define the constants

$$Q := \min_{\gamma \in (1,\overline{\gamma}]} f'(p_{\max}) \quad \text{and} \quad M := \max_{\gamma \in (1,\overline{\gamma}]} f'(p_{\min}), \tag{B.3}$$

only depending on $p_{\min}$, $p_{\max}$ and $\overline{\gamma}$. This gives us the following estimate

$$Q\,|p_2 - p_1\,| \leq |(s_2 - r_2) - (s_1 - r_1)\,| \leq M\,|p_2 - p_1\,|\,. \tag{B.4}$$

B.2. **Estimates for interactions of Type Ba and Type Bb.** We now prove the estimates for interactions between two waves or fronts where no contact discontinuity is present. These interactions are classified as Type Ba and Type Bb in the papers, and, more important, these interactions are the same for the Glimm scheme and for front tracking. Thus, we will no longer distinguish between waves and fronts, and we choose to use the term wave for the rest of this section.

We follow the same notation as used in the papers: The two incoming waves connect $U_l$ to $U_r$ with $U_1$ as the intermediate state. Since no contact discontinuity is present, the interactions have at most two outgoing waves, a 1-wave connecting $U_l$ to the intermediate state $\tilde{U}$, and a 3-wave connecting $\tilde{U}$ to $U_r$.

*Interactions of Type Ba.* These are the interactions where the incoming waves are of the same family. There are six interactions of this form, where three are symmetric to one of the others. Before we discuss each interaction, we define the constant

$$\tilde{C} = \frac{Q}{M} \min_{\gamma \in (1,\overline{\gamma}]} C_0, \tag{B.5}$$

where $C_0$ is the positive constant in the estimates given in [2, Lemma 4] and $Q$ and $M$ are given by (B.3). Thus, $\tilde{C}$ is a positive constant depending only on $p_{\min}$, $p_{\max}$ and $\overline{\gamma}$.

(i) $\alpha_1 + \alpha_2 \to \alpha' + \nu'$, symmetric to $\beta_1 + \beta_2 \to \mu' + \beta'$: For this interaction we do not need to use estimates from [2] because the estimates follows directly: We have $p_l \leq p_1 \leq p_r$ and $p_l \leq \tilde{p} \leq p_r$, see Figure 2, and the sum of the strengths of the incoming waves equals the sum of the strengths of the outgoing waves. Therefore,

$$|\alpha'\,| - |\alpha_1\,| - |\alpha_2\,| = -\,|\nu'\,|\,.$$

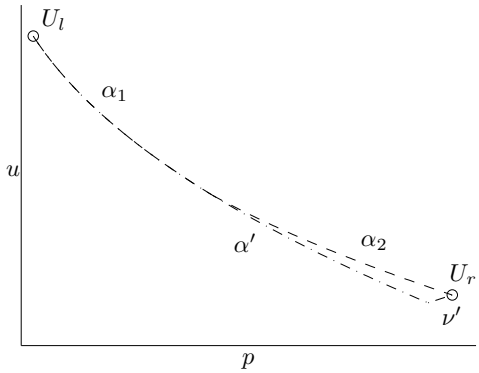


FIGURE 2. The interaction $\alpha_1 + \alpha_2 \to \alpha' + \nu'$ in the $(p, u)$-plane.

(ii) $\alpha + \mu$, symmetric to $\nu + \beta$. This interaction has two possible combinations of outgoing waves. In both cases we have an outgoing 3-shock wave connecting $\tilde{U}$ to $U_r$, thus,

$$|\tilde{p} - p_r| \le \frac{1}{Q} |(\tilde{s} - \tilde{r}) - (s_r - r_r)| = \frac{1 - q_3}{Q} |\tilde{s} - s_r| \le \frac{1}{Q} |\tilde{s} - s_r|, \tag{B.6}$$

since $0 < q_3 < 1$.

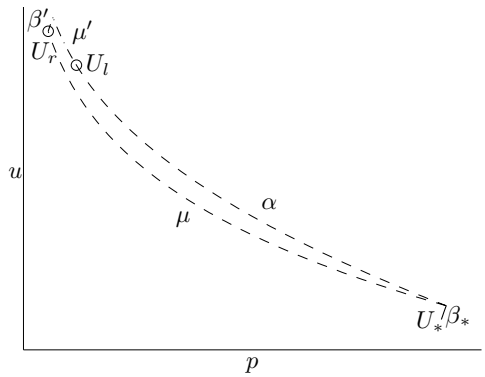


(a) In the $(p, u)$-plane: $\alpha + \mu \to \mu' + \beta'$.

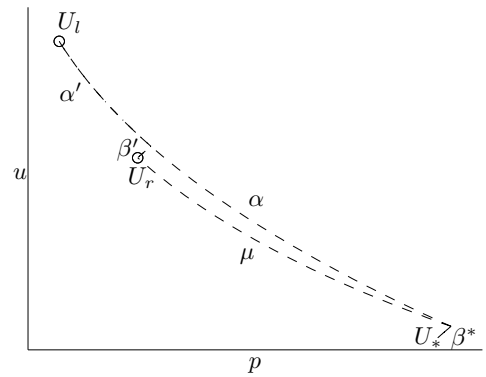


(b) In the $(p, u)$-plane: $\alpha + \mu \to \alpha' + \beta'$.

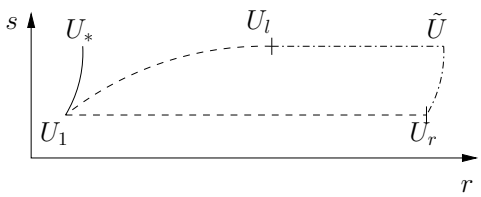


(c) In the $(r, s)$-plane: $\alpha + \mu \to \mu' + \beta'$.

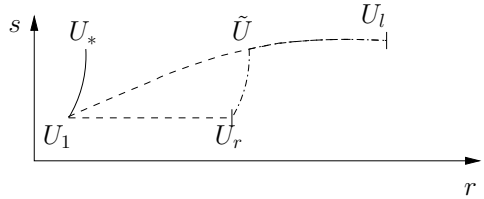


(d) In the $(r, s)$-plane: $\alpha + \mu \to \alpha' + \beta'$.

FIGURE 3. The interaction $\alpha + \mu$.

- $\alpha + \mu \to \mu' + \beta'$: With respect to $p$, $U_r$ is in this case to the left of the 3-shock wave starting at $U_l$, see Figure 3(a). The interaction is depicted in the $(r,s)$-plane in Figure 3(c). From [2] we have that

$$|r_l - r_1| = \frac{1}{q_1}|s_l - s_1| = (1 + C_0)|\tilde{s} - s_r|, \tag{B.7}$$

where $C_0 > 0$ is a constant. Using this, we want to estimate $|\alpha| - |\beta'|$ where the strengths are measured in $p$. First, we have to introduce an auxiliary curve; let $\beta^*$ be a copy of $\beta'$ that starts at $U_1$, and let the point where $\beta^*$ ends be $U_*$. Then, $|\alpha| - |\beta'| = |p_* - p_l|$ in the $(p,u)$-plane, and $r_* = r_1 + \tilde{r} - r_r$ and $s_* = \tilde{s}$ in the $(r,s)$-plane. We get

$$\begin{aligned}
|\alpha| - |\beta'| = |p_* - p_l| &\geq \frac{1}{M}|(s_* - r_*) - (s_l - r_l)| \\
&= \frac{1}{M}|r_l - r_1 - \tilde{r} + r_r| = \frac{1}{M}||r_l - r_1| - |\tilde{r} - r_r|| \\
&= \frac{1}{M}||r_l - r_1| - q_3|\tilde{s} - s_r|| \geq \frac{1}{M}C_0|\tilde{s} - s_r| \\
&\geq \frac{Q}{M}C_0|\tilde{p} - p_r| \geq \tilde{C}|\beta'|,
\end{aligned}$$

since $0 < q_3 < 1$ and we first used (B.7), then (B.6). Thus, we have proved that

$$|\beta'| - |\alpha| \leq -\tilde{C}|\beta'|, \tag{B.8}$$

where $\tilde{C}$ given by (B.5) only depends on $p_{\min}$, $p_{\max}$ and $\overline{\gamma}$.

- $\alpha + \mu \to \alpha' + \beta'$: With respect to $p$, $U_r$ is in this case to the right of the 3-shock wave starting at $U_l$. Figure 3(b) and Figure 3(d) show the interaction in the $(p,u)$-plane and $(r,s)$-plane, respectively. Moreover, we have from [2] that

$$|r_l - r_1| - |r_l - \tilde{r}| = |\tilde{r} - r_1| = \frac{1}{q_1}|\tilde{s} - s_1| = (C_0 + 1)|\tilde{s} - s_r|, \tag{B.9}$$

for a constant $C_0 > 0$. In order to obtain an estimate of $|\alpha| - |\alpha'| - |\beta'|$, we again introduce an auxiliary curve $\beta^*$ which is a copy of $\beta'$, starting at $U_1$ and ending at $U_*$. Then, we have $|\alpha| - |\alpha'| - |\beta'| = |p_* - \tilde{p}|$ in the $(p,u)$-plane, and $r_* = r_1 + \tilde{r} - r_r$ and $s_* = \tilde{s}$ in the $(r,s)$-plane. We get

$$\begin{aligned}
|\alpha| - |\alpha'| - |\beta'| = |p_* - \tilde{p}| &\geq \frac{1}{M}|(s_* - r_*) - (\tilde{s} - \tilde{r})| \\
&= \frac{1}{M}|\tilde{r} - r_1 - \tilde{r} + r_r| \\
&= \frac{1}{M}||r_l - r_1| - |r_l - \tilde{r}| - |\tilde{r} - r_r|| \\
&= \frac{1}{M}||r_l - r_1| - |r_l - \tilde{r}| - q_3|\tilde{s} - s_r|| \\
&\geq \frac{1}{M}C_0|\tilde{s} - s_r| \geq \frac{Q}{M}C_0|\tilde{p} - p_r| \geq \tilde{C}|\beta'|,
\end{aligned}$$

since $0 < q_3 < 1$ and we used (B.9) and (B.6). Hence,

$$|\alpha'| + |\beta'| - |\alpha| \leq -\tilde{C}|\beta'|, \tag{B.10}$$

where $\tilde{C}$ given by (B.5) only depends on $p_{\min}$, $p_{\max}$ and $\overline{\gamma}$.

(iii) $\mu + \alpha$, symmetric to $\nu + \beta$: This interaction has two possible combinations of outgoing waves.

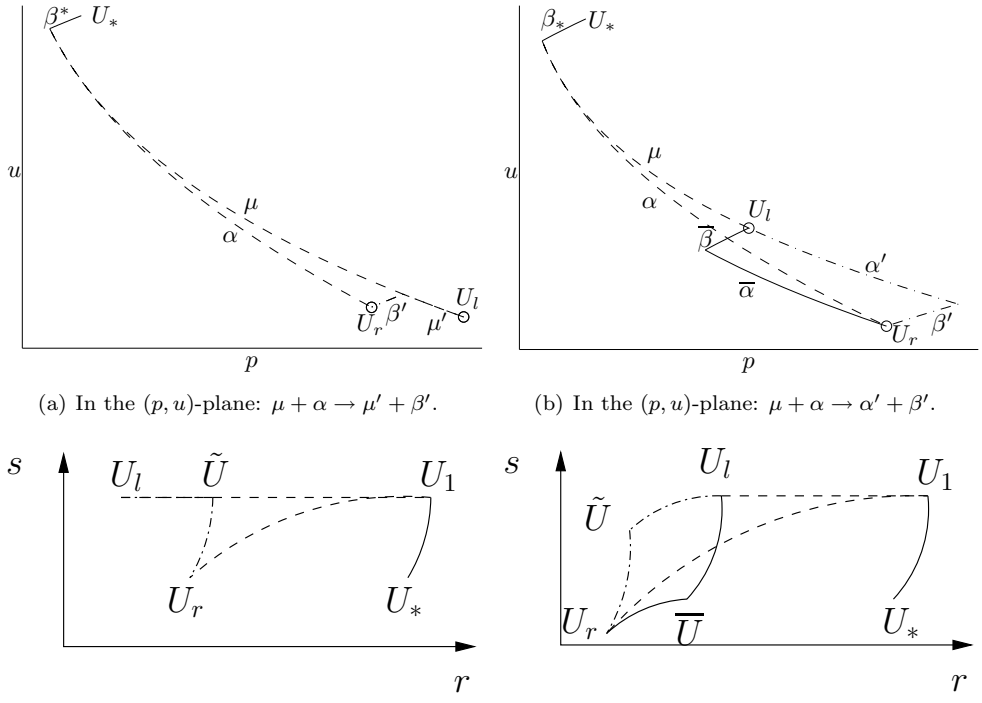


(a) In the $(p,u)$-plane: $\mu+\alpha\to\mu'+\beta'$.

(b) In the $(p,u)$-plane: $\mu+\alpha\to\alpha'+\beta'$.

(c) In the $(r,s)$-plane: $\mu+\alpha\to\mu'+\beta'$.

(d) In the $(r,s)$-plane: $\mu+\alpha\to\alpha'+\beta'$.

FIGURE 4. The interaction $\mu+\alpha$.

- $\mu+\alpha\to\mu'+\beta'$: With respect to $p$, $U_r$ is in this case to the left of the 3-shock wave starting at $U_l$, see Figure 4(a). The interaction in the $(r,s)$-plane is depicted in Figure 4(c), and from [2] we have

$$|r_1-r_r\,|=\frac{1}{q_1}\,|s_1-s_r\,|=(1+C_0)\,|\tilde{s}-s_r\,|\,, \tag{B.11}$$

where $C_0>0$ is a constant. Moreover, (B.6) also holds for this interaction because it has an outgoing 3-shock wave connecting $\tilde{U}$ to $U_r$. As above, we introduce an auxiliary curve $\beta^*$ which is a copy of $\beta'$, starting at $U_1$ and ending at $U_*$. Then, we have $|\alpha\,|-|\beta'\,|=|p_r-p_*\,|$ in the $(p,u)$-plane, and $r_*=r_1+r_r-\tilde{r}$ and $s_*=s_r$ in the $(r,s)$-plane. Furthermore,

$$\begin{aligned}
|\alpha\,|-|\beta'\,|=|p_r-p_*\,|&\geq\frac{1}{M}\,|(s_r-r_r)-(s_*-r_*)\,|\\
&=\frac{1}{M}\,|r_1+r_r-\tilde{r}-r_r\,|=\frac{1}{M}\,||r_1-r_r\,|-|\tilde{r}-r_r\,|\,|\\
&=\frac{1}{M}\,||r_1-r_r\,|-q_3\,|\tilde{s}-s_r\,|\,|\geq\frac{1}{M}C_0\,|\tilde{s}-s_r\,|\\
&\geq\frac{Q}{M}C_0\,|\tilde{p}-p_r\,|\geq\tilde{C}\,|\beta'\,|\,,
\end{aligned}$$

since $0<q_3<1$ and we used (B.11) and (B.6). Furthermore, the constant $\tilde{C}$ is given by (B.5) and depends only on $p_{\min}$, $p_{\max}$ and $\overline{\gamma}$.

- $\mu + \alpha \to \alpha' + \beta'$: With respect to $p$, $U_r$ is in this case to the right of the 3-shock wave starting at $U_l$, and we use the same strategy as Nishida and Smoller [2] replacing the interaction with a new one, $\overline{\beta} + \overline{\alpha} \to \alpha' + \beta'$, where $\overline{\beta} + \overline{\alpha}$ connects $U_l$ to $U_r$. Figure 4(b) and Figure 4(d) show the interaction in the $(p, u)$-plane and $(r, s)$-plane, respectively. The new interaction is of Type Bb which is covered below, thus, we only need to show that

$$|\overline{\alpha}| + |\overline{\beta}| - |\alpha| \le -\tilde{C}\,|\overline{\beta}|\,. \tag{B.12}$$

Let $\overline{U}$ denote the new intermediate state so that $\overline{\beta}$ connects $U_l$ to $\overline{U}$ and $\overline{\alpha}$ connects $\overline{U}$ to $U_r$. In the $(r, s)$-plane we then have from [2] that

$$|r_1 - r_r| - |\overline{r} - r_r| \ge (1 + C_0)\,|s_l - \overline{s}|\,, \tag{B.13}$$

for a constant $C_0 > 0$. Moreover,

$$|p_l - \overline{p}| \le \frac{1}{Q}\,|(s_l - r_l) - (\overline{s} - \overline{r})| = \frac{1 - q_3}{Q}\,|s_l - \overline{s}| \le \frac{1}{Q}\,|s_l - \overline{s}|\,. \tag{B.14}$$

Once more we introduce an auxiliary curve, and now $\beta^*$ is a copy of $\overline{\beta}$, starting at $U_1$ and ending at $U_*$. Thus, $|\alpha| - |\overline{\alpha}| - |\overline{\beta}| = |\overline{p} - p_*|$ in the $(p, u)$-plane, and $r_* = r_1 + \overline{r} - r_l$ and $s_* = \overline{s}$ in the $(r, s)$-plane, and

$$\begin{aligned}
|\alpha| - |\overline{\alpha}| - |\overline{\beta}| = |\overline{p} - p_*| &\ge \frac{1}{M}\,|(\overline{s} - \overline{r}) - (s_* - r_*)| \\
&= \frac{1}{M}\,|r_1 + \overline{r} - r_l - \overline{r}| \\
&= \frac{1}{M}\,||r_1 - r_r| - |\overline{r} - r_r| - |r_l - \overline{r}||\\
&= \frac{1}{M}\,||r_1 - r_r| - |\overline{r} - r_r| - q_3\,|s_l - \overline{s}||\\
&\ge \frac{1}{M} C_0\,|s_l - \overline{s}| \ge \frac{Q}{M} C_0\,|p_l - \overline{p}| \ge \tilde{C}\,|\overline{\beta}|\,,
\end{aligned}$$

since $0 < q_3 < 1$ and we used (B.13) and (B.14). This proves (B.12) with $\tilde{C}$ given by (B.5).

*Interactions of Type Bb.* These are the interactions between a 3-wave and a 1-wave. There are four interactions of this kind, and one of these is symmetric to one of the others.

(i) $\nu + \mu \to \mu' + \nu'$: Since $s$ and $r$ are constant along 1- and 3-rarefaction waves, respectively, we have

$$r_l = r_1, \quad \tilde{r} = r_r, \quad s_1 = s_r, \quad s_l = \tilde{s},$$

as illustrated in Figure 5(b). Thus,

$$\begin{aligned}
|u_r - \tilde{u}| &= \left|\frac{1}{2}(s_r + r_r) - \frac{1}{2}(\tilde{s} + \tilde{r})\right| = \left|\frac{1}{2}(s_r - \tilde{s})\right| \\
&= \left|\frac{1}{2}(s_1 - s_l)\right| = \left|\frac{1}{2}s_1 - \frac{1}{2}s_l + \frac{1}{2}r_1 - \frac{1}{2}r_l\right| \\
&= \left|\frac{1}{2}(s_1 + r_1) - \frac{1}{2}(s_l + r_l)\right| = |u_1 - u_l|\,.
\end{aligned}$$

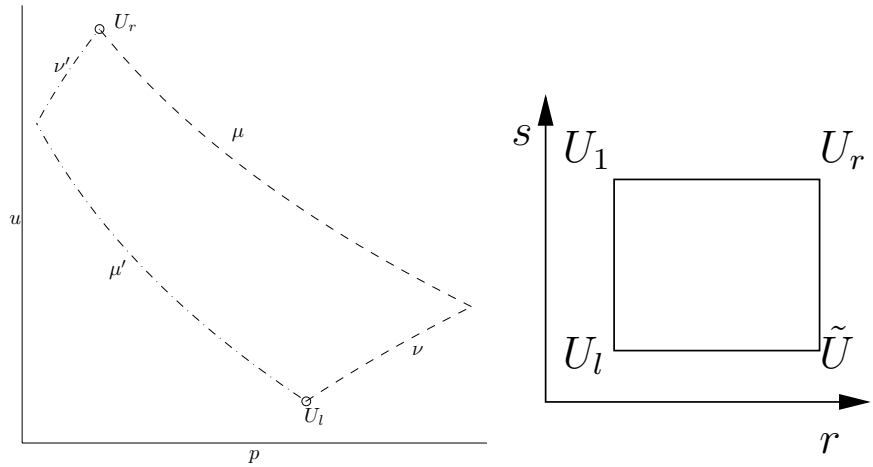


(a) In the $(p,u)$-plane: $\nu+\mu \to \mu'+\nu'$. (b) In the $(r,s)$-plane: $\nu+\mu \to \mu'+\nu'$.

FIGURE 5. The interaction $\nu+\mu$.

We furthermore know that a 3-rarefaction wave is steeper the smaller $p$ is. Since $|u_r-\tilde{u}\,| = |u_1-u_l\,|$ and $p_r < p_1$, we have

$$\frac{|u_r-\tilde{u}\,|}{|p_r-\tilde{p}\,|} \geq \frac{|u_1-u_l\,|}{|p_1-p_l\,|} \quad \Rightarrow \quad |p_r-\tilde{p}\,| \leq |p_1-p_l\,|\,,$$

hence, $|\nu'\,| \leq |\nu\,|$. Figure 5(a) shows the interaction in the $(p,u)$-plane, and we observe that

$$|\mu'\,|+|\nu\,| = |\mu\,|+|\nu'\,| \quad \Rightarrow \quad |\mu'\,|-|\mu\,| = |\nu'\,|-|\nu\,| \leq 0.$$

Thus, we have proved the estimates

$$|\mu'\,| \leq |\mu\,| \quad \text{and} \quad |\nu'\,| \leq |\nu\,|\,.$$

(ii) $\beta+\alpha \to \alpha'+\beta'$: In [2], three different estimates are given in Riemann invariants for this interaction, depending on which of three given regions the intermediate state $\tilde{U}$ is in. The positive constant $C$ in the estimates in [2, Lemma 4] will here be denoted by $C_{\rm ns}$ and may depend on $\gamma$. Furthermore, the three regions are denoted $I$, $II$ and $III$, and they are shown in Figure 6(b). First, we introduce an auxiliary point $U_*$: Let $\alpha_*$ be a copy of $\alpha$ that starts at the point $U_l$, and let $\beta_*$ be a copy of $\beta$ that ends at $U_r$, as shown in the $(p,u)$-plane in Figure 6(a). Then, the intersection point between $\alpha_*$ and $\beta_*$ is $U^*$. In Figure 6(b), where the interaction is depicted in the $(r,s)$-plane, the solid curves are the copy of $\alpha$, $\alpha^*$, and the copy of the backward 3-shock wave connecting $U_1$ to $U_l$. These two curves also intersect at $U_*$, and they bound the three different regions. We have that $r_* = r_r+r_l-r_1$ and $s_* = s_l+s_r-s_1$. Furthermore, due to the properties of shock curves, $p_* \leq \tilde{p}$, where $\tilde{U}$ is the intersection point between $\alpha'$ and $\beta'$. Moreover, we have $|\alpha\,|+|\beta'\,| = |\alpha'\,|+|\beta\,|$ in the $(p,u)$-plane, hence

$$|\alpha'\,|-|\alpha\,| = |\beta'\,|-|\beta\,| = \tilde{p}-p_*. \tag{B.15}$$

If $(\tilde{r},\tilde{s})$ is in Region $II$, as in Figure 6(b), then $\tilde{r} \leq r_*$ and $\tilde{s} \geq s_*$, and we have from [2] that

$$|r_l-\tilde{r}\,|-|r_1-r_r\,| \leq C_{\rm ns}(\gamma-1)\,|r_1-r_l\,|\,|s_l-s_1\,|\,,$$

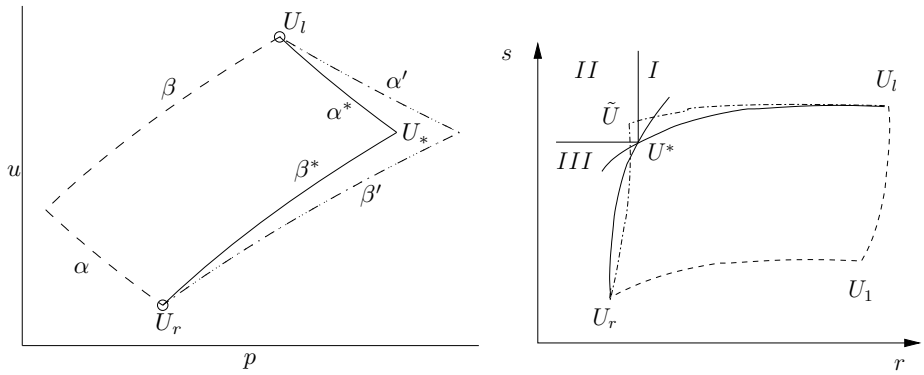


(a) In the $(p, u)$-plane. (b) In the $(r, s)$-plane.

FIGURE 6. The interaction $\beta + \alpha \to \alpha' + \beta'$.

$$|\tilde{s} - s_r\,| - |s_l - s_1\,| \le C_{\rm ns}(\gamma - 1)\,|r_1 - r_l\,|\,|s_l - s_1\,|\,,$$

where $C_{\rm ns}$ is a positive constant. Thus,

$$\begin{aligned} |\tilde{p} - p_*\,| &\le \frac{1}{Q}\,|(\tilde{s} - \tilde{r}) - (s_* - r_*)\,| = \frac{1}{Q}(\tilde{s} - s_* + r_* - \tilde{r}) \\ &= \frac{1}{Q}(\tilde{s} - s_r - s_l + s_1 + r_l + r_r - r_1 - \tilde{r}) \\ &= \frac{1}{Q}(|\tilde{s} - s_r\,| - |s_l - s_1\,| + |r_l - \tilde{r}\,| - |r_1 - r_r\,|) \\ &\le \frac{2C_{\rm ns}(\gamma - 1)}{Q}\,|r_1 - r_l\,|\,|s_l - s_1\,|\,. \end{aligned} \tag{B.16}$$

For $(\tilde{r}, \tilde{s})$ in Region $I$, we have $\tilde{r} \ge r_*$ and $\tilde{s} \ge s_*$, and according to [2];

$$\begin{aligned} &|r_l - \tilde{r}\,| - |r_1 - r_r\,| = -q_\epsilon, \\ &|\tilde{s} - s_r\,| - |s_l - s_1\,| \le C_{\rm ns}(\gamma - 1)\,|r_1 - r_l\,|\,|s_l - s_1\,| + q_\eta, \end{aligned}$$

where $q_\eta < q_\epsilon$ and $C_{\rm ns}$ is a positive constant.[2] Thus,

$$\begin{aligned} |\tilde{p} - p_*\,| &\le \frac{1}{Q}\,|(\tilde{s} - \tilde{r}) - (s_* - r_*)\,| \\ &= \frac{1}{Q}\,|\tilde{s} - s_r - s_l + s_1 + r_l + r_r - r_1 - \tilde{r}\,| \\ &= \frac{1}{Q}\,||\tilde{s} - s_r\,| - |s_l - s_1\,| + |r_l - \tilde{r}\,| - |r_1 - r_r\,|\,| \\ &\le \frac{1}{Q}\,|C_{\rm ns}(\gamma - 1)\,|r_1 - r_l\,|\,|s_l - s_1\,| + q_\eta - q_\epsilon\,| \\ &\le \frac{C_{\rm ns}(\gamma - 1)}{Q}\,|r_1 - r_l\,|\,|s_l - s_1\,|\,. \end{aligned} \tag{B.17}$$

Finally, if $(\tilde{r}, \tilde{s})$ is in Region $III$, then $\tilde{r} \le r_*$ and $\tilde{s} \le s_*$, and from [2] we have

$$|r_l - \tilde{r}\,| - |r_1 - r_r\,| \le C_{\rm ns}(\gamma - 1)\,|r_1 - r_l\,|\,|s_l - s_1\,| + q_\eta,$$

[2]The constants $q_\epsilon$ and $q_\eta$ correspond to the constants $\epsilon$ and $\eta$ in [2], respectively.

$$|\tilde{s} - s_r| - |s_l - s_1| = -q_\epsilon,$$

where $q_\eta < q_\epsilon$ and $C_{\rm ns}$ is a positive constant. Thus,

$$\begin{aligned}
|\tilde{p} - p_*| &\le \frac{1}{Q}\,|(\tilde{s} - \tilde{r}) - (s_* - r_*)| \\
&= \frac{1}{Q}\,|\tilde{s} - s_r - s_l + s_1 + r_l + r_r - r_1 - \tilde{r}| \\
&= \frac{1}{Q}\,||\tilde{s} - s_r| - |s_l - s_1| + |r_l - \tilde{r}| - |r_1 - r_r||
\end{aligned} \tag{B.18}$$

$$\begin{aligned}
&\le \frac{1}{Q}\,|-q_\epsilon + C_{\rm ns}(\gamma - 1)\,|r_1 - r_l|\,|s_l - s_1| + q_\eta| \\
&\le \frac{C_{\rm ns}(\gamma - 1)}{Q}\,|r_1 - r_l|\,|s_l - s_1|.
\end{aligned}$$

From equation (B.15), together with estimates (B.16)–(B.18), we get

$$|\alpha'| - |\alpha| = |\beta'| - |\beta| \le \frac{2C_{\rm ns}(\overline{\gamma} - 1)}{Q}\,|r_1 - r_l|\,|s_l - s_1|,$$

regardless of the region $\tilde{U}$ is in. Furthermore, we have

$$\begin{aligned}
|\alpha| = |p_r - p_1| &\ge \frac{1}{M}\,|(s_r - r_r) - (s_1 - r_1)| \\
&= \frac{1}{M}\,|(r_1 - r_r) - (s_1 - s_r)| = \frac{1}{M}(1 - q_1)\,|(r_1 - r_r)|,
\end{aligned}$$

where $0 < q_1 < 1$, and

$$\begin{aligned}
|\beta| = |p_l - p_1| &\ge \frac{1}{M}\,|(s_l - r_l) - (s_1 - r_1)| \\
&= \frac{1}{M}\,|(s_l - s_1) - (r_l - r_1)| = \frac{1}{M}(1 - q_3)\,|(s_l - s_1)|,
\end{aligned}$$

where $0 < q_3 < 1$. Hence

$$|\alpha'| - |\alpha| = |\beta'| - |\beta| \le C_1(\overline{\gamma} - 1)\,|\alpha|\,|\beta|,$$

where

$$C_1 = \frac{2M^2}{Q} \sup_{\gamma \in (1, \overline{\gamma}]} \frac{C_{\rm ns}}{(1 - q_1)(1 - q_3)},$$

only depends on $p_{\min}$, $p_{\max}$ and $\overline{\gamma}$.

(iii) $\nu + \alpha \to \alpha' + \nu'$, symmetric to $\beta + \mu \to \mu' + \beta'$. As for the first interaction, we only need to consider this interaction in the $(p, u)$-plane to obtain the estimates. First, we introduce an auxiliary point $U_*$ as follows: Let $\alpha_*$ be a copy of $\alpha'$ that ends at the point $U_r$, and let $\nu_*$ be a copy of $\nu'$ starting at $U_l$. Thus, $\alpha_*$ and $\nu_*$ have the same shape as $\alpha'$ and $\nu'$, respectively, but start and end at different points, see Figure 7. The intersection point between $\alpha_*$ and $\nu_*$ is $U_*$. Recall that slope of a 3-rarefaction wave only depends on $p$ and decreases as $p$ increases. Since $\nu$ starts at $p_l$ and $\nu'$ starts at $\tilde{p}$, where $p_l \le \tilde{p}$, the first part of $\nu$ is steeper than the first part of $\nu'$. The curve $\nu^*$ has the same slope as $\nu'$, therefore, $\nu_*$ lies below $\nu$, as depicted in Figure 7. The slope of a 1-shock wave depends both on the starting point and on $p$. The starting point of $\alpha'$ is less than the starting point of $\alpha$, therefore, the first part of $\alpha'$ is steeper than $\alpha$.

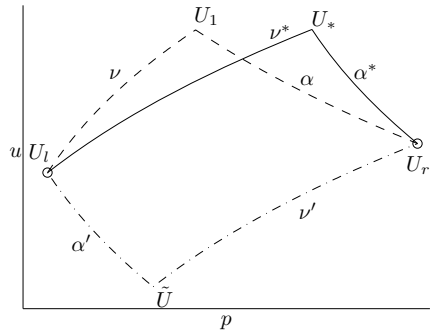


FIGURE 7. The interaction $\nu + \alpha \to \alpha' + \nu'$ in the $(p, u)$-plane.

Since $\alpha_*$ has the same slope as $\alpha'$, but ends in the same point as $\alpha$, $\alpha_*$ has to lie above $\alpha$. Thus, $p_* \geq p_1$ and $|\nu'| - |\nu| = p_* - p_1 \geq 0$. Furthermore,

$$|\alpha| + |\nu| = |\alpha'| + |\nu'| \quad \Rightarrow \quad |\alpha'| - |\alpha| = |\nu| - |\nu'|,$$

hence

$$|\nu'| - |\nu| = q, \quad \text{and} \quad |\alpha'| - |\alpha| = -q,$$

where $q \geq 0$.

This concludes the detailed discussion of the estimates for interactions of Type Ba and Type Bb, that is, the interactions between two waves not involving a contact discontinuity. The remaining interactions between two waves are discussed in detail in Paper I. These are the interactions of Type Bc; the interactions between a contact discontinuity and another wave, also called $\gamma$-collisions in Paper II.

## REFERENCES

[1] C. Dafermos *Hyperbolic Conservation Laws in Continuum Physics.* Springer-Verlag, 2005.
[2] T. Nishida and J. A. Smoller. Solution in the large for some nonlinear hyperbolic conservation laws. *Comm. Pure Appl. Math.*, 26:183–200, 1973.